Alternative paths to proliferation

Joseph Ryan

▶ **To cite this version:**

HAL Id: tel-04058167
https://theses.hal.science/tel-04058167

Submitted on 4 Apr 2023

THESE DE DOCTORAT DE

UNIVERSITÉ DE RENNES 1

L'UNIVERSITE DE RENNES 1

ECOLE DOCTORALE N° 605
Biologie Santé
Spécialité: *Biologie cellulaire, biologie du développement*

Par

Joseph RYAN

Alternative Paths to Proliferation

Thèse présentée et soutenue à Rennes, le 07/12/2022
Unité de recherche: UMR 6290

Rapporteurs avant soutenance :

Sandra LOPEZ-AVILES   Group Leader – Centre for Molecular Medicine Norway, Oslo, Norway
Lionel PINTARD   Group Leader – Institut Jacques Monod, Paris, France

Composition du Jury :

Président :   Lionel PINTARD   Group Leader – Institut Jacques Monod, Paris, France
Examinateurs : Sandra LOPEZ-AVILES   Group Leader – Centre for Molecular Medicine Norway, Oslo, Norway
                Isabelle SAGOT   Institut de Biochimie et Génétique Cellulaires, Bordeaux, France
Dir. de thèse : Damien COUDREUSE   Institut de Biochimie et Génétique Cellulaires, Bordeaux, France

Summary in French

Le travail présenté dans cette thèse combine le cadre de la biologie synthétique avec l'outil de l'évolution expérimentale afin de découvrir des voies précédemment inconnues impliquées dans la régulation du cycle cellulaire. En utilisant les propriétés uniques d'un réseau synthétique du cycle cellulaire minimal dans la levure de fission (MCN, Coudreuse et Nurse 2010), nous avons pu explorer les stratégies évolutives que les cellules peuvent employer pour surmonter la perte de mécanismes de régulation normalement essentiels à la prolifération. De façon remarquable, nos résultats démontrent que la modulation de processus mal compris peut compenser, au moins partiellement, la perte de la boucle de rétroaction hautement conservée Wee1/Cdc25. De tels mécanismes auraient été difficiles à identifier dans les cellules de type sauvage en raison de la prédominance de cette boucle de rétroaction réglementaire. Cette thèse s'est principalement concentrée sur la dissection d'un des mécanismes évolués responsables de la récupération du potentiel de prolifération des cellules dépourvues du commutateur d'entrée mitotique. Nous avons démontré que la perte de la petite protéine hautement désordonnée, Spo12, favorise la croissance des cellules MCN dans lesquelles les sites cibles de Wee1/Cdc25 sont mutés. Nous avons également montré que Spo12 est impliquée dans une boucle de rétroaction positive sur l'activité de Cdk au début de la mitose.

La première étape de cette étude a consisté en un test d'évolution expérimental de 70 jours réalisé à l'aide de trois souches de levure de fission distinctes : une avec un réseau de contrôle du cycle cellulaire normal (cellules de type sauvage, WT), et deux réseaux de contrôle du cycle cellulaire minimal (MCN et MCN-AF ; dans le fond MCN-AF, les résidus T14 et Y15 de Cdc2/Cdk1, qui sont les sites cibles de Wee1, sont mutés en A et F, respectivement). Au cours de l'essai d'évolution, les populations ont été maintenues à une croissance végétative constante, ce qui a permis de sélectionner les cellules à croissance plus rapide. Ce dispositif expérimental nous a permis d'explorer deux questions clés : 1) Le réseau simplifié de contrôle du cycle cellulaire reste-t-il robuste malgré son manque de complexité par rapport au réseau de type sauvage (WT vs MCN), et 2) quelles voies peuvent être ciblées par l'évolution dans les cellules ne contrôlant pas strictement l'entrée en mitose pour surmonter la perte inhérente du potentiel prolifératif des cellules MCN-AF. Tout d'abord, sur la base de la caractérisation des populations évoluées WT et MCN présentée dans ce travail, nous pouvons voir que les cellules avec un réseau simplifié de contrôle du cycle cellulaire ne semblent pas avoir de pressions inhérentes pour se recomplexifier, et ne sont pas moins robustes lorsqu'elles sont maintenues en croissance végétative prolongée par rapport à WT. Il s'agit d'un résultat frappant, car il contribue à un ensemble croissant de preuves que le principe fondamental du cycle cellulaire est de maintenir l'oscillation correcte de l'activité Cdk (Fisher et Nurse 1996 ; Coudreuse et Nurse 2010b ; Santamaría et al. 2007). Cependant, l'augmentation du nombre de couches de complexité dans le réseau de contrôle du cycle cellulaire normal par rapport au réseau MCN peut être significative pour maintenir l'intégrité du cycle cellulaire dans des conditions de croissance spécifiques et d'autres études seront nécessaires pour explorer cette question. En fait, les travaux de notre équipe ont montré que les cellules MCN et WT ont des propriétés très différentes lorsqu'elles sont en quiescence et un profil de vieillissement chronologique différent (données non publiées).

Ensuite, afin d'étudier les stratégies évolutives que les cellules peuvent employer pour surmonter la perte de la boucle de rétroaction Wee1/Cdc25, nous avons spécifiquement exploré une des altérations génétiques qui a été identifiée dans notre essai d'évolution expérimental. En effet, une mutation ponctuelle dans le gène spo12 qui entraîne une perturbation de la protéine Spo12 s'est avérée être la cause de l'amélioration observée de la croissance des cellules MCN-AF évoluées. Cette amélioration du potentiel prolifératif s'est accompagnée d'un raccourcissement de la phase G1 et d'une réduction de la taille à la division (SAD). Il est intéressant de noter que ces améliorations semblent être des caractéristiques communes à chacune des populations MCN-AF évoluées indépendamment, ce qui implique que l'amélioration de la croissance dans

le contexte de ce test implique le retour à un état du cycle cellulaire plus similaire à celui des cellules WT. La perte de la fonction de Spo12 a été confirmée comme étant responsable de la capacité proliférative retrouvée des cellules MCN-AF, car la délétion complète du cadre de lecture ouvert a démontré des avantages clairs pour la croissance par rapport aux cellules parentales, tant au niveau de la population que de la cellule unique.

Le rôle de Spo12 chez la levure de fission reste inconnu, et ne partage pas de fonction avec son homologue chez la levure bourgeonnante, qui est impliqué dans la libération précoce de Cdc14 dans le cadre du réseau FEAR (Chen et al. 2006 ; Samuel et al. 2000). Il est intéressant de noter que Spo12 de la levure de fission (90aa) est beaucoup plus petit que SPO12 de la levure bourgeonnante (173aa), avec seulement un petit domaine Spo12 conservé entouré de structures largement désorganisées. Dans le domaine Spo12, il y a deux sites cibles Cdk putatifs, dont l'un a été montré comme étant phosphorylé par Cdc2/Cdk1 (Swaffer et al. 2016). Cela démontre une interaction fonctionnelle claire entre Spo12 et Cdc2/Cdk1. En effet, nos résultats montrent que Spo12 fonctionne comme un potentialisateur de l'activité de Cdk, et fait partie d'une nouvelle boucle de rétroaction positive sur la cycline B/Cdk1. Spo12 est transloqué vers le noyau de manière dépendante de Cdk au début de la mitose où il reste transitoirement jusqu'à l'anaphase. Il est intéressant de noter que les niveaux cellulaires de Spo12 ne changent pas au cours du cycle cellulaire. C'est en fait sa translocation vers le noyau induite par le Cdk lors de la mitose qui semble être le médiateur d'une augmentation de l'activité des Cdk. Ainsi, notre travail démontre pour la première fois que Spo12 est un nouveau régulateur de l'activité de Cdk qui fonctionne dans une boucle de rétroaction positive spatiale sur Cdc2. Bien que nous ayons découvert la manière dont Cdc2 régule Spo12, le mécanisme responsable de la potentialisation de l'activité de Cdk par Spo12 reste obscur. Cependant, nous espérons le découvrir grâce à l'identification d'interacteurs de Spo12 à l'aide de la balise TurboID combinée à la spectrométrie de masse (Larochelle et al. 2019).

Notre étude a montré que la perte de la fonction de Spo12 était suffisante pour améliorer la croissance des cellules dépourvues du commutateur d'entrée mitotique en réduisant les niveaux d'activité de Cdk. En effet, nous avons constaté que les populations MCN-AF présentent un pourcentage plus élevé de cellules non-divisées par rapport à WT, qui est réduit en abrogeant la fonction Spo12. Nous supposons que le pourcentage plus élevé de cellules qui ne se divisent pas dans les cultures MCN-AF est dû à l'augmentation du nombre de cellules entrant prématurément en mitose, ce qui entraînerait l'incapacité de compléter correctement la ségrégation des chromosomes. Ceci est le résultat d'une augmentation plus progressive de l'activité des Cdk au cours de la G2, causée par l'absence de la boucle de rétroaction Wee1/Cdc25, qui conduit alors les cellules à atteindre le seuil de la phase M plus tôt. De façon remarquable, nos données suggèrent que, contrairement à l'un des modèles communément admis, les cellules MCN-AF ne présentent pas une activité Cdk globale plus élevée que les cellules WT. Cela implique également que le seuil mitotique Cdk peut être plus bas que prévu et qu'il existe un dépassement important de l'activité Cdk lorsque les cellules WT entrent en mitose. En diminuant l'activité de Cdk pendant cette phase du cycle cellulaire par la perte de la fonction de Spo12, on dispose de plus de temps pendant la G2, car le moment où le seuil mitotique de Cdk est atteint est retardé. Cela facilite l'achèvement complet de la duplication du génome et une préparation plus optimale de la ségrégation des chromosomes, réduisant ainsi l'occurrence d'une entrée délétère en mitose. Par conséquent, nous proposons que les cellules dépourvues du commutateur d'entrée en mitose puissent surmonter sa perte pour améliorer la prolifération en réduisant l'activité de Cdk au début de la mitose sans affecter son profil dynamique progressif. Dans l'ensemble, nos résultats suggèrent la possibilité que Spo12 agisse comme un régulateur archaïque de l'activité de Cdk à la mitose, dont la fonction a été minimisée par l'évolution de la boucle de rétroaction Wee1/Cdc25, plus dominante. Alternativement, la fonction de Spo12 peut être cruciale dans des environnements plus spécifiques qui ne sont pas reproduits dans des conditions de laboratoire. Les résultats de ce travail démontrent également la valeur ajoutée significative de l'approche d'évolution expérimentale adoptée par ce projet, car il n'aurait pas été facile de découvrir une telle voie dans des stratégies plus standard ou dans des modèles alternatifs, étant donné l'importance du commutateur d'entrée mitotique.

Une partie importante des données présentées dans ce travail a été générée par l'analyse de cellules uniques d'événements dynamiques du cycle cellulaire, ce qui n'a été possible que grâce aux nouvelles techniques expérimentales utilisées. Plus précisément, l'analyse de cellules uniques a été réalisée à l'aide d'expériences time-lapse combinant la microfluidique et la microscopie à haute résolution. Nous avons ainsi pu surveiller la progression du cycle cellulaire, ce qui nous a permis de suivre les changements dynamiques en temps réel des marqueurs pertinents qui ont été marqués avec des protéines fluorescentes. Nous avons généré de grandes quantités d'images en temps réel à partir de ces expériences, qui ont ensuite été utilisées pour produire des données quantitatives et qualitatives afin de caractériser le rôle de Spo12 dans la progression du cycle cellulaire. Cependant, afin d'acquérir des données significatives à partir de ces essais, il était nécessaire de marquer un nombre important de cellules pour chaque expérience. Cet aspect de notre travail a pris beaucoup de temps, car il a nécessité une évaluation manuelle de tous les marqueurs indépendants. Il s'agit en soi d'un goulot d'étranglement courant dans l'analyse des images de microscopie time-lapse. En effet, si la capacité d'acquérir des données à haut contenu a considérablement augmenté, notamment grâce au développement de nouvelles technologies telles que la microfluidique, l'analyse automatisée des images reste une tâche complexe qui nécessite une expertise très spécifique. Ainsi, bien que nous ne l'ayons pas utilisée dans le cadre de l'étude Spo12, nous avons cherché à améliorer cet aspect de notre travail en mettant en œuvre un pipeline récemment développé pour l'analyse automatique d'images, DetecDiv. Cette plateforme est un logiciel très polyvalent qui utilise des techniques d'apprentissage profond pour entraîner des réseaux neuronaux pour l'analyse à haut débit de données d'imagerie unicellulaire (Aspert, Hentsch et Charvin 2022). Associé à une nouvelle conception de puce microfluidique, DetecDiv a été initialement développé pour étudier la durée de vie réplicative des cellules de levure bourgeonnante individuelles dans différentes conditions de croissance. L'objectif de cette partie de notre travail était d'adapter ce pipeline à l'analyse du cycle cellulaire de la levure de fission. De manière importante, notre approche a sondé pour la première fois la capacité de Detecdiv à déterminer l'organisation temporelle d'un processus complexe basé sur 1) la segmentation de cellules individuelles et 2) l'utilisation de plusieurs marqueurs fluorescents au sein d'une même souche, une stratégie qui n'avait pas été testée dans l'étude originale. Ce travail a été réalisé en collaboration avec le Dr Gilles Charvin, qui a développé Detecdiv.

Tout d'abord, nous avons adapté la conception du microdispositif à la levure de fission en modifiant les structures qui permettent de piéger et de surveiller les cellules individuelles. Ensuite, nous avons développé de nouveaux classificateurs pour l'analyse de caractéristiques cellulaires spécifiques (par exemple, la longueur et le volume des cellules) et des événements du cycle cellulaire à l'aide de marqueurs fluorescents (par exemple, l'apparition de S et M). Pour ce faire, le réseau neuronal a été entraîné avec des données acquises lors d'expériences de time-lapse avec des souches hébergeant les marqueurs spécifiques du cycle cellulaire Nhp6::mCherry (ADN), Plo1::GFP (mitose) et Tos4::GFP (G1/S). Nous avons validé nos résultats en utilisant le réseau entraîné pour analyser automatiquement des ensembles de données qui avaient été précédemment évalués manuellement, ce qui nous a permis de comparer les résultats avec les caractérisations de la vérité terrain. En parallèle, nous avons construit de nouvelles souches qui expriment nos différents reporters tout en ayant des propriétés de cycle cellulaire modifiées, ce qui servira de preuve de concept pour la capacité du pipeline nouvellement formé à extraire des données significatives à partir d'images d'événements du cycle cellulaire. Bien que cette étude soit encore en cours de finalisation, nous avons maintenant utilisé avec succès Detecdiv pour cartographier les événements du cycle cellulaire et la dynamique du cycle cellulaire au niveau de la cellule unique. Dans l'ensemble, il s'agit d'un outil puissant pour la communauté des levures de fission, car il permettra l'analyse à haut débit des données de cycle cellulaire en temps réel, produisant des données quantitatives et qualitatives solides. En effet, comme nous avons utilisé des marqueurs généraux pour suivre les événements du cycle cellulaire chez la levure de fission, d'autres laboratoires pourront utiliser directement notre réseau formé pour traiter leurs propres ensembles de données en utilisant ces mêmes marqueurs. Cet outil nous permettra également de renforcer les résultats obtenus par notation manuelle dans notre étude Spo12. De plus, grâce à la polyvalence du pipeline DetecDiv, d'autres personnes pourront contribuer à ce logiciel libre et partager des classificateurs formés à l'aide de marqueurs alternatifs, générant ainsi une base de données

d'outils prêts à l'emploi pour l'analyse d'images. Notre étude représente la première étape de cette dynamique. Enfin, comme nous démontrons maintenant comment la combinaison de Detecdiv avec un ensemble complexe de marqueurs est un outil puissant pour l'analyse de n'importe quel processus de manière à haut débit, nous pensons que ce travail sera également intéressant dans d'autres domaines et pour les laboratoires utilisant d'autres modèles que la levure de fission.

Enfin, dans le cadre de cette thèse, nous avons cherché à examiner les changements dans la régulation de la taille des cellules qui se produisent en l'absence de Spo12. Pour ce faire, nous avons utilisé des mesures de la longueur des cellules à la division comme indicateur de la taille des cellules, une approche classique pour déterminer l'efficacité du contrôle de la taille chez la levure de fission. Cependant, le volume cellulaire est une autre mesure qui est maintenant largement utilisée dans notre équipe pour surveiller la taille des cellules. Le volume cellulaire est une mesure plus pertinente de la taille des cellules, car il est plus critique pour la physiologie cellulaire que la longueur des cellules. En effet, des changements significatifs du volume cellulaire entraînent une modification de la biochimie intracellulaire, et la surface, qui est également liée au volume, définit l'interaction des cellules avec leur environnement. Il est important de noter que dans le contexte de la cellule de levure de fission en forme de bâtonnet, la mesure de la longueur de la cellule ignore les petits changements potentiels du diamètre de la cellule, malgré leur fort impact sur le volume de la cellule. Ainsi, en mesurant les changements dynamiques du volume des cellules de levure de fission au cours du cycle cellulaire, nous pouvons obtenir de nouvelles informations sur les mécanismes responsables de la prolifération améliorée des clones MCN-AF évolués. Cependant, il n'existait pas de méthode permettant de mesurer directement le volume des cellules de levure, et toutes les techniques existantes disponibles à cet effet présentent de forts biais. Nous avons donc mis en œuvre une nouvelle méthodologie pour mesurer le volume cellulaire chez la levure de fission en utilisant comme point de départ une stratégie initialement développée pour les cellules de mammifères (García-Ruano et al. 2022). Dans cet article, nous démontrons que les changements de volume cellulaire peuvent être suivis avec précision au niveau de la cellule unique en utilisant la microfluidique et un pipeline d'analyse dédié. Cet outil passionnant améliorera notre compréhension de la façon dont les cellules régulent leur taille et sera potentiellement utilisé pour découvrir de nouvelles informations sur les voies alternatives de la prolifération. En particulier, le laboratoire évaluera le volume cellulaire dans le contexte de notre étude Spo12. Pour conclure, le travail présenté dans ce manuscrit était centré sur l'étude de Spo12, où nous avons impliqué son rôle dans une nouvelle boucle de rétroaction positive sur l'activité de Cdk. En outre, nous avons été incités à améliorer le type d'analyse que nous avons effectué, de sorte que ce manuscrit détaille également la mise en œuvre d'un outil nouveau et puissant pour l'analyse microfluidique time-lapse.

Acknowledgements

The past 4 years have been a period of growth and development that has allowed me to reach a personal goal I had previously thought unachievable. That said it is clear that this journey of mine has not been easy and would not have been possible without the important individuals in my life who have supported me through the ups and downs.

First, I would like to thank Damien for the opportunity and trust you bestowed upon me to take on such an exciting project. I have learned a lot about being a scientist but also gained more insight into myself as a person. I hope that I have delivered this work to a level that brings pride to the both of us.

Next I would like to thank my family (Dad, Mum, James, Su, Nanny, and Grandad) for their support of me, I would not be in a position to do my thesis if it weren't for them. I understand that my choices in life have sometimes felt heavier than we would have wanted, but hopefully from this I have a foundation to continue my evolution to where I can begin to give back. Just know that this achievement of mine would not have been possible without your encouragement and love, for which I am forever grateful.

I would also like to thank my friends: Manu, Celine, and Redwane for being very patient roommates who were there to help me get a break from the lab, and Aebert and Vivek for keeping me company when I needed it – albeit virtually. I want to thank my lab mates, both past and present, for their contributions to my thesis and more importantly their friendship: Vasantha, Aude, Greta, Dani, Ninon, Akanksha, Larisa, Jenny, Balveer, Diane, Julia, Tony, Celia, and Alicia.

Lastly, I want to thank Catarina and Norris, the family I chose, who motivate me to keep pushing to be better everyday. Thank you for making it easier for me to wake up every morning (not really Norris) by knowing I'll eventually get to move on to the next phase of my life with you. I will always appreciate you for being there.

Table of Contents

Chapter 1:

General Introduction

1.1 Synthetic Biology

1.1.1 Synthetic biology as a tool for fundamental research

Complex cellular behaviours such as growth and division, intracellular signalling, and environmental response, rely on networks of interacting genes and proteins. Our current understanding of these networks has largely depended on studies that perturbed the natural systems, allowing for the determination of the role of the molecules involved and the characteristics of the systems as a whole (Nandagopal and Elowitz 2011; Davies 2017). However, recent advances in technology have allowed the generation of vast amounts of genomic and proteomic data, which has improved our understanding of the hierarchy of the networks, their core features, and their biological relevance (Mertz 2016). Nevertheless, we still lack insight into why specific circuits of interacting proteins or genes exist in the naturally evolved configuration (Nandagopal and Elowitz 2011; Coudreuse 2016).

Synthetic biology is a relatively new idea, which was originally a denotation of bioengineering. However synthetic biology can be used more broadly to describe the assembly of new biological parts from components that are already found in nature (Benner and Sismour 2005). In fundamental research, this methodology aims to understand natural biology through logically designed and biologically integrated synthetic modules, where we can infer the fundamental principles of the natural system as a whole. Traditionally, the primary strategy for studying biological systems was a top-down approach. This involved the disruption of existing systems to better understand their regulation and necessary components, yet alone this method is limited especially in light of the vast complexity and interconnectedness present in biological systems. Indeed, synthetic biology offers a complementary and ground-breaking strategy to the classical top-down approach to improve our knowledge of the design principles of natural systems (Zakeri 2015; Nandagopal and Elowitz 2011).

In other engineering disciplines, the development of simple modules that can be used to construct predictable systems is relatively easy, although in biology this is not the case. The variables involved in biological systems (i.e. proteins, molecules, environmental insults etc.) are intertwined in a massive amount of complexity, making it difficult to accurately predict outcomes. So in biology, the novel functions of engineered systems often do not behave exactly as predicted, because they are

built with imperfectly characterised components. Biological engineering has provided a vast array of tools to manipulate living organisms and has allowed for many different strategies to improve our understanding of living systems. Synthetic biology represents a novel conceptual framework that takes a bottom-up approach to studying biological systems, although much like the classical top-down approach, it alone is not sufficient. This methodology requires the iteration of design cycles incorporating both bottom-up and top-down strategies (Figure 1).

Top-down perspective

Interactions   Orthogonality

Analysis in context

Biological design

Construction and implementaion

Configurations   Modules

Bottom-up perspective
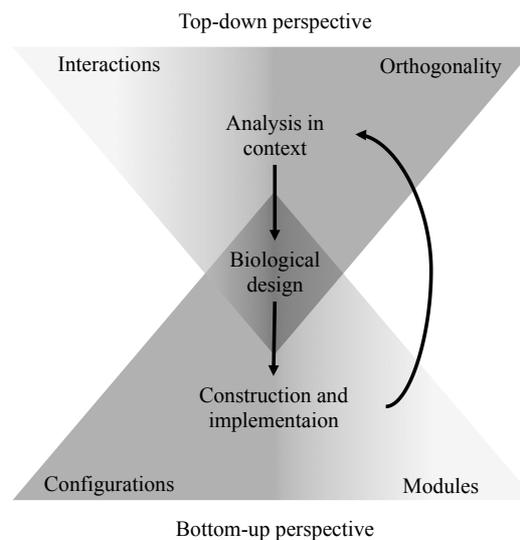
Figure 1: The paradigm of biological design
Biological design requires both top-down and bottom-up approaches. The iteration of constructing rationally designed modules and their analysis in a biological context improves our understanding of the design principles in biology. Adapted from (Leonard et al. 2010).

A bottom-up approach involves the design and assembly of biological systems with synthetic modules (or alternatively the simple reorganisation of natural systems), which then exhibit novel functions/topologies. This process is dependent on the prior characterisation of the biological parts used, which has been achieved by: 1) the iteration of the non-natural systems in the natural endogenous context, and 2) perturbation of natural systems itself. This is where the framework of a top-down approach complements synthetic biology, and vice versa (Figure 1). A top-down approach focuses on the development of strategies for taking advantage of, or compensating for, the potential interactions in biological systems in order to configure desired function. The combination of these two approaches provides a powerful methodology for studying the evolutionary design and the basic principles of biological systems. Synthetic biology can be seen as a useful methodology to extract

principles in evolutionary design, topologies of natural systems, and population dynamics and behaviour. This can be clearly seen in the following examples.

1.1.2 Building molecular circuits to study their characteristics

Synthetic biology was initially based on designing circuits that were independent of the endogenous cellular network with no interference with cell behaviour (Nandagopal and Elowitz 2011; Gardner, Cantor, and Collins 2000; Elowitz and Leibler 2000). An example is the bistable toggle switch, a simple genetic circuit composed of two repressors and two constitutive promoters (Figure 2). This approach provided a highly controlled and highly simplified example of gene regulation that exhibits complex dynamics. The bistable toggle switch is a proof of concept of how bistable dynamics can be genetically achieved in a relatively simple manner. This is in contrast to natural systems, which achieve such dynamics through more complex systems that are integrated in cellular behaviours (Sha et al. 2003; Tyson and Novak 2008; Yang and Ferrell 2013).
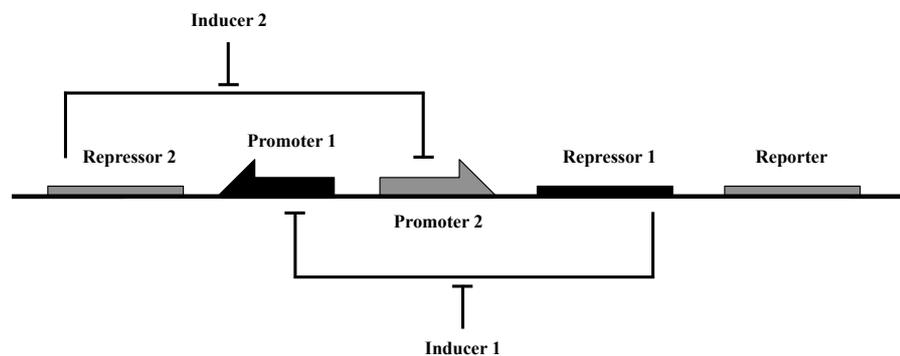
Figure 2: The bistable toggle switch
Repressor 1 inhibits promoter 1 and repressor 2 inhibits promoter 2. Through the modulation of promoter of inducers 1 & 2, two stable states can be attained in a predictable fashion – the reporter is either expressed or not expressed. Adapted from (Gardner, Cantor, and Collins 2000).

The simplicity of synthetic systems such as the bistable toggle switch allows us to study the minimal mechanistic architecture necessary to sustain complex natural behaviours. This provides us with unprecedented foundations to identify simple regulatory modules within complex mechanisms, onto which complexity has been added throughout evolution, possibly to 'fine-tune' the system or even to repurpose its function entirely. Understanding complex biological systems is incredibly difficult, as biological circuits are typically comprised of many components, with some unknown,

but synthetic biology provides us with a tool to decipher such complexity through the engineering of minimal architectures (Nandagopal and Elowitz 2011).

1.1.3 Understanding biological phenomena through synthetic design

The advantage of replacing endogenous circuits with redesigned versions of these networks *in vivo* is that it allows us to test different topologies for the same regulatory system, and assess the output of these distinct artificial circuits, even if they are predicted to operate similarly. Unanticipated differential behaviours for such networks provide valuable insights into the evolutionary rationale of the circuit architectures that exist in natural systems. In this context, synthetic biology may be one of the only ways to test the advantages of the naturally evolved mechanisms, thereby explaining the way cellular functions are wired in cells, as we know them.
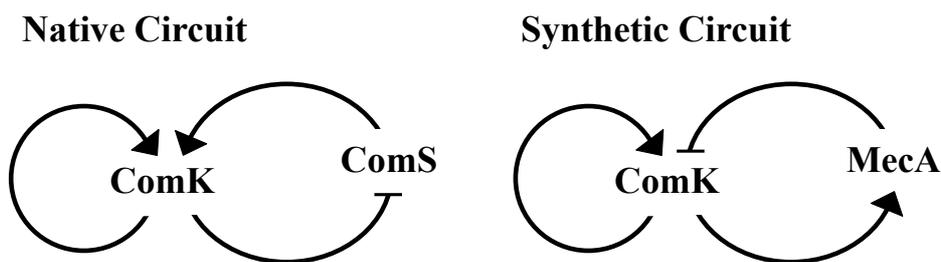
Figure 3: Endogenous regulation of ComK vs. an alternatively engineered synthetic circuit
The native circuit is composed of both a positive and a negative feedback loop. ComK inhibiting its activator ComS constituting the negative feedback loop. In the synthetic circuit, the topology of the negative feedback loop is changed as ComK promotes its own inhibition through the activation of its inhibitor MecA. While the two networks were predicted to behave similarly in silico, the native system showed clear advantage in vivo. Adapted from (Çağatay et al. 2009).

A pioneering example of this is the study of bacterial competence in *Bacillus subtilis*, which is controlled by the combination of positive and negative feedback loops. Under environmental stress, *B. subtilis* can transiently differentiate into a state of competence in which cells are can uptake extracellular DNA and integrate it into their genome. Competence is regulated by the transcription factor ComK, which controls the expression of over 140 genes (Çağatay et al. 2009). The native regulation of ComK relies on two integrated feedback loops: 1) positive; ComK promotes its own expression, and 2) negative; ComK indirectly represses the expression of ComS, an indirect activator of ComK that acts through inhibition of the MecA-mediated degradation of ComK (Figure 3). The combination of these feedback loops constitutes a noise-driven excitable system. Interestingly, an

alternative and artificial negative feedback loop could be used to fulfil the same function. Thus, a circuit in which ComK directly activates MecA in conditions where ComS function is constant may be as efficient as the native system. Why was such alternative possibility not selected by evolution? To understand this, Çağatay and colleagues rewired the endogenous system to generate a synthetic feedback look with this opposite topology. Through this approach, characteristics that were unique to the native circuitry could be uncovered, providing novel insight into the rational for the design of the natural mechanisms regulating competence (Çağatay et al. 2009).

1.1.4 Reconstructing endogenous systems with synthetic circuits

The redesigning of an endogenous circuit can be taken further by replacing the native system with a synthetic alternative that has been simplified through either the deletion of non-essential components, or the construction of a functional equivalent that is less complex. By studying the *in vivo* effect of switching to a minimal system, we can decipher the fundamental principles and basic requirements that underlie the function sustained by the native circuit. Furthermore, potential limitations of the minimal architecture provide an opportunity to elucidate the rational of the added layers of complexity in the endogenous system.

An example of an integrated minimal system is the Minimal Cell cycle Network (MCN) that was implemented in fission yeast. The fission yeast cell cycle is comprised of a single cyclin-dependent kinase (Cdk) known as Cdc2, which associates with different cyclins throughout the cell cycle. There are two distinct events during the cell cycle that require Cdk activity; the transition into replication (G1/S), and into chromosome segregation (G2/M). During these events, Cdc2 binds to specific cyclins that are present at each of the particular stages, thereby regulating Cdk activity and the successful progression of the phases through these key transitions. During G1/S, the cyclins Puc1, Cig1, and Cig2 are predominantly expressed, while at the G2/M transition it is Cdc13.

In MCN cells, this complex regulation is replaced by a simple module, namely a unique chimeric Cyclin B/Cdc13- Cdk1/Cdc2 fusion expressed under the control of the *cdc13* regulatory elements (Coudreuse and Nurse 2010). Surprisingly, in this minimal background (the genes encoding for the endogenous Cdc2 and cell cycle cyclins are deleted), cells are virtually wild type despite bypassing a number of regulatory branches of cell cycle control. These include the specific expression and degradation programs of the different cell cycle cyclins, the regulation of their

localisation and association with Cdc2 as well as the qualitative inputs from distinct cyclins. In addition, the commonly accepted requirement for reaching specific ratios of cyclins/Cdk at different points of the cell cycle is abrogated in this 1:1 system. The absence of phenotype in these cells demonstrated that oscillation of a single qualitative Cdk activity between two thresholds is sufficient to autonomously drive cell cycle progression in fission yeast. This showed that in contrast to the general model of cell cycle control based on cyclin diversity, the core engine of the cell cycle relies on a purely quantitative model. Interestingly, evidence suggests that this model may also apply in more complex organisms (Santamaría et al. 2007; Dinarina, Santamaria, and Nebreda 2009; Echalier et al. 2012; Helfrid Hochegger, Takeda, and Hunt 2008).

Altogether, the MCN is a good example of how rewiring and simplifying *in vivo* the regulatory network of a highly conserved and complex process like cell division can dramatically advance our understanding of the evolutionary design of the native mechanisms. Revealing the fundamental principles of biological systems that are hidden behind layers of complexity is one of the powers of applying synthetic biology for fundamental research.

1.1.5 Designing the behaviour of organisms through gene drives

Synthetic biology has also been recently used to engineer specific characteristics and behaviours at the level of the organism in more complex systems. One such example is the work that was performed to limit malaria and dengue epidemics through the use of transgenic flies (Wang et al. 2021; C. Chen et al. 2007). While mosquitos with a decreased ability to transmit pathogens have been found in the wild and/or engineered in laboratories, the lack of fitness advantage of these organisms make it unlikely that they become dominant in a population through Mendelian transmission alone.

Chen *et al.* proposed a solution by coupling resistance genes with genetic elements that have a greater frequency of transmission. This would allow the genetic elements to act as "gene drivers", allowing for transgenic flies to have a selection advantage in a population. This idea was demonstrated by engineering *Drosophila* to have a maternal-effect selfish gene elements, from flour beetles, linked with the desired gene of interest (Figure 4). The selfish gene elements are composed of maternal toxin (an miRNA that targets an essential gene in embryonic development) and an antidote (a copy of the essential gene that is resistant to miRNA degradation). This means that

transgenic females will impair the development of offspring in the germ line that do not inherit the transgenic element. So by coupling the genetic element with a resistant gene, for example, there will be a synthetic genetic selection imposed on the population. Indeed, the results of this approach showed that with this synthetic component, populations can become dominated by transgenic flies in about 10-20 generations (C. Chen et al. 2007). This example shows how synthetic biology can be used to manipulate population dynamics, and that integrated synthetic circuits have a wider reach than just biological systems in single cell organisms.
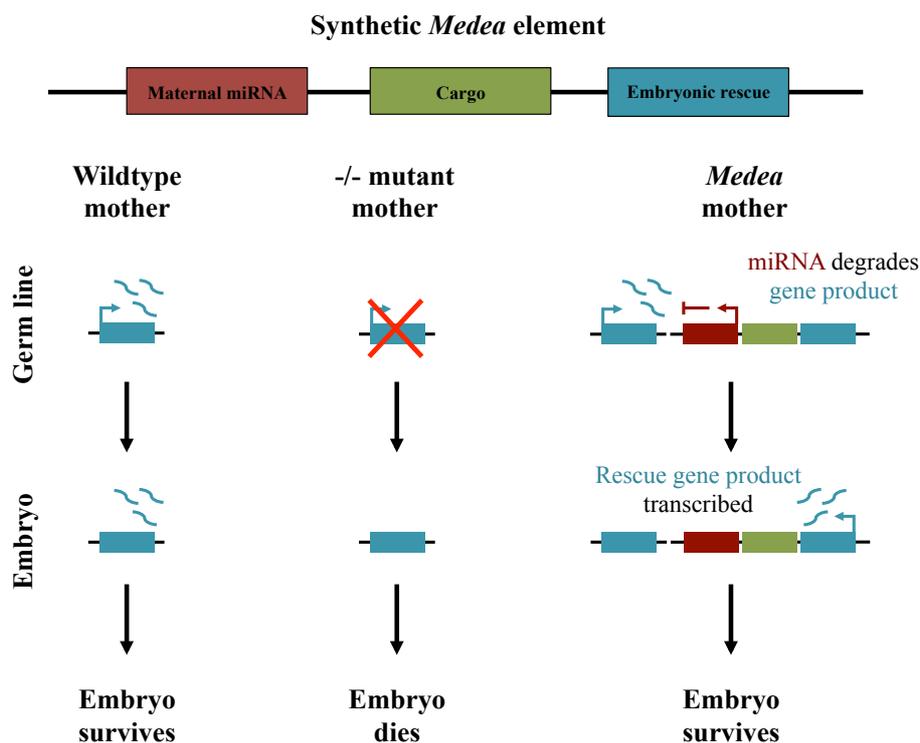
Figure 4: A schematic representation of a selfish gene element
The synthetic Medea (maternal-effect dominant embryonic arrest) element (top). The transgenic vector produces an miRNA, which degrades an essential gene in embryonic development that is expressed only in maternal cell lines and contains a modified version of the essential gene that is resistant to degradation. The integrated circuit modulates the development and population dynamics of transgenic flies. Adapted from (Nandagopal and Elowitz 2011).

Altogether, these examples demonstrate the impact of synthetic biology in expanding our understanding of the principles that govern biological systems. This relatively new methodology is only possible due to the exciting new technological innovations in research and the groundwork produced from more conventional strategies, such as a top-down approaches. Thus, it is necessary to couple synthetic biology with our current framework of approaching questions in biology in order to maximise our ability to dissect complex biological systems.

1.2 Experimental Evolution

Recently, experimental evolution (EE) has established the possibility of combining both top-down and bottom-up approaches as a means to studying biological design. EE is a framework for exploring the evolutionary trajectories of organisms in laboratory conditions (Colegrave and Collins 2008). The process of evolution is driven by natural selection, where organisms will be selected for their increased fitness in challenging conditions. These challenges could involve environmental stress (i.e. temperature, the presence of toxic agents, lack of nutrients, etc.), or genetic impairment of essential existing biological processes. Imposing such conditions to organisms in controlled conditions and evolving them in the laboratory allows for the dissection of the evolutionary strategies that can arise to overcome deleterious environments or challenges to endogenous cellular functions (Remigi, Masson-Boivin, and Rocha 2019). EE is an ideal platform to combine a bottom-up and top-down approach, as we can engineer organisms with alternative biological systems, and subsequently improve on the rational design process through the incorporation of biological evolution. To understand this more clearly, I will first discuss the significance of EE followed by its relevance in studying biological systems. Lastly, it should be noted that most EE studies have been done bacteria and yeast due to their short generation time and genetic manipulability, which would be constraint in more complex organisms.

Evolutionary biology has long aimed to understand a number of key concepts in evolution such as the variety of evolutionary solutions, the repeatability of the trajectories, and the interplay between evolution and complex cellular networks (Jagdish and Nguyen Ba 2022). These concepts are virtually impossible to explore outside of controlled laboratory conditions due to the vast number of variables that would need to be considered. EE therefore emerged as an ideal methodology to isolate specific variables, allowing us to cater to more specific biological questions. Dr. Richard Lenski pioneered one of the first major EE studies, where his team addressed the question of repeatability in evolutionary strategies by performing long-term experimental evolution assays with *Escherichia coli* (Lenski et al. 2016). Twelve *E. coli* populations, descended from a common ancestor, were evolved in carbon-limited minimal media for over 73,000 generations. These population were selected for growth by being maintained at a constant optical density (OD) through periodical dilutions (Maddamsetti, Lenski, and Barrick 2015; Kawecki et al. 2012; Maddamsetti and Grant 2020). One of the major observations of these studies was the appearance of populations with impairment to their DNA repair processes, which led to an increased occurrence of point mutations,

reflecting an increased mutation rate (Maddamsetti and Grant 2020). Interestingly, these results question the relevance of "hypermutator populations" and their potential roles in driving evolutionary strategies. Studies such as this have contributed to our understanding of evolutionary dynamics of adaptation, in which cell size, temperature tolerance, and metabolism have been demonstrated to be targets of adaptive strategies (Cooper 2018).
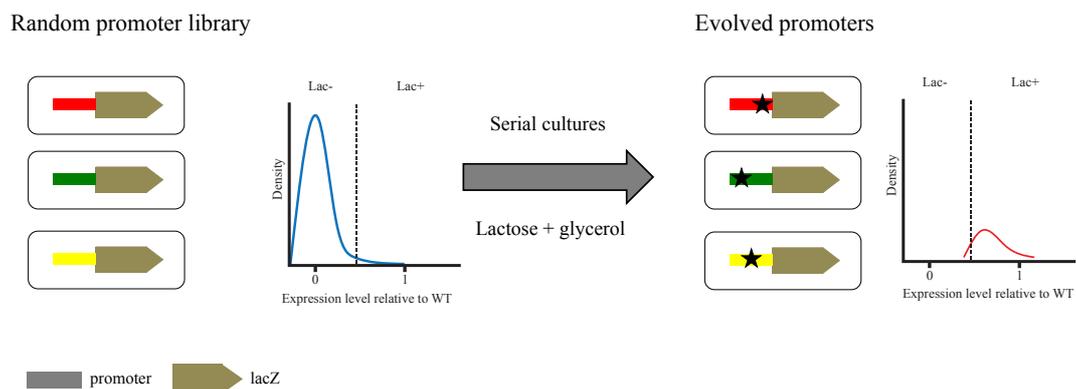
Figure 5: Evolution of de novo synthetic lacZ promoters
The lac promoter was replaced by randomised sequences in *E. coli*. The *E. coli* were then evolved by serial dilutions in liquid cultures of 0.05% glycerol and 0.2% lactose. Initially, only glycerol was utilised by the bacteria, but over the course of the experimental evolution, the randomised lac promoters acquired mutations allowing for lactose to be used. At the end of the assay, approximately 60% of promoters had acquired single point mutations (black star), and exhibited an average of 50% wild type lac promoter activity. Adapted from (Remigi, Masson-Boivin, and Rocha 2019).

Since the initial work done by the Lenski group, there have been a variety of different EE studies, examining different concepts of evolutionary biology (Lind and Andersson 2008; Wistrand-Yuen et al. 2018; M. Martin et al. 2016; Hoang, Morran, and Gerardo 2016). These experiments were made possible due to improvements in how experimenters were able to set-up the controlled conditions for evolution. One of the major improvements includes the development of bioreactors such as chemostats or ministats (Callens et al. 2017; Remigi, Masson-Boivin, and Rocha 2019), which allowed for the up-scaling of EE assays (a particular asset for more directed evolution of protein engineering). An even more recent example of such a development is the eVOLVER system, which provides an increased ease of management for evolving cultures, allowing the experimenter to develop more complex conditions (Wong et al. 2018).

Remarkably, the development of bioengineering techniques has also allowed for a modify-and-evolve approach. Thus, strains can be engineered with modifications to genes and/or genetic networks that perturb the endogenous systems and subsequently evolved. This allows for uncovering novel topologies associated with specific functions as well as determine the evolutionary strategies

cells can take to adapt (Remigi, Masson-Boivin, and Rocha 2019). Therefore, EE can be viewed as a tool to help microbiologists identify novel components in signaling networks, new connections between known regulatory systems, and interactions between signaling and metabolic pathways (Remigi, Masson-Boivin, and Rocha 2019; Carroll and Marx 2013). An interesting example of how bioengineered organisms can be used as starting biological materials in EE is the replacement of the *lac* promoter in bacteria with randomised sequences (Yona, Alm, and Gore 2018). Yona *et al.* evolved bacteria with non-functional *lac* promoters in media supplemented with 0.2% lactose and 0.05% glycerol (Figure 5). Over time, the bacterial populations accumulated mutations in the randomised sequences at the promoter to restore *lacZ* expression. From this, single point mutations were found that bring about approximately 50% of the LacZ activity of wild type, identifying novel *lac* promoter sequences (Figure 5).

Finally, EE can also be used to study the architecture of biological systems and thus the rationale of natural evolutionary designs. By examining how evolution remodels regulatory networks, we can gain valuable insight into the role of individual components and the overall topology of biological systems. An example is the inherent evolvability of the bacterial motility control checkpoint in *E. coli* (Ni et al. 2017). The control of cellular decisions is largely governed by regulatory networks that frequently have specific "bow-tie" organization (Csete and Doyle 2004). The topology of these networks connects multiple inputs and outputs to a central regulator. In the case of *E. coli* motility, the central regulator is a global regulatory motif comprised of a promoter-specific sigma factor of the bacterial RNA polymerase, and a counteracting anti-sigma factor. Interestingly though EE, Ni *et al.* demonstrated that the "bow-tie" topology of the network provides evolutionary plasticity by substantially increasing the number of possible mutations to affect the central process. This result exemplifies how the use of EE can provide insight into the evolutionary architecture of biological systems.

In conclusion, by combining experimental evolution with synthetic biology, we have a unique opportunity to explore how simplified biological systems can be redesigned through evolution or how cells can adapt to sub-optimal synthetic circuits. This provides us with a view of the evolutionary trajectories possible for ancestral biological systems to develop key regulatory pathways, which are seen in more complex native systems. Correspondingly, this method could also allow us to dissect complex cellular networks, and identify novel components and regulatory motifs within them. My thesis project took advantage of such an approach, unravelling novel regulators of the fission yeast cell cycle through experimental evolution.

1.3 The Cell Cycle

1.3.1 The eukaryotic cell cycle

Cell division is a fundamental feature of life where cells duplicate into two daughter cells. The duplication of cells is central to processes such as development and growth, and its deregulation can lead to pathologies such as cancer (P. Nurse 2002; Morgan 2007; Hanahan and Weinberg 2011). In eukaryotes, the different events that are required for cell proliferation are organised in a complex, highly regulated and highly conserved multi-step process known as the cell cycle (Morgan 2007). The series of events that encompass the cell cycle are specifically ordered in time to ensure its correct execution, and its mechanisms of control have been the subject of a large body of research in the past century (Cvrčková 2018). The central component in the cell cycle is a family of enzymes known as Cyclin-dependent protein kinases (Cdks), whose activities drive progression through the different phases of the cell cycle. The activities of these enzymes are dependent on their association with regulatory subunits of the cyclin family (Morgan 1997a; P. M. Nurse 2002), ensuring the timely execution of the different phases and transitions of the cell cycle. In this section I will provide an overview of the cell cycle and its regulation.

1.3.2 Cell cycle control – Cdks and cyclins

Cdks are highly conserved across eukaryotes and their regulation drives the timing of events in the cell cycle (Morgan 2007; M. G. Lee and Nurse 1987; H Hochegger, A, and Hunt 2008). Although Cdks are conserved, there is diversity in the number of Cdks and cyclins in different organisms. For example, yeast have only one major Cdk that plays a central role in the cell cycle, Cdc28 and Cdc2 for *S. cerevisiae* and *S. pombe* respectively, while vertebrates have a wider array of Cdks (Bloom & Cross, 2007; Lee & Nurse, 1987; Morgan, 1997). Indeed, animal cells have up to nine Cdks, although only four contribute to cell cycle progression (Cdk1, 2, 4 and 6) (Morgan 2007; Martínez-Alonso and Malumbres 2020). The implications of having more Cdks may elicit the idea that the systems level regulation is more complex and thus different, but it should be noted that the fundamental mechanisms of control remain remarkably consistent (Morgan, 1997).
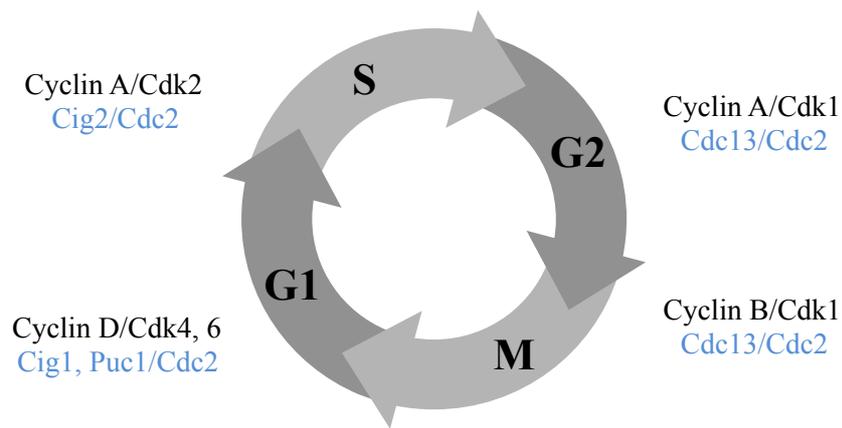
Figure 6: The cyclin/Cdk complexes involved in the different phases of the cell cycle of mammalian and fission yeast cells
Unlike in mammalian cells, fission yeast has a simpler cell cycle control system with only one major Cdk, known as Cdc2. Cdc2 forms phase specific complexes with the four major cell cycle cyclins: Cig1, Cig2, Puc1, and Cdc13.

A key component and first level of regulation of Cdk activity is cyclins, which bind to a domain in Cdks known as the cyclin box. This causes conformational changes in Cdk structure that unlocks the active site of the kinase (Morgan, 1997). Cyclins can be placed in categories based on the different phases during which they associate with Cdks and the timing of their expression: G1/S cyclins, S cyclins, M cyclins, and G1 cyclins (Figure 6). Each of these cyclin groups are directly influenced by cell cycle events, except for the latter which reacts to both extracellular and internal factors (Morgan 2007; Martínez-Alonso and Malumbres 2020). Much like Cdks, the number of cyclins that have a functional role in the cell cycle can vary across organisms. For example, humans Cdks associate with eleven cyclins, which are organised in five major cyclin classes (A, B, C, D, and E). While in fission yeast, there are only four cyclins involved in this process: Cig1, Cig2, Puc1, and Cdc13 (Figure 6) (Martínez-Alonso and Malumbres 2020; Daniel Fisher and Nurse 1995). It was initially thought that the timing of action of specific cyclins provides substrate specificity to Cdks at the relevant phases, but this has since been proven to not be the case. Indeed, it was shown in fission yeast that the oscillation of a single qualitative Cdk activity is necessary and sufficient to drive cell proliferation (D. L. Fisher and Nurse 1996; Coudreuse and Nurse 2010b; Stern and Nurse 1996). In addition to cyclin binding, a number of other regulatory mechanisms have evolved to modulate Cdk activity, allowing the necessary oscillations in activity observed during the eukaryotic cell cycle. Interestingly, there is increasing evidence that this observed quantitative model of Cdk activity regulation is highly conserved (Santamaría et al. 2007; Gutiérrez-Escribano and Nurse 2015; Pickering et al. 2021; Berthet et al. 2003).

1.3.3 Interphase

The cell cycle includes two major phases known as interphase and mitosis (M). Interphase is further divided into Gap phase 1 (G1), Synthesis phase (S) and Gap phase 2 (G2). The cell replicates its genetic material during S phase, which is between the two gap phases during which the cell grows and duplicates its contents in preparation for division (Figure 7) (Morgan 2007; McIntosh 2016).
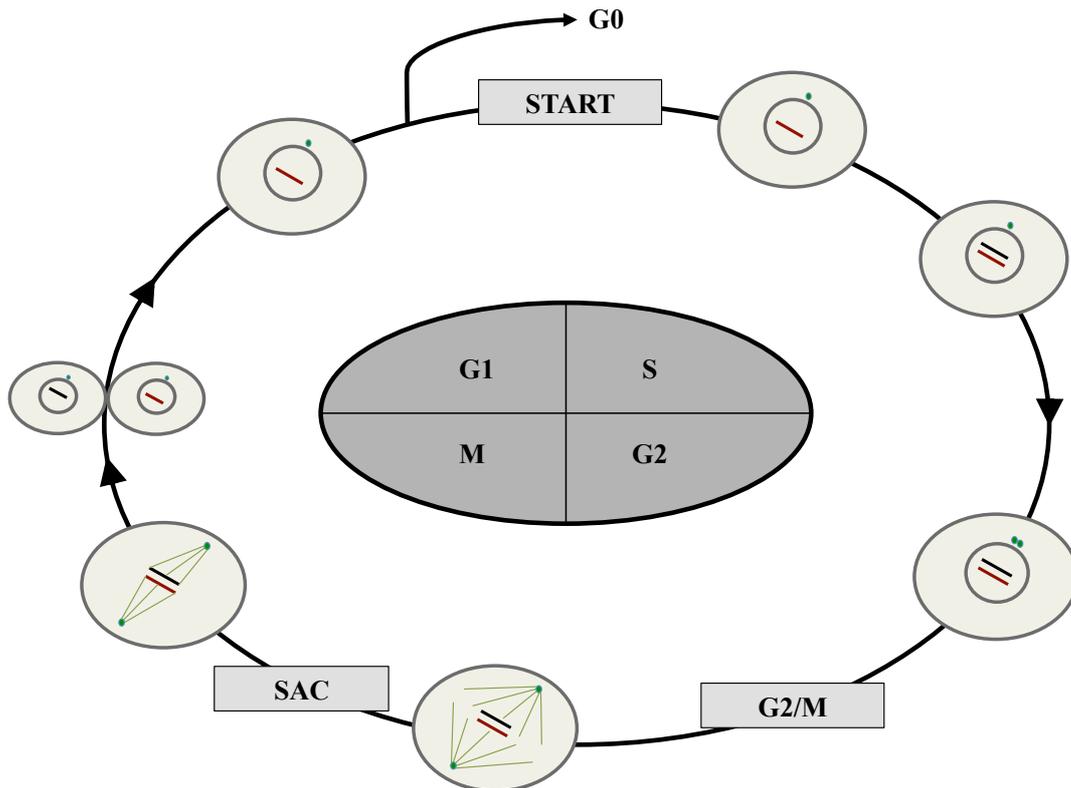
Figure 7: The mitotic cell cycle in eukaryotes
The main events of the mitotic cell cycle are represented in this schematic. During G1, cells will make the decision to commit to a new cell cycle (START), or exit into a quiescent state (G0). During S phase, the chromosomes are duplicated and the cell subsequently enters a period of growth (G2). In G2, the cell will prepare for mitosis, which is delayed until replication is complete (G2/M). Prior to mitotic entry the centrosome (green dot) is duplicated. In M, the sister chromatids will condense and the spindle will begin to emanate form the centrosomes, located at opposite ends of the cell. The spindles will then attach to the kinetochores of the sister chromatids. Progression to mitotic exit is delayed by the spindle assembly checkpoint (SAC) until the spindles are correctly attached. Once the SAC is deactivated, the cell will enter anaphase where the structures holding the sister chromatids together, cohesins, will be cleaved. The microtubules will then depolymerise pulling the chromosomes to the cell tips, where the nucleus will reform around them. Lastly, cytokinesis will give rise to two daughter cells.

G1 is the first regulatory period where the decision on whether to commit to a new cell cycle is taken. Interestingly, unlike later in the cell cycle where internal signals largely control cell cycle progression, entering into a new division cycle from G1 is mainly influenced by external factors

(Yanagida et al. 2011; De Virgilio and Loewith 2006). For example, in poor nutrient conditions, the cell will not enter the cell cycle and will instead enter a quiescent state known as G0. Target of rapamycin (TOR), which is part of a nutrient sensing pathway, has been implicated in this decision (De Virgilio and Loewith 2006; Jorgensen et al. 2004). However, in favorable conditions for cellular division, the cell will commit to completing a cell cycle. Once the decision to divide has been made, cells progress into S phase: this critical transition is referred to as Start and Restriction Point in yeast and mammalian cells, respectively.

The next step in interphase is S phase during which genome duplication occurs. Preparation for DNA replication begins in G1 when the pre-replicative complex (pre-RC) binds to specific sites along the genome called origins (Fragkos et al. 2015; Bell and Dutta 2002). The loading of origins with the pre-RC is necessary for DNA replication and is referred to as origin licensing. Origin licensing is not only an important step in the preparation of DNA replication, but it is also a mechanism to ensure that replication occurs only once per cell cycle (Fragkos et al. 2015). Indeed, while loading of the pre-RC components Cdc6 and Mcm2-7 onto yeast replication origins was observed using protein extract from G1-arrested cells, which was not the case for G2/M extracts. This is the result of mitotic cyclin/Cdk complexes outcompeting an essential component of the pre-RC, Cdc4. Interestingly, it was thought that this interaction stabilises the pre-RC in an inactive state outside of DNA replication (Mimura et al. 2004; Fragkos et al. 2015).

At the G1/S transition, additional components are added to the pre-RC, transforming the complex into the pre-initiation complex (pre-IC) (Bell and Dutta 2002; Fragkos et al. 2015). The assembly of the pre-IC is controlled by at least two different types of kinases: Cdks, and Ddks (Cdc7 in fission yeast). Ddks stands for Dbf4-dependent kinases, as their activity requires the association with a protein subunit known as Dbf4 (Bell and Dutta 2002). Once all the factors of the replication machinery have been recruited, the replication forks are formed and duplicate the entire genome (Fragkos et al. 2015; Méchali 2010). The result of S phase is a duplicated pair of sister chromatids which are tightly bound together via DNA catenation and protein complexes called cohesins. DNA catenation is the intertwining of duplicated DNA molecules that occurs at replication forks, and cohesin is a multi-subunit complex which holds together the sister chromatids via mechanisms involving its ring-like structure (Nasmyth and Haering 2009; Peters, Tedeschi, and Schmitz 2008; Morgan 2007).

The cells then enter a period of growth known as G2, where a number of checkpoints are present to ensure that replication has been executed correctly. These checkpoints are important to delay mitotic onset, giving cells the necessary time to complete DNA replication or DNA repair. Several of these checkpoints operates through the modulation of Cdk activity via a feedback loop on the mitotic cyclin/Cdk complex (cyclin B/Cdk1) (Gould and Nurse 1989; Lundgren et al. 1991). The checkpoints are necessary to overcome DNA damage and replicative stress, which will be detailed in a later section. Only once the checkpoints have been fulfilled and a threshold level of Cdk activity has been reached will the cell commit to mitosis and progress through chromosome segregation (Coudreuse and Nurse 2010a; Mochida et al. 2016).

1.3.4 Mitosis

1.3.4.1 Preparing for chromosome separation

Once the cell has successfully completed DNA replication, it will eventually exit interphase and enter mitosis. The main objective of mitosis is the equal segregation of duplicated chromosomes into two daughter cells. This critical step of the cell cycle requires preparation and accurate execution, thus commitment to mitosis is tightly regulated, ensuring that cells only commit to chromosome segregation when it can be done faithfully. Indeed, unequal segregation of the genome can lead to aneuploidy in the daughter cells, which is potentially lethal (Morgan 2007; Santaguida and Amon 2015). Mitosis is composed of four main events: prophase, metaphase, anaphase, and telophase (McIntosh 2016; Morgan 2007).

In prophase, there is an observed slowing down in protein synthesis (McIntosh 2016; Morgan 2007). Centrosomes (known as the spindle pole body (SPB) in yeast) will be duplicated in a process known as centrosome maturation, where they are surrounded by a large structure known as the pericentriolar material (PCM) and will recruit ϒ-tubulin (Conduit et al. 2014; Petronczki, Lénárt, and Peters 2008; Fu, Hagan, and Glover 2015). The centrosomes are the central organisers of microtubules in eukaryotic cells but also act as a regulatory centre for several cell cycle regulators and cell cycle checkpoint proteins (Andersen et al. 2003; Müller et al. 2010; Doxsey, Zimmerman, and Mikule 2005). AurA is an enzyme with a significant role in early mitosis, where it recruitments the PCM, contributing to centrosome maturation, separation, and duplication (Barr and Gergely 2007; Fu, Hagan, and Glover 2015; Mori et al. 2007). AurA is part of a conserved group of serine/threonine kinases (AurA, AurB, and AurC) that have been implicated in a number of steps in

mitosis (Barr and Gergely 2007). For example, these kinases have roles in the stabilisation of microtubules that emanate from the centrosome (Barros et al. 2005; Mori et al. 2007; Eot-Houllier et al. 2018).

Another kinase important early in mitosis is Polo-like kinases (Plks), which localise to the centrosomes. Plks were initially identified in genetic screens in yeast and *Drosophila*, where their loss prevented the assembly of a proper bipolar spindle (Petronczki, Lénárt, and Peters 2008). They are essential for several mitotic events and can be considered to be as crucial as Cdks for cell cycle progression. Indeed, Plk1 (Plx1, Cdc5 and Plo1 in *Xenopus,* budding yeast, and fission yeast, respectively) is necessary for the proper timing of mitotic entry in humans and *Xenopus* (Qian et al. 1998; Sumara et al. 2004), and is required for mitotic exit in budding yeast (Yoshida et al. 2006). Furthermore, Plks are part of the control network for mitotic entry through regulating the phosphatases Cdc25 and Myt1, two key modulators of Cdk activity which will be detailed in a later section (Kumagai and Dunphy 1996; Nakojima et al. 2003; Tavernier et al. 2015; Singh et al. 2021). Interestingly, a recent EE study in fission yeast demonstrated that the requirement for Plo1 function in mitosis can be bypassed by alterations of downstream microtubule regulators and glucose transporters (J. Kim and Goshima 2022). These results indicate that the loss of normally essential regulators of mitosis can be overcome through EE. It further highlights how such a strategy makes it possible to uncover novel mechanisms that cells can utilise to compensate for the absence of conserved components that have naturally evolved.

During prophase, chromosomes are condensed into more compact forms by protein complexes known as condensins (Antonin and Neumann 2016). The compaction of the chromosomes is necessary to facilitate the segregation of the DNA material equally by the microtubules in the latter stages. Similar to cohesins, condensins are multi-subunit protein complexes containing Smc ATPases, and have been shown to induce DNA supercoiling and looping in an ATP-dependent manner (Hirano 2005). Vertebrate cells have two different condensin complexes, condensin I and condensin II (although in yeast cells, there is only one complex) (Morgan 2007; Hirano 2005). Condensin II has a nuclear localization and participates early in chromosome segregation, while condensin I is located in the cytoplasm and thus only gains access to the chromosomes after nuclear envelope breakdown during the transition to metaphase, known as prometaphase (Hirano 2005; Losada, Hirano, and Hirano 2002).

On the other hand, the nuclear envelope breakdown associated with open mitosis is not a feature of all eukaryotic cells. For example in fission yeast, the nucleus remains intact throughout the entire process, which is often qualified as closed mitosis (Boettcher and Barral 2013). The dynamics of specific components will therefore be drastically different between these two distinct types of mitosis. For example, as the condensin complexes in fission yeast are cytoplasmic, they must be actively translocated into the nucleus, a mechanism that is regulated by Cdk activity. Indeed, the Smc core of fission yeast condensin contains Cut14 and Cut3, both of which require cyclin B/Cdk1 phosphorylation to localise to the nucleus (Sutani et al. 1999). The nuclear translocation of Cut3 upon modification by Cdc2 has been used as a proxy to quantify Cdk activity levels in fission yeast (Patterson 2017).

1.3.4.2 The spindle assembly checkpoint

In metaphase, microtubules from opposite poles attach to the centromeric regions of the chromosomes at large structures known as kinetochores, and arrange the chromosomes to the centre of the cell in a formation described as the metaphase plate (Cheeseman 2014; McIntosh 2016). Kinetochores not only have an essential role as the site spindle attachment but also are important for the regulation of mitotic exit. Cdks promote the recruitment of key components of the kinetochores to the centromeres, many of which have important functions in delaying mitotic exit until all chromosomes are correctly attached (Gascoigne and Cheeseman 2013; Singh et al. 2021). Plk1 accumulates at the kinetochores during prometaphase, binding to the kinase Bub1 at the conserved CENP-U histone (Petronczki, Lénárt, and Peters 2008; Liu, Davydenko, and Lampson 2012; Singh et al. 2021). In this context, Plk1 contributes to maintaining the activation of the spindle assembly checkpoint (SAC), which prevents the onset of anaphase until all the kinetochores have been correctly attached to the spindle (Liu, Davydenko, and Lampson 2012). Additionally, AurB is also recruited to the kinetochores in a Cdk-dependent manner (Gascoigne and Cheeseman 2013).

Progression into anaphase depends on the secure attachment of microtubules to the sister chromatids in a bi-orientated fashion. The faithful segregation of chromosomes is crucial for the integrity of the cell cycle and more significantly for cell survival. Mis-segregation and the subsequent aneuploidy that can arise from it are largely prevented through the SAC (Musacchio and Salmon 2007; Roy et al. 2022; Papini, Levasseur, and Higgins 2021; Kadura and Sazer 2005) and the DNA damage repair checkpoint. These mechanisms function to arrest cell cycle progression via the

maintenance or inhibition of Cdk activity, respectively. When the SAC is active, it delays chromosome segregation until all chromosomes are correctly attached. An important regulator of the SAC is the mitotic checkpoint complex (MCC), which is recruited to the kinetochores at sites of unattached spindle microtubules. This protein complex maintains the activation of the checkpoint, preventing chromosome segregation and progression into anaphase (Pachis and Kops 2018). Early in mitosis, the kinase Mps1 phosphorylates components of the kinetochores to recruit and facilitate the assembly of the MCC (Musacchio and Salmon 2007). The MCC is composed of Mad2, BubR1 and Bub3, which sequesters the Cdc20 activating subunit of the anaphase-promoting complex/cyclosome (APC/C) via phosphorylation (Jia, Li, and Yu 2016; Morrow et al. 2005; Elowe 2011). The APC/C is the key driver of mitotic exit as it targets cyclin B for degradation by ubiquitinylation, thereby reducing Cdk activity. By preventing the function of APC/C, the SAC delays mitotic exit.

In addition to delaying anaphase onset via the SAC, the kinetochores also have an error-correcting mechanism to prevent syntelic, monotelic and merotelic attachments (Kadura and Sazer 2005; Santaguida and Amon 2015). AurB, which is localized at the kinetochore, stabilises many of its substrates through direct phosphorylation, and as microtubules become correctly attached, the tension on the centromeric region is increased (Santaguida et al. 2010; Roy et al. 2022). The tension-induced spatial separation of the outer kinetochore components reduces their exposure to AurB activity; this is due to a gradient in its activity that is concentrated at the spindle midzone (Papini, Levasseur, and Higgins 2021). The subsequent destabilization of the kinetochores promotes the inactivation of the SAC (Liu, Davydenko, and Lampson 2012; Cheeseman 2014), and as a consequence the localization of Mad2 to the MCC decreases (Waters et al. 1998; Elowe 2011). This allows for SAC signalling to progressively be turned off as all the kinetochores become correctly attached, promoting the activation of the APC/C via Cdc20. Interestingly, this mechanism includes a negative feedback loop that allows for the rapid on and off of the SAC (Nijenhuis et al. 2014), thus enabling for the quick disconnection and reconnection of microtubules.

The now-activated APC/C targets both cyclin B and securin for ubiquitinylation and subsequent proteolysis (Bokros and Wang 2016; Bokros et al. 2016). This leads to a drop in Cdk activity and the activation of separase in the absence of securin (McIntosh 2016). Separase in turn cleaves cohesin, allowing for the separation and equal distribution of sister chromatids between daughter cells driven by the mitotic spindle (Losada, Hirano, and Hirano 2002). A signal transduction cascade known as the mitotic exit network (MEN) initiates mitotic exit and has been well-characterised in budding yeast (de Bettignies and Johnston 2003).

1.3.4.3 Mitotic exit - MEN and FEAR

Mitotic exit involves the inactivation of mitotic regulators, the disassembly of the mitotic apparatus, and the transition back into interphase (Hotz and Barral 2014). In budding yeast, these events are triggered through the MEN, a signalling cascade which promotes the release of Cdc14, a highly conserved phosphatase (Rock and Amon 2009; Krapp, Gulli, and Simanis 2004). Cdc14 is sequestered in the nucleolus for the majority of the cell cycle, where it is bound to Cfi1/Net1 as part of the regulator of nucleolar silencing and telophase exit (RENT) complex (Azzam et al. 2004). Cdc14 activity is highly dependent on localisation, and upon activation of the MEN, it is released into the cytoplasm. The relocalisation of Cdc14 allows the phosphatase to dephosphorylate the APC/C subunit Cdh1 and the transcription factor Swi5 that transcribes the Cdk1 inhibitor *sic1* (Baro, Queralt, and Monje-Casas 2017; Yellman and Roeder 2015). Additionally, Cdc14 also promotes Sic1 function directly, constituting a feed-forward loop (Yellman and Roeder 2015). Dephosphorylation of these substrates leads to a decrease in Cdk activity, shifting the balance of phosphorylated Cdk targets to a dephosphorylated state. Thus, the activation of the MEN leads to a decrease in Cdk activity via 1) cyclin B degradation through the full activation of the APC/C, and 2) inhibition of Cdk1, thereby allowing the cell to exit mitosis.

The primary driver of the MEN is the GTPase Tem1, which signals Cdc14 release via the kinase Cdc15. During anaphase, Tem1 and Cdc15 localize at the SPB along with two other kinases, Dfb20 and Dfb2/Mob1 (Hotz and Barral 2014; Visintin and Amon 2001). The interaction of Tem1 and Cdc15 is necessary for the activation of the MEN (Figure 8). Upon activation, Cdc15 activates the Dfb2/Mob1 complex, promoting Cdc14 release (Queralt and Uhlmann 2008; Visintin and Amon 2001). Counteracting the activity of Tem1 is a protein complex of Bub2 and Bfa1, which together form a bipartite GTPase-activating protein (GAP) that prevents Cdc15 localisation at the SPB (Visintin and Amon 2001). The Bud2/Bfa1 complex thus isolates Tem1 from Cdc15 until the SPB enters the bud at which time both the complex and Cdc15 relocalise to the SPB, allowing for Cdc15 to become activated by Tem1 (de Bettignies and Johnston 2003). However, it should be noted that evidence also suggests that this process may be more complicated as cells lacking Tem1 or overexpressing Cdc15 reportedly still show wild type timing for mitotic exit, implying that mitotic exit does not solely depend on the MEN (Hotz and Barral 2014).

Although Cdc14 requires the MEN for its full release, another pathway has been implicated in a potentially more partial release, possibly 'priming' the full activation of the MEN and improving

the efficiency of mitotic exit (Yellman and Roeder 2015). Indeed, the initial release of Cdc14 from the nucleolus is triggered by the Cdc14 early anaphase release (FEAR) network, creating a pulse of Cdc14 activity before MEN activation (Azzam et al. 2004; Rock and Amon 2009). The FEAR network is comprised of Cdc5, Esp1, Slk19 (a kinetochore protein), and Spo12 (Figure 8) (Stegmeier, Visintin, and Amon 2002). The activation of this network is not essential for the full activation of the MEN, but it has been shown to improve the viability of budding yeast during anaphase by contributing to spindle stability (Tomson et al. 2009; Rock and Amon 2009; D'Amours and Amon 2004). Moreover, the FEAR-dependent release of Cdc14 was also reported to play a role in the segregation of ribosomal DNA, the nucleolus, and telomeres (C.-T. Chen et al. 2006; Tomson et al. 2009; D'Amours and Amon 2004).
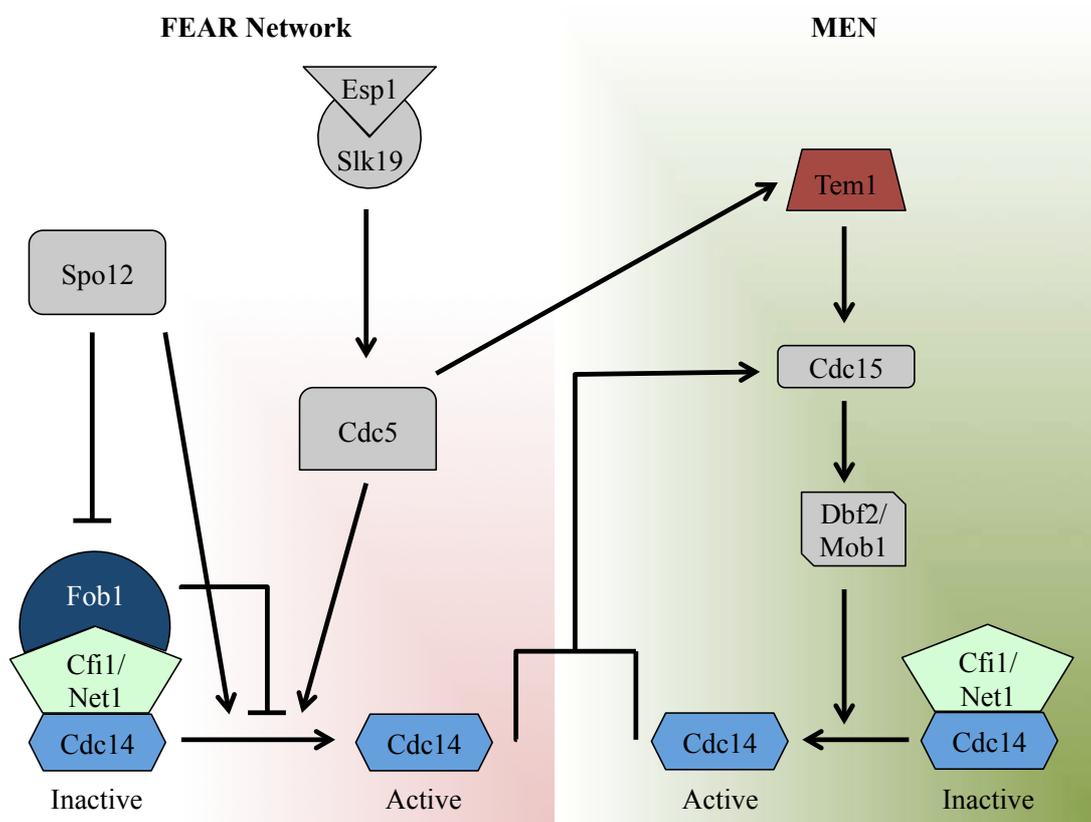
Figure 8: The FEAR and mitotic exit network
Early in anaphase the FEAR network is triggered, leading to a partial release of Cdc14 primarily into the nucleus. This is followed by the full activation of the MEN where Cdc14 is fully released into the cytoplasm driving a cascade of events for mitotic exit. Adapted from (D'Amours and Amon 2004).

The FEAR-dependent release of Cdc14 is thought to be limited to the nucleus, as imaging of the protein indicates a largely nuclear localisation (Mohl et al. 2009), although it is likely there is also some export to the cytoplasm (Yellman and Roeder 2015). The activation of the FEAR network first requires the phosphorylation of Net1 by Cdks. Before the reduction in Cdk activity by the

APC/C, the activation of separase (Esp1 in budding yeast) results in the downregulation of the phosphatase PP2A^{Cdc55}. PP2A are heterotrimeric holoenzymes that contain a scaffold and catalytic subunit, which includes a range of regulatory subunits that provide substrate specificity (Touati et al. 2019). In this case, the Cdc55 subunit provides substrate specificity to Net1 (a component of the RENT complex sequestering Cdc14 to the nucleolus), counteracting its Cdk-dependent phosphorylation. This allows cyclin B/Cdk complexes to promote the activation and timing of the FEAR network (Touati et al. 2019; Yellman and Roeder 2015).

Spo12, the Esp1/Slk9 complex, and Cdc5 all promote the release of active Cdc14 from the nucleolus through its separation from the RENT complex (Stegmeier, Visintin, and Amon 2002). Specifically, Spo12 is required for FEAR network function, and its phosphorylation has been shown to act on the same downstream target as the Esp1/Slk9 complex (Tomson et al. 2009). Spo12 is a nucleolar phosphoprotein that binds to an inhibitor of the FEAR network, Fob1. Fob1 inhibits FEAR function by preventing Cdc14 release as it also binds to Cfi1/Net1 (Rata et al. 2018; D'Amours and Amon 2004). Loss of Spo12 or inhibition of its phosphorylation in budding yeast is not lethal but does induce a delay in the timing of mitotic exit of approximately 10-15 minutes (Stegmeier, Visintin, and Amon 2002; Tomson et al. 2009). Interestingly, budding yeast Spo12 contains an LxF docking motif that is required for cyclin B/Cdk1 phosphorylation, and subsequently FEAR network function, indicating a likely interaction of Spo12 with Cdks (Örd, Venta, et al. 2019).

1.3.4.4. Sister chromatid separation

In late anaphase, the chromosomes are pulled to opposite ends of the cell by the action of the attached microtubules (Cheeseman 2014; McIntosh 2016). All sister chromatid pairs separate at the same time, and the process is stimulated by a wave of activity of separase (Morgan 2007). Separase is a protease that cleaves the Scc1/Mcd1 subunit of the cohesin complex, which holds the sister chromatids together (Morgan 2007; Luo and Tong 2021). Additionally, separase has also been demonstrated to have several other functions in a broad range of processes including DNA damage repair (Hellmuth et al. 2018; McAleenan et al. 2013) and centrosome duplication (Matsuo et al. 2012). Deregulation of separase can lead to aneuploidy and chromosome instability, thus it is tightly regulated by two inhibitors: securin and cyclin B/Cdk1 (Luo and Tong 2021; Uhlmann 2001; Karasu et al. 2019). Securin tightly binds to separase, thereby inhibiting its activity, but also acts as a chaperon stabilising the enzyme (Luo and Tong 2021; Hornig et al. 2002). Hence, the loss of securin

in *Drosophila* and fission yeast causes a decrease in separase activity (Uhlmann 2001). Inhibition of separase by cyclin B/Cdk1 is achieved via direct phosphorylation, and thus as cyclin B and securin are targeted for destruction by the APC/C at the metaphase to anaphase transition, there is a subsequent activation of separase (Luo and Tong 2021). The cleavage of the cohesion structures binding the sister chromatids is followed by their abrupt separation.

Finally, with the chromosomes separated at the poles of the cell, the mitotic spindles are depolymerized and the chromosomes begin to decondense, with the nuclear envelope reassembling in telophase (Cheeseman 2014; McIntosh 2016; Antonin and Neumann 2016). After the two nuclei are formed, the cell will undergo cytokinesis, producing two daughter cells with equal numbers of chromosomes (McIntosh 2016).

1.4 DNA Damage and Stress Responses

Disruptions in normal cell cycle progression can be fatal, thus cells have evolved mechanisms known as checkpoints to delay or arrest cell cycle progression (D'Urso and Nurse 1995). Cell cycle checkpoints are regulated by multiple proteins which are conserved across eukaryotes, and their impairment is a common feature of cancers (Laiho and Latonen 2003). In previous sections, checkpoints that ensure optimal conditions for cell cycle commitment and faithful chromosome segregation, Start and the SAC respectively, have already been discussed. The other major checkpoints in the cell cycle are operating in response to replicative stress or DNA damage, allowing cells to delay mitotic entry (Melo and Toczyski 2002). The response pathway of both instances will arrest the cell cycle via the same downstream target, the Cdc25 phosphatase, which leads to a reduction in Cdk activity. However, although the downstream result is shared, the upstream activation for either DNA stress or DNA replication is different. The proteins involved in DNA damage response are highly conserved across eukaryotes (Melo and Toczyski 2002).

The DNA damage checkpoint involves two specific groups of PI3K-like kinase damage sensors known as ATR and ATM (Melo and Toczyski 2002). The recruitment of these complexes to the sites of DNA stress is considered to be the most upstream event of checkpoint signaling. Both ATR and ATM are localised in the nucleus and are recruited to sites of DNA damage (Harrison and Haber 2006). The recruitments of ATM and ATR are mediated by the MRN complex (which consists of the proteins Mre11, Rad50, and Nbs1), and the ATR partner ATRIP (Melo and Toczyski 2002; Harrison and Haber 2006), respectively. The subsequent increase in the concentration of checkpoint machinery components at the sites of DNA stress leads to the local phosphorylation of the histone H2AX, which acts as a platform for mediator proteins (Crb2 and Mrc1 in fission yeast) to amplify the signal (Yata and Esashi 2009; Melo and Toczyski 2002).

Specifically in yeast, ATR (Mec1 & Rad3 respectively for budding and fission yeast) appears to be the most critical pathway of the two (Abraham 2001; Melo and Toczyski 2002), where Mec1 phosphorylates its regulatory subunit Ddc2 (Rad26 in fission yeast), forming a complex which associates with DNA breaks. The DNA damage sensor ATM is a complex of proteins consisting of Rad9, Hus1, and Rad1. These factors form the 9-1-1-complex, and with the assistance of Rad17, it binds to chromatin after DNA damage or replicative stress (i.e. stalled forks) (Burtelow, Kaufmann, and Karnitz 2000; Melo and Toczyski 2002). The downstream kinases of the DNA damage and

replicative stress pathways are Chk1 and Chk2 (Sancar et al. 2004). Chk1 is part of the DNA replication checkpoint, while Chk2 acts as an effector kinase for the DNA damage checkpoint (Melo and Toczyski 2002; Sancar et al. 2004). It is important to note that Chk1 and Chk2 homologs in *S. pombe* are Chk1 and Cds1, respectively. Chk1 in fission yeast is involved in the DNA damage reponse checkpoint, while Cds1 is part of the replicative stress pathway (Rhind and Russell 2001; Melo and Toczyski 2002).
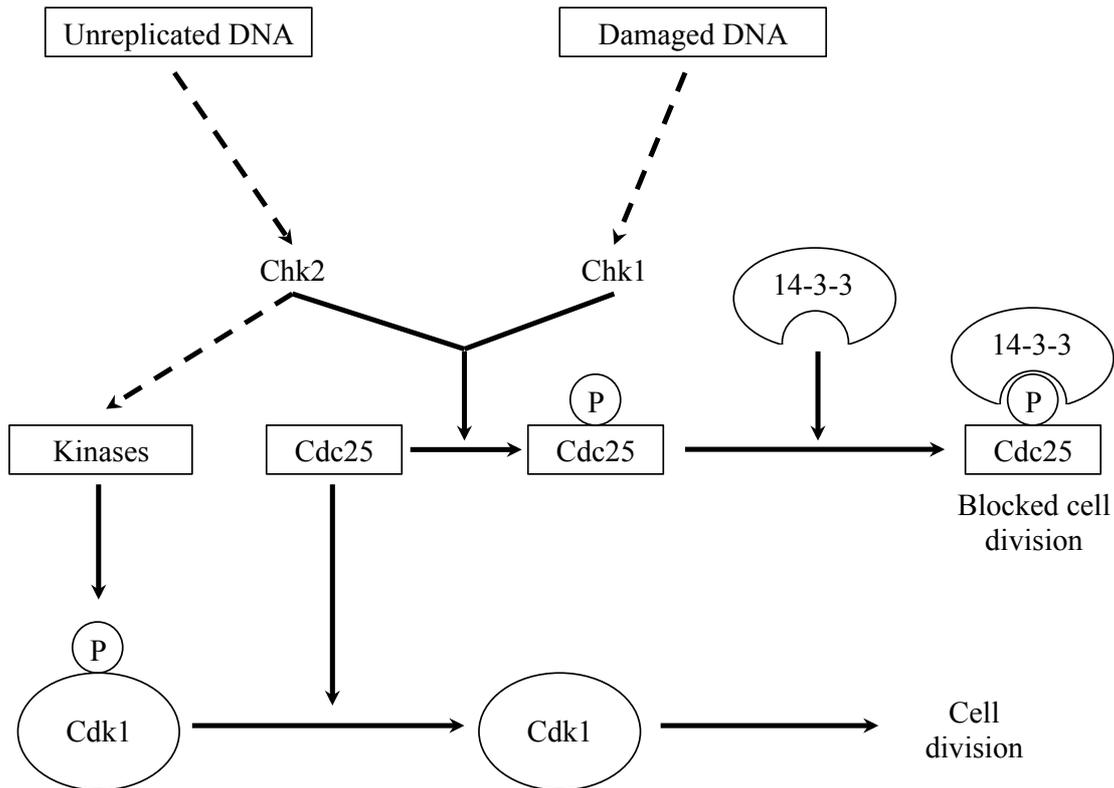
Figure 9: The replicative stress and DNA damage response pathways
Cells will activate pathways specific depending on the type of DNA stress. These pathways will arrest the cell cycle through the downstream repression of Cdk activity via the mitotic feedback loop. Adapted from (Zeng et al. 1998).

Chk1 and Chk2 are serine/threonine kinases that, when activated, phosphorylate Cdc25, inactivating the phosphatase by nuclear exclusion (Figure 9) (Sancar et al. 2004; Hermeking and Benzinger 2006). Evidence suggests that the 14-3-3-complex is involved in the translocation of Cdc25 to the cytoplasm by binding to phosphorylated Cdc25. The nuclear-excluded Cdc25 is unable to interact with Cdk1, and subsequently cannot activate Cdk activity, preventing mitotic entry (Hermeking and Benzinger 2006). Interestingly, in fission yeast, Chk1 and Cds1 were demonstrated to also up-regulate Wee1, which inhibits Cdc2, contributing to the reduction in Cdk activity (Rhind and Russell 2001; Raleigh and O'Connell 2000). The regulatory mechanisms of checkpoints are made possible by the modulation of kinase activity via biologically conserved network motifs.

1.5 Network Motifs in Cell Cycle Control

1.5.1 Feedback loops

Cells can be viewed as devices composed of integrated systems, which involve thousands of interacting proteins (Alon 2006). These proteins form complicated networks that allow cells to react to internal and external signals in order to transition to the required state via the timely activation of the associated processes. These intricate circuits are vast and difficult to interpret. Interestingly, recurring topologies, or network motifs, can be extracted and are often conserved between species. Studying the dynamics of these network motifs as well as their biological context provides important insights not only into the way regulatory networks operate and interact but also into the rationale for the selection of specific topologies throughout evolution.

Network motifs were first systematically identified in *E. coli*, where specific patterns occurred more often than randomised patterns in the transcription network (Alon 2006, 2007). Strikingly, these same motifs have been identified in yeast, plants and animal cells (Milo et al. 2002; Alon 2007; T. I. Lee et al. 2002). Investigating motif operation in simple and genetically amenable model systems is therefore a powerful approach to understand the biology of more complex organisms. The dynamics of many network topologies have been described in the context of the control of gene expression, with sometimes relatively slow, protein synthesis-dependent outputs. However, cellular functions can also be regulated by shifting existing proteins between active and inactive states via post-translational modifications such as phosphorylation, which provides more rapid responses (Alon 2007; Derouiche, Cousin, and Mijakovic 2012). In the context of the cell cycle, the events are coordinated by the fluctuations in Cdk activity that is generated by interacting positive and negative feedback loops. Such feedbacks allow for inducing fast and hypersensitive changes in Cdk activity levels, which in turn trigger fast changes in cell physiology through modulation of the Cdk-dependent phosphoproteome (Csikász-Nagy et al. 2009; Novak et al. 2007; Ferrell 2013). Furthermore, many of the proteins that are periodically expressed during the cell cycle are Cdk substrates, indicating the importance of the regulation of their phosphorylation status. The systems level regulation of Cdks and Cdk substrates is therefore a central feature of cell cycle regulation, and understanding the fundamental principles are essential for elucidating the mechanisms of cell cycle control (Ferrell 2013).

The cell cycle is a series of events that allow for genome duplication and the equal distribution of the DNA into two daughter cells. Orderly and irreversible progression through cell cycle relies on the activation of the mechanisms that trigger the main cell cycle transitions e.g. phosphatases preventing cells returning to mitosis at mitotic exit (Deritei et al. 2019; Morgan 2007). The characteristic irreversibility of the cell cycle has been suggested to be due to hysteresis at the G2/M transition, which creates a state of bistability. Hysteresis is a concept where the input required to change the state of a system is greater than what is required to maintain the new state, in part due to a dynamic lag between the input and the output (Solomon 2003). For this reason, bistable systems exist in only one of two possible steady states and do not fluctuate in response to small perturbations, making them robust. In the context of the cell cycle, hysteresis was proposed to be a central aspect of irreversibility. The bistability of the cell cycle system is brought about by positive and negative feedback loops that generate oscillations between the two steady states of Cdk activity (Ferrell 2013). The feedback loops are necessary for the correct functioning of the cell cycle since they are essential for maintaining the irreversibility of the transitions between phases (Ferrell 2013; López-Avilés et al. 2009; D. Fisher et al. 2012). Studying these motifs will provide insight into the basic principles of cell cycle control.
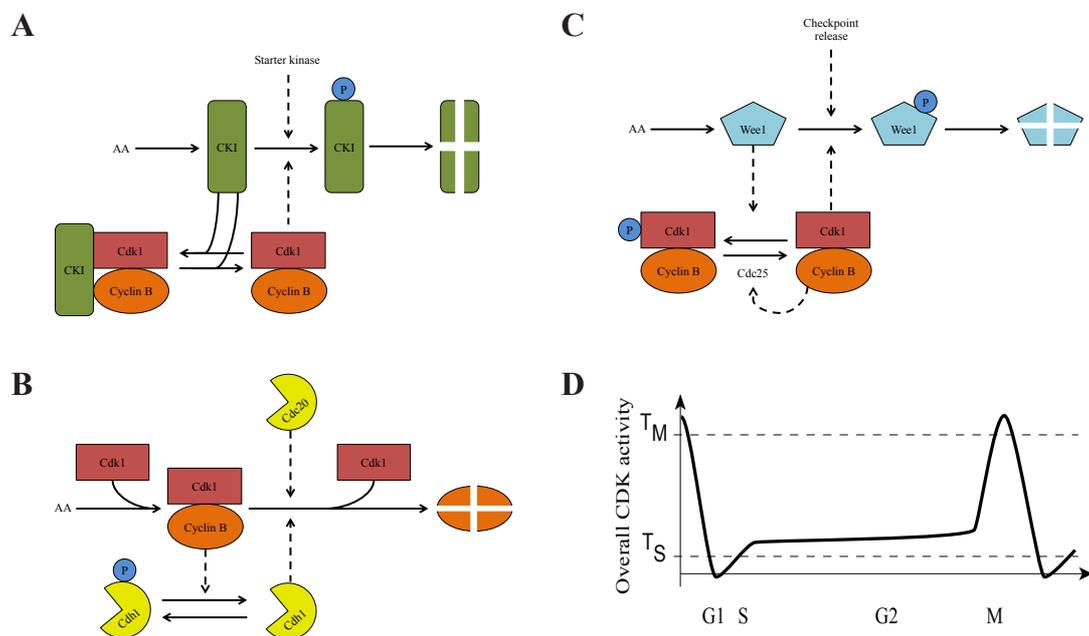
Figure 10: Feedback loops create oscillations in CDK activity
(A) G1-S. CKIs inhibit active cyclin B/Cdk1 complexes and keep Cdk activity low, but the increased concentration of resistant 'starter kinases' counteracts CKI inhibition through SCF-mediated destruction. Once CKIs reach a threshold of inhibition, the cyclin B/Cdk1 complexes quickly overcome them and Cdk activity subsequently increases. **(B)** Mitotic entry. A balance of Wee1 and Cdc25 activity controls the active state of cyclin B/Cdk1 complexes. Once the level of active cyclin B/Cdk1 reaches a critical level, Wee1 becomes sufficiently inhibited, leading to an abrupt increase in Cdk activity through cyclin B/Cdk1 dephosphorylation by Cdc25. **(C)** Mitotic exit. The high levels of CDK activity instigate

the activation the APC/C, which is initiated to degrade cyclin B at the metaphase-to-anaphase transition by the subunit Cdc20. The proteolysis of cyclin B allows for the dephosphorylation of another APC/C subunit, Cdh1, which stabilizes cyclin B levels, keeping it low. **(D)** The feedback loops impose a specific profile of Cdk activity oscillations throughout the cell cycle, maintaining its integrity and the bistability between cell cycle transitions. Figure was partially adapted from (Novak et al. 2007).

Following Cdk inhibition at mitotic exit, the binding of the G1 Cdk-inhibitors (CKIs: Sic1 in budding yeast and Rum1 in fission yeast) to the remaining or newly assembled cyclin B/Cdk1 complexes keep the activity low (Correa-Bordes and Nurse 1995; Mondesert, McGowan, and Russell 1996). Together with the function of the APC/C, this prevents G1 cells to revert to a mitotic state. CKIs are themselves targets of inhibitory phosphorylation by cyclin/Cdk complexes, representing a first feedback loop on cell cycle progression. At this point, if the cell is in favourable growth conditions (i.e. nutrient-rich, or in the presence of growth stimuli), the decision is made to commit to a new cell cycle, as previously mentioned (Moreno-Torres, Jaquenoud, and De Virgilio 2015). Once the cell passes Start, CKIs are rapidly phosphorylated and subsequently ubiquitinylated for degradation. Cyclin/Cdk complexes that are resistant to CKI-mediated inhibition will increasingly phosphorylate CKIs as they increase in levels, and this will subsequently reduce the impact of CKIs on Cdk activity over time (Mondesert, McGowan, and Russell 1996; Martín-Castellanos et al. 2000). As the cell then grows in size, cyclins are synthesized, allowing for the cell to accumulate sufficient amounts of the resistant cyclin/Cdk complexes necessary to counteract the inhibitory mechanisms in G1 (this factor is more crucial in the G2 phase of the cell cycle). This condition creates a state of bistability, where Cdk activity is kept low until CKIs are inhibited by the resistant kinases. Once CKIs have been sufficiently downregulated, the inhibited cyclin B/Cdk1 complexes are able to overcome the CKIs and further contribute to their inhibition, quickly tipping the balance in favour of the kinases (Novak et al. 2007). In budding yeast, it is necessary for the cyclin B/Cdk1 complexes (known as Clb5/Cdc28 and Clb6/Cdc28) to be activated in order to initiate DNA replication (Nash et al. 2001). The increase in Cdk activity during this phase is coupled with the inhibition of the Cdh1 subunit of the APC/C, which is phosphorylated by the active cyclin/Cdk complex, contributing to the overall rise in cyclin B/Cdk1 levels (Novak et al. 2007). This positive feedback loop allows for a rapid switch of momentum from lowering Cdk activity to increasing it, initiating DNA replication (Figure 10A).

After progressing through S phase, cells enter G2 and then mitosis. The onset of mitosis is tightly controlled by modulation of Cdk activity. From late G1 until late G2, cyclin B/Cdk1 complexes increase in concentration but their activity remains low, precluding the entry into mitosis.

This is brought about by inhibitory phosphorylation of Cdk1 on a conserved residue by the kinase Wee1 (Lundgren et al. 1991; Russell and Nurse 1986). Wee1 is a small and highly conserved kinase that phosphorylates Tyr15 on Cdk1 (in fission yeast, Thr14 of Cdc2 is also a target of Wee1 phosphorylation), inhibiting it regardless of whether it is bound to a cyclin (although it has been shown to better target cyclin B/Cdk1 complexes) (Crncec and Hochegger 2019; Lundgren et al. 1991). Thus, despite the increase in the concentration of Cyclin B/Cdk1 complexes throughout G2 due to the synthesis of cyclin B, Wee1 maintains overall Cdk activity low enough to prevent mitotic onset. Importantly, Wee1 is directly inhibited by Cdk1-dependent phosphorylation, representing another feedback loop motif in cell cycle control. Thus, when the level of Wee1-inhibited Cdk activity reaches a certain threshold (this has not been experimentally quantified but it is based on the hypothesis that Wee1-phosphorylated Cdk1 is not fully inactive), it becomes sufficient to inhibit Wee1 function, promoting further increase in Cyclin B/Cdk1 activity. Importantly, the phosphatase Cdc25 counteracts Wee1 function and is activated by Cdk1 (Russell and Nurse 1986; Crncec and Hochegger 2019), contributing to another embedded positive feedback on Cdk1 function. This system of double feedback loops allows for a rapid and abrupt increase in Cdk1 activity, triggering the onset of mitosis (Novak et al. 2007; Coudreuse and Nurse 2010a) (Figure 10B), and ensures that this transition is an all-or-nothing process (López-Avilés et al. 2009).

Upon commitment to mitosis, the cell enters a state where the necessary Cdk substrates are phosphorylated and the events of chromosome segregation are initiated (Domingo-Sananes et al. 2011). The phosphorylation of these substrates is a consequence of the increased Cdk activity, and thus in order for cells to exit mitosis, a decrease in the activity is necessary to allow for substrate dephosphorylation. The switching from one state to another (mitosis back into interphase) is brought about by the negative feedback loop between the APC/C and cyclin B/Cdk1 (Figure 10C). As previously mentioned, the APC/C deactivates cyclin B/Cdk1 complexes through the targeted ubiquitinylation of cyclin B, instigating mitotic exit (Peters 2006). The APC/C remains inactive from late G1 until early mitosis, allowing for its target substrates to accumulate during this period (Pines 2011). Once the cell reaches the required threshold of Cdk activity, it progresses into mitosis, and subsequently activates the APC/C through direct phosphorylation by Cdk1/cyclin B complexes (Kraft et al. 2003). This constitutes a negative feedback loop, where the increase in Cdk activity also stimulates its decrease via the activation of an inhibitor. This negative feedback loop is essential for mitotic exit, as circuits containing non-degradable forms of cyclin B or inhibition of the APC/C cause an arrest in mitosis (Ferrell 2013; Yang and Ferrell 2013). However, it should be noted that decrease in Cdk activity alone is not sufficient to drive mitotic exit, as the desphosphorylation of Cdk

substrates is logically required (D. Fisher et al. 2012). More details into the role of phosphatases will be provided in a later part.

In conclusion, the cell cycle is comprised of a series of events that require a temporal ordering to ensure the correct execution of successive and often incompatible processes (e.g. genome duplication and mitosis). This strict unidirectional ordering of the cell cycle has been achieved through the evolution of feedback loops that create irreversible transitions between the states of Cdk substrates. Indeed, the changes in the substrates are, in principle, consequences of the oscillating levels of Cdk activity (Figure 10D) (Coudreuse and Nurse 2010a). Contributing to the changes are phosphatases, a group of enzymes that counteract Cdk activity. The regulation of phosphatases is complex in terms of their activity, localisation, and role in the cell cycle, as they are still not fully understood. The following section is an overview of phosphatases in the cell cycle and their relevance in the dynamic oscillation of the phosphorylation states of cell cycle components.

1.5.2 Phosphatases in cell cycle regulation

Cell cycle substrates can be viewed as balancing between two steady states where they are either phosphorylated or dephosphorylated (Domingo-Sananes et al. 2011). The dynamic positive and double negative feedback loops on cyclin B/Cdk1 activity, brought about by Cdc25 and Wee1, were thought to be the major regulators of these two cellular states. However, more recent work has indicated the existence of significant upstream regulations via phosphatases.

It had been long known that phosphatases play a significant role in controlling cell cycle progression, as it has been demonstrated that treatment with the phosphatase inhibitor okadaic acid induces entry into mitosis in cells (Izumi and Maller 1993). More recently, two phosphatases are known as PP2A/B55 (Pab1 in fission yeast) and PP1 have been reported to counteract cyclin B/Cdk1-mediated phosphorylation (Wu et al. 2009; Grallert et al. 2015). Indeed, the importance of their activity can be seen at mitotic exit, where cyclin B/Cdk1 inactivation is not sufficient, as the targets of Cdk1 must be dephosphorylated to progress to G1 and prevent a deleterious return to a mitotic state (Wu et al. 2009). Consistent with this, it has been demonstrated that PP2A/B55 upregulation prevents entry into mitosis as observed in *Xenopus* (Mochida et al. 2009).
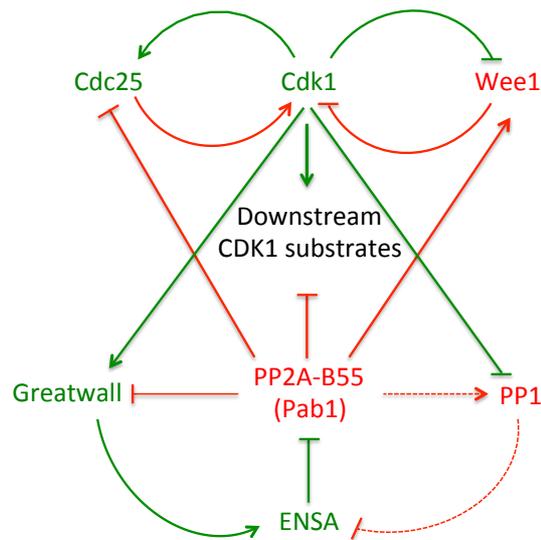
Figure 11: Phosphatase regulation of the phosphorylation of cell cycle substrates
Phosphatase and kinase activities are balanced in two states that regulate the phosphorylation of cell cycle components. The switch between interphase and mitosis is controlled by the counteracting activities of PP2A and Cdk. The figure was adapted from (Domingo-Sananes et al. 2011).

Moreover, PP2A/B55 counteracts cyclin B/cdk1 activity by inhibiting and activating Cdc25 and Wee1, respectively (Figure 11). Its activity is also amplified in a positive feedback loop involving PP1 (Lucena et al. 2017; Grallert et al. 2015). Indeed, PP2A/B55 activates PP1, which in turn inhibits endosulfine and Arpp19 (ENSA) (Gharbi-Ayachi et al. 2010). Importantly, ENSA are inhibitors of PP2A/B55 (Arpp19 specifically directly inhibits PP2A): the regulation of ENSA by PP1, therefore, represents a positive feedback loop on PP2A activity. In addition, the kinase Greatwall (Gwl), which is inhibited by PP2A, is an activator of ENSA. Thus, the regulation of Gwl by PP2A constitutes another positive feedback loop. Gwl depletion in *Xenopus* egg extracts results in rapid mitotic exit, which is due to the potentiation of PP2A activity as a result of a reduction in ENSA function (Lorca and Castro 2013; Gharbi-Ayachi et al. 2010). These feedback loops are highly conserved in eukaryotic organisms and are clearly present in fission yeast (Domingo-Sananes et al. 2011). This again highlights the organization of cell cycle control in an intricate network of feedback motifs.

In principle, cell cycle progression depends on the temporal modulation of Cdk activity. The regulation of Cdk has evolved as a complex system of interacting components including a variety of kinases and counteracting phosphatases. The output of this circuit is a specific dynamic profile of the balance of Cdk and phosphatase activity, which is likely the evolutionary consequence of the

necessary directionality of events. In any case Cdk activity modulation is an essential feature of cell cycle regulation in eukaryotic cell, and understanding the underlying principles provide novel insights into this highly conserved mechanism of control. The complex network of the cell cycle includes a vast array of different components involved in drastically different functions. However, the principle of its regulation is dissectible with the use of rationally designed motifs, which can elucidate the fundamentals of cell cycle control.

1.6 Studying the cell cycle with fission yeast

1.6.1 *Schizosaccharomyces pombe* as a model organism

The fission yeast *Schizosaccharomyces pombe* is a unicellular eukaryotic organism that divides symmetrically by radial fission. It has a small genome of 14Mb and only three chromosomes. *S. pombe* has been a model of choice for studying a number of subjects including translation, RNA splicing, chromosome structure, meiosis, mitosis and the cell cycle, with the latter being of particular significance after pioneering work done by Sir Paul Nurse (Moreno, Klar, and Nurse 1991; Hayles and Nurse 1992). There are a number of appealing reasons to work with fission yeast to study the cell cycle.

First, it is easy to handle and manipulate given that many of the established protocols used in other models such as *Saccharomyces cerevisiae* are transferable (Hayles and Nurse 1992; Vyas et al. 2021). Furthermore, *S. pombe* grows much faster than mammalian cells: at 32˚C in synthetic minimal medium (EMM6S) fission yeast has a generation time of approximately 140 minutes. This fast generation time is also coupled with a dynamic and easily measurable cell length (fission yeast are generally considered to maintain a constant diameter throughout its life cycle). Changes in generation time and cell length in *S. pombe* reflect the changes in the organisation of cell cycle events. Thus, manipulation of components involved in proliferation can have their role in the cell cycle inferred based on changes in these easily measurable characteristics (Vyas et al. 2021). For example, the identification of the role of the kinase Wee1 at mitotic entry was discovered through a temperature sensitive mutation that leads to a reduction in cell length at division (*wee1-50*) (P. Nurse and Thuriaux 1980). Strains carrying the *wee1-50* mutation have a temperature-sensitive loss of function of the kinase, and will as a consequence have a shorter G2 period of growth prior to mitotic entry.

Second, as already mentioned, the eukaryotic cell cycle is conserved in fission yeast with the same identifiable phases (G1, S, G2 and M), but with fewer conserved Cdks and cyclins, making it a simpler model of investigation (Figure 12). The cyclins Cig1, Cig2 and Puc1 regulate Cdc2 activity from Start through G1 (Martín-Castellanos et al. 2000; Benito, Martín-Castellanos, and Moreno 1998), and Cdc13 has a more prominent role during S phase and G2 (Russell and Nurse 1986; Lundgren et al. 1991). Cdc2 is the primary Cdk in the fission yeast cell cycle and was initially

discovered as necessary for entry into mitosis (Gould and Nurse 1989). Since, it has also been implicated in a number of events throughout the cell cycle including Start and transcription (Baum, Wuarin, and Nurse 1997), DNA replication (Fragkos et al. 2015; Noguchi et al. 2002), and the expression of cycling genes (Banyai et al. 2016). The reduced complexity in Cdks and cyclins involved make it an attractive model for studying the cell cycle, as there is are a number of conserved mechanisms, and likely fundamental principles will remain relevant for other eukaryotic organism. More recently, the importance of a specific profile of oscillations in Cdc2 activity has been demonstrated for the proper execution and progression of cell cycle events, supporting a quantitative model of regulation (Banyai et al. 2016; Coudreuse and Nurse 2010a; Pickering et al. 2021; Örd, Möll, et al. 2019).

1.6.2 Cell cycle control in *Schizosaccharomyces pombe*

The general principles of cell cycle regulation discussed earlier are conserved in fission yeast. In G1, Cdk activity is kept low until the decision to commit to another round of division is made by passing Start (Morgan 2007; Simanis, Hayles, and Nurse 1987). During this phase, the activity of Cig2/Cdc2 and Cdc13/Cdc2 complexes are inhibited due to Rum1, which maintains an overall low Cdk activity post-mitosis (Gérard et al. 2015; Benito, Martín-Castellanos, and Moreno 1998; Correa-Bordes and Nurse 1995). However, Cig1/Cdc2 and Puc1/Cdc2 complexes are not inhibited by Rum1 and are active during this period, albeit are low in relative quantity. If the cell is in favourable conditions, growth will lead to an increase in the quantity of these Rum1-resistant Cdc2 complexes. This eventually leads to phosphorylation of Rum1 on T58 and T62, targeting it for degradation (Martín-Castellanos et al. 2000). As Cig1/Cdc2 and Puc1/Cdc2 progressively promote Rum1 degradation, Cig2/Cdc2 activity levels also rise. The combined activities of Cig1/Cdc2, Puc1/Cdc2, and Cig2/Cdc2 eventually reach the Cdc2 activity threshold necessary for the cell to progress into S phase (Martín-Castellanos et al. 2000).

Following progression into DNA replication, the overall Cdk activity will be above the S phase threshold but much below the mitotic entry requirement. However, during S and G2, the mitotic cyclin/Cdk complex, Cdc13/Cdc2, will increase in concentration. The increasing level of Cdc13/Cdc2 is instigated by the inhibition of the APC/C via phosphorylation by the Cig1/Cdc2, Cig2/Cdc2, and Puc1/Cdc2 complexes. These complexes will inhibit the APC/C, reducing the degradation of Cdc13 by ubiquitinylation, which in turn lead to an increase in Cdc13/Cdc2

complexes (Blanco et al. 2000). Although the concentration of Cdc13/Cdc2 complexes increases over S and G2, Cdk activity remains low as a result of inhibitory phosphorylation on Y15 by the Wee1 and Mik1 kinases (Gould and Nurse 1989; Russell and Nurse 1986). It should be noted that Mik1 has an overlapping function with Wee1, but has a more specific role in response to replicative stress (Dutta and Rhind 2009).
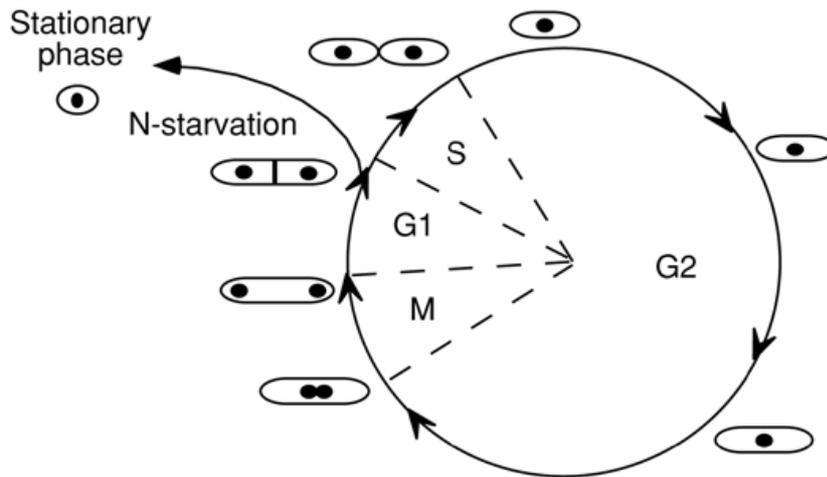

Figure 12: The fission yeast mitotic cell cycle
The fission yeast cell cycle maintains the same conserved phases as other eukaryotes. However, *S. pombe* cells spend the majority of their cell cycle in G2 (approximately 70%), with M taking about 10-15 minutes, followed by a short G1 and S phase. The process of septation overlaps with G1 and S phase.

In G2, the cell continues to grow, accumulating Cdc13/Cdc2 complexes, which are inhibited by the aforementioned kinases. Interestingly, the high concentration of phosphorylated mitotic cyclin/Cdk complexes at this stage creates a unique condition for an abrupt change in Cdk activity levels. The inhibitory phosphorylation by Wee1 and Mik1 is counteracted by the phosphatase Cdc25 that dephosphorylates the same residue on Cdc2. The activity of the phosphatase alone is insufficient to out compete the kinases, and in order for the cell to progress into mitosis, a specific threshold of Cdk activity needs to be reached. Interestingly, the active form of the Cdc13/Cdc2 complex both inhibits and potentiates the Wee1/Mik1 and Cdc25, respectively. This creates two positive feedback loops, which once the balance of active to non-active Cdc13/Cdc2 complexes shifts to a critical point, they allow for a sudden increase in the dephosphorylation of the complexes and a subsequent increase in Cdk activity that triggers entry into mitosis (S. Y. Kim and Ferrell 2007; Izumi and Maller 1993; Novak et al. 2007).

1.6.3 Size control in *Schizosaccharomyces pombe*

Size control is a subject of large interest, as experimental observations imply that cells are able to regulate their size through mechanisms that are not fully understood (Amodeo and Skotheim 2015; Cook and Tyers 2007). As size and growth are important factors in cell division, it is likely that size control is regulated by the timing of cell cycle events (P. A. Fantes et al. 1975; Wood and Nurse 2015; Amodeo and Skotheim 2015). Fission yeast is an ideal model for studying size control due to its homogeneity of size at division (SAD) (Á. Sveiczer and Horváth 2017; Wood and Nurse 2015). Indeed, wild type *S. pombe* cells have a diameter of ~4μm and grow from approximately 8 to 14μm during the cell cycle in synthetic minimal media (EMM) at 32˚C (Navarro and Nurse 2012).

A number of models have attempted to explain size homeostasis in fission yeast but the mechanisms underlying this important feature of their life cycle remain elusive. One proposed concept involves a fixed timer for division, which would represent a passive control mechanism. In this case, linearly growing cells would always divide at the same size, maintaining a constant cell size in the absence of checkpoints (Conlon and Raff 2003). However, experimental observations clearly show that fission yeast cells adjust their cell cycle duration in order to reach a critical size before entry into mitosis i.e. cells that are born smaller will have longer cell cycles and vice versa (P. Fantes and Nurse 1977; Wood and Nurse 2013). Additionally, neither budding yeast nor fission yeast accumulate mass linearly throughout the cell cycle as their growth varies over the different periods of the cell cycle (Wood and Nurse 2015). An alternative model was therefore proposed that involves direct cell size sensing.

Fission yeast appears to have an active size sensing mechanism, as variations in their size at birth are adjusted in the length of their cell cycle. Indeed, the average length of *S. pombe* at division is approximately 14 μm, with a variation of about 6% (A. Sveiczer, Novak, and Mitchison 1996; Wood and Nurse 2015). This can be interpreted in two ways: 1) that *S. pombe* cells sense their size has been reached or, 2) there is a fixed timer for when division occurs. The latter model is unlikely as fission yeast cells blocked in G2, and subject to extended growth, will correct back to their average SAD in successive division cycles (P. A. Fantes et al. 1975; Wood and Nurse 2013; Coudreuse and Nurse 2010b). So the question remains on how cells are able to interpret their size. Size in this sense in not necessarily a measurement of cell volume or length, but could include a variety of properties including total protein, ribosome content, or biosynthetic capacity (Amodeo and Skotheim 2015).
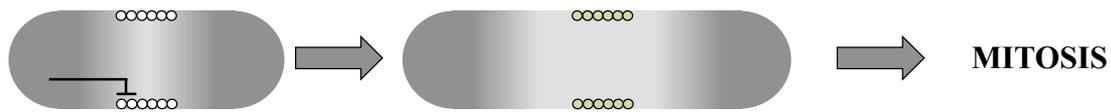
MITOSIS

Figure 13: Representative schematic of Pom1 Gradient
In Fission yeast, the mitotic inhibitor Pom1 forms polarized gradients at the cell tips (dark shading). Cortical nodes (Cdr1 and Cdr2) are localised at the centre of the cell (circles; white indicates inactive, green indicates activated) and are inhibited by Pom1. Smaller cells have sufficient Pom1 at the middle of the cell to inhibit the nodes, but as the cell gets bigger the inhibition by Pom1 decreases. Figure was adapted from (Moseley and Nurse 2010).

A proposed mechanism of how fission yeast cells can sense their size is the Pom1-gradient model (Moseley et al. 2009; S. G. Martin and Berthelot-Grosjean 2009). This model shows that Pom1, a dual specificity tyrosine-phosphorylation regulated kinase (DYRK), acts as a "molecular ruler". Pom1 localises at the cell tips, forming a gradient (Moseley et al. 2009; Allard et al. 2018). The kinase phosphorylates two nodes at the centre of the cell known as Cdr1 and Cdr2, and when there is sufficient Pom1 at the nodes, they will be inhibited. Cdr1 and Cdr2 promote mitotic entry through the inhibition of Wee1. Interestingly, as the cell grows the Pom1 gradient will become less concentrated at the centre, causing Cdr1 and Cdr2 to become increasingly activated, increasing Cdk activity. Despite the appeal of the model, it was not sufficient to fully address size control in fission yeast.

Indeed, it has since been shown that it is likely that the Pom1 gradient is not as consistent as first proposed given there was an observed large cell-to-cell variability in the distribution of the protein, and no difference in the medial concentration between short and long cells (Saunders et al. 2012; Pan et al. 2014). Furthermore, Δ*pom1* cells maintain a size control mechanism: although there is a heterogeneous size at birth in these strains (due to the increased asymmetric division in this background), their SAD has a low variation, implying that cells are able to correct for size over the course of a cell cycle (Wood and Nurse 2013). This indicates that the regulation of size homeostasis cannot solely rely on a potential Pom1 gradient. Finally, the model of Pom1 does not address all facets of size control such as ploidy, multinucleated cells, and shape mutants (Wood and Nurse 2015).

Although the Pom1 gradient model does not fully address the question of how cells control their size, it may contribute to a larger network regulating size homeostasis. In fact, more recent work has highlighted that Cdr2 activity itself is size-dependent, and that Wee1 localisation occurs in

short bursts at these nodes that increase in frequency as the cell gets bigger (Allard et al. 2018). The increasing frequency of Wee1 to the nodes promotes mitotic entry, and ends the G2 period of growth. Additionally, Cdc25 transcription levels are also size-dependent (Keifenheim et al. 2017), which would implicate another regulatory mechanism upstream of the Wee1/Cdc25 feedback loop. Interestingly, although the mitotic entry switch was considered to be the downstream regulator of size in fission yeast, cells devoid of this control are still exhibit size correction, albeit not perfectly (Wood and Nurse 2013; Coudreuse and Nurse 2010a). Thus, it is likely that a number of processes, and not a singular mechanism, are integrated to maintain size homeostasis.
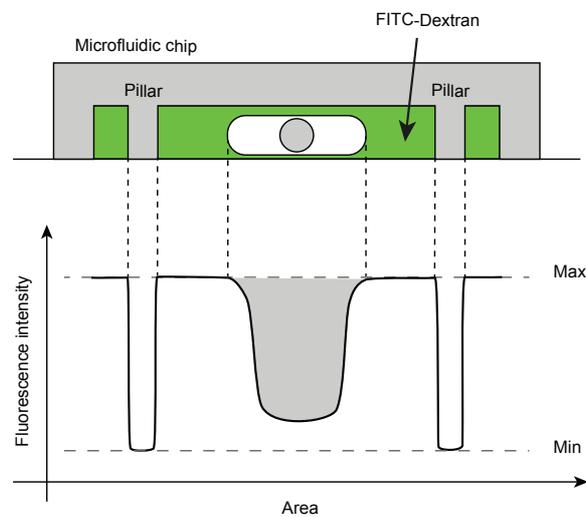
Figure 14: A schematic representation of the principles of FXm
Top: cells are injected into a microfluidic chip with FITC-Dextran. The chamber is supported by pillars, which are also used for image normalisation. Bottom: Cell volume is determined by measuring the displacement of fluorescence by the cell, after normalisation using the pillars. Figure was adapted from (García-Ruano et al. 2021).

To study size control in cells, it may be more useful to consider volume instead of length for several reasons. Firstly, length in fission yeast is highly specific to the model, and does not apply to other non-rod shaped cells. Second, length does not provide insight into the internal chemistry, and given proteins such as enzymes are highly influenced by changes in concentrations, volume would be a far more useful parameter in this regard. Finally, exchanges cells have with the environment are dependent on surface area, and this can only be considered through volume and not length. For this reason, cell length on its own may be unreliable because it does not account for the broad spectrum of size control, so the consideration of volume may provide further insight into size control.

To study the implication of volume is size regulation, our lab has adapted a newly developed method for measuring cell volume using fluorescent exclusion in fission yeast (Figure 14). The

method will allow us to measure the volume of entire populations of fission yeast of various shapes and sizes, and has proven to be more broadly relevant for size control in cells. Furthermore, we have also demonstrated the possibility to track the dynamic change in volume of individual cells using microfluidics, which would allow us to explore how changes in cell cycle regulation are influenced by cell volume. We expect to uncover novel mechanisms for size control regulation, and potentially cell cycle control by developing a more accurate characterisation of cell size using the parameter of volume. This work has resulted in a publication presented in Chapter 3 of this thesis.

1.7 A Minimal Cdk Network

The fission yeast cell cycle regulatory network is controlled by the activity of Cdc2, which associates and dissociates with specific cyclins at different phases of the process. The kinase activity of Cdc2 is balanced between two steady states, active and inactive, creating an oscillation between states of phosphorylation and dephosphorylation (mitosis and interphase respectively) of the cell cycle substrates. The transition from interphase to mitosis and vice versa is predominantly controlled by the Wee1/Cdc25 feedback loop and the action of the APC/C, as previously discussed, which act as tightly controlled bistable switch mechanisms. Additionally, in wild type fission yeast, the cyclins Cig1, Cig2, Puc1, and Cdc13 follow specific expression and degradation programs, which act as an additional regulatory element of Cdc2 activity (García-Blanco and Moreno 2019; Chang et al. 2001; Daniel Fisher and Nurse 1995). Ultimately, all of these features of the fission yeast cell cycle regulatory network function specifically to modulate the activity of Cdc2.
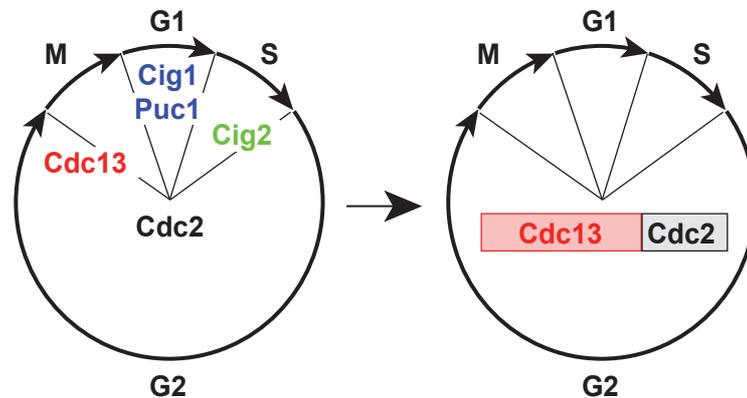
Figure 15: The integrated synthetic regulatory circuit of the MCN
The MCN is able to drive the cell cycle by maintaining the necessary oscillations in CDK activity through a chimeric fusion protein of Cdc13::Cdc2.

The presence of different cyclins that are temporally expressed to modulate the timing of Cdc2 activity has long been interpreted as a model of control that is dependent on qualitative inputs influencing substrate specificity at different stages of the cell cycle. Given the diversity and variety of cyclins and Cdks, this qualitative model of cell cycle control has been implicated across all eukaryotes. Indeed, events of the cell cycle, such as replication and chromosome segregation, are vastly different and require very different substrates to be phosphorylated, which favours the idea of a qualitative model. However, experimental results indicated the contrary, as there was a surprising

amount of redundancy observed in the cell cycle regulatory network, which has been demonstrated in fission yeast (Stern and Nurse 1996).

Three of the cell cycle cyclins (Cig1, Cig2, and Puc1) were demonstrated to be dispensable, with triple mutants shown to be capable of completing a full cell cycle, albeit with a delayed S phase (Daniel L. Fisher and Nurse 1996). Specifically, Cig2 and Puc1 were previously shown to play a role in G1 for the initiation of replication (Mondesert, McGowan, and Russell 1996), but it is not required as Δ*cig2* and Δ*puc1* cells are able to undergo replication, albeit with a slight delay to the onset of S phase (Stern and Nurse 1996; Martín-Castellanos et al. 2000). Only the mitotic B type cyclin, Cdc13, is essential, as Δ*cdc13* strains do not enter mitosis and instead enter continuous rounds of replication, in part due to a loss in Cdk activity required to enter mitosis (Daniel L. Fisher and Nurse 1996). These results indicated that Cdc13 alone was potentially able to drive the cell cycle in the absence of the other cyclins, and that possibly the oscillation of Cdc13/Cdc2 activity was all that was necessary to execute events such as replication and chromosome segregation (Stern and Nurse 1996).

To demonstrate the hypothesis of a quantitative model of cell cycle control, the MCN was constructed with the goal of replacing the complex endogenous cell cycle machinery with an integrated synthetic circuit (Figure 15). The MCN's cell cycle regulatory network is composed of a single chimeric fusion protein of Cdc13::Cdc2 which is under the *cdc13* regulatory elements, and is integrated into a background that lacks the core elements of the endogenous cell cycle network (Δ*cdc2* Δ*cig1* Δ*cig2* Δ*puc1* Δ*cdc13*) (Coudreuse and Nurse 2010a). This network bypasses a number of key aspects of the normal system: there is no cyclin diversity, Cdc13 and Cdc2 are in a 1:1 ratio, and both components are subject to the same expression, degradation and localisation programs. Impressively, cells with this integrated synthetic regulatory circuit behave essentially like wild-type cells, with no observable differences in proliferation or cell cycle organisation. Furthermore, manipulation of these MCN cells demonstrated that the core principle of the cell cycle regulatory network is to maintain the correct oscillation of Cdk activity between the S and M phase thresholds.

The correct oscillation of Cdk activity is maintained in MCN cells through intact regulation of mitotic entry by the Wee1/Cdc25 feedback loop, and the degradation program of the fusion protein at mitotic exit by the APC/C. Interestingly, the dynamic interaction of Cdc13/Cdc2 and Rum1 in G1 is predicted to be different in the MCN compared to wild type, as simulations imply that Rum1 more tightly interacts with the phosphorylated form of Cdc13/Cdc2 complexes (Gérard et al. 2015). This means that as Cdc25 increasingly dephosphorylates the fusion protein, the

unphosphorylated complex will progressively inhibit Rum1, allowing the overall Cdk activity to rise. Normally in wild type this is achieved through the action of Cig2/Cdc2 and Puc1/Cdc2 complexes, as explained earlier (Martín-Castellanos et al. 2000). Although Rum1 appears to be inhibited differently in the MCN, the resulting cell cycle phase duration remains unchanged, but it does provide us with a unique setting to further simplify the cell cycle regulatory network.

This hypothesised difference between the MCN and wild-type backgrounds explains a unique feature of MCN cells, in which abrogation of the Wee1/Cdc25 feedback loop remains viable. In a wild-type background as loss of the mitotic entry switch causes cells to prematurely enter M phase and undergo "mitotic catastrophe" (when chromosome segregation occurs before replication is complete) (Coudreuse and Nurse 2010a). However, in simulations of MCN Δ*wee1* Δ*mik1* there were increased levels of unphosphorylated Cdc13::Cdc2 complexes which were more tightly bound to Rum1 and thus remain inhibited for longer, this provided more time for cells to complete DNA replication before entry into mitosis (Gérard et al. 2015). Thus, MCN cells with a non-functioning Wee1/Cdc25 regulatory mechanism have a reduced lethality by mitotic catastrophe, because of the additional time to prepare properly before entry into mitosis.

This means that using the MCN; we have the possibility to bypass an essential and highly conserved feedback loop that controls mitotic entry in eukaryotic cells. The absence of the Wee1/Cdc25 feedback loop in the MCN allows us to explore the alternative mechanisms that cells can utilise to regain cell cycle control. In MCN cells, we are able to abrogate the mitotic entry switch through mutating the Wee1 target sites on Cdc2 (T14A Y15F). These cells are referred to as MCN-AF, and are a further simplification of the cell cycle regulatory network that have severely impaired growth. The reduced proliferative potential of MCN-AF make for an interesting start point for experimental evolution, where we can uncover mechanism that compensate for the loss of mitotic entry switch (Coudreuse and Nurse 2010a).

1.8 Aim of Thesis: Alternative Paths to Proliferation

Cell cycle regulation is an essential aspect of the biology of eukaryotic cells, playing a key role in a host of processes during development and in adult tissues. Furthermore, deregulation of the controls that delineate cell cycle progression can result in abnormal cell proliferation, a feature that is common to all tumors. Despite decades of investigation, a number of key aspects of the mechanisms that underlay cell proliferation remain unclear, and in particular how cells enhance their proliferation rate in adverse conditions or when critical cell cycle controls are altered, a process that is key for adaptation and evolution. In my project, I will take a unique and unprecedented strategy to investigate how cells, in which signals that are essential to cell cycle progression are impaired, can remodel their cell cycle control network to bypass these controls and recover a high proliferative potential.

MCN-AF cells were subject to experimental evolution, and this led to the identification of genetic alterations that bypass the requirement for essential branches of the cell cycle network, which allowed for the significant recovery of the proliferation potential. The goal of the project is to study the molecular and dynamic mechanisms underlying this improved growth. From this we will be able to identify novel pathways for regulating proliferation and possibly alternative mechanisms of cell cycle control that are normally hidden behind the dominant Wee1/Cdc25 feedback loop.

This study demonstrates a strategy cells can take to overcome the loss of the Wee1/Cdc25 feedback loop, through the modulation of Cdk activity. Indeed, through population and single cell characterisations of the evolved MCN-AF clones, we have examined the extent of the recovery the beneficial mutation has provided. Additionally, using molecular genetics, we have successfully uncovered how the evolved clones are improved, and identified new regulatory pathways for proliferation. Spo12, a protein of unknown function, was shown to potentiate Cdk activity, and thus acts in a novel feedback loop on Cdk1. This discovery highlights two key concepts: 1) hidden behind the dominance of the Wee1/Cdc25 feedback loop are alternative pathways that influence the dynamics of Cdk activity, and 2) cells can mutate these pathways to change Cdk activity in order to recover their proliferations potential. The results presented here encompass the value of combining a synthetic biology approach with experimental evolution to further understand cell cycle control.

The output of this multidisciplinary project will therefore be two-fold. On one hand, it will bring new insights into the dynamic principles of the core control of cell proliferation in eukaryotes. Through uncovering and describing alternative pathways, previously unknown, which modulate Cdk activity we can better understand the rational for the highly conserved Wee1/Cdc25 feedback loop in eukaryotes. Furthermore, we can explore other mechanisms of control that may be present in cells and better understand their relevance. On the other hand, cancer cells are often referred to as models of rapid evolution. Based on the results of laboratory evolution experiments, this work will allow us to reveal novel mechanisms by which the acquisition of resistance to therapy may be brought about.

1.9 References

Abraham, Robert T. 2001. "Cell Cycle Checkpoint Signaling through the ATM and ATR Kinases." *Genes and Development* 15 (17): 2177–96. https://doi.org/10.1101/gad.914401.

Allard, Corey A.H., Hannah E. Opalko, Ko Wei Liu, Uche Medoh, and James B. Moseley. 2018. "Cell Size-Dependent Regulation of Wee1 Localization by Cdr2 Cortical Nodes." *Journal of Cell Biology* 217 (5): 1589–99. https://doi.org/10.1083/jcb.201709171.

Alon, Uri. 2006. *An Introduction to Systems Biology*. Chapman and Hall/CRC. https://doi.org/10.1201/9781420011432.

———. 2007. "Network Motifs: Theory and Experimental Approaches." *Nature Reviews Genetics* 8 (6): 450–61. https://doi.org/10.1038/nrg2102.

Amodeo, Amanda A, and Jan M Skotheim. 2015. "Cell-Size Control."

Andersen, Jens S., Christopher J. Wilkinson, Thibault Mayor, Peter Mortensen, Erich A. Nigg, and Matthias Mann. 2003. "Proteomic Characterization of the Human Centrosome by Protein Correlation Profiling." *Nature* 426 (6966): 570–74. https://doi.org/10.1038/nature02166.

Antonin, Wolfram, and Heinz Neumann. 2016. "Chromosome Condensation and Decondensation during Mitosis." *Current Opinion in Cell Biology* 40: 15–22. https://doi.org/10.1016/j.ceb.2016.01.013.

Azzam, Ramzi, Susan L. Chen, Wenying Shou, Angie S. Mah, Gabriela Alexandru, Kim Nasmyth, Roland S. Annan, Steven A. Carr, and Raymond J. Deshaies. 2004. "Phosphorylation by Cyclin B-Cdk Underlies Release of Mitotic Exit Activator Cdc14 from the Nucleolus." *Science* 305 (5683): 516–19. https://doi.org/10.1126/science.1099402.

Banyai, Gabor, Feriel Baïdi, Damien Coudreuse, and Zsolt Szilagyi. 2016. "Cdk1 Activity Acts as a Quantitative Platform for Coordinating Cell Cycle Progression with Periodic Transcription." *Nature Communications* 7. https://doi.org/10.1038/ncomms11161.

Baro, Bàrbara, Ethel Queralt, and Fernando Monje-Casas. 2017. "Regulation of Mitotic Exit in Saccharomyces Cerevisiae." *Methods in Molecular Biology* 1505: 3–17. https://doi.org/10.1007/978-1-4939-6502-1_1.

Barr, Alexis R., and Fanni Gergely. 2007. "Aurora-A: The Maker and Breaker of Spindle Poles." *Journal of Cell Science* 120 (17): 2987–96. https://doi.org/10.1242/jcs.013136.

Barros, Teresa P., Kazuhisa Kinoshita, Anthony A. Hyman, and Jordan W. Raff. 2005. "Aurora A Activates D-TACC-Msps Complexes Exclusively at Centrosomes to Stabilize Centrosomal Microtubules." *Journal of Cell Biology* 170 (7): 1039–46. https://doi.org/10.1083/jcb.200504097.

Baum, Buzz, Jérôme Wuarin, and Paul Nurse. 1997. "Control of S-Phase Periodic Transcription in the Fission Yeast Mitotic Cycle." *EMBO Journal* 16 (15): 4676–88. https://doi.org/10.1093/emboj/16.15.4676.

Bell, Stephen P., and Anindya Dutta. 2002. "DNA Replication in Eukaryotic Cells." *Annual Review of Biochemistry* 71: 333–74. https://doi.org/10.1146/annurev.biochem.71.110601.135425.

Benito, Javier, Cristina Martín-Castellanos, and Sergio Moreno. 1998. "Regulation of the G1 Phase of the Cell Cycle by Periodic Stabilization and Degradation of the P25(Rum1) CDK Inhibitor." *EMBO Journal* 17 (2): 482–97. https://doi.org/10.1093/emboj/17.2.482.

Benner, Steven A., and A. Michael Sismour. 2005. "Synthetic Biology." *Nature Reviews Genetics* 6 (7): 533–43. https://doi.org/https://doi.org/10.1038/35002125.

Berthet, Cyril, Eiman Aleem, Vincenzo Coppola, Lino Tessarollo, and Philipp Kaldis. 2003. "Cdk2 Knockout Mice Are Viable." *Current Biology* 13 (20): 1775–85. https://doi.org/10.1016/j.cub.2003.09.024.

Bettignies, Geoffroy de, and Leland H. Johnston. 2003. "The Mitotic Exit Network." *Current Biology : CB* 13 (8): 301. https://doi.org/10.1016/s0960-9822(03)00230-6.

Blanco, Miguel a, Alberto Sánchez-Díaz, José M. de Prada, and Sergio Moreno. 2000. "APC Ste9/Srw1 Promotes Degradation of Mitotic Cyclins in G 1 and Is Inhibited by Cdc2 Phosphorylation." *The EMBO Journal* 19 (15): 3945–55. https://doi.org/10.1093/emboj/19.15.3945.

Bloom, Joanna, and Frederick R. Cross. 2007. "Multiple Levels of Cyclin Specificity in Cell-Cycle Control." *Nature Reviews Molecular Cell Biology* 8 (2): 149–60. https://doi.org/10.1038/nrm2105.

Boettcher, Barbara, and Yves Barral. 2013. "The Cell Biology of Open and Closed Mitosis." *Nucleus (United States)* 4 (3): 160–65. https://doi.org/10.4161/nucl.24676.

Bokros, Michael, Curtis Gravenmier, Fengzhi Jin, Daniel Richmond, and Yanchang Wang. 2016. "Fin1-PP1 Helps Clear Spindle Assembly Checkpoint Protein Bub1 from Kinetochores in Anaphase." *Cell Reports* 14 (5): 1074–85. https://doi.org/10.1016/j.celrep.2016.01.007.

Bokros, Michael, and Yanchang Wang. 2016. "Spindle Assembly Checkpoint Silencing and Beyond." *Cell Cycle* 15 (13): 1661–62. https://doi.org/10.1080/15384101.2016.1176396.

Burtelow, Matthew A., Scott H. Kaufmann, and Larry M. Karnitz. 2000. "Retention of the Human Rad9 Checkpoint Complex in Extraction-Resistant Nuclear Complexes after DNA Damage." *Journal of Biological Chemistry* 275 (34): 26343–48. https://doi.org/10.1074/jbc.M001244200.

Çağatay, Tolga, Marc Turcotte, Michael B. Elowitz, Jordi Garcia-Ojalvo, and Gürol M. Süel. 2009. "Architecture-Dependent Noise Discriminates Functionally Analogous Differentiation Circuits." *Cell* 139 (3): 512–22. https://doi.org/10.1016/j.cell.2009.07.046.

Callens, Céline, Nelson C. Coelho, Aaron W. Miller, Maria Rosa Domingo Sananes, Maitreya J. Dunham, Matthieu Denoual, and Damien Coudreuse. 2017. "A Multiplex Culture System for the Long-Term Growth of Fission Yeast Cells." *Yeast* 34 (8): 343–55. https://doi.org/10.1002/yea.3237.

Carroll, Sean Michael, and Christopher J. Marx. 2013. "Evolution after Introduction of a Novel Metabolic Pathway Consistently Leads to Restoration of Wild-Type Physiology." *PLoS Genetics* 9 (4). https://doi.org/10.1371/journal.pgen.1003427.

Chang, L., J. L. Morrell, A. Feoktistova, and K. L. Gould. 2001. "Study of Cyclin Proteolysis in Anaphase-Promoting Complex (APC) Mutant Cells Reveals the Requirement for APC Function in the Final Steps of the Fission Yeast Septation Initiation Network." *Molecular and Cellular Biology* 21 (19): 6681–94. https://doi.org/10.1128/mcb.21.19.6681-6694.2001.

Cheeseman, Iain M. 2014. "The Kinetochore." *Cold Spring Harbor Perspectives in Biology* 6 (7): 1–18. https://doi.org/10.1101/cshperspect.a015826.

Chen, C.-T., M.-P. Peli-Gulli, V. Simanis, and D. McCollum. 2006. "S. Pombe FEAR Protein Orthologs Are Not Required for Release of Clp1/Flp1 Phosphatase from the Nucleolus during Mitosis." *Journal of Cell Science* 119 (21): 4462–66. https://doi.org/10.1242/jcs.03220.

Chen, Chun-hong, Haixia Huang, Catherine M. Ward, Jessica T. Su, Lorian V Schaeffer, Ming Guo, and Bruce a Hay. 2007. "A Synthetic Maternal-Effect Selfish Genetic Element Drives Population Replacement in Drosophila." *Science* 316 (5824): 597–600. https://doi.org/10.1126/science.1138595.

Colegrave, N., and S. Collins. 2008. "Experimental Evolution: Experimental Evolution and Evolvability." *Heredity* 100 (5): 464–70. https://doi.org/10.1038/sj.hdy.6801095.

Conduit, Paul T., Zhe Feng, Jennifer H. Richens, Janina Baumbach, Alan Wainman, Suruchi D. Bakshi, Jeroen Dobbelaere, Steven Johnson, Susan M. Lea, and Jordan W. Raff. 2014. "The Centrosome-Specific Phosphorylation of Cnn by Polo/Plk1 Drives Cnn Scaffold Assembly and Centrosome Maturation." *Developmental Cell* 28 (6): 659–69. https://doi.org/10.1016/j.devcel.2014.02.013.

Conlon, Ian, and Martin Raff. 2003. "Differences in the Way a Mammalian Cell and Yeast Cells Coordinate Cell Growth and Cell-Cycle Progression." *Journal of Biology* 2 (1): 1–10.

Cook, Mike, and Mike Tyers. 2007. "Size Control Goes Global." *Current Opinion in Biotechnology* 18 (4): 341–50. https://doi.org/10.1016/j.copbio.2007.07.006.

Cooper, Vaughn S. 2018. "Experimental Evolution as a High-Throughput Screen for Genetic Adaptations." *MSphere* 3 (3): 1–7. https://doi.org/10.1128/msphere.00121-18.

Correa-Bordes, Jaime, and Paul Nurse. 1995. "P25rum1 Orders S Phase and Mitosis by Acting as an Inhibitor of the P34cdc2 Mitotic Kinase." *Cell* 83 (6): 1001–9. https://doi.org/10.1016/0092-8674(95)90215-5.

Coudreuse, Damien. 2016. "Insights from Synthetic Yeasts." *Yeast* 33 (9): 483–92. https://doi.org/10.1002/yea.3169.

Coudreuse, Damien, and Paul Nurse. 2010a. "Driving the Cell Cycle with a Minimal CDK Control Network." *Nature* 468 (7327): 1074–80. https://doi.org/10.1038/nature09543.

———. 2010b. "Driving the Cell Cycle with a Minimal CDK Control Network." *Nature* 468 (December): 1074. https://doi.org/10.1038/nature09543.

Crncec, Adrijana, and Helfrid Hochegger. 2019. "Triggering Mitosis." *FEBS Letters* 593 (20): 2868–88. https://doi.org/10.1002/1873-3468.13635.

Csete, Marie, and John Doyle. 2004. "Bow Ties, Metabolism and Disease." *Trends in Biotechnology* 22 (9): 446–50. https://doi.org/10.1016/j.tibtech.2004.07.007.

Csikász-Nagy, Attila, Orsolya Kapuy, Attila Tóth, Csaba Pál, Lars Juhl Jensen, Frank Uhlmann, John J. Tyson, and Béla Novák. 2009. "Cell Cycle Regulation by Feed-Forward Loops Coupling Transcription and Phosphorylation." *Molecular Systems Biology* 5 (236). https://doi.org/10.1038/msb.2008.73.

Cvrčková, Fatima. 2018. "A Brief History of Eukaryotic Cell Cycle Research." *Plant Cell Monographs* 23 (January): 67–93. https://doi.org/10.1007/978-3-319-69944-8_4.

D'Amours, Damien, and Angelika Amon. 2004. "At the Interface between Signaling and Executing Anaphase - Cdc14 and the FEAR Network." *Genes and Development* 18 (21): 2581–95. https://doi.org/10.1101/gad.1247304.

D'Urso, Gennaro, and Paul Nurse. 1995. "Checkpoints in the Cell Cycle of Fission Yeast." *Current Opinion in Genetics and Development* 5 (1): 12–16. https://doi.org/10.1016/S0959-437X(95)90047-0.

Davies, Jamie. 2017. "Using Synthetic Biology to Explore Principles of Development." *Development (Cambridge)* 144 (7): 1146–58. https://doi.org/10.1242/dev.144196.

Deritei, Dávid, Jordan Rozum, Erzsébet Ravasz Regan, and Réka Albert. 2019. "A Feedback Loop of Conditionally Stable Circuits Drives the Cell Cycle from Checkpoint to Checkpoint." *Scientific Reports* 9 (1): 1–19. https://doi.org/10.1038/s41598-019-52725-1.

Derouiche, Abderahmane, Charlotte Cousin, and Ivan Mijakovic. 2012. "Protein Phosphorylation from the

Perspective of Systems Biology." *Current Opinion in Biotechnology* 23 (4): 585–90. https://doi.org/10.1016/j.copbio.2011.11.008.

Dinarina, Ana, Patricia G. Santamaria, and Angel R. Nebreda. 2009. "Cell Cycle Regulation of the Mammalian CDK Activator RINGO/Speedy A." *FEBS Letters* 583 (17): 2772–78. https://doi.org/10.1016/j.febslet.2009.07.028.

Domingo-Sananes, Maria Rosa, Orsolya Kapuy, Tim Hunt, and Bela Novak. 2011. "Switches and Latches: A Biochemical Tug-of-War between the Kinases and Phosphatases That Control Mitosis." *Philosophical Transactions of the Royal Society B: Biological Sciences* 366 (1584): 3584–94. https://doi.org/10.1098/rstb.2011.0087.

Doxsey, Stephen, Wendy Zimmerman, and Keith Mikule. 2005. "Centrosome Control of the Cell Cycle." *Trends in Cell Biology* 15 (6): 303–11. https://doi.org/10.1016/j.tcb.2005.04.008.

Dutta, Chaitali, and Nicholas Rhind. 2009. "The Role of Specific Checkpoint-Induced S-Phase Transcripts in Resistance to Replicative Stress." *PLoS ONE* 4 (9). https://doi.org/10.1371/journal.pone.0006944.

Echalier, Aude, Emilie Cot, Alain Camasses, Elsie Hodimont, Franois Hoh, Philippe Jay, Felix Sheinerman, Liliana Krasinska, and Daniel Fisher. 2012. "An Integrated Chemical Biology Approach Provides Insight into Cdk2 Functional Redundancy and Inhibitor Sensitivity." *Chemistry and Biology* 19 (8): 1028–40. https://doi.org/10.1016/j.chembiol.2012.06.015.

Elowe, Sabine. 2011. "Bub1 and BubR1: At the Interface between Chromosome Attachment and the Spindle Checkpoint." *Molecular and Cellular Biology* 31 (15): 3085–93. https://doi.org/10.1128/mcb.05326-11.

Elowitz, Michael B., and Stanislas Leibler. 2000. "A Synthetic Oscillatory Network of Transcriptional Regulators." *Nature* 403 (6767): 335–38. https://doi.org/10.1038/35002125.

Eot-Houllier, Grégory, Laura Magnaghi-Jaulin, Géraldine Fulcrand, François Xavier Moyroud, Solange Monier, and Christian Jaulin. 2018. "Aurora A-Dependent CENP-A Phosphorylation at Inner Centromeres Protects Bioriented Chromosomes against Cohesion Fatigue." *Nature Communications* 9 (1). https://doi.org/10.1038/s41467-018-04089-9.

Fantes, P. A., W. D. Grant, R. H. Pritchard, P. E. Sudbery, and A. E. Wheals. 1975. "The Regulation of Cell Size and the Control of Mitosis." *Journal of Theoretical Biology* 50 (1): 213–44. https://doi.org/10.1016/0022-5193(75)90034-X.

Fantes, P., and P. Nurse. 1977. "Control of Cell Size at Division in Fission Yeast by a Growth-Modulated Size Control over Nuclear Division." *Experimental Cell Research* 107 (2): 377–86. https://doi.org/10.1016/0014-4827(77)90359-7.

Ferrell, James E. 2013. "Feedback Loops and Reciprocal Regulation: Recurring Motifs in the Systems Biology of the Cell Cycle." *Current Opinion in Cell Biology* 25 (6): 676–86. https://doi.org/10.1016/j.ceb.2013.07.007.

Fisher, D., L. Krasinska, D. Coudreuse, and B. Novak. 2012. "Phosphorylation Network Dynamics in the Control of Cell Cycle Transitions." *Journal of Cell Science* 125 (20): 4703–11. https://doi.org/10.1242/jcs.106351.

Fisher, D. L., and P. Nurse. 1996. "A Single Fission Yeast Mitotic Cyclin B P34cdc2 Kinase Promotes Both S-Phase and Mitosis in the Absence of G1 Cyclins." *EMBO Journal* 15 (4): 850–60. https://doi.org/10.1002/j.1460-2075.1996.tb00420.x.

Fisher, Daniel L., and Paul Nurse. 1996. "A Single Fission Yeast Mitotic Cyclin B P34cdc2 Kinase Protoes Both S-Phase and Mitosis in the Absence of G1 Cyclins." *The EMBO Journal* 15 (4): 850–60. https://doi.org/10.1016/j.neubiorev.2011.05.014.

Fisher, Daniel, and Paul Nurse. 1995. "Cyclins of the Fission Yeast Schizosaccharomyces Pombe." *Seminars in Cell Biology* 6 (2): 73–78. https://doi.org/10.1016/1043-4682(95)90003-9.

Fragkos, Michalis, Olivier Ganier, Philippe Coulombe, and Marcel Méchali. 2015. "DNA Replication Origin Activation in Space and Time." *Nature Reviews Molecular Cell Biology* 16 (6): 360–74. https://doi.org/10.1038/nrm4002.

Fu, Jingyan, Iain M. Hagan, and David M. Glover. 2015. "The Centrosome and Its Duplication Cycle." *Cold Spring Harbor Perspectives in Medicine* 5 (1): 1–36. https://doi.org/10.1101/cshperspect.a015800.

García-Blanco, Natalia, and Sergio Moreno. 2019. "Down-Regulation of Cdk1 Activity in G1 Coordinates the G1/S Gene Expression Programme with Genome Replication." *Current Genetics* 65 (3): 685–90. https://doi.org/10.1007/s00294-018-00926-y.

García-Ruano, Daniel, Akanksha Jain, Joseph C Ryan, Vasanthakrishnan Radhakrishnan Balasubramaniam, Larisa Venkova, Matthieu Piel, and Damien Coudreuse. 2021. "Fluorescence Exclusion: A Rapid, Accurate and Powerful Method for Measuring Yeast Cell Volume." *BioRxiv*, January, 2021.10.07.463508. https://doi.org/10.1101/2021.10.07.463508.

Gardner, Timothy S, Charles R Cantor, and James J Collins. 2000. "Construction of a Genetic Toggle Switch in Escherichia Coli." *Nature* 403 (6767): 339–42. https://doi.org/10.1038/35002131.

Gascoigne, Karen E., and Iain M. Cheeseman. 2013. "CDK-Dependent Phosphorylation and Nuclear Exclusion Coordinately Control Kinetochore Assembly State." *Journal of Cell Biology* 201 (1): 23–32. https://doi.org/10.1083/jcb.201301006.

Gérard, Claude, John J. Tyson, Damien Coudreuse, and Béla Novák. 2015. "Cell Cycle Control by a Minimal Cdk Network." *PLoS Computational Biology* 11 (2): 1–27. https://doi.org/10.1371/journal.pcbi.1004056.

Gharbi-Ayachi, Aicha, Jean Claude Labbé, Andrew Burgess, Suzanne Vigneron, Jean Marc Strub, Estelle Brioudes, Alain Van-Dorsselaer, Anna Castro, and Thierry Lorca. 2010. "The Substrate of Greatwall Kinase, Arpp19, Controls Mitosis by Inhibiting Protein Phosphatase 2A." *Science* 330 (6011): 1673–77. https://doi.org/10.1126/science.1197048.

Gould, Kathleen L., and Paul Nurse. 1989. "Tyrosine Phosphorylation of the Fission Yeast Cdc2+ Protein Kinase Regulates Entry into Mitosis." *Nature* 342 (6245): 39–45. https://doi.org/10.1038/342039a0.

Grallert, Agnes, Elvan Boke, Anja Hagting, Ben Hodgson, Yvonne Connolly, John R. Griffiths, Duncan L. Smith, Jonathon Pines, and Iain M. Hagan. 2015. "A PP1-PP2A Phosphatase Relay Controls Mitotic Progression." *Nature* 517 (7532): 94–98. https://doi.org/10.1038/nature14019.

Gutiérrez-Escribano, Pilar, and Paul Nurse. 2015. "A Single Cyclin-CDK Complex Is Sufficient for Both Mitotic and Meiotic Progression in Fission Yeast." *Nature Communications* 6. https://doi.org/10.1038/ncomms7871.

Hanahan, Douglas, and Robert A. Weinberg. 2011. "Hallmarks of Cancer: The next Generation." *Cell* 144 (5): 646–74. https://doi.org/10.1016/j.cell.2011.02.013.

Harrison, Jacob C., and James E. Haber. 2006. "Surviving the Breakup: The DNA Damage Checkpoint." *Annual Review of Genetics* 40: 209–35. https://doi.org/10.1146/annurev.genet.40.051206.105231.

Hayles, Jacqueline, and Paul Nurse. 1992. "Genetics of the Fission Yeast Schizosaccharomyces Pombe."
Annual Review of Genetics 26: 373–402. https://doi.org/10.1146/annurev.ge.26.120192.002105.

Hellmuth, Susanne, Cristina Gutiérrez‑Caballero, Elena Llano, Alberto M Pendás, and Olaf Stemmann. 2018.
"Local Activation of Mammalian Separase in Interphase Promotes Double‑strand Break Repair and
Prevents Oncogenic Transformation." *The EMBO Journal* 37 (22): 1–17.
https://doi.org/10.15252/embj.201899184.

Hermeking, Heiko, and Anne Benzinger. 2006. "14-3-3 Proteins in Cell Cycle Regulation." *Seminars in Cancer
Biology* 16 (3): 183–92. https://doi.org/10.1016/j.semcancer.2006.03.002.

Hirano, Tatsuya. 2005. "Condensins: Organizing and Segregating the Genome." *Current Biology* 15 (7): 265–
75. https://doi.org/10.1016/j.cub.2005.03.037.

Hoang, Kim L., Levi T. Morran, and Nicole M. Gerardo. 2016. "Experimental Evolution as an Underutilized
Tool for Studying Beneficial Animal-Microbe Interactions." *Frontiers in Microbiology* 7 (SEP): 1–16.
https://doi.org/10.3389/fmicb.2016.01444.

Hochegger, H, Takeda. A, and T Hunt. 2008. "PersPectives Cyclin-Dependent Kinases and Cell-Cycle
Transitions : Does One Fit All ?" *Nature* 9 (NOvEmBER): 911–16. https://doi.org/10.1038/nrm2510.

Hochegger, Helfrid, Shunichi Takeda, and Tim Hunt. 2008. "Cyclin-Dependent Kinases and Cell-Cycle
Transitions: Does One Fit All?" *Nature Reviews Molecular Cell Biology* 9 (11): 910–16.
https://doi.org/10.1038/nrm2510.

Hornig, Nadine C.D., Philip P. Knowles, Neil Q. McDonald, and Frank Uhlmann. 2002. "The Dual Mechanism
of Separase Regulation by Securin." *Current Biology* 12 (12): 973–82. https://doi.org/10.1016/S0960-
9822(02)00847-3.

Hotz, Manuel, and Yves Barral. 2014. "The Mitotic Exit Network: New Turns on Old Pathways." *Trends in
Cell Biology* 24 (3): 145–52. https://doi.org/10.1016/j.tcb.2013.09.010.

Izumi, T., and J. L. Maller. 1993. "Elimination of Cdc2 Phosphorylation Sites in the Cdc25 Phosphatase Blocks
Initiation of M-Phase." *Molecular Biology of the Cell* 4 (12): 1337–50.
https://doi.org/10.1091/mbc.4.12.1337.

Jagdish, Tanush, and Alex N Nguyen Ba. 2022. "Microbial Experimental Evolution in a Massively Multiplexed
and High-Throughput Era." *Current Opinion in Genetics & Development* 75: 101943.
https://doi.org/10.1016/j.gde.2022.101943.

Jeffares, Daniel C., Charalampos Rallis, Adrien Rieux, Doug Speed, Martin Převorovský, Tobias Mourier,
Francesc X. Marsellach, et al. 2015. "The Genomic and Phenotypic Diversity of Schizosaccharomyces
Pombe." *Nature Genetics* 47 (3): 235–41. https://doi.org/10.1038/ng.3215.

Jia, Luying, Bing Li, and Hongtao Yu. 2016. "The Bub1-Plk1 Kinase Complex Promotes Spindle Checkpoint
Signalling through Cdc20 Phosphorylation." *Nature Communications* 7: 1–14.
https://doi.org/10.1038/ncomms10818.

Jorgensen, Paul, Ivan Rupeš, Jeffrey R. Sharom, Lisa Schneper, James R. Broach, and Mike Tyers. 2004. "A
Dynamic Transcriptional Network Communicates Growth Potential to Ribosome Synthesis and Critical
Cell Size." *Genes and Development* 18 (20): 2491–2505. https://doi.org/10.1101/gad.1228804.

Kadura, Sheila, and Shelley Sazer. 2005. "SAC-Ing Mitotic Errors: How the Spindle Assembly Checkpoint
(SAC) Plays Defense against Chromosome Mis-Segregation." *Cell Motility and the Cytoskeleton* 61 (3):

145–60. https://doi.org/10.1002/cm.20072.

Karasu, Mehmet E., Nora Bouftas, Scott Keeney, and Katja Wassmann. 2019. "Cyclin B3 Promotes Anaphase i Onset in Oocyte Meiosis." *Journal of Cell Biology* 218 (4): 1265–81. https://doi.org/10.1083/jcb.201808091.

Kawecki, Tadeusz J., Richard E. Lenski, Dieter Ebert, Brian Hollis, Isabelle Olivieri, and Michael C. Whitlock. 2012. "Experimental Evolution." *Trends in Ecology and Evolution* 27 (10): 547–60. https://doi.org/10.1016/j.tree.2012.06.001.

Keifenheim, Daniel, Xi Ming Sun, Edridge D'Souza, Makoto J. Ohira, Mira Magner, Michael B. Mayhew, Samuel Marguerat, and Nicholas Rhind. 2017. "Size-Dependent Expression of the Mitotic Activator Cdc25 Suggests a Mechanism of Size Control in Fission Yeast." *Current Biology* 27 (10): 1491-1497.e4. https://doi.org/10.1016/j.cub.2017.04.016.

Kim, Juyoung, and Gohta Goshima. 2022. "Mitotic Spindle Formation in the Absence of Polo Kinase." *Proceedings of the National Academy of Sciences of the United States of America* 119 (12): 1–11. https://doi.org/10.1073/pnas.2114429119.

Kim, Sun Young, and James E. Ferrell. 2007. "Substrate Competition as a Source of Ultrasensitivity in the Inactivation of Wee1." *Cell* 128 (6): 1133–45. https://doi.org/10.1016/j.cell.2007.01.039.

Kraft, Claudine, Franz Herzog, Christian Gieffers, Karl Mechtler, Anja Hagting, Jonathon Pines, and Jan Michael Peters. 2003. "Mitotic Regulation of the Human Anaphase-Promoting Complex by Phosphorylation." *EMBO Journal* 22 (24): 6598–6609. https://doi.org/10.1093/emboj/cdg627.

Krapp, Andrea, Marie Pierre Gulli, and Viesturs Simanis. 2004. "SIN and the Art of Splitting the Fission Yeast Cell." *Current Biology* 14 (17): 722–30. https://doi.org/10.1016/j.cub.2004.08.049.

Kumagai, Akiko, and William G. Dunphy. 1996. "Purification and Molecular Cloning of Plx1, a Cdc25-Regulatory Kinase from Xenopus Egg Extracts." *Science* 273 (5280): 1377–80. https://doi.org/10.1126/science.273.5280.1377.

Laiho, Marikki, and Leena Latonen. 2003. "Cell Cycle Control, DNA Damage Checkpoints and Cancer." *Annals of Medicine* 35 (6): 391–97. https://doi.org/10.1080/07853890310014605.

Lee, Melanie G., and Paul Nurse. 1987. "Complementation Used to Clone a Human Homologue of the Fission Yeast Cell Cycle Control Gene Cdc2." *Nature* 327 (6117): 31–35. https://doi.org/10.1038/327031a0.

Lee, Tong Ihn, Nicola J. Rinaldi, François Robert, Duncan T. Odom, Ziv Bar-Joseph, Georg K. Gerber, Nancy M. Hannett, et al. 2002. "Transcriptional Regulatory Networks in Saccharomyces Cerevisiae." *Science* 298 (5594): 799–804. https://doi.org/10.1126/science.1075090.

Lenski, Richard E, Michael R Rose, Suzanne C Simpson, and Scott C Tadler. 2016. "Long-Term Experimental Evolution in Escherichia Coli . I . Adaptation and Divergence During 2 , 000 Generations Author (s): Richard E . Lenski , Michael R . Rose , Suzanne C . Simpson and Scott C . Tadler Published by : The University of Chicago Press F" 138 (6): 1315–41.

Leonard, Joshua N., Brian R. Fritz, Laura E. Timmerman, Nichole M. Daringer, and Michael C. Jewett. 2010. "Biology by Design: From Top to Bottom and Back." *Journal of Biomedicine and Biotechnology* 2010. https://doi.org/10.1155/2010/232016.

Lind, Peter A., and Dan I. Andersson. 2008. "Whole-Genome Mutational Biases in Bacteria." *Proceedings of the National Academy of Sciences of the United States of America* 105 (46): 17878–83.

https://doi.org/10.1073/pnas.0804445105.

Liu, Dan, Olga Davydenko, and Michael A. Lampson. 2012. "Polo-like Kinase-1 Regulates Kinetochore-Microtubule Dynamics and Spindle Checkpoint Silencing." *Journal of Cell Biology* 198 (4): 491–99. https://doi.org/10.1083/jcb.201205090.

López-Avilés, Sandra, Orsolya Kapuy, Béla Novák, and Frank Uhlmann. 2009. "Irreversibility of Mitotic Exit Is the Consequence of Systems-Level Feedback." *Nature* 459 (7246): 592–95. https://doi.org/10.1038/nature07984.

Lorca, T., and A. Castro. 2013. "The Greatwall Kinase: A New Pathway in the Control of the Cell Cycle." *Oncogene* 32 (5): 537–43. https://doi.org/10.1038/onc.2012.79.

Losada, Ana, Michiko Hirano, and Tatsuya Hirano. 2002. "Cohesin Release Is Required for Sister Chromatid Resolution, but Not for Condensin-Mediated Compaction, at the Onset of Mitosis." *Genes and Development* 16 (23): 3004–16. https://doi.org/10.1101/gad.249202.

Lucena, Rafael, Maria Alcaide-Gavilán, Steph D. Anastasia, and Douglas R. Kellogg. 2017. "Wee1 and Cdc25 Are Controlled by Conserved PP2A-Dependent Mechanisms in Fission Yeast." *Cell Cycle* 16 (5): 428–35. https://doi.org/10.1080/15384101.2017.1281476.

Lundgren, Karen, Nancy Walworth, Robert Booher, Marlene Dembski, Marc Kirschner, and David Beach. 1991. "Mik1 and Wee1 Cooperate in the Inhibitory Tyrosine Phosphorylation of Cdc2." *Cell* 64 (6): 1111–22. https://doi.org/10.1016/0092-8674(91)90266-2.

Luo, Shukun, and Liang Tong. 2021. "Structure and Function of the Separase-Securin Complex." In *Physiology & Behavior*, 176:217–32. https://doi.org/10.1007/978-3-030-58971-4_4.

Maddamsetti, Rohan, and Nkrumah A. Grant. 2020. "Divergent Evolution of Mutation Rates and Biases in the Long-Term Evolution Experiment with Escherichia Coli." *Genome Biology and Evolution* 12 (9): 1591–1603. https://doi.org/10.1093/GBE/EVAA178.

Maddamsetti, Rohan, Richard E. Lenski, and Jeffrey E. Barrick. 2015. "Adaptation, Clonal Interference, and Frequency-Dependent Interactions in a Long-Term Evolution Experiment with Escherichia Coli." *Genetics* 200 (2): 619–31. https://doi.org/10.1534/genetics.115.176677.

Martín-Castellanos, Cristina, Miguel A. Blanco, José M. De Prada, and Sergio Moreno. 2000. "The Puc1 Cyclin Regulates the G1 Phase of the Fission Yeast Cell Cycle in Response to Cell Size." *Molecular Biology of the Cell* 11 (2): 543–54. https://doi.org/10.1091/mbc.11.2.543.

Martin, Marivic, Theresa Hölscher, Anna Dragoš, Vaughn S. Cooper, and Ákos T. Kovács. 2016. "Laboratory Evolution of Microbial Interactions in Bacterial Biofilms." *Journal of Bacteriology* 198 (19): 2564–71. https://doi.org/10.1128/JB.01018-15.

Martin, Sophie G., and Martine Berthelot-Grosjean. 2009. "Polar Gradients of the DYRK-Family Kinase Pom1 Couple Cell Length with the Cell Cycle." *Nature* 459 (7248): 852–56. https://doi.org/10.1038/nature08054.

Martínez-Alonso, Diego, and Marcos Malumbres. 2020. "Mammalian Cell Cycle Cyclins." *Seminars in Cell and Developmental Biology* 107 (March): 28–35. https://doi.org/10.1016/j.semcdb.2020.03.009.

Matsuo, Kazuhiko, Keita Ohsumi, Mari Iwabuchi, Toshio Kawamata, Yoshitaka Ono, and Mikiko Takahashi. 2012. "Kendrin Is a Novel Substrate for Separase Involved in the Licensing of Centriole Duplication." *Current Biology* 22 (10): 915–21. https://doi.org/10.1016/j.cub.2012.03.048.

McAleenan, Alexandra, Andres Clemente-Blanco, Violeta Cordon-Preciado, Nicholas Sen, Miguel Esteras, Adam Jarmuz, and Luis Aragón. 2013. "Post-Replicative Repair Involves Separase-Dependent Removal of the Kleisin Subunit of Cohesin." *Nature* 493 (7431): 250–54. https://doi.org/10.1038/nature11630.

McIntosh, J. Richard. 2016. "Mitosis." *Cold Spring Harbor Perspectives in Biology* 8 (9): a023218. https://doi.org/10.1101/cshperspect.a023218.

Méchali, Marcel. 2010. "Eukaryotic DNA Replication Origins: Many Choices for Appropriate Answers." *Nature Reviews Molecular Cell Biology* 11 (10): 728–38. https://doi.org/10.1038/nrm2976.

Melo, Justine, and David Toczyski. 2002. "A Unified View of the DNA-Damage Checkpoint." *Current Opinion in Cell Biology* 14 (2): 237–45. https://doi.org/10.1016/S0955-0674(02)00312-5.

Mertz, Leslie. 2016. "All It Takes Is Vision: Synthetic Biology Opens the Doors to Vast Possibilities: \"Ideas Just Pop Into Your Head\"." *IEEE Pulse* 7 (2): 4–9. https://doi.org/10.1109/MPUL.2015.2513538.

Milo, R., S. Shen-Orr, S. Itzkovitz, N. Kashtan, D. Chklovskii, and U. Alon. 2002. "Network Motifs: Simple Building Blocks of Complex Networks." *Science* 298 (5594): 824–27. https://doi.org/10.1126/science.298.5594.824.

Mimura, Satoru, Takashi Seki, Seiji Tanaka, and John F.X. Diffley. 2004. "Phosphorylation-Dependent Binding of Mitotic Cyclins to Cdc6 Contributes to DNA Replication Control." *Nature* 431 (7012): 1118–23. https://doi.org/10.1038/nature03024.

Mochida, Satoru, Satoshi Ikeo, Julian Gannon, and Tim Hunt. 2009. "Regulated Activity of PP2A-B55 Is Crucial for Controlling Entry into and Exit from Mitosis in Xenopus Egg Extracts." *EMBO Journal* 28 (18): 2777–85. https://doi.org/10.1038/emboj.2009.238.

Mochida, Satoru, Scott Rata, Hirotsugu Hino, Takeharu Nagai, and Béla Novák. 2016. "Two Bistable Switches Govern M Phase Entry." *Current Biology* 26 (24): 3361–67. https://doi.org/10.1016/j.cub.2016.10.022.

Mohl, Dane A., Michael J. Huddleston, Therese S. Collingwood, Roland S. Annan, and Raymond J. Deshaies. 2009. "Dbf2-Mob1 Drives Relocalization of Protein Phosphatase Cdc14 to the Cytoplasm during Exit from Mitosis." *Journal of Cell Biology* 184 (4): 527–39. https://doi.org/10.1083/jcb.200812022.

Mondesert, O, C H McGowan, and P Russell. 1996. "Cig2, a B-Type Cyclin, Promotes the Onset of S in Schizosaccharomyces Pombe." *Molecular and Cellular Biology* 16 (4): 1527–33. https://doi.org/10.1128/mcb.16.4.1527.

Moreno-Torres, Marta, Malika Jaquenoud, and Claudio De Virgilio. 2015. "TORC1 Controls G 1 -S Cell Cycle Transition in Yeast via Mpk1 and the Greatwall Kinase Pathway." *Nature Communications* 6: 1–10. https://doi.org/10.1038/ncomms9256.

Moreno, Sergio, Amar Klar, and Paul Nurse. 1991. "Molecular Genetic Analysis of Fission Yeast Schizosaccharomyces Pombe." *Methods in Enzymology* 194 (C): 795–823. https://doi.org/10.1016/0076-6879(91)94059-L.

Morgan, David O. 1997a. "Cyclin-Dependent Kinases: Engines, Clocks, and Microprocessors." *Annual Review of Cell and Developmental Biology* 13: 261–91. https://doi.org/10.1146/annurev.cellbio.13.1.261.

Morgan, David O. 1997b. "CYCLIN-DEPENDENT KINASES: Engines, Clocks, and Microprocessors." *Annual Review of Cell and Developmental Biology* 13 (1): 261–91. https://doi.org/10.1146/annurev.cellbio.13.1.261.

———. 2007. *Primers in Biology The Cell Cycle Primers in Biology : Protein Structure and Function*

Forthcoming Titles :

Mori, Daisuke, Yoshihisa Yano, Kazuhito Toyo-oka, Noriyuki Yoshida, Masami Yamada, Masami Muramatsu, Dongwei Zhang, et al. 2007. "NDEL1 Phosphorylation by Aurora-A Kinase Is Essential for Centrosomal Maturation, Separation, and TACC3 Recruitment." *Molecular and Cellular Biology* 27 (1): 352–67. https://doi.org/10.1128/mcb.00878-06.

Morrow, Christopher J., Anthony Tighe, Victoria L. Johnson, Maria I.F. Scott, Claire Ditchfield, and Stephen S. Taylor. 2005. "Bub1 and Aurora B Cooperate to Maintain BubR1-Mediated Inhibition of APC/CCdc20." *Journal of Cell Science* 118 (16): 3639–52. https://doi.org/10.1242/jcs.02487.

Moseley, James B., and Paul Nurse. 2010. "Cell Division Intersects with Cell Geometry." *Cell* 142 (2): 189–93. https://doi.org/10.1016/j.cell.2010.07.004.

Moseley, James B, Adeline Mayeux, Anne Paoletti, and Paul Nurse. 2009. "A Spatial Gradient Coordinates Cell Size and Mitotic Entry in Fission Yeast." *Nature* 459 (May): 857. https://doi.org/10.1038/nature08074.

Müller, Hannah, David Schmidt, Sandra Steinbrink, Ekaterina Mirgorodskaya, Verena Lehmann, Karin Habermann, Felix Dreher, et al. 2010. "Proteomic and Functional Analysis of the Mitotic Drosophila Centrosome." *EMBO Journal* 29 (19): 3344–57. https://doi.org/10.1038/emboj.2010.210.

Musacchio, Andrea, and Edward D. Salmon. 2007. "The Spindle-Assembly Checkpoint in Space and Time." *Nature Reviews Molecular Cell Biology* 8 (5): 379–93. https://doi.org/10.1038/nrm2163.

Nakojima, Hiroyuki, Fumiko Toyoshima-Morimoto, Eri Taniguchi, and Eisuke Nishida. 2003. "Identification of a Consensus Motif for PlK (Polo-like Kinase) Phosphorylation Reveals Myt1 as a Plk1 Substrate." *Journal of Biological Chemistry* 278 (28): 25277–80. https://doi.org/10.1074/jbc.C300126200.

Nandagopal, Nagarajan, and Michael B. Elowitz. 2011. "Synthetic Biology: Integrated Gene Circuits." *Science* 333 (6047): 1244–48. https://doi.org/10.1126/science.1207084.

Nash, Piers, Xiaojing Tang, Stephen Orlicky, Qinghua Chen, Frank B. Gertler, Michael D. Mendenhall, Frank Sicheri, Tony Pawson, and Mike Tyers. 2001. "Multisite Phosphorylation of a CDK Inhibitor Sets a Threshold for the Onset of DNA Replication." *Nature* 414 (6863): 514–21. https://doi.org/10.1038/35107009.

Nasmyth, Kim, and Christian H. Haering. 2009. "Cohesin: Its Roles and Mechanisms." *Annual Review of Genetics* 43: 525–58. https://doi.org/10.1146/annurev-genet-102108-134233.

Navarro, Francisco J., and Paul Nurse. 2012. "A Systematic Screen Reveals New Elements Acting at the G2/M Cell Cycle Control." *Genome Biology* 13 (5): R36. https://doi.org/10.1186/gb-2012-13-5-r36.

Ni, Bin, Bhaswar Ghosh, Ferencz S. Paldy, Remy Colin, Thomas Heimerl, and Victor Sourjik. 2017. "Evolutionary Remodeling of Bacterial Motility Checkpoint Control." *Cell Reports* 18 (4): 866–77. https://doi.org/10.1016/j.celrep.2016.12.088.

Nijenhuis, Wilco, Giulia Vallardi, Antoinette Teixeira, Geert J.P.L. Kops, and Adrian T. Saurin. 2014. "Negative Feedback at Kinetochores Underlies a Responsive Spindle Checkpoint Signal." *Nature Cell Biology* 16 (12): 1257–64. https://doi.org/10.1038/ncb3065.

Noguchi, Eishi, Paul Shanahan, Chiaki Noguchi, and Paul Russell. 2002. "CDK Phosphorylation of Drc1 Regulates DNA Replication in Fission Yeast." *Current Biology* 12 (7): 599–605. https://doi.org/10.1016/S0960-9822(02)00739-X.

Novak, Bela, John J. Tyson, Bela Gyorffy, and Attila Csikasz-Nagy. 2007. "Irreversible Cell-Cycle Transitions

Are Due to Systems-Level Feedback." *Nature Cell Biology* 9 (7): 724–28.
https://doi.org/10.1038/ncb0707-724.

Nurse, Paul. 2002. "Cyclin Dependent Kinases and Cell Cycle Control (Nobel Lecture)." *ChemBioChem* 3 (7):
596–603. https://doi.org/10.1002/1439-7633(20020703)3:7<596::AID-CBIC596>3.0.CO;2-U.

Nurse, Paul M. 2002. "Cyclin Dependent Kinases and Cell Cycle Control." *Bioscience Reports* 22 (5–6): 487–
99. https://doi.org/10.1023/A:1022017701871.

Nurse, Paul, and Pierre Thuriaux. 1980. "REGULATORY GENES CONTROLLING MITOSIS IN THE
FISSION YEAST SCHIZOSACCHAROMYCES POMBE." *Genetics* 96 (3): 627–37.
https://doi.org/10.1093/genetics/96.3.627.

Örd, Mihkel, Kaidi Möll, Alissa Agerova, Rait Kivi, Ilona Faustova, Rainis Venta, Ervin Valk, and Mart Loog.
2019. "Multisite Phosphorylation Code of CDK." *Nature Structural and Molecular Biology* 26 (7): 649–
58. https://doi.org/10.1038/s41594-019-0256-4.

Örd, Mihkel, Rainis Venta, K. Möll, E. Valk, and Mart Loog. 2019. "Cyclin-Specific Docking Mechanisms
Reveal the Complexity of M-CDK Function in the Cell Cycle." *Molecular Cell* 75 (1): 76-89.e3.
https://doi.org/10.1016/j.molcel.2019.04.026.

Pachis, Spyridon T., and Geert J.P.L. Kops. 2018. "Leader of the SAC: Molecular Mechanisms of Mps1/TTK
Regulation in Mitosis." *Open Biology* 8 (8). https://doi.org/10.1098/rsob.180109.

Pan, Kally Z., Timothy E. Saunders, Ignacio Flor-Parra, Martin Howard, and Fred Chang. 2014. "Cortical
Regulation of Cell Size by a Sizer Cdr2p." *ELife* 2014 (3): 1–24. https://doi.org/10.7554/eLife.02040.

Papini, Diana, Mark D. Levasseur, and Jonathan M.G. Higgins. 2021. "The Aurora B Gradient Sustains
Kinetochore Stability in Anaphase." *Cell Reports* 37 (6): 109818.
https://doi.org/10.1016/j.celrep.2021.109818.

Patterson, James O. 2017. "Quantitative Biology of Cell Cycle Decision Making - A Thesis Submitted for the
Degree of Doctor of Philosophy University College London," no. August.

Peters, Jan Michael. 2006. "The Anaphase Promoting Complex/Cyclosome: A Machine Designed to Destroy."
Nature Reviews Molecular Cell Biology 7 (9): 644–56. https://doi.org/10.1038/nrm1988.

Peters, Jan Michael, Antonio Tedeschi, and Julia Schmitz. 2008. "The Cohesin Complex and Its Roles in
Chromosome Biology." *Genes and Development* 22 (22): 3089–3114.
https://doi.org/10.1101/gad.1724308.

Petronczki, Mark, Péter Lénárt, and Jan Michael Peters. 2008. "Polo on the Rise-from Mitotic Entry to
Cytokinesis with Plk1." *Developmental Cell* 14 (5): 646–59. https://doi.org/10.1016/j.devcel.2008.04.014.

Pickering, Mary, Mira Magner, Dan Keifenheim, and Nicholas Rhind. 2021. "The Fission Yeast S-Phase Cyclin
Cig2 Can Drive Mitosis." *Genetics* 217 (1). https://doi.org/10.1093/GENETICS/IYAA002.

Pines, Jonathon. 2011. "Cubism and the Cell Cycle: The Many Faces of the APC/C." *Nature Reviews Molecular
Cell Biology* 12 (7): 427–38. https://doi.org/10.1038/nrm3132.

Qian, Yue-Wei, Eleanor Erikson, Chuan Li, and James L. Maller. 1998. " Activated Polo-Like Kinase Plx1 Is
Required at Multiple Points during Mitosis in Xenopus Laevis ." *Molecular and Cellular Biology* 18 (7):
4262–71. https://doi.org/10.1128/mcb.18.7.4262.

Queralt, Ethel, and Frank Uhlmann. 2008. "Cdk-Counteracting Phosphatases Unlock Mitotic Exit." *Current
Opinion in Cell Biology* 20 (6): 661–68. https://doi.org/10.1016/j.ceb.2008.09.003.

Raleigh, Jeanette M., and Matthew J. O'Connell. 2000. "The G2 DNA Damage Checkpoint Targets Both Wee1 and Cdc25." *Journal of Cell Science* 113 (10): 1727–36. https://doi.org/10.1242/jcs.113.10.1727.

Rata, Scott, Maria F. Suarez Peredo Rodriguez, Stephy Joseph, Nisha Peter, Fabio Echegaray Iturra, Fengwei Yang, Anotida Madzvamuse, et al. 2018. "Two Interlinked Bistable Switches Govern Mitotic Control in Mammalian Cells." *Current Biology* 28 (23): 3824-3832.e6. https://doi.org/10.1016/j.cub.2018.09.059.

Remigi, Philippe, Catherine Masson-Boivin, and Eduardo P.C. Rocha. 2019. "Experimental Evolution as a Tool to Investigate Natural Processes and Molecular Functions." *Trends in Microbiology* 27 (7): 623–34. https://doi.org/10.1016/j.tim.2019.02.003.

Rhind, Nicholas, and Paul Russell. 2001. " Roles of the Mitotic Inhibitors Wee1 and Mik1 in the G 2 DNA Damage and Replication Checkpoints ." *Molecular and Cellular Biology* 21 (5): 1499–1508. https://doi.org/10.1128/mcb.21.5.1499-1508.2001.

Rock, Jeremy M., and Angelika Amon. 2009. "The FEAR Network." *Current Biology* 19 (23): R1063–68. https://doi.org/10.1016/j.cub.2009.10.002.

Roy, Babhrubahan, Simon J.Y. Han, Adrienne N. Fontan, Soubhagyalaxmi Jema, and Ajit P. Joglekar. 2022. "Aurora B Phosphorylates Bub1 to Promote Spindle Assembly Checkpoint Signaling." *Current Biology* 32 (1): 237-247.e6. https://doi.org/10.1016/j.cub.2021.10.049.

Russell, Paul, and Paul Nurse. 1986. "Cdc25+ Functions As an Inducer in the Mitotic Control of Fission Yeast." *Cell* 45 (1): 145–53. https://doi.org/10.1016/0092-8674(86)90546-5.

Sancar, Aziz, Laura A. Lindsey-Boltz, Keziban Ünsal-Kaçmaz, and Stuart Linn. 2004. "Molecular Mechanisms of Mammalian DNA Repair and the DNA Damage Checkpoints." *Annual Review of Biochemistry* 73: 39–85. https://doi.org/10.1146/annurev.biochem.73.011303.073723.

Santaguida, Stefano, and Angelika Amon. 2015. "Short- and Long-Term Effects of Chromosome Mis-Segregation and Aneuploidy." *Nature Reviews Molecular Cell Biology* 16 (8): 473–85. https://doi.org/10.1038/nrm4025.

Santaguida, Stefano, Anthony Tighe, Anna Morena D'Alise, Stephen S. Taylor, and Andrea Musacchio. 2010. "Dissecting the Role of MPS1 in Chromosome Biorientation and the Spindle Checkpoint through the Small Molecule Inhibitor Reversine." *Journal of Cell Biology* 190 (1): 73–87. https://doi.org/10.1083/jcb.201001036.

Santamaría, David, Cédric Barrière, Antonio Cerqueira, Sarah Hunt, Claudine Tardy, Kathryn Newton, Javier F. Cáceres, Pierre Dubus, Marcos Malumbres, and Mariano Barbacid. 2007. "Cdk1 Is Sufficient to Drive the Mammalian Cell Cycle." *Nature* 448 (7155): 811–15. https://doi.org/10.1038/nature06046.

Saunders, Timothy E., Kally Z. Pan, Andrew Angel, Yinghua Guan, Jagesh V. Shah, Martin Howard, and Fred Chang. 2012. "Noise Reduction in the Intracellular Pom1p Gradient by a Dynamic Clustering Mechanism." *Developmental Cell* 22 (3): 558–72. https://doi.org/10.1016/j.devcel.2012.01.001.

Sha, Wei, Jonathan Moore, Katherine Chen, Antonio D. Lassaletta, Chung Seon Yi, John J. Tyson, and Jill C. Sible. 2003. "Hysteresis Drives Cell-Cycle Transitions in Xenopus Laevis Egg Extracts." *Proceedings of the National Academy of Sciences of the United States of America* 100 (3): 975–80. https://doi.org/10.1073/pnas.0235349100.

Simanis, V., J. Hayles, and P. Nurse. 1987. "Control over the Onset of DNA Synthesis in Fission Yeast." *Philosophical Transactions of the Royal Society of London. Series B, Biological Sciences* 317 (1187):

507–16. https://doi.org/10.1098/rstb.1987.0077.

Singh, Priyanka, Marion E. Pesenti, Stefano Maffini, Sara Carmignani, Marius Hedtfeld, Arsen Petrovic, Anupallavi Srinivasamani, Tanja Bange, and Andrea Musacchio. 2021. "BUB1 and CENP-U, Primed by CDK1, Are the Main PLK1 Kinetochore Receptors in Mitosis." *Molecular Cell* 81 (1): 67-87.e9. https://doi.org/10.1016/j.molcel.2020.10.040.

Solomon, Mark J. 2003. "Hysteresis Meets the Cell Cycle." *Proceedings of the National Academy of Sciences of the United States of America* 100 (3): 771–72. https://doi.org/10.1073/pnas.0430083100.

Stegmeier, Frank, Rosella Visintin, and Angelika Amon. 2002. "Separase, Polo Kinase, the Kinetochore Protein Slk19, and Spo12 Function in a Network That Controls Cdc14 Localization during Early Anaphase." *Cell* 108 (2): 207–20. https://doi.org/10.1016/S0092-8674(02)00618-9.

Stern, Bodo, and Paul Nurse. 1996. "A Quantitative Model for the Cdc2 Control of S Phase and Mitosis in Fission Yeast." *Trends in Genetics* 12 (9): 345–50. https://doi.org/10.1016/S0168-9525(96)80016-3.

Sumara, Izabela, Juan F. Giménez-Abián, Daniel Gerlich, Toru Hirota, Claudine Kraft, Consuelo de la Torre, Jan Ellenberg, and Jan-Michael Peters. 2004. "Roles of Polo-like Kinase 1 in the Assembly of Functional Mitotic Spindles." *Current Biology* 14 (19): 1712–22. https://doi.org/10.1016/j.cub.2004.09.049.

Sun, Siyu, and David Gresham. 2021. "Cellular Quiescence in Budding Yeast." *Yeast* 38 (1): 12–29. https://doi.org/10.1002/yea.3545.

Sutani, Takashi, Tatsuro Yuasa, Takeshi Tomonaga, Naoshi Dohmae, Koji Takio, and Mitsuhiro Yanagida. 1999. "Fission Yeast Condensin Complex: Essential Roles of Non-SMC Subunits for Condensation and Cdc2 Phosphorylation of Cut3/SMC4." *Genes & Development* 13 (17): 2271–83. https://doi.org/10.1101/gad.13.17.2271.

Sveiczer, A., B. Novak, and J. M. Mitchison. 1996. "The Size Control of Fission Yeast Revisited." *Journal of Cell Science* 109 (12): 2947–57. https://doi.org/10.1242/jcs.109.12.2947.

Sveiczer, Ákos, and Anna Horváth. 2017. "How Do Fission Yeast Cells Grow and Connect Growth to the Mitotic Cycle?" *Current Genetics* 63 (2): 165–73. https://doi.org/10.1007/s00294-016-0632-0.

Tavernier, Nicolas, Anna Noatynska, Costanza Panbianco, Lisa Martino, Lucie Van Hove, Françoise Schwager, Thibaut Léger, Monica Gotta, and Lionel Pintard. 2015. "Cdk1 Phosphorylates SPAT-1/Bora to Trigger PLK-1 Activation and Drive Mitotic Entry in C. Elegans Embryos." *Journal of Cell Biology* 208 (6): 661–69. https://doi.org/10.1083/jcb.201408064.

Tomson, Brett N., Rami Rahal, Vladimír Reiser, Fernando Monje-Casas, Karim Mekhail, Danesh Moazed, and Angelika Amon. 2009. "Regulation of Spo12 Phosphorylation and Its Essential Role in the FEAR Network." *Current Biology* 19 (6): 449–60. https://doi.org/10.1016/j.cub.2009.02.024.

Touati, Sandra A., Lorena Hofbauer, Andrew W. Jones, Ambrosius P. Snijders, Gavin Kelly, and Frank Uhlmann. 2019. "Cdc14 and PP2A Phosphatases Cooperate to Shape Phosphoproteome Dynamics during Mitotic Exit." *Cell Reports* 29 (7): 2105-2119.e4. https://doi.org/10.1016/j.celrep.2019.10.041.

Tyson, John J., and Bela Novak. 2008. "Temporal Organization of the Cell Cycle." *Current Biology* 18 (17): 759–68. https://doi.org/10.1016/j.cub.2008.07.001.

Uhlmann, F. 2001. "Secured Cutting: Controlling Separase at the Metaphase to Anaphase Transition." *EMBO Reports* 2 (6): 487–92. https://doi.org/10.1093/embo-reports/kve113.

Virgilio, Claudio De, and Robbie Loewith. 2006. "The TOR Signalling Network from Yeast to Man."

International Journal of Biochemistry and Cell Biology 38 (9): 1476–81. https://doi.org/10.1016/j.biocel.2006.02.013.

Visintin, R., and A. Amon. 2001. "Regulation of the Mitotic Exit Protein Kinases CDc15 and Dbf2." *Molecular Biology of the Cell* 12 (10): 2961–74. https://doi.org/10.1091/mbc.12.10.2961.

Vyas, Aditi, Anna V. Freitas, Zachary A. Ralston, and Zhaohua Tang. 2021. "Fission Yeast Schizosaccharomyces Pombe: A Unicellular 'Micromammal' Model Organism." *Current Protocols* 1 (6): 1–40. https://doi.org/10.1002/cpz1.151.

Wang, Guan Hong, Stephanie Gamez, Robyn R. Raban, John M. Marshall, Luke Alphey, Ming Li, Jason L. Rasgon, and Omar S. Akbari. 2021. "Combating Mosquito-Borne Diseases Using Genetic Control Technologies." *Nature Communications* 12 (1): 1–12. https://doi.org/10.1038/s41467-021-24654-z.

Waters, Jennifer C., Rey Huei Chen, Andrew W. Murray, and E. D. Salmon. 1998. "Localization of Mad2 to Kinetochores Depends on Microtubule Attachment, Not Tension." *Journal of Cell Biology* 141 (5): 1181–91. https://doi.org/10.1083/jcb.141.5.1181.

Wistrand-Yuen, Erik, Michael Knopp, Karin Hjort, Sanna Koskiniemi, Otto G. Berg, and Dan I. Andersson. 2018. "Evolution of High-Level Resistance during Low-Level Antibiotic Exposure." *Nature Communications* 9 (1). https://doi.org/10.1038/s41467-018-04059-1.

Wong, Brandon G, Christopher P Mancuso, Szilvia Kiriakov, Caleb J Bashor, and Ahmad S Khalil. 2018. "Precise , Automated Control of Conditions for High- Throughput Growth of Yeast and Bacteria with EVOLVER." *Nature Publishing Group*, no. June. https://doi.org/10.1038/nbt.4151.

Wood, Elizabeth, and Paul Nurse. 2013. "Pom1 and Cell Size Homeostasis in Fission Yeast." *Cell Cycle* 12 (19): 3417–25. https://doi.org/10.4161/cc.26462.

———. 2015. "Sizing up to Divide: Mitotic Cell-Size Control in Fission Yeast." *Annual Review of Cell and Developmental Biology* 31 (1): 11–29. https://doi.org/10.1146/annurev-cellbio-100814-125601.

Wu, Judy Qiju, Jessie Yanxiang Guo, Wanli Tang, Chih Sheng Yang, Christopher D. Freel, Chen Chen, Angus C. Nairn, and Sally Kornbluth. 2009. "PP1-Mediated Dephosphorylation of Phosphoproteins at Mitotic Exit Is Controlled by Inhibitor-1 and PP1 Phosphorylation." *Nature Cell Biology* 11 (5): 644–51. https://doi.org/10.1038/ncb1871.

Yanagida, Mitsuhiro, Nobuyasu Ikai, Mizuki Shimanuki, and Kenichi Sajiki. 2011. "Nutrient Limitations Alter Cell Division Control and Chromosome Segregation through Growth-Related Kinases and Phosphatases." *Philosophical Transactions of the Royal Society B: Biological Sciences* 366 (1584): 3508–20. https://doi.org/10.1098/rstb.2011.0124.

Yang, Qiong, and James E. Ferrell. 2013. "The Cdk1-APC/C Cell Cycle Oscillator Circuit Functions as a Time-Delayed, Ultrasensitive Switch." *Nature Cell Biology* 15 (5): 519–25. https://doi.org/10.1038/ncb2737.

Yata, Keiko, and Fumiko Esashi. 2009. "Dual Role of CDKs in DNA Repair: To Be, or Not to Be." *DNA Repair* 8 (1): 6–18. https://doi.org/10.1016/j.dnarep.2008.09.002.

Yellman, Christopher M., and G. Shirleen Roeder. 2015. "Cdc14 Early Anaphase Release, FEAR, Is Limited to the Nucleus and Dispensable for Efficient Mitotic Exit." *PLoS ONE* 10 (6): 1–24. https://doi.org/10.1371/journal.pone.0128604.

Yona, Avihu H., Eric J. Alm, and Jeff Gore. 2018. "Random Sequences Rapidly Evolve into de Novo Promoters." *Nature Communications* 9 (1): 1–10. https://doi.org/10.1038/s41467-018-04026-w.

Yoshida, Satoshi, Keiko Kono, Drew M. Lowery, Sara Bartolini, Michael B. Yaffe, Yoshikazu Ohya, and David Pellman. 2006. "Polo-like Kinase Cdc5 Controls the Local Activation of Rho1 to Promote Cytokinesis." *Science* 313 (5783): 108–11. https://doi.org/10.1126/science.1126747.

Zakeri, Bijan. 2015. "Synthetic Biology: A New Tool for the Trade." *ChemBioChem* 16 (16): 2277–82. https://doi.org/10.1002/cbic.201500372.

Zeng, Yan, Kristi Chrispell Forbes, Zhiqi Wu, Sergio Moreno, Helen Piwnica-Worms, and Tamar Enoch. 1998. "Replication Checkpoint Requires Phosphorylation of the Phosphatase Cdc25 by Cds1 or Chk1." *Nature* 395 (6701): 507–10. https://doi.org/10.1038/26766.

Identification of a novel positive feedback loop on Cdc2/Cdk1 activity at mitosis

Identification of a novel positive feedback loop on Cdc2/Cdk1 activity at mitosis

Joseph C. Ryan[1,2], Akanksha Jain[1,2], Nelson Castilho Coelho[1], Maria Rosa Domingo Sananes[1] and Damien Coudreuse[1,2]

[1] Institute of Biochemistry and Cellular Genetics, CNRS UMR 5095, Bordeaux, France

[2] Institute of Genetics and Development of Rennes, CNRS UMR 6290, Rennes, France

Correspondence : damien.coudreuse@ibgc.cnrs.fr

ABSTRACT

Cell cycle progression is an essential process whose regulation is highly conserved among eukaryotes. Cyclin-dependent protein kinases (Cdks) are key components of the cell cycle control network and interact with various cyclins to drive robust cell proliferation. In eukaryotic cells, entry into mitosis is regulated by essential feedback loops on Cdk activity, referred to as the mitotic switch, which rely on the activities of the kinase Wee1 and counteracting phosphatase Cdc25. Although this control system is essential in most organisms, we previously demonstrated that cells operating with a simplified minimal cell cycle circuit (MCN) but lacking the Wee1/Cdc25 regulation (MCN-AF) were surprisingly viable. However, MCN-AF cells show a significant heterogeneity in cell size at division, a reduced growth rate, an extended G1 phase, and a hypersensitivity to DNA stress. This makes them an ideal model to investigate how cells can adapt to the lack of mitotic switch and enhance their proliferative potential. Using an experimental evolution approach, we found that alteration of Spo12, a small nuclear protein of unknown function, improves the growth of MCN-AF cells. We further show that Spo12 is a positive regulator of Cdk activity that acts at the time of mitosis in a Cdk-dependent manner. Remarkably, while loss of Spo12 does not change the distinct temporal pattern of Cdk activity observed in the MCN-AF background, it results in an overall decrease in activity levels. Furthermore, mutation of the Cdk target site on Spo12 mimics deletion of the *spo12* gene and leads to a reduction in Spo12 nuclear localisation at the onset of mitosis. Altogether, our work reveals the existence of a novel feedback loop on Cdk activity in fission yeast, in which the regulation of Cdk by Spo12 is modulated by the control of Spo12 nuclear localisation by Cdk at the G2/M transition.

INTRODUCTION

Cell cycle control is an essential feature in eukaryotes, playing a key role in a host of processes during development and in adult tissues. Importantly, deregulation of the controls that delineate cell cycle progression can result in abnormal cell proliferation, a common trait to all tumours, and the pathways that are involved in modulating the cell cycle represent primary targets for cancer therapies. Deciphering how cell proliferation is brought about in healthy cells is therefore an essential step in our understanding of the way this process is altered in pathological contexts and also serves to improve our understanding of the fundamental principles that govern this highly regulated process.

The eukaryotic cell cycle is highly conserved at a systems level. Its regulatory network has evolved to be specifically organised and tightly controlled for the proper coordination of the progression through the various phases of the cell cycle: G1, S, G2, and M (Morgan 2007; McIntosh 2016; Morgan 1997; Mochida et al. 2016; Peters 2006; Harper and Brooks 2005). Cyclin-dependent protein kinases (Cdks) are a family of enzymes that are central to this process and play a critical role in ensuring the faithful execution of cell cycle events (Morgan 1997). In metazoans, the regulation of Cdk activity is complex, in part due to the number of qualitatively different cyclin/Cdk complexes that form at different stages of the cell cycle. This complexity in the array of regulatory component of cell proliferation varies across species, but many of the Cdks and cyclins remain homologous (Martínez-Alonso and Malumbres 2020; Morgan 1997).

In the fission yeast *Schizosaccharomyce pombe*, cell cycle control relies on only one major Cdk, Cdc2, and four cyclins, namely Cig1, Cig2, Puc1, and Cdc13 (A Bueno and Russell 1993; Avelino Bueno and Russell 1993; Forsburg and Nurse 1991). Cig1, Cig2 and Puc1 have been implicated in G1 and the transition to S, while Cdc13 plays a primary role at the G2/M transition (Martín-Castellanos et al. 2000; Gould and Nurse 1989; Russell and Nurse 1986). Importantly, the association of these different cyclins with Cdc2 contributes to the temporal and quantitative modulation of Cdk activity during the different phases of the cell cycle. Interestingly, Cdk activity is tightly controlled by a network of positive and negative feedback loops that are conserved among eukaryotes. In particular, the Wee1 and Mik1 kinases and Cdc25 phosphatase are part of a double negative and a positive feedback loop, respectively, that are essential for the abrupt increase in Cdc2 activity at mitotic onset. Mitotic exit is then ensured by a negative feedback mediated by the anaphase-promoting complex (APC), which inhibits Cdc2 function through induced cyclin

degradation. Altogether, these conserved feedback motifs are crucial for maintaining the oscillation of activity necessary for the correct progression and integrity of the cell cycle (Morgan 1997; Mondesert, McGowan, and Russell 1996; Gould and Nurse 1989).

Since cyclin expression is temporally ordered, it was thought that the specific association of Cdc2 with distinct cyclins throughout the cell cycle brings about the substrate specificity of the kinase that was proposed to be necessary for the different phases of the division cycle (Nurse, Thuriaux, and Nasmyth 1976). This idea was however challenged as only one cyclin was shown to be essential for fission yeast proliferation, leading to a new quantitative model of cell cycle progression (Stern and Nurse 1996; Coudreuse and Nurse 2010a; Pickering et al. 2021; Fisher and Nurse 1995). Based on this hypothesis, the Minimal Cell cycle Network (MCN) was constructed in S. pombe, in which a simplified synthetic circuit replaces the endogenous Cdc2 regulatory network. More specifically, the MCN consists of a fusion between Cdc13 and Cdc2 expressed under the control of the cdc13 regulatory elements, in the absence of the endogenous copies of *cdc2*, *cdc13*, *cig1*, *cig2* and *puc1*. Analysis and manipulation of the MCN provided insight into the basic principles of the cell cycle, demonstrating that the orderly progression of the fission yeast cell cycle solely relies on the oscillation of a single qualitative Cdk activity between two thresholds (S and M), rather than on distinct qualitative inputs of the different cyclins at each critical phase of the process (Coudreuse and Nurse 2010a). Interestingly, the MCN allowed for a further simplification of the network via the abrogation of the Wee1/Cdc25 feedback loop, which regulates mitotic entry. In wild type cells and the vast majority of eukaryotic models, loss of this conserved feature is lethal (Lundgren et al. 1991; Nurse 1990). The MCN background is therefore a unique tool to explore cell cycle control beyond normallsy essential and highly conserved regulatory elements (Izumi and Maller 1993; Coudreuse and Nurse 2010a).

The network motifs that regulate cell cycle progression also have an active role in the surveillance of potential problems, which could have dramatic consequences on cell cycle progression (Zeng et al. 1998; Simanis, Hayles, and Nurse 1987). One of the major checkpoints in the control of cell proliferation operates at the G2/M transition, delaying chromosome segregation when replication has not be completed or in case of DNA damage (Boddy et al. 1998; Y. Chen and Sanchez 2004; Rhind and Russell 2000). If activated, the downstream target of the checkpoint, Cdc25 phosphatase, is inhibited. This prevents Cdk activation and mitotic entry, maintaining the Cdc13/Cdc2 complex in an inhibited, phosphorylated state as a result of Wee1 and Mik1 functions (Zeng et al. 1998). Thus, the loss of ability to inhibit Cdc2 through phosphorylation abrogates the

DNA damage and replicative stress checkpoint. Such cells are thus predicted to be hypersensitive to these challenges.

Abrogation of the Wee1/Cdc25 feedback loop can be achieved through mutation of the phosphorylation sites on Cdc2 (T14A Y15F; AF), which are targets of the Wee1 and Mik1 kinase as well as the Cdc25 phosphatase (Coudreuse and Nurse 2010a). This cannot be achieved in a wild-type background, as the Wee1/Cdc25 feedback loop is essential for viability, but is possible in the MCN background (Coudreuse and Nurse 2010b; Gérard et al. 2015). MCN cells harbouring these mutations are referred to as MCN-AF, and were shown to surprisingly grow despite a slower doubling time (Coudreuse and Nurse 2010a). In addition to slow growth, MCN-AF cells have a heterogeneous distribution of size at division (SAD) and an extended G1 phase. These characteristics imply that in the absence of the mitotic entry switch, MCN-AF cells have lost cell size homeostasis control and a reorganised cell cycle (Coudreuse and Nurse 2010a). MCN-AF cells therefore represent a unique and promising model to investigate unknown mechanisms that may exist in the cells or that may be developed to enhance their proliferation despite the lack of the mitotic entry switch. This may unravel novel branches of the cell cycle control network or shed light on alternative paths to growth that cell may employ to proliferate. Here we use the MCN-AF background as a starting point for experimental evolution assays that select cell populations for their growth rate.

Our work shows that cells lacking a fundamental regulatory mechanism for entry into mitosis can evolve alternative compensatory pathways to modulate their Cdk activity. Indeed, we have uncovered a novel feedback loop on Cdk activity involving the previously undefined protein, Spo12. Our findings demonstrate that Spo12 is directly phosphorylated by Cdc2, translocating it to the nucleus, which leads to a potentiation of Cdk activity. The function of Spo12 to modulate Cdk activity is more pronounced in the absence of the Wee1/Cdc25 feedback loop, and its abrogation will reduce overall Cdk activity. The Spo12/Cdc2 feedback loop constitutes a new regulatory mechanism on Cdk activity that, at least in laboratory growth conditions, is non-essential in the presence a functioning Wee1/Cdc25 feedback loop. Thus, by combining a synthetic biological approach with experimental evolution we have identified an alternative pathway for cell cycle control, and improved our understanding of the mechanisms cells can employ to modulate Cdk activity.

RESULTS

Experimental evolution of cells lacking the mitotic entry switch

By combining a synthetic approach to cell cycle control in fission yeast (MCN and MCN-AF cells) and experimental evolution, genetic alterations that allow cells to bypass the requirement for essential branches of the cell cycle network can be identified. This methodology relies on the isolation of evolved populations that improve their proliferation potential over time despite the lack of critical controls.

We therefore performed experimental evolution assays to select for improved proliferation of MCN-AF cells in vegetative growth for several generations. Three backgrounds were used for our experiments: 1) MCN-AF cells, in which the Wee1/Cdc25 feedback loop is abrogated through mutation of the Wee1 target residues on Cdc2 (T14A Y15F); while viable, these cells show significantly slower generation time and an increased heterogeneity in cell cycle progression, and 2) MCN and wild-type (WT) cells, which were used as a controls for mutations that may occur as a result of the conditions in our continuous culture system and MCN background (see below). MCN and WT cells have a normal generation time in the medium that was used for our assays. To perform these experiments, we used a long-term culture system, the ministats, which was optimised for fission yeast in the lab (Callens et al. 2017). These devices make it possible to maintain cells in exponential growth for hundreds of generations and monitor the emergence of clones that show an improvement in proliferation potential over time compared to the parental strains.

The experimental evolution assay was maintained over a period of 70 days, in triplicates of each cell cycle background (M1, M3: MCN-AF; M4, M6: MCN; M7, M9: WT) (Figure 1A). Within the first 20 days, all MCN-AF strains (M1, M3) showed a visible decrease in generation time (Figure 1B & C), indicating that evolved clones with improved proliferation rates had emerged in these cultures. In contrast, no changes were observed for MCN and WT cells. Measurements of size at division also revealed a decrease in the average cell size if the MCN-AF evolved clones compared to the parental strains (Figure 1D), an observation that was again specific to the populations lacking the mitotic entry switch. The decrease in size at division for all MCN-AF populations may indicate that: 1) the size control regulatory system is altered, and 2) the features of the Cdk oscillator (e.g. dynamics, thresholds, levels) have changed, as SAD is commonly used as a marker for evaluating the timing of mitotic entry in fission yeast. Interestingly, the decrease in SAD

in all evolved MCN-AF populations may suggest that their improved growth may rely on a common evolutionary strategy.

DNA content analysis performed throughout the experimental evolution assay also showed significant alterations in cell cycle organisation in evolved MCN-AF cells. Wild type fission yeast cells spend most of their life cycle in G2, thus in asynchronous cultures, the majority of cells have a 2C DNA content. Removal of the Wee1/Cdc25 feedback control results in an extension of G1, thereby increasing the percentage of cells with 1C DNA content (Figure 2) (Coudreuse and Nurse 2010a; Gérard et al. 2015; Peter A. Fantes and Nurse 1978). Strikingly, over the course of the experimental evolution assay, the fraction of cells with a 1C DNA content in the MCN-AF population decreased (Figure 2), with a reduction in the 1C peak compared to the ancestor at D35 and D70. No changes were observed in MCN and WT cells. These results indicate that the evolved MCN-AF cells partially restore an organisation of the cell cycle phase that is more similar to that in wild type cells. Interestingly, cells in the M1 population show a fully normal, wild type 2C profile. Altogether, these results suggest that MCN-AF cells can evolve to improve their growth despite the absence of the mitotic entry switch and that this may involve a strong evolutionary pressure for shortening G1.

As discussed above, WT and MCN cells remained stable throughout the experimental evolution assay, with no observable changes in growth, size at division, or cell cycle phase durations (Figure 1 & 2). This suggests that MCN cells are as robust as cells operating with the more complex, wild type cell cycle control network, questioning the relevance of this complexity. Such robustness also supports the principle that quantitative changes in Cdk activity are the sole driver of the cell division cycle, and that in optimal growing conditions; complexity is not a pre-requisite at the population level. Altogether, we successfully evolved cells that lack the Wee1/Cdc25 feedback loop, isolating fast-growing cells that may have rewired their cell cycle regulatory network or altered unknown mechanisms that promote their growth.

Isolation of evolved clones from evolved MCN-AF populations

Importantly, populations at the end of the evolution assays may not be clonal and may be constituted of different subpopulations that contribute to overall growth. To sequence the evolved populations, identify the mutations causal for the improved growth and study the underlying mechanisms, it was, therefore, necessary to first isolate and characterise individual clones from

each evolved ministat cultures to identify those that would be further studied for their improved growth rate. We thus analysed three independent colonies for each evolved population, assessing their generation time, SAD, and DNA content. In addition, clones from different time points during the evolution assay were also isolated and characterised, allowing us to track the evolutionary dynamics of each culture over time.

For these assays, the individual clones were isolated from samples at D35 and D70 for all the MCN-AF evolved populations (M1, M2, and M3), and one from each of the MCN (M4) and WT (M7) cultures (no changes were observed, as discussed above, for M5, M6, M8 and M9). As a control, the ancestral strain (D0) was also characterised for each vial. First, as observed at the level of the full evolved populations (Figure 1 and 2), there were no significant changes in generation time, SAD, and cell cycle organisation for either the MCN or WT subclones (Figure 3). Although there was no alteration in the SAD or in the covariance (CV) for the majority of individual evolved clones in these backgrounds (Figure 3B & C), we measured a drastic increase in SAD for WT clone 3 at day 70 (Figure 3B). Although it is not clearly seen at the population level of the FACS profiles, a possible explanation could be that diploids are in the WT vials. Indeed, as S. pombe can undergo diploidisation when exposed to starvation conditions, it may have been invoked via errors in the serial dilution of the cultures during the experimental evolution assay (Figure 1C) (Ekwall and Thon 2017). Overall these results indicate that WT and MCN cells do not improve their proliferation rate further in standard conditions.

Strikingly, the single-evolved clones isolated from the MCN-AF populations all showed decreases in generation times compared with the ancestor strains at both time points (D35 and D70, Figure 3A). These results demonstrate that our observations at the population level were reflected at the individual clone level and that these cells are under sufficient selective pressure to improve their growth. Remarkably, all clones isolated from M1 confirm the population analysis, with a complete restoration of wild-type generation time and SAD and a decreased CV by day 70 (Figure 3A, B & C). The potential genetic alteration responsible for this recovery is likely to have appeared before D35, as clone 3 of this specific time-point already shows a normal wild-type phenotype. Furthermore, our data suggest that by day 70, this clone has overtaken the entire population and grow efficiently without the Wee1/Cdc25 feedback loop. This is also apparent in our DNA content analyses (Figure 4): the single clones from the M1 population at day 70 have an essentially wild-type profile, indicating that the organisation of the cell cycle phases and their lengths are also wild type.

Characterisation of the M2 and M3 populations (Figure 1B) already showed a significant decrease in generation time by day 35, implying that sub-populations growing faster than the ancestral MCN-AF already represented a significant fraction of the population at this time point. This was also reflected in the individual clones at day 35, as those isolated from both M2 and M3 grew faster than the ancestral strain (Figure 3A). Finally, the doubling times of the evolved clones from M3 at day 70 were all shorter than those from day 35 (Figure 3A), consistent with the further improvement in growth observed at a population level (Figure 1B).

Interestingly, in terms of SAD, the analysed evolved clones from M2 and M3 were smaller than the ancestor strain at day 35 but then increased in size and variability by day 70 (Figure 3B). This might indicate that independently evolved MCF-AF populations may eventually share a common evolutionary trajectory. In any case, both the SAD and the heterogeneity of SAD were reduced in all the evolved MCN-AF clones compared to the ancestral MCN-AF, indicating a general trend towards decreasing cell size and improving size homeostasis when improving growth in the absence of the mitotic switch. Another common feature of all the MCN-AF evolved clones is a reduction in the length of G1, with a reduction in the 1C peak observed in each individual clone at both D25 and D70 (Figure 4).

The conclusions of these results are two-fold. Firstly, based on population and clonal characterisation of evolved MCN and WT cells, there is no observable difference in their evolutionary trajectories with regards to their phenotypes. MCN cells, which are longer than WT, do not change in SAD or size variability, and their generation time remains consistent from day 0 to day 70. This result implies that cells with a minimal architecture for cell cycle control remain robust and stable over long-term growth, and are similar to wild type cells in this regard. Secondly, MCN-AF cells subject to long-term sustained growth will compensate the absence of the mitotic entry switch, improving their growth potential, align their cell cycle organisation more similarly to wild type, and potentially improve their size control. Demonstrating that the loss of a dominant regulatory motif, the Wee1/Cdc25 feedback loop, could potentially be overcome through alternative mechanisms. The next steps are to identify the specific genetic alterations that the evolved clones have acquire, as they will help us to understand the mechanisms that have evolved to overcome the loss of mitotic entry control.

Altogether, these data show that cells can adapt to the lack of mitotic switch and enhance their proliferation, suggesting that alterations of existing pathways or development of novel functions can occur that render the Wee1/Cdc25 loop dispensable.

Whole genome sequencing to identify the dynamics of the mutational landscape of the evolved populations

To identify the molecular mechanisms involved in the improved proliferation of the evolved MCN-AF populations, we took advantage of whole genome sequencing approaches and individual fast-growing clones isolated from the different populations at different time-points. By correlating the genetic mutations to the phenotypic improvements of the MCN-AF, this approach aims to pinpoint the genetic changes linked with overcoming the loss of the mitotic entry switch. For this, we used WT (M7), MCN (M4) and evolved MCN-AF (M1, M2, M3) clones from M1, M2, M3, M4 and M7. These analyses were performed in collaboration with the team of Dr. Gianni Liti (IRCAN, Nice, France), and provided a global picture of the specific mutations that occurred over time in our experimental cultures (Figure 5). While this analysis did not allow for the identification of the causal mutations, as each clone harbours a number of genetic alterations (a result that is expected in these types of assays), it did allow for interesting observations. First, the full recovery observed in the M1 population was simply the result of a reversion of the Y15F mutation. Strikingly, the T14A mutation was still present, excluding a potential experimental error. This suggests a strong selective pressure on the mitotic switch. This population was not further studied. Second, we only identified few known cell cycle regulators, including the G1 Cdc2 inhibitor Rum1. Alteration of Rum1 was in fact observed in independent cultures. However, while sub-populations harbouring a mutation in rum1 were dominant at D35, they were often reduced of even disappeared by D70. This indicates that altering Rum1 function is a common strategy for MCN-AF cells to improve their growth, but other unknown or unanticipated mechanisms are likely to be more beneficial to these cells. These results also suggest that our experimental evolution assay led to the identification of novel processes that promote growth in eukaryotic cells, in particular in the absence of mitotic switch.

Identifying mutations responsible for improving the MCN-AF proliferation potential

To directly identify the individual genes that are responsible for the improved growth of our evolved MCN-AF populations, individual evolved clones were backcrossed several times with the ancestral strains and all four colonies emerging for individual tetrads were both sequenced and

phenotyped for their capacity to grow more efficiently despite the lack of Wee1/Cdc25 loop. This approach allows for the random shuffling of all genetic alterations during the meiotic process. Analysis of multiple tetrads, therefore, makes it possible to identify mutations that systematically segregate with the growth phenotype. Except in the case of physical linkage, only the causal mutations are expected to always be associated with the enhanced proliferation phenotype. A representative example of such analysis is shown in Figure 6. For the rest of the project, we focused on one specific evolved population in which mutation of the *spo12* gene results in an improved growth rate in MCN-AF cells.

Loss of Spo12 promotes growth in MCN-AF cells

Our experimental evolution and genetic analyses showed that alteration in Spo12 (Q19X, Figure 7) might promote the growth of cells lacking the mitotic entry switch. Spo12 is an unusually small and disorganized nuclear protein of 90 amino acids (Figure 7). Fission yeast Spo12 owes its name to the short homology domain (~20aa) which is the only feature shared with the longer budding yeast Spo12 protein. *spo12* is part of a cluster of genes that also includes plo1, ace2 and sid2, and that is periodically expressed in the late M- and early G1-phase (Buck et al. 2004; Anderson et al. 2002). This cluster is regulated by the forkhead transcription factor Fkh2, which targets a shared promoter sequence known as the Pombe Cell Cycle Box (PCB) (Anderson et al. 2002). Fkh2 is part of the PBF (PCB binding factor) transcriptional complex, which also involves another forkhead-like protein, Sep1, and the MADS box-like protein Mbx1 (Suárez et al. 2015; Buck et al. 2004). Deletion of fkh2 abolishes periodic expression of the M/G1 cluster and leads to defects in the position, timing and contraction of the actomyosin ring as well as a delay in mitotic entry (Buck et al. 2004). Many of the gene products of the PCB cluster are involved in spindle formation, anaphase onset, and septation (Buck et al. 2004; Anderson et al. 2002). However, the function of Spo12 in fission yeast remains unknown. Interestingly, overexpression of plo1 was shown to further promote PCB gene expression, indicating the potential existence of a positive feedback loop on the activation of this cluster (Anderson et al. 2002; Papadopoulou et al. 2008).

In fission yeast, Spo12 was first identified as a multi-copy suppressor of the mcs3-12 wee1-50 cdc25-22 conditional G2 arrest (Samuel et al. 2000). The wee1-50 and cdc25-22 mutations produce temperature-sensitive variants of Wee1 and Cdc25, which are partially impaired at the restrictive temperature of 36.5°C (P. A. Fantes 1981; Russell and Nurse 1987). The double wee1-50 cdc25-22 mutant is therefore related to the MCN-AF strains (note that these are partial loss-of-

function as the double deletion of wee1 and cdc25 is lethal). Interestingly, the viability of wee1-50 cdc25-22 cells requires the mitotic catastrophe suppressor gene mcs3, as mcs3-12 (a temperature-sensitive allele) induces G2 arrest in this background (Millar et al. 1992; Samuel et al. 2000). Consistent with these data, and while it remains unidentified; Mcs3 was proposed to have a role in mitotic entry. However, overexpression of in wee1-50 cdc25-22 mcs3-12 and wee1-50 cdc25-22 win1-1 cells rescued the G2-arrest at restrictive-temperature. These results are consistent with our experimental evolution data, which suggest interplay between Spo12 function and the Wee1/Cdc25 feedback loop.

Budding yeast Spo12 was first identified in a screen for genes involved in meiosis. Thus, loss of Spo12 in S. cerevisiae altered the capacity of cells to execute properly the two successive rounds of meiosis, leading to the formation of only two-spore asci (Klapholz and Esposito 1980; Chaves and Blobel 2001). Budding yeast Spo12 has since been shown to be part of the FEAR network (see Introduction), promoting the release of Cdc14 from the nucleolus (Tomson et al. 2009b). Overexpression of Spo12 in budding yeast therefore promotes Cdc14 release (Visintin, Stegmeier, and Amon 2003). Remarkably, the function of fission yeast Spo12 remains unknown, but it was shown that it differs from that in budding yeast. Indeed, neither overexpression nor deletion of *spo12* in S. pombe affects the localisation of the Cdc14 homolog Clp1 (Samuel et al. 2000; C.-T. Chen et al. 2006), and Δ*spo12* cells were able to undergo meiosis and produce four spore asci.

Finally, fission yeast Spo12 (90aa) is considerably smaller than in budding yeast (173aa) and lacks the docking motif that was shown to be required for S. cerevisiae Spo12 activation by cyclin B/Cdk1 (Örd et al. 2019). Altogether, these results indicate that fission yeast Spo12 does not fulfil the same function as budding yeast Spo12, and the mechanisms by which its loss allows cells to bypass the mitotic switch and improve their proliferation remain unknown. Interestingly, fission yeast Spo12 harbours two putative Cdc2 target sites (S47, S54) (Figure 7). However, although both are Cdk consensus sites, only S54 was identified to be phosphorylated by Cdc2 (Swaffer et al. 2016). This hints towards a potential novel feedback motif in cell cycle control, in which Spo12 and Cdc2 may regulate each other. Additionally, a putative Fin1 target site was also identified on the Spo12 protein sequence, which may hint at a possible interaction. Although, the site was not examined in this study, it remains a site of interest, and will be considered in future analysis. Finally, Spo12 was shown to be enriched in response to DNA damage in fission yeast cells,

however not in the absence of Cds1 and Rad3 (Willis et al. 2016). The targeted phosphorylation of Spo12 by these proteins implies it may be involved in Cdk activity regulation.

Construction of Δ*spo12* cells

To understand if loss of Spo12 is causal for the improvement in generation time observed in the evolved clone, we deleted *spo12* in the parental MCN-AF background by homologous recombination. Additionally, to examine if loss of Spo12 only impacts MCN-AF cells, *spo12* was also deleted in wild type (WT) and MCN cells. All the strains that we obtained carrying Δ*spo12* were fully characterised as asynchronous populations in EMM6S at 32°C, with generation time, SAD and DNA content measured.

First, we found that loss of Spo12 in the WT and MCN backgrounds had no apparent impact on their growth, indicating that Spo12 function is not critical for cell cycle progression in optimal lab conditions (Figure 8A). WT and MCN cells also exhibited no change in SAD or DNA content (Figure 8B & C). In contrast, in MCN-AF cells, deletion of *spo12* significantly promotes proliferation, with a reduction of ~25 minutes in generation time. At the level of a yeast population, this is a very significant growth advantage. Furthermore, our results show that the improvement in growth is coupled with a reorganised cell cycle (as indicated by the reduction in 1C cells) and a decrease in SAD (Figure 8B, C). These results demonstrate that deletion of *spo12* in the MCN-AF background recapitulates the impact of the point mutation identified in our experimental evolution assay. Collectively, these data show that Spo12 is an unusual regulator of the cell cycle, whose function is revealed in the sensitised MCN-AF background.

Next, we investigated whether loss of Spo12 affects other phenotypes associated with cells proliferating in the absence of the mitotic entry switch. In fission yeast, entry into mitosis is delayed in the presence of damaged DNA or incomplete replication. This is achieved through checkpoints which depend on the downstream inhibition of Cdc25, preventing the dephosphorylation of Cdc2 and subsequent progression into mitosis (Hermeking and Benzinger 2006; Sancar et al. 2004). Thus, MCN-AF cells exhibit a loss of DNA damage and replicative checkpoints (Coudreuse and Nurse 2010a). To examine if loss of Spo12 can partially rescue these controls over mitotic entry, we assessed the response of cells to both hydroxyurea (HU; depletes nucleotide pools), and camptothecin (CPT; an inhibitor of Topoisomerase I). As expected MCN-AF cells are hypersensitive to both drugs (Figure 8D) (Coudreuse and Nurse 2010a). Remarkably, while loss of

Spo12 did not impact the responses of WT and MCN cells to these concentrations of HU and CPT, the MCN-AF Δ*spo12* strain showed a striking resistance compared to the parental MCN-AF (Figure 8D). This result suggests that in cells lacking the Wee1/Cdc25 feedback loop, a potential alteration of the regulation of mitotic entry upon deletion of *spo12* may allow cells to cope with replication stress even in the absence of the canonical checkpoint pathways.

Altogether, these data demonstrate that Spo12 affects cell cycle progression, and may affects different aspects of the control of cell proliferation, hinting towards interplay between Spo12 function and Cdk activity.

Effect of loss of Spo12 on cell proliferation at the single cell level

Next, we addressed whether the observed improvement in population growth of MCN-AF cells lacking *spo12* can be observed at the single-cell level. This was a key step for understanding if the phenotype we observe results from an improved growth in all cells or only affects a specific subpopulation. To this end, we took advantage of dedicated microfluidic chips that allowed us to track the growth dynamics of individual cells over an extended period of time. In this system, cells are maintained in optimal growth conditions as a constant flow of fresh medium is applied to the chip. Using this approach, we characterised individual cells carrying Δ*spo12* in both WT and MCN-AF backgrounds in EMM6S at 32˚C.

The microfluidic device used for the single cell characterisations integrates a 2000 of cell traps, allowing for individual cells to be easily followed (Figure 9A). The trap design, which was initially developed for budding yeast (Aspert, Hentsch, and Charvin 2022) was first adapted for the use of fission yeast. This made it possible to track cells in real time over successive generations. Note that a mild size selection, likely due to the cell loading process, may be introduced, as suggested by the slight difference in cell size between standard bulk approaches and our microfluidic-based strategy (Figure 9B). However, this may also result from differences in growth conditions, as cells growing in flasks are exposed to a changing environment as the population grows, while cells in the microfluidic traps are exposed to a more controlled and constraint environment.

Firstly, we compared the growth rate of individual cells to see if the improvement of growth, which is seen at a population level, can be recapitulated in every individual cell of the population.

For WT and Δ*spo12* cells, we observed a median generation time that was higher than what is observed in population experiments (Figure 9C). This result is not unusual as previous generation time measurements of fission and budding yeast cells in microfluidic devices have been previously shown to be ~10% higher than those from bulk cultures (Nobs and Maerkl 2014). This higher generation time could be the consequence of a number of factors. In particular, as mentioned above, cells in the chip are exposed to a constantly renewed media. This may notably wash away pheromones that are known to affect growth. In addition, this results in very different nutritional conditions between flasks and chips that must be taken into account and controlled for, as this impacts cell growth. We observed a significant difference in growth of MCN-AF cells in the microfluidic device compared to when in culture (compare Figure 8A with Figure 9C & E), where these cells have a faster generation time in these conditions accompanied with a reduced median single cell SAD. However, when using bulk cultures, determination of the population doubling time integrates all cells, including those that fail to divide. In contrast, only dividing cells are accounted for when scoring cycle time in the chips. This is likely to contribute to the observed differences between the two conditions, as MNC-AF cells show a significant fraction of non-dividing cells compared to WT (Figure 9D). Importantly, despite the overall faster growth as determined in the cell trap system for MCN-AF cells, the improvement in proliferation potential upon loss of Spo12 was also striking a the single-cell level (Figure 9C). This was also accompanied by a reduction in the number of non-dividing cells, albeit still considerably higher than in WT (Figure 9D). Altogether, this indicates that loss of Spo12 function improves the growth of individual MCN-AF cells and reduces cell mortality.

Strikingly, MCN-AF Δ*spo12* cells showed a clear change in the distribution of single-cell doubling time compared to MCN-AF cells. In the latter, we observed a clear bimodal pattern, with two distinct sub-populations of cells growing at different median rates (Figure 9C). Remarkably, the loss of Spo12 leads to a more homogenous population that shows an overall lower generation time. These results indicate the loss of the Wee1/Cdc25 feedback loop induces cells to either undergo a relatively fast cell cycle (<120), or a longer one (>150 minutes), and this dichotomy is lost when Spo12 is absent.

Next, we also analysed the strength of the size control mechanism in the MCN-AF vs. MCN-AF Δ*spo12* strains. As discussed earlier, loss of Spo12 in the MCN-AF background makes cells smaller and more homogenous in doubling time. This may indicate a change in the regulation of size homeostasis, a process that is tightly linked to cell cycle control. In the microfluidic device,

the difference in SAD between the MCN-AF and MCN-AF Δ*spo12* was still present (Figure 9E), however less pronounced (this could be a consequence of the mild size selection in the traps discussed earlier, Figure 9B). To analyse the strength of cell size control, we used a common approach in fission yeast (P. A. Fantes et al. 1975; Wood and Nurse 2013; Sveiczer, Novak, and Mitchison 1996), in which single-cell generation time is plotted against size at birth (Figure 9F). Essentially, wild type fission yeast cells have an observed average size at division of ~14μm that is tightly maintained in a population. This is brought about by an extension and a reduction of the cycle time in newly born cells that are small and large, respectively. The strength of this size control process can be quantified by the slope of the linear regression of doubling time against size at birth (P. A. Fantes et al. 1975; Sveiczer, Novak, and Mitchison 1996; Wood and Nurse 2013). A slope of -1 would imply that all size deviations are corrected within one cell cycle, which is impossible in fission yeast as there is an incompressible period for G2, which corresponds to the minimum necessary amount of time required to prepare for mitosis (P. A. Fantes et al. 1975; P. Fantes and Nurse 1977; Wood and Nurse 2013). Thus, excessively large cells require more than one round of division in order to reach the correct homeostatic size. The mechanisms underlying cell size control are still not fully understood but cell cycle checkpoints, for example those present at the G2/M transition, are likely to have a role via the modulation of the cell cycle timings.

WT and Δ*spo12* cells scored in our microdevices showed a slope value of -0.71 and -0.73 respectively (Figure 9F), which is similar to what has been previously reported (P. A. Fantes et al. 1975; Wood and Nurse 2013). Loss of Spo12 in these backgrounds therefore does not impact cell size homeostasis. For MCN-AF cells, despite the observed heterogeneous SAD at the population level, a size control mechanism seems to still operate. While surprising, this is consistent with previously published data using standard bulk cultures and single cells (Wood and Nurse 2013; Coudreuse and Nurse 2010a). However, the effectiveness of this process is reduced compared to WT (Figure 9F) and loss of Spo12 did not appear to improve size control (Figure 9F), suggesting that not all Wee1/Cdc25-dependent processes are affected by the absence of Spo12 function.

Taken together, we demonstrated that the loss of Spo12 function in WT cells grown in optimal laboratory conditions does not impact proliferation or cell size at both the population and single-cell levels. In contrast, there is a clear improvement in generation time for single cells lacking the mitotic switch. This is associated with homogenisation of cell cycle duration between cells coupled with a decrease in the fraction of cells that fail to undergo a division cycle. Thus, our

approach using MCN-AF cells unravelled a novel regulation of cell cycle progression that may modulate the operation of the cell cycle control network.

Timing and localisation of Spo12 function

While our results clearly show that Spo12 has a role in modulating the division cycle of cells lacking the Wee1/Cdc25 feedback loop, how this is brought about remained unclear. We therefore set out to determine the behaviour of the Spo12 protein throughout the cell cycle. First, Spo12 was N-terminally HA-tagged and the amounts of Spo12 in asynchronous cultures of different genotypes (WT, MCN and MCN-AF) were determined (Figure 8E). Western blot analyses showed no observable difference in Spo12 levels between these strains. This indicates that neither the minimal cell cycle regulatory network nor the loss the Wee1/Cdc25 feedback loop appear to change the overall expression of Spo12. As Spo12 amount doesn't appear to change in the respective genetic backgrounds, we next looked to understand how its localisation might differ.

To visualise Spo12 in our models, we engineered both an N-terminally and C-terminally tagged versions of the protein using msGFP2, and assessed its localisation in WT, MCN, and MCN-AF. In both the WT and MCN strains, Spo12 appears transiently in the nucleus of dividing cells (Figure 10). It has been reported that *spo12* mRNA is periodically expressed throughout the cell cycle, peaking during mitosis (Samuel et al. 2000; Swaffer et al. 2016; Tomson et al. 2009a). This expression pattern is consistent with the increase in Spo12 nuclear localisation in dividing cells, as seen using the fluorescently tagged Spo12 (Figure 10). However, to investigate the potential regulation of Spo12 during the cell cycle, we determined the changes in the Spo12 levels during the cell cycle. To this end, MCN cells were synchronised in G2, after which protein samples were taken periodically following release for two rounds of division (Figure 11A).

Spo12 localisation to the nucleus is triggered when cells enter mitosis. Indeed, G2 arrested cells showed no nuclear localisation of Spo12 (Figure 11B). However, once cells are released to enter mitosis in our assay, we observed a rapid increase in nuclear Spo12, which peaks approximately 10 minutes after the G2 release (Figure 11B & C). Our results on the levels of Spo12 throughout the cell cycle suggest that this is mostly the result of a change in localisation rather than a dramatic change in overall Spo12 concentration in the cells. This is consistent with previous observations focusing on *spo12* mRNA expression (Samuel et al. 2000; Tomson et al. 2009b). Surprisingly, the periodic expression of *spo12* mRNA was not reflected at the protein level (Figure

11D). Indeed, immunostaining for GFP from total protein lysates taken at 15 minutes intervals showed no change in protein level throughout the time course. This implies that Spo12 remains stable throughout the cell cycle but translocates to the nucleus at during mitosis, after which it eventually is released. Given our results on the level of Spo12 throughout the cell cycle, we clearly see a dynamic regulation of Spo12 subcellular localisation that is linked to mitosis. Similar results were obtained in MCN-AF cells (Figure 10), although with an apparently stronger nuclear intensity. This suggests that Spo12 may be translocated or retained the nucleus more efficiently in MCN-AF cells.

Interestingly, we found that Spo12 nuclear intensity to be different depending on whether it was tagged at the N-terminal or the C-terminal of the protein, with the latter appearing weaker (Figure 10). This led us to compare both forms of the protein by western blot, which showed that Spo12 might undergo C-terminal proteolysis (Figure 12A). The apparent cleavage of Spo12 remained consistent in the different genetic backgrounds (Figure 12B). Thus, the monitoring of Spo12::msGFP2 may in fact mostly reflect the localisation of a cleavage product: the ~30 kDa band on our Western blot would thus correspond to the entire msGFP2 tag associated with a small C-terminal fraction of Spo12 (~10 kDa). Interestingly, this also indicates that Spo12 regulation may involve its C-terminal cleavage. To assess whether this is not physiological but rather the result of tagging the 10 kDa Spo12 protein with a large msGFP2 tag (~28 kDa), we used the same approach with the smaller 3xHA tag. In this context, we observed a similar C-terminal cleavage (Figure 12C), hinting at a regulatory process for Spo12 function.

Collectively, our data show that Spo12 levels are stable during the cell cycle, despite the reported periodic expression of *spo12* mRNA. However, the protein shows a dynamic modulation of its subcellular localisation, with a rapid and transient translocation into the nucleus around the time of mitosis. Although Spo12 appears to undergo C-terminal proteolytic cleavage, it is unclear how this is controlled. The cleavage site as well as the role of this modification for Spo12 function remains to be elucidated. Finally, our results combining population and single-cell analyses hint toward a nuclear role for Spo12 at the G2/M transition. Given our observations on the sensitivity of MCN-AF cells to replication stress and the fact that the importance of Spo12 was specifically revealed using cells lacking the Wee1/Cdc25 feedback loop, Spo12 may act through regulating Cdk activity.

Progression through mitosis in the absence of Spo12

Given the potential role of Spo12 during mitosis, we set out to investigate the potential effects of *spo12* deletion on mitotic events in both WT and MCN-AF cells. To this end, we generated strains carrying fluorescent markers that allows for tracking cell cycle events. More specifically, we used tagged versions of 1) the polo-like kinase Plo1 (Plo1::GFP; mitotic entry) which is recruited to the spindle pole body (SPB) at the onset of mitosis (Mulvihill et al. 1999), and 2) the non-histone protein 6 (Nhp6::mCherry, DNA marker), which allows to monitor anaphase, chromosome segregation and mitotic exit. Combining these markers, we characterised the timing of various mitotic events and their integrity in our different backgrounds.

First, to assess whether the timing of mitosis is impacted by the loss of Spo12, we measured the length of mitosis in WT and MCN-AF +/- Δ*spo12* cells. The start of mitosis was defined as SPB maturation, which occurs shortly after the cell has reached the mitotic Cdk threshold and committed to completing chromosome segregation. At this point, Plo1 is recruited to the SPB as it is involved in the maturation process (Conduit et al. 2014; Petronczki, Lénárt, and Peters 2008; Fu, Hagan, and Glover 2015). Thus, as cells enter mitosis, a rapid increase in the Plo1::GFP signal, at the SPB can be observed, followed by SPB duplication (Figure 13A; top panel). The duplicated SPBs then migrate to the poles of the nucleus as the cell prepares for anaphase. Plo1 is then released from the SPB and chromosome segregation occurs. For our experiment, the loss of SPB GFP signal was therefore used to define the start of chromosome segregation, and mitosis considered to be completed once the separated nuclear masses reach their furthest distance apart (Figure 13A; top panel).

The duration of mitosis in WT cells was measured at a median of 16 minutes with a very narrow distribution, indicating a consistent timing for this key cell cycle process (Figure 13B). Similar results were obtained in cells lacking Spo12 (Figure 13B). In contrast, MCN-AF cells took longer to complete mitosis (~28 minutes, Figure 13B). This increase in timing was also accompanied by a striking increase in cell-to-cell heterogeneity in mitosis duration. Loss of Spo12 in the MCN-AF background resulted in a mild but reproducible decrease of 2 minutes in the length of mitosis, with a clear increase in the percentage of cells completing mitosis in less than 25 minutes (Figure 13B). However, MCN-AF Δ*spo12* cells still required more time to execute mitosis than WT cells, demonstrating that loss of Spo12 may only partially rescue the MCN-AF defect in mitosis progression.

To further dissect the execution of mitosis in our models, we assessed the residency time of Plo1 at the SPB. This may provide insight into potential mechanisms by which Spo12 may affect Cdk activity. Indeed, the recruitment of Plo1 to the SPB has been previously shown to require both Cdc25 and Cdc2 activity (Mulvihill et al. 1999), and Plo1 has been shown to potentiate Cdk activity via a feedback loop with Cdc25 (Kumagai and Dunphy 1996; Mulvihill et al. 1999; Anderson et al. 2002). Plo1 may thus be considered as a downstream marker for the dynamics of Cdk activity at the onset of mitosis, and changes in Plo1 function could reflect modulations of Cdk activity before mitotic entry. The median duration of Plo1 residency at the SPB in our experimental setup was ~10 minutes in WT, and remained unaffected by the loss of Spo12 (Figure 13C). In MCN-AF cells, this was extended by 6 minutes, indicating that the loss of mitotic entry switch prolongs the time during which Plo1 kinase activity is present at the SPB (Figure 13C). This is consistent with the idea of a more progressive increase in Cdk1 activity in the absence of the Wee1/Cdc25 feedback loop (Gérard et al. 2015). However, the extended duration of Plo1 is unchanged in MCN-AF Δ*spo12* cells, indicating that the reduction of the length of mitosis is not due to a dynamic change in Plo1 activity.

We next examined how chromosome segregation was impacted by the loss of Spo12. Chromosome segregation is regulated by a negative feedback loop on Cdk activity, where high Cdk activity activates the APC/C, which in turn targets Cdc13 for degradation (Peters 2006; Chang et al. 2001; Blanco et al. 2000; Gérard, Tyson, and Novák 2013). The downregulation of Cdc13 results in a rapid decrease in Cdk activity, allowing cells to progress through anaphase and exit mitosis. However, this transition can be delayed if the mitotic spindle is not correctly attached to the kinetochores of the chromosomes. This delay is regulated by the spindle assembly checkpoint (SAC), which involves surveillance mechanisms that ensure the correct attachment of the spindle before the full activation of the APC/C (Roy et al. 2022; Pines 2011). Thus, differences in the duration of chromosome segregation may reflect defects in spindle attachment and organisation. The median duration for chromosome segregation in WT with and without Spo12 was ~6 minutes (Figure 13D). This is consistent with our observation that the overall duration of mitosis is unchanged in WT cells lacking Spo12 (Figure 13B). In contrast, MCN-AF cells show an increase in the time required for cells to complete chromosome segregation, which is reduced in absence of Spo12 (Figure 13D). The extended period of segregation required for MCN-AF cells may result from prolonged activation of the SAC compared to WT, which could be due to difficulties in executing correct kinetochore attachment or to efficiently reduce Cdk activity. This may also result

from chromosome segregation defects. The possibility that Spo12 may promote this phase of the cell cycle and potentially prevent SAC activation in MCN-AF cells is a hypothesis that could give insight into the role of Spo12.

Interestingly, MCN-AF Δ*spo12* cells exhibited a specific chromosome segregation phenotype at a significantly higher frequency than the parental MCN-AF background (Figure 13E). Indeed, a fraction of cells appeared to abort chromosome segregation after anaphase onset, a phenotype that we refer to as 'mitotic reversion' (Figure 13A; bottom panel). The cells that underwent mitotic reversion resulted in the asymmetrical separation of the chromosomes in the two daughter cells, after septation. It is unclear how this may be beneficial for MCN-AF Δ*spo12* cells, as the resulting 4C cells from mitotic reversion appear not to re-enter mitosis, at least within the time frame of this experiment. These results potentially describe a phenotype where chromosome segregation is impacted by the loss of Spo12 in MCN-AF cells.

Altogether, these time-lapse analyses of mitotic events show that the loss of Spo12 in cells lacking the mitotic entry switch reduces the duration of chromosome segregation and shortens mitosis. A possible explanation could be that the requirements to transition to anaphase are met sooner in the absence of Spo12 for MCN-AF cells, which could implicate a change in Cdk activity dynamics. Intriguingly, the MCN-AF Δ*spo12* cells showed a considerably higher occurrence of mitotic reversion, although it is unclear why this occurs more frequently in these cells or how it would be beneficial for growth. Importantly, our results link Spo12 function with events that are tightly linked with Cdc2 activity. This prompted us to investigate whether the loss of Spo12 affects Cdk activity levels. Indeed, we previously showed that cell cycle progression in fission yeast relies on quantitative changes in Cdc2 activity (Coudreuse and Nurse 2010a).

Regulation of Cdk activity by Spo12

MCN-AF cells lack a fundamental and evolutionary conserved regulatory motif on Cdk activity (Coudreuse and Nurse 2010a). The Wee1/Cdc25 feedback loop is the gatekeeper of mitotic entry. It is thus often the target of upstream responses such as DNA stress (Sancar et al. 2004; Hermeking and Benzinger 2006) and is key to balancing the phosphorylation state of cell cycle substrates (Domingo-Sananes et al. 2011). Interestingly, as discussed above, deleting *spo12* in the absence of this regulation leads to a remarkable improvement in growth accompanied with a decrease in size, a reorganisation of the cell cycle phases, and partial resistance to DNA stress

(Figure 8). Additionally, we observed a decreased length in mitosis and a reduction in the time required for chromosome segregation (Figure 13). A potential strategy for evolving fission yeast cells that lack the mitotic entry switch would be to restore some level of Cdk activity control. To determine whether the loss of Spo12 function impacts Cdc2 activity in our different models, we took advantage of a novel Cdk activity marker known as synCut3::mCherry (Patterson 2017). Cut3 is a condensin protein that translocate to the nucleus during mitosis in a Cdk-dependent manner (Sutani et al. 1999; Patterson 2017). synCut3::mCherry consists of a fragment of Cut3 that is fused with the fluorescent protein mCherry. This chimaera was shown to undergo nuclear translocation, a process that is quantitatively correlated to the ratio of Cdk and phosphatase activities (Patterson 2017, Figure 14A). Using this tool, we could compare the changes in Cdk activity levels and their dynamics throughout the cell cycle.

We first focused on the maximum Cdc2 activity reached in our different backgrounds using the peak intensity of nuclear synCut3 as a marker. Interestingly, we first found that this peak is significantly higher in WT than in MCN-AF cells (Figure 14B). This implies that the maximum Cdk activity in WT cells is higher than in the MCN-AF background. It has been shown that Cdk activity needs to reach a specific threshold to pass the G2/M transition (Coudreuse and Nurse 2010a; Gérard, Tyson, and Novák 2013). Our results, therefore, suggest that the activity threshold for mitotic entry is significantly lower than the activity level attained in dividing WT cells, as MCN-AF cells meet the mitotic threshold despite a lower activity. Importantly, loss of Spo12 in WT cells led to a wider spread in the peak of Cdk activity, with an increased fraction of cells showing lower peak synCut3::mCherry, and in the MCN-AF background, this resulted in a clear reduction in maximum signal, suggesting that Spo12 may be a positive regulator of Cdc2 activity.

In fission yeast, M phase is triggered by the phosphorylation of key substrates by the mitotic cyclin/Cdk complex, Cdc13/Cdc2. Importantly, the Wee1/Cdc25 regulatory mechanism imposes a unique dynamic profile of Cdk activity at the G2/M transition: the activity remains low as Cdk1 is inhibited throughout G1, S and G2, and then undergo an abrupt increase to pass the mitotic threshold as a result of the feedback loop motif. APC-dependent degradation of cyclin B at mitotic exit then leads to a rapid decrease in Cdk activity. This predicts that in cells lacking the Wee1/Cdc25 feedback loop, this switch-like behaviour may be lost and Cdk activity may increase more progressively throughout interphase. To evaluate if the temporal profile of Cdc2 activity is altered in the absence of Spo12, we tracked the translocation of synCut3::mCherry in individual

cells (Figure 14C) by time-lapse imaging and established the dynamic changes in Cdc2 activity at the single-cell level.

In WT cells, as expected, the rate of synCut3 phosphorylation by Cdc2 and its subsequent translocation showed a similar dynamic profile from what has been described for Cdk activity at the G2/M transition (Gérard, Tyson, and Novák 2013; Novak et al. 2007) (Figure 14C): nuclear synCut3 remained low during most of the cell cycle, rapidly increased at mitotic onset and then quickly dropped as cells entered the next cycle. In contrast, Cdk activity in MCN-AF cells increased more gradually (Figure 14C), and consistent with our peak activity analyses above, these cells entered mitosis with a lower apparent level of Cdc2 activity. This demonstrates that the loss of Wee1/Cdc25 feedback loop abolishes the tightly controlled timing of mitotic entry. Interestingly, although loss of Spo12 in WT cells does not change the profile of synCut3 translocation and only mildly affected its peak nuclear intensity (see above, Figure 14C), it has a strong impact in the MCN-AF background: MCN-AF Δ*spo12* cells show a significant reduction in the level of nuclear synCut3 (Figure 14C) at all stage of the cell cycle. This supports the hypothesis that Spo12 function potentiates Cdk activity. Furthermore, our data demonstrate that with an even lower apparent Cdk activity than the parental MCN-AF cells, MCN-AF Δ*spo12* cells are still able to reach the mitotic threshold and pass the G2/M transition.

Altogether, our data provide a potential explanation for the effect of *spo12* deletion in MCN-AF cells. Indeed, comparison of the temporal profiles of Cdc2 activity in MCN-AF vs. MCN-AF Δ*spo12* cells suggests that in the absence of Spo12, the probability for cells to prematurely cross the mitotic threshold is reduced. This may promote the proper separation of S and M as well as reduce potential alterations in chromosome segregation. This is consistent with our results showing a reduction in the percentage of non-dividing cells (Figure 9D) in MCN-AF Δ*spo12* and the shorter delay in mitotic exit (Figure 13D).

To validate further the hypothesis that Spo12 potentiate Cdc2 activity, we tested the impact of the loss of Spo12 in other sensitised backgrounds. More specifically, we deleted *spo12* in the wee1-50 and cdc25-22 mutants. As previously mentioned, these mutations produce temperature-sensitive variations of Wee1 and Cdc25. At the restrictive temperature of 36.5°C, cdc25-22 cannot enter mitosis and arrest in G2, while wee1-50 show an advance in mitosis and divide at a very small size. Even at the permissive temperature of 25°C, these mutations alter cell cycle progression (P. A. Fantes 1981; Russell and Nurse 1987): wee1-50 and cdc25-22 cells have a smaller and longer SAD

compared to WT, respectively. We, therefore, assessed whether loss of Spo12 further affects SAD in these backgrounds grown at 25˚C. However, neither the wee1-50 Δ*spo12* nor cdc25 Δ*spo12* cells appear to show any clear change in SAD (Figure 15).

To confirm that Spo12 potentiates Cdk activity, we then took an alternative approach and investigated the effects of *spo12* overexpression. Indeed, previous work demonstrated that excess of Spo12 can rescue the G2 arrest of the mcs3-12 wee1-50 cdc25-22 and win1-1 wee1-50 cdc25-22 mutants (Samuel et al. 2000), which again implicates Spo12 the regulation of Cdk activity. For these experiments, we expressed *spo12* under the control of the thiamine-repressible Pnmt1 promoter (Maundrell 1990) in WT, MCN, and MCN-AF backgrounds. This promoter is widely used for overexpression studies in fission yeast, as it leads to high expression levels when cells are grown in the absence of thiamine. In addition, the synCut3::mCherry was used in these assays to measure differences in Cdk activity. First, we did not observe any effect of Spo12 overexpression on the generation time of WT and MCN cells (Figure 16A). Note that the faster generation time for strains growing with thiamine was due to the supplementation of thiamine itself (this is a known effect of growing cells in the thiamine). However, excess of Spo12 led to a clear decrease in SAD of about 1 and 2 μm in WT and MCN, respectively (Figure 16A & C). Decrease in SAD of fission yeast generally reflects an advance in mitotic entry, which is a consequence of Cdk activity prematurely reaching the mitotic threshold. Consistent with this, the average nuclear synCut3::mCherry intensity was higher upon *spo12* overexpression in WT and MCN cells, as anticipated if Cdk activity is increased (Figure 16D). Interestingly, in MCN cells, we also observed an apparent reorganisation of the cell cycle, as populations growing with *spo12* overexpressed exhibited a longer G1 as seen from the appearance of a 1C peak in DNA content analyses (Figure 16B). This suggests that Spo12 has a potentially different effect on cells operating with a simplified cell cycle regulatory network. Spo12 may for instance be more specific of the Cdc13/Cdc2 complex, which is the only Cdk pair regulating cell proliferation in the MCN background. Collectively, these results support the model in which Spo12 potentiates Cdk activity in fission yeast cells.

Strikingly, overexpression of *spo12* in MCN-AF cells was strongly detrimental to the cells. The generation time and SAD of MCN-AF *Pnmt1::spo12* cells increased dramatically and cells appeared to be very sick (Figure 17). It is unclear as to exactly why the overexpression of *spo12* in the MCN-AF background has such a negative impact, because even though we do observe a loss of synCut3::mCherry in the cells, we cannot conclude that there is necessarily a reduction in Cdk

activity (the marker could no longer be expressed due to the overall sick state of the cells). However, this does further implicate Spo12 as having a more impactful role in the absence of the Wee1/Cdc25 feedback loop.

In conclusion, our results demonstrate that Spo12 is a positive regulator of Cdk activity in fission yeast cell. When Spo12 function is enhanced through overexpression, there is a change in the timing of mitotic entry in both WT and MCN cells which is likely results from the observed increase in Cdk activity. Given MCN-AF cells become very sick and eventually die after prolonged overexpression. Our data prompted us to determine whether Spo12 directly interacts with Cdc2. To assess this, we performed co-immunoprecipitation experiments, using the msGFP2::Spo12 fusion, the GFP trap approach for pulling down Spo12, and an anti-PSTAIR antibody to evaluate whether Cdc2 co-precipitate with Spo12. However, we could not detect Cdc2 in our pull-down samples (Figure 18A). This implies that Cdc2 may not directly interact with Spo12. Alternatively, their interaction may be either, weak and affected by the buffers used for the immunoprecipitation, or transient (for instance at very specific phases of the cell cycle). Assessing the binding of Spo12 to Cdc2 in synchronised cells may thus be necessary prior to concluding whether these two proteins interact. However, we are currently preparing all reagents to analyse more broadly Spo12 interactors using TurboID and mass spectrometry (see Discussion).

Next, we investigated the impact of loss of Spo12 on meiosis, as it has been recently shown that a reduction of Cdk activity can impede the progression from meiosis I to meiosis II (Gutiérrez-Escribano and Nurse 2015). This would result in the formation of incomplete (1, 2, or 3 spores) tetrads after crossing cells. To assess this, we crossed Δ*spo12* mutants of opposite mating types and with WT and determined the frequency of apparently successful meiosis. Surprisingly, we observed an increase in the percentage of 2 and 3-spore tetrads in both the Δ*spo12* x WT and Δ*spo12* x Δ*spo12* compared to WT x WT (Figure 18B). These results contradicts previously published data on Spo12, where no impact on meiosis was reported (Samuel et al. 2000; C.-T. Chen et al. 2006). This may be due to the approach, as we crossed heterothallic strains of opposite mating type while previous studies focused on homothallic h90 cells. The apparent defect in meiosis observed in our assay in the absence of Spo12 suggests that it may have a function in meiosis, potentially through modulating Cdk activity. This is an aspect of Spo12 function that requires further investigation.

Spo12 is a target of Cdk1

Our work provides strong evidence that Spo12 positively regulates Cdk activity in fission yeast cells. As discussed earlier, the cell cycle control network integrates a number of feedback motifs that contribute to the ordered and irreversible progression through the cell cycle. As previously mentioned, Spo12 has two Cdk consensus sites, and one of them, S54, was previously identified to be phosphorylated by Cdc2, indicating that Spo12 is a Cdk substrate (Swaffer et al. 2016). This led us to hypothesise that Spo12 is part of an additional, novel feedback loop on Cdc2 activity.

To test the role of the Cdk-dependent phosphorylation of Spo12 on its function, we altered the main Cdk target site (S54A) on Spo12 and expressed the protein in MCN-AF cells. Strikingly, MCN-AF *spo12(S54A)* mutants exhibited an improved growth, a reduced sensitivity to HU and CPT, a reorganisation of their cell cycle, and a reduced SAD, all similar to the MCN-AF Δ*spo12* (Figure 8). This suggests that Cdc2-dependent phosphorylation of Spo12 on S54A is critical for Spo12 function. Consistent with this, the overexpression of *spo12(S54A)* had no effect in WT or MCN cells with no changes in SAD or Cdk activity and no increase in G1 length in MCN cells (Figure 16). MCN-AF cells overexpressing *spo12(S54A)* did not show the strong increase in generation time observed when overexpressing *spo12* and showed a smaller SAD similar to the MCN-AF Δ*spo12* cells (Figure 16 & 17), suggesting that excess of the mutated form of Spo12 may act as a dominant negative. Altogether, these results suggest that Spo12 is part of a novel positive feedback loop on Cdc2 activity, in which Spo12 potentiate Cdc2 function in a Cdc2-dependent manner. Implicating that Spo12 could have a more prominent role in certain growth conditions, which are not apparent in laboratory conditions.

The loss of Cdk phosphorylation of Spo12 changes localisation

We next investigated how Cdc2 phosphorylation of Spo12 may control its function. As discussed earlier, the expression of *spo12* is periodic and peaks at the G2/M transition (Samuel et al. 2000), although this is not reflected at the protein level, which remains constant throughout the cell cycle (Figure 11D). However, we showed a clear change in Spo12 localisation, which transiently translocates into the nucleus at the onset of mitosis. Strikingly, using a similarly tagged version of Spo12(S54A), we found that the mutant does not significantly accumulate in the nucleus (Figure 11A). This was not due to a change in protein levels of Spo12(S54A) vs Spo12 as shown by

Western blot analysis (Figure 8E and 11D). Intriguingly, although Spo12(S54A) is largely absent from the nucleus compared to Spo12, we did observe a specific localisation at the mitotic spindle during mitosis (Figure 11E). The relevance of this remains unclear. These results suggest that Spo12 translocates to the nucleus in a Cdk-dependent manner, providing insight into the mechanisms underlying this novel feedback loop. This may be an example of a spatial positive feedback, where localisation acts as a trigger for the positive regulation of Cdk activity (Santos et al. 2012). The loss of phosphorylation of Spo12 impairs this feedback, and subsequently the positive regulation of Cdk activity.

Finally, we tested whether the Cdk-dependent phosphorylation of Spo12 is linked to its C-terminal cleavage, which may contribute to its localisation. However, we did not observe any change in Spo12(S54A) cleavage (Figure 8E & 12A), suggesting that these two processes may be uncoupled. How Spo12 cleavage is regulated and how it impacts its function will be an important future development of the work presented here.

DISCUSSION

In this study, we took a synthetic biology approach to explore what alternative strategies cells can take to overcome the loss of the highly conserved mitotic entry switch. To this end, we performed experimental evolution of cells with different cell cycle regulatory architectures in constant growth conditions (in ministats). While being maintained in constant vegetative growth, MCN-AF populations were under selective pressure for faster growing cells. Both WT and MCN populations were also evolved to act as controls, so mutations that were random and due to the ministat conditions could be identified. Furthermore, using the MCN as a control also allowed us to conclude that cells do not have an inherent selective pressure, when under constant growth, to reinstate the more complex regulatory network of wild type. This is an interesting result that implies that the fundamental principle in cell cycle control is centered on maintaining the correct oscillation of Cdk activity, and would add to a growing body of evidence in favour of a quantitative model of cell cycle control (Kozar et al. 2004; Hochegger, Takeda, and Hunt 2008; Pickering et al. 2021).

Next, the results of the experimental evolution also provided insight into the possible mechanisms cells can employ to overcome the loss of normal mitotic entry control. Fission yeast proliferation relies on an essential and conserved feedback loop on Cdc2 activity mediated by the kinase-phosphatase pair Wee1 and Cdc25. In wild type, this feedback loop is essential and its abrogation leads to cell death. However, the MCN is one of the only known in vivo model in which cells lacking this feedback loop are viable, albeit with severe impairments to growth. This provides us with a unique model for investigating novel regulations of cell cycle progression beyond the mitotic switch. By subjecting MCN-AF cells to experimental evolution, we observed that cells lacking the mitotic feedback loop could overcome their inherent impairments to growth. Indeed, over the course of the assay, we observed a consistent reduction in generation time for all independently growing MCN-AF populations. This indicates that MCN-AF cells are under sufficient selective pressure to acquire genetic alterations that compensate for the loss of the normal mitotic entry switch. Interestingly, one of the isolated evolved clones showed a reversion of the mutated Y15 residue on Cdc2. This suggests that while various mechanisms may be employed by cells to enhance their proliferation in the absence of the Wee1/Cdc25 regulation, the presence of an operational feedback loop remains highly beneficial and strongly selected for. However, none of the other evolved clones did show a reversion of the Wee1/Cdc25 regulation. This implies that alternative mechanisms can be altered for cells lacking the mitotic entry switch to promote their growth and partially recover aspects of the normal cell cycle. By coupling our experimental

evolution strategy with whole genome sequencing and genetic assays, we were able to identify various causal mutations that significantly suppressed the MCN-AF growth defect.

For our studies, we focused on the role of Spo12, as loss of Spo12 function in one of our evolved clones allowed these cells to grow with a faster generation time. This phenotype was accompanied with a reorganisation of cell cycle phases that is more similar to that in WT cells. Our study demonstrates that Spo12 is a positive regulator of Cdc2 that is part of a novel feedback loop promoting Cdk activity. Importantly, disruption of Spo12 in cells lacking the Wee1/Cdc25 feedback loop improves cell cycle progression by lowering the overall Cdk activity during the cell cycle. Normally, cells with tight control over mitotic entry maintain Cdk activity below the mitotic threshold until they are prepared to correctly execute chromosome segregation (Fisher et al. 2012; Mochida et al. 2016; Coudreuse and Nurse 2010). However, our experiments demonstrate that MCN-AF cells are unable to consistently maintain Cdk activity below the threshold during G2. This leads to a more progressive increase in activity, which likely results in pre-mature entry into mitosis and subsequent defects in the division process that increase cell lethality. Reducing Cdk activity narrows the temporal window during which cells have a level of Cdk activity that is above the mitotic threshold, thereby delaying mitotic entry. This provides more time for cells to complete adequate preparation for mitosis, such as DNA replication (Morgan 2007; Santaguida and Amon 2015), and therefore improves overall population growth.

Spo12 function is dependent on Cdc2 phosphorylation, as mutation of the S54 phosphorylation site (S54A) mimics the full deletion of the *spo12* open-reading frame and promotes the proliferation of MCN-AF cells. Interestingly, in contrast to wild type Spo12, we found that Spo12(S54A) does not translocate to the nucleus during mitosis. Our experiments show that this observation is not the result of an alteration of Spo12 stability but rather reflects a direct control of Spo12 subcellular localisation by Cdc2. This change in localisation dynamics coupled with the observed reduction the ability of Spo12 to potentiate Cdk activity implies that the Spo12-mediated increase in Cdk activity may be specific to mitosis and dependent on Spo12 nuclear translocation. This may entail a spatial positive feedback loop, where the Cdc13/Cdc2 phosphorylation of Spo12 induces the translocation of Spo12 to the nucleus, which in turn positively regulate Cdk activity. This type of spatial feedback loop has already been demonstrated with the translocation of Cdc13/Cdc2 to the nucleus in fission yeast (Santos et al. 2012). Altogether, our strategy using experimental evolution revealed the existence of a novel feedback loop on Cdc2 activity and

provides a mechanism for the regulation of Spo12 function by Cdc2. Further investigation is required to decipher the molecular pathway by which Spo12 modulates Cdc2 activity.

Loss of the Spo12 positive feedback loop appears to have a more prominent impact in cells lacking the mitotic entry switch. In wild-type and MCN cells, there is an overall higher Cdk activity level compared to MCN-AF, and entry into mitosis in these backgrounds relies on the abrupt burst in Cdk activity that is mediated by the positive and double-negative feedback loops on Cdc2 by Wee1 and Cdc25. Furthermore, our data suggest that there is a strong overshoot of the Cdk mitotic threshold when these cells enter division. In this context, lowering Cdk activity may not change cell cycle progression, as cells would still reach the mitotic threshold with similar dynamics. In contrast, MCN-AF cells show a lower and, more importantly, progressive increase in Cdc2 activity. In this situation, the temporal window where cells have sufficient activity to commit to mitosis is broad, resulting in an increased change of premature entry into M. We propose that lowering further Cdk activity by altering Spo12 function reduces this window and delays mitosis, thereby preventing deleterious advance in mitosis onset.

Spo12 is part of the PCB group of proteins that are expressed in during mitosis and early G1, as its mRNA expression has been reported to be specifically timed during the cell cycle (Buck et al. 2004; Anderson et al. 2002). However, our results indicate that at a protein level, Spo12 remains constant throughout the cell cycle, which further demonstrates that a change in the localisation is likely what is relevant for Spo12 function. Interestingly, in the absence of the Wee1/Cdc25 feedback loop, the overexpression of Spo12 appears to heavily impair cell cycle progression. MCN-AF cells overexpressing Spo12 also show an increase in the percentage of 1C cells in the population, implying an extension of the G1 phase. This might indicate that an increase in Cdc13/Cdc2 activity, induced by Spo12 overexpression, outside of mitosis may prevent cells from completing DNA replication. This is consistent with previous observations where the elevated levels of the mitotic cyclin/Cdk prevent loading of pre-RC components, as Cdc4 is outcompeted (Mimura et al. 2004; Fragkos et al. 2015). And may also explain why there is an observed increase in G1 for MCN cells but not wild type cells, given the former has a simplified regulatory network comprised of only the mitotic cyclin/Cdk.

As discussed above, the translocation of Spo12 to the nucleus appears to be largely under the regulation of Cdc2. However, not all nuclear Spo12 is lost during mitosis in the absence of Cdk phosphorylation, a transient localisation at the mitotic spindle can be observed using Spo12(S54A).

This may indicate a possible secondary layer of regulation for Spo12 that is independent of Cdc2 phosphorylation. It is possible that Spo12 always appears transiently at the mitotic spindle (regardless of S54 phosphorylation), but it is difficult to see, as it is also present throughout the nucleus and therefore masks it. Alternatively, the phosphorylation of Spo12 by Cdc2 may change the stability of Spo12 at the spindle, meaning the protein will have a reduced duration at the site, once again masking its localisation there. This would mean that the introduction of the S54A mutation could increase the stability of Spo12 at the mitotic spindle; expanding the window it transiently appears there. Interestingly, Spo12 has a conserved target site (T81) for the NIMA kinase Fin1. Fin1 has been shown to regulate spindle formation via the SPB, which could be a possible common localisation where Spo12 interacts with Fin1 (Grallert and Hagan 2002). The may hint at the possibility that Spo12 localisation to the spindle is dependent on Fin1 rather than Cdc2, and through this interaction, Fin1 may contribute to Cdc2 regulation.

Indeed, Fin1 has been shown to promote mitotic commitment. Both cyclin B/Cdk1 and Fin1 phosphorylate Cut12, preventing the recruitment of the phosphatase PP1/Dis2, promoting the recruitment of Plo1 kinase to Cut12 and the SPB. This in turn triggers a positive feedback loop, where Plo1 enhances Cdc25 activity and inhibits Wee1 (Karaiskou et al. 1999; Grallert et al. 2013). Additionally, Fin1 also regulates the timing of Wee1 inhibition by the Cdr1 and Cdr2 nodes, although the molecular mechanism of this remains to be elucidated (Grallert et al. 2013). Thus, Fin1-dependent phosphorylation of Spo12 may represent an upstream mechanism for the potentiation of Cdc2 activity, and may be a critical part of a pathway for Spo12 to increase Cdk activity. More work will need to be done to understand the relevance of the Fin1 target site, but this remains a potential avenue of interest given the direct connection with regards to Cdk activity regulation.

To explore Spo12 function via its interactors, we are planning to do mass spectrometry analysis of Spo12 using the novel TurboID tag (Larochelle et al. 2019). This method involves a tag on Spo12 that will biotinylate interactors in vivo. This is a powerful method because it is an enzymatic reaction, so it will not only act on proteins that are physically bound to Spo12 but also those that are in close proximity. This means we have the potential to identify interactors that are more transiently associated with the protein, which may be the case of key regulators such as Cdc2 based on our results. To this end, we plan on running samples of both Spo12 and Spo12(S54A) as it would allow us to see changes in binding partners, complex formations, and also potential modifications that are associated with Cdk1 phosphorylation at S54. Currently, we have finished

building strains that express Spo12 and Spo12(S54A) tagged with the TurboID component, as well as two control strains. These control strains include: 1) TurboID::Spo12 expressed in the MCN-AF background, and 2) TurboID expressed on its own in the WT background. The first strain will allow us to identify any possible differences that are associated to the simplified cell cycle control network, while the latter will act as a control for off target interactions. Furthermore, all strains also included a 3xHA, so we would be able ensure that the expression of the protein was not changed with the addition of the TurboID component. So far all tests have been completed, and the next steps will be to isolate the biotinylated proteins from the relevant strains through pruification using a streptavidin-based affinity protocol. The purified interactors will then to be identified via mass spectrometry, which we expect to provide us with a comprehensive list of proteins that have both a strong or even transient interaction with Spo12. This would direct us to the relevant pathways involved in the mechanism of the Spo12 positive feedback loop on Cdk activity.

Another reason for us to take the approach of using TurboID to identify Spo12 interactors comes from the unique characteristics of the protein. Indeed, Spo12 shares features with phase separating proteins (e.g. disorganised N- and C-terminal, and a C-terminal coiled-coil domain) (Alberti et al. 2018), raising the possibility that it organises cell cycle control by compartmentalising key factors in phase-separating condensates. Using TurboID specifically, we have the possibility to identify proteins that would be in the same condensate, even if they were not directly bound to Spo12. Although it is a hypothesis, it would contribute to a growing body of work that suggests an increasingly apparent role for phase separation in the cell cycle (Liu et al. 2020). In any case, more work is needed to explore this idea further, but in the meantime the TurboID approach has added value.

Lastly, a significant observation made in our work indicates that Spo12 likely has a specific interaction with the cyclin B/Cdk1 complex. Although budding yeast Spo12 is not conserved with regards to its function with fission yeast Spo12, this interaction of the protein appears to be a shared feature of the two (Örd et al. 2019). This conserved interaction with cyclin B/Cdk1 proposes the question of whether Spo12 is conserved in other eukaryotes. Spo12 is small, and contains only a short Spo12 domain with the remainder of the protein being disorganised, which may explain why it is difficult to identify any sequence homolog beyond yeast. Furthermore, the disorganised structure of the protein means that it is fast evolving (Schlessinger et al. 2011), given the disorder within the protein can be achieved in many ways, which may result in proteins with the same function but entirely different structures. So despite not finding any sequence homology, it is still

possible that the protein is functionally conserved, as has been reported for other cell cycle regulators (Harashima, Dissmeyer, and Schnittger 2013).

Interestingly, the fact that Spo12 contains an inherent property to associate with a key regulator of the cell cycle, like cyclin B/Cdk1, while being largely disordered makes it a malleable target for evolution. Since, as previously stated, a disorganised structures are fast evolving and can be easily reshaped (Schlessinger et al. 2011). Thus, could the fundamental interaction Spo12 has with cyclin B/Cdk1 represent a 'swiss army knife' that can be repurposed by evolution to influence the cell cycle control network? This would not be a novel idea, as malleable components of complex networks that are drivers of evolution have been previously demonstrated (Ni et al. 2017). This would implicate Spo12 in providing plasticity in the cell cycle control network, allowing the system to quickly reshape in the event of its disruption.

Alternatively, the role of Spo12 could be more linked to challenging conditions, as our data suggest the protein is more crucial when cells are starved, like when inducing meiosis. This would imply that Spo12 is key when cells are under certain stresses and that its function is not obvious in optimal lab conditions. More work is required to test this idea, but in any case, the results of the Spo12 interactors using the TurboID may shed light on this possibility, and thus should be considered when analysing the mass spectrometry data.

Overall, our data suggests the possibility that Spo12 may have played a key role in a less complex cell cycle network and that evolution of the Wee1/Cdc25 feedback may have masked its function in vegetative growth. Spo12 function relies on Cdc2 mediated translocation, where its concentration in the nucleus, where it will promote Cdk activity. Our work provides evidence of a possible strategy of reducing overall Cdk activity to improve proliferation for cells lacking normal mitotic entry, as well as a novel pathway for Cdk activity regulation.

MATERIALS AND METHODS

Fission yeast strains and growth conditions

Standard media and methods were used (Moreno, Klar, and Nurse 1991; Hayles and Nurse 1992). Strains used in this study can be found in Supplementary table 1. All experiments were performed using liquid minimal media with supplements (EMM6S), unless otherwise noted. Spot assays were performed on rich medium (YE4S) and supplemented with either hydroxyurea (HU) or camptothecin (CPT), where indicated. The sporulation assay was done on EMM without Nitrogen and supplemented with glutamate plates.

Deletions of spo12, cig1, cig2, puc1, and cdc2 were constructed by replacing their open reading frames with antibiotic cassettes by homologous recombination. The tagging of Spo12 with msGFP2 and HA, and the S54A point mutation, were engineered using the SpEdit CRISPR method (Torres-garcia et al. 2021). All strains with the synCut3::mCherry::ura4+ component were generated from an initial strain received from the Nurse Lab (Patterson 2017).

The overexpression of Spo12 assay used EMM6S, which was supplemented with thiamine (10mg/ml) where indicated. The strains used were generated with the No Message Thiamine Promoter 1 (Pnmt1) (Maundrell 1990), which is inhibited in the presence of thiamine in the media. After the promoter has been repressed, over 24 hours is required to derepress it. This specific variation of the promoter has a high level of expression, for this reason it was chosen to for the overexpression assay.

Microscopy

Experiments were either performed using a Zeiss Axio Observed (Carl Zeiss Inc.) equipped with a laser bench (Visitron GmbH) and spinning disc confocal head (CSU-W1, Yokogawa) as well as a Lumencor Spectra X illumination system. Images were acquired with a Hamamatsu Orca Flash 4.0V2 sCMOS camera via VisiView (Visitron GmbH). For cell size measurements, live cells were stained with Blankophor (MP Biochemicals) and size was determined from microscopy images using Fiji and the Pointpicker plugin (National Institutes of Health).
Microfabrication of single-cell time-lapse chip

PDMS microfluidic chips for all time-lapse microscopy analyses in this study were prepared following standard microfabrication protocols (McDonald and Whitesides 2002). The microfluidic device is composed of an array of 2000 geometric microstructures that allow mother cell trapping and flushing of successive daughter cells (Figure 9A). The device also included a particle filter with a cut-off size of 15μm to prevent debris or dust particles from blocking media flow.

The first layer, which includes the traps chamber, was spin-coated with SU8-2005 at 3000rpm and baked at 95˚C for 3 minutes to achieve a trap height of approximately 5μm. The second layer, which includes the inlet and outlet channels, was spin-coated with SU8-2025 at 3000rpm and baked for 3 minutes to achieve a height of approximately 60μm. Both layers were exposed to 365nm UVs at 120mJ/cm2 with a mask aligner (UV-KUB3, Kloé, France). A detailed protocol for the parameters used in the microfabrication process can be found in (Aspert, Hentsch, and Charvin 2022).

For the time-lapse chips, a 1:10 mixture of PDMS (Sylgard 184, Dow Corning, USA) was cast onto the master mould and cured at 70˚C for 2 hours. Inlets were made using 0.75mm biopsy punches, and the chips were bonded to microscopy-grade coverslips by plasma activation (3 minutes) (Harrick Plasma, USA).

Medium flow control

All time-lapse experiments were performed in PDMS microfluidic chips with a flow rate of 5 μl/min of EMM6S at 32˚C. Flow rates were maintained through flow sensors that regulate pressure controllers (Elvesys).

Single-cell time-lapse experiments

All strains were grown at 32ºC. Cells were inoculated in 10 ml overnight static cultures, followed by dilution in 30 ml of EMM6S. Cultures were maintained in exponential growth for at least 36 hours. Subsequently, 0.5 ml of an exponentially growing culture (approximately OD 0.4) was diluted in 1 ml of fresh medium before being sonicated once for 10s on/off at 10% with Branson Sonifier (Branson Rev.0803). The 1 ml sample was then injected into the PDMS microfluidic chip using a syringe (needle dimension: 0.5mm x 16mm). The microfluidic chip mould was provided by the Charvin lab (Aspert, Hentsch, and Charvin 2022).

Characterisation of single-cell growth

For analysis of cell growth and proliferation, DIC images were taken at 10-minute intervals for ~10 hours. Size at division and size at birth was measured using the Fiji Point Picker plugin. Generation time was calculated from the time of birth, where there is a visible 'pop' when the mother cell disconnects into two daughter cells, until a complete round of division ends with the same visible disconnection in the specific daughter cell. The time between the two disconnections for a single cell was determined by the number of frames multiplied by the time interval for the experiment (10 minutes), which constituted the single-cell generation time.

The percentage of non-dividing cells was determined by scoring the number of cells within individual traps that did not undergo septation over the course of the time-lapse. The percentage was then calculated from the total number of cells identified from the traps at the start of the experiment.

Characterisation of mitosis in single cells

To assess mitotic events in single cells, images were taken at 2-minute intervals for ~5 hours. Images were taken at each time point with DIC as well as with the 488 nm and 561 nm lasers. To visualize Pol1::GFP, 488 nm images were taken as z-stacks with 0.3μm steps between images. Maximum projections of each stack were generated before analysis. Quantification of 'early mitosis' was calculated based on the duration of Plo1::GFP at the SPB. Plo1 is a kinase that associates with the SPB at the onset of mitosis, and thus is a clear marker for identifying commitment to M. The timing of this was determined as starting from the sudden increase in the signal of Plo1 at the SPB, which followed the duplication of the SPB and its subsequent migration to the poles of the nucleus until the signal eventually disappears. The duration of this entire period of events was calculated by the number of frames multiplied by the time interval of acquisition (2 minutes).

To assess both the duration of 'late mitosis' (more specifically the duration of chromosome segregation) and the 'mitotic reversion' phenotype, the fluorescent marker Nhp6::mCherry was used. Single plane images were image taken at each time interval, following the acquisition of the Plo1::GFP stack, using the 561nm laser. Additionally, the hardware autofocus was set using this plane for each time-lapse experiment involving the Nhp6::mCherry marker. The duration of this

event was determined as starting when Plo1::GFP signal disappeared until the singular Nhp6::mCherry signal separated into two and reached their furthest distance apart before septation. The time between these points was calculated from the number of frames multiplied by the time interval (2 minutes). Using this marker, the occurrence of the 'mitotic reversion' phenotype was quantified. 'Mitotic reversion' was identified as occurring when the Nhp6::mCherry appears to expand before complete separation but then instead abruptly aborts retaining a single mass. Cells that presented this phenotype were excluded from the calculation of chromosome segregation duration. The percentage of cells that exhibited the 'mitotic reversion' phenotype was determined by the number of cells positive for the phenotype divided by the total number of cells scored in the experiment (completed a round of division or had an induced 'mitotic reversion').

The duration of mitosis was calculated from the start point of the 'early mitosis' parameter until the end point of the 'late mitosis' parameter. The timing of mitosis was then calculated as the number of frames between these events multiplied by the time interval (2 minutes).

Quantification of Cdk activity using SynCut3::mCherry in single cells

Cells were grown in PDMS microfluidic chips as described above. Z-stacks of images at 0.3μm steps were taken every 2 minutes using the 561nm laser. Maximal projections of each z-stack were generated. Cdk activity was subsequently quantified by measuring the average signal at the peak intensity of synCut3::mCherry signal in the nuclei of individual cells. The average pixel intensity of an area within the nucleus was calculated using Fiji (National Institute of Health).

Spot assays and determination of colony-forming units

Exponentially growing cells (approximately OD 0.4) were harvested and washed in fresh medium. The number of cells per millilitre was determined using a haemocytometer, and approximately 15625 were diluted in 1ml of fresh EMM6S medium. Using these cells, a dilution series of 6 was done with a ratio of 1:5, all in fresh EMM6S. Spots were made with 2 μL of each dilution in sequential order onto YE4S or YE4S plates containing either 3mM hydroxyurea or 2.5μM camptothecin. The plates were then incubated at 32°C for 3-4 days.

Protein extraction

Protein samples were prepared using the IPP50 extraction method: samples were prepared in IPP50 buffer (10 mM Tris-HCl pH 8, 150 mM NaCl, 0.1% NP-40) supplemented with protease inhibitors (100 mM PMSF, cOmplete ULTRA (ref: 05892953001, Roche)). Samples were maintained on ice at all times unless otherwise stated. Cells were harvested and resuspended in IPP50 + proteases and lysed using glass beads (BioSpec Products) in the Precellys Evolution (Bertin Instruments). The lysis program used with the Precellys was: 2 x 20 seconds at 8000 rpm, with 1-2 minutes on ice between. Protein extract was then transferred to a fresh tube, and 2 rounds of centrifugation at 4˚C each for 20 minutes (between which lysate was transferred to a fresh tube, and used in the subsequent centrifugation) were done to clear the debris. Quantification of protein concentrations was determined using the Bradford Protein Assay (Bio-Rad Protein Assay Dye Reagent Concentrate #5000006, 1:5 dilution in MilliQ H2O).

Western blots

Required protein amounts were diluted in 2x sample buffer (120 mM Tris/Cl pH 6.8, 20 % glycerol, 4 % SDS, 0.04 % bromophenol blue, 10 % ß-mercaptoethanol) before western blot analysis. Western blots were performed on total protein extracts. For the analysis of GFP-tagged strains, 30 µg of protein extract (1µg of extracts from overexpression strains) were loaded on 12% polyacrylamide gels. msGFP2 was detected using a monoclonal α-GFP (Roche # 11814460001, 1:1000) and a secondary α-mouse-HRP (Abcam (ab97046); 1:10000). For the immunostaining of HA-tagged strains, 30 µg (10µg of protein extracts from overexpression strains) were loaded on 15% polyacrylamide gels. HA was detected using a polyclonal α-HA HRP (Abcam (ab1190), 1:1000). For immunostaining of tubulin, 10 µg of protein extracts were loaded on 12% polyacrylamide gels. HA staining was done with a monoclonal α-TAT1 (a gift from K. Gull, 1:1000) and a secondary α-mouse-HRP (Abcam (ab97046); 1:10000).

GFP trap pull-down

The pull-down of GFP-tagged Spo12 was achieved using magnetic agarose beads that are conjugated with a GFP nanobody (ChromoTek (AB2631358)). 25 µl of beads were used for each protein sample of 500 µg. First, beads were equilibrated with a 3x wash of dilution buffer (10 mM Tris/Cl pH 7.5, 150 mM NaCl, 0.5 mM EDTA). 500 µg of protein extract in IPP50 was diluted up

to 500 µl with dilution buffer and added to the agarose beads. Samples were incubated overnight at 4˚C with continuous rotation. The beads were then washed 3x with wash buffer (10 mM Tris/Cl pH 7.5, 150 mM NaCl, 0.05 % Nonidet, P40 Substitute, 0.5 mM EDTA) and then transferred to a new tube. Proteins were eluted by resuspension of the beads in sample buffer and IPP50 buffer followed by 5 minutes boiling at 95˚C. The supernatant was used for western blot analysis.

DNA content analysis

Flow cytometry was used to perform DNA content analyses. Cells were fixed in 70% cold ethanol, washed with sodium citrate, and treated with RNAse A (0.1 mg/ml) overnight at 37˚C. Cells were then stained with propidium iodide (2 mg/ml), sonicated, and analysed using the BD Accuri C6 flow cytometer. The haploid fission yeast cell cycle has a short G1 period with cytokinesis occurring before DNA replication. Therefore, in asynchronous cultures, the majority of fission yeast cells will be cycling through G2 with a 2C DNA content. In synchronised cultures, cells will have a transient 4C peak as S phase occurs in post-mitotic binucleated cells, which is resolved upon cytokinesis resulting in mono-nucleated 2C cells. This 4C peak is not observed in asynchronous cultures as only a minority of cells are undergoing DNA replication at any given time. The appearance of a higher 1C peak in asynchronous cultures indicates an elongation of the G1 phase, indicating that cytokinesis is occurring before DNA replication.

Overexpression of Spo12 and Spo12(S54A)

Strains were constructed to integrate the nmt1 promoter upstream of *spo12* and *spo12(S54A)* (Supplementary Table 1). Strains were initially cultured in EMM6S supplemented with thiamine at 32˚C. 10 ml overnight static cultures were diluted into 30 ml and grown for a period of 24 hours with agitation. Cultures were then split, with one maintained in EMM6S supplemented with thiamine (nmt1 repressed), and the other without thiamine (overexpression of Spo12). For this, cultures were centrifuged at 3000 rpm for 5 minutes and washed with either EMM6S + thiamine or EMM6S. The wash step was repeated 3 times before inoculation into the respective media (with thiamine: OD~0.006, without thiamine: OD~0.01). Cultures were then maintained for a period of 36 hours in exponential growth before characterisation.

Quantification of Cdk activity in Spo12 overexpression strains

Images of exponentially growing cells with and without induced Spo12 overexpression were taken during live-cell imaging experiments (575/25 excitation, LED power at 15%, 200 ms exposure time). Cdk activity was quantified by measuring the average intensity of the synCut3::mCherry nuclear signal in each strain under the different conditions. At least 50 synCut3::mCherry nuclei were measured in mono-nucleated cells for each sample. Average pixel intensity was quantified using Fiji (National Institute of Health). MCN-AF XS-Spo12 and MCN-AF XS-Spo12(S54A) (Supplementary Table 1) were not determined because too few cells displayed synCut3::mCherry nuclear signal while in exponential growth.

Block and release of MCN strains

All MCN and MCN-AF (Supplementary Table 1) cells in this study harboured an amino acid alteration (F84G) in the Cdc2 component of the fusion protein (Bishop et al. 2000; Coudreuse and Nurse 2010). This change renders Cdc2 sensitive to inhibition by the non-hydrolysable ATP analogue 3-MBPP1 (Bishop et al. 2000; Coudreuse and Nurse 2010). Individual cultures of exponentially growing MCN msGFP2::Spo12, MCN msGFP2::Spo12(S54A), and MCN-AF msGFP2::Spo12 cells at OD595 = 0.3 were treated with 1 µM for 2 hours and 30 minutes, resulting in G2 arrest. Cells were released from the G2 block by washing 3x with pre-warmed EMM6S before re-inoculation of the culture. GFP images were then taken every 10 minutes starting at the moment of release.

Sporulation assay

The efficiency of fission yeast with and without Δ*spo12* to complete meiosis was determined via the percentage of 4-, 3-, and 2-spore tetrads observed after mating. Crosses were performed by mixing equal amounts of the indicated strains on EMM-N+glutamate plates. Crosses were incubated at 25˚C for 2.5 days before DIC images were taken. The percentages of asci with different numbers of spores were scored from the images acquired.

ACKNOWLEDGMENTS

REFERENCES

Alberti, Simon, Shambaditya Saha, Jeffrey B. Woodruff, Titus M. Franzmann, Jie Wang, and Anthony A. Hyman. 2018. "A User's Guide for Phase Separation Assays with Purified Proteins." *Journal of Molecular Biology* 430 (23): 4806–20. https://doi.org/10.1016/j.jmb.2018.06.038.

Anderson, Mark, Szu Shien Ng, Vanessa Marchesi, Fiona H. MacIver, Frances E. Stevens, Tracy Riddell, David M. Glover, Iain M. Hagan, and Christopher J. McInerny. 2002. "Plo1+ Regulates Gene Transcription at the M-G1 Interval during the Fission Yeast Mitotic Cell Cycle." *EMBO Journal* 21 (21): 5745–55. https://doi.org/10.1093/emboj/cdf564.

Aspert, Théo, Didier Hentsch, and Gilles Charvin. 2022. "DetecDiv, a Generalist Deep-Learning Platform for Automated Cell Division Tracking and Survival Analysis." *ELife* 11 (August): 2021.10.05.463175. https://doi.org/10.7554/eLife.79519.

Bishop, Anthony C., Jeffrey A. Ubersax, Dejah T. Pøtsch, Dina P. Matheos, Nathanael S. Gray, Justin Blethrow, Eiji Shimizu, et al. 2000. "A Chemical Switch for Inhibitor-Sensitive Alleles of Any Protein Kinase." *Nature* 407 (6802): 395–401. https://doi.org/10.1038/35030148.

Blanco, Miguel a, Alberto Sánchez-Díaz, José M. de Prada, and Sergio Moreno. 2000. "APC Ste9/Srw1 Promotes Degradation of Mitotic Cyclins in G 1 and Is Inhibited by Cdc2 Phosphorylation." *The EMBO Journal* 19 (15): 3945–55. https://doi.org/10.1093/emboj/19.15.3945.

Buck, Vicky, Szu Shien Ng, Ana Belen Ruiz-Garcia, Kyriaki Papadopoulou, Saeeda Bhatti, Jane M. Samuel, Mark Anderson, Jonathan B.A. Millar, and Christopher J. McInerny. 2004. "Fkh2p and Sep1p Regulate Mitotic Gene Transcription in Fission Yeast." *Journal of Cell Science* 117 (23): 5623–32. https://doi.org/10.1242/jcs.01473.

Chang, L., J. L. Morrell, A. Feoktistova, and K. L. Gould. 2001. "Study of Cyclin Proteolysis in

Anaphase-Promoting Complex (APC) Mutant Cells Reveals the Requirement for APC Function in the Final Steps of the Fission Yeast Septation Initiation Network." *Molecular and Cellular Biology* 21 (19): 6681–94. https://doi.org/10.1128/mcb.21.19.6681-6694.2001.

Chaves, Susana R., and Günter Blobel. 2001. "Nuclear Import of Spo12p, a Protein Essential for Meiosis." *Journal of Biological Chemistry* 276 (21): 17712–17. https://doi.org/10.1074/jbc.M010760200.

Chen, C.-T., M.-P. Peli-Gulli, V. Simanis, and D. McCollum. 2006. "S. Pombe FEAR Protein Orthologs Are Not Required for Release of Clp1/Flp1 Phosphatase from the Nucleolus during Mitosis." *Journal of Cell Science* 119 (21): 4462–66. https://doi.org/10.1242/jcs.03220.

Conduit, Paul T., Zhe Feng, Jennifer H. Richens, Janina Baumbach, Alan Wainman, Suruchi D. Bakshi, Jeroen Dobbelaere, Steven Johnson, Susan M. Lea, and Jordan W. Raff. 2014. "The Centrosome-Specific Phosphorylation of Cnn by Polo/Plk1 Drives Cnn Scaffold Assembly and Centrosome Maturation." *Developmental Cell* 28 (6): 659–69. https://doi.org/10.1016/j.devcel.2014.02.013.

Coudreuse, Damien, and Paul Nurse. 2010a. "Driving the Cell Cycle with a Minimal CDK Control Network." *Nature* 468 (7327): 1074–80. https://doi.org/10.1038/nature09543.

———. 2010b. "Driving the Cell Cycle with a Minimal CDK Control Network." *Nature* 468 (December): 1074. https://doi.org/10.1038/nature09543.

Domingo-Sananes, Maria Rosa, Orsolya Kapuy, Tim Hunt, and Bela Novak. 2011. "Switches and Latches: A Biochemical Tug-of-War between the Kinases and Phosphatases That Control Mitosis." *Philosophical Transactions of the Royal Society B: Biological Sciences* 366 (1584): 3584–94. https://doi.org/10.1098/rstb.2011.0087.

Fantes, P. A. 1981. "Isolation of Cell Size Mutants of a Fission Yeast by a New Selective Method: Characterization of Mutants and Implications for Division Control Mechanisms." *Journal of Bacteriology* 146 (2): 746–54. https://doi.org/10.1128/jb.146.2.746-754.1981.

Fantes, P. A., W. D. Grant, R. H. Pritchard, P. E. Sudbery, and A. E. Wheals. 1975. "The Regulation of Cell Size and the Control of Mitosis." *Journal of Theoretical Biology* 50 (1): 213–44. https://doi.org/10.1016/0022-5193(75)90034-X.

Fantes, P., and P. Nurse. 1977. "Control of Cell Size at Division in Fission Yeast by a Growth-Modulated Size Control over Nuclear Division." *Experimental Cell Research* 107 (2): 377–86. https://doi.org/10.1016/0014-4827(77)90359-7.

Fisher, D., L. Krasinska, D. Coudreuse, and B. Novak. 2012. "Phosphorylation Network Dynamics in the Control of Cell Cycle Transitions." *Journal of Cell Science* 125 (20): 4703–11. https://doi.org/10.1242/jcs.106351.

Fragkos, Michalis, Olivier Ganier, Philippe Coulombe, and Marcel Méchali. 2015. "DNA
    Replication Origin Activation in Space and Time." *Nature Reviews Molecular Cell Biology* 16
    (6): 360–74. https://doi.org/10.1038/nrm4002.

Fu, Jingyan, Iain M. Hagan, and David M. Glover. 2015. "The Centrosome and Its Duplication
    Cycle." *Cold Spring Harbor Perspectives in Medicine* 5 (1): 1–36.
    https://doi.org/10.1101/cshperspect.a015800.

Gérard, Claude, John J. Tyson, Damien Coudreuse, and Béla Novák. 2015. "Cell Cycle Control by
    a Minimal Cdk Network." *PLoS Computational Biology* 11 (2): 1–27.
    https://doi.org/10.1371/journal.pcbi.1004056.

Gérard, Claude, John J. Tyson, and Béla Novák. 2013. "Minimal Models for Cell-Cycle Control
    Based on Competitive Inhibition and Multisite Phosphorylations of Cdk Substrates."
    Biophysical Journal 104 (6): 1367–79. https://doi.org/10.1016/j.bpj.2013.02.012.

Grallert, Agnes, Kuan Yoow Chan, Maria Luisa Alonso-Nuñez, Marisa Madrid, Ashapurna Biswas,
    Isabel Alvarez-Tabarés, Yvonne Connolly, et al. 2013. "Removal of Centrosomal PP1 by
    NIMA Kinase Unlocks the MPF Feedback Loop to Promote Mitotic Commitment in S.
    Pombe." *Current Biology* 23 (3): 213–22. https://doi.org/10.1016/j.cub.2012.12.039.

Grallert, Agnes, and Iain M. Hagan. 2002. "Schizosaccharomyces Pombe NIMA-Related Kinase,
    Fin1, Regulates Spindle Formation and an Affinity of Polo for the SPB." *EMBO Journal* 21
    (12): 3096–3107. https://doi.org/10.1093/emboj/cdf294.

Gutiérrez-Escribano, Pilar, and Paul Nurse. 2015. "A Single Cyclin-CDK Complex Is Sufficient for
    Both Mitotic and Meiotic Progression in Fission Yeast." *Nature Communications* 6.
    https://doi.org/10.1038/ncomms7871.

Harashima, Hirofumi, Nico Dissmeyer, and Arp Schnittger. 2013. "Cell Cycle Control across the
    Eukaryotic Kingdom." *Trends in Cell Biology* 23 (7): 345–56.
    https://doi.org/10.1016/j.tcb.2013.03.002.

Hayles, Jacqueline, and Paul Nurse. 1992. "Genetics of the Fission Yeast Schizosaccharomyces
    Pombe." *Annual Review of Genetics* 26: 373–402.
    https://doi.org/10.1146/annurev.ge.26.120192.002105.

Hermeking, Heiko, and Anne Benzinger. 2006. "14-3-3 Proteins in Cell Cycle Regulation."
    Seminars in Cancer Biology 16 (3): 183–92. https://doi.org/10.1016/j.semcancer.2006.03.002.

Hochegger, Helfrid, Shunichi Takeda, and Tim Hunt. 2008. "Cyclin-Dependent Kinases and Cell-
    Cycle Transitions: Does One Fit All?" *Nature Reviews Molecular Cell Biology* 9 (11): 910–16.
    https://doi.org/10.1038/nrm2510.

Karaiskou, Anthi, Catherine Jessus, Thierry Brassac, and René Ozon. 1999. "Phosphatase 2A and

Polo Kinase, Two Antagonistic Regulators of Cdc25 Activation and MPF Auto-Amplification." *Journal of Cell Science* 112 (21): 3747–56. https://doi.org/10.1242/jcs.112.21.3747.

Klapholz, Sue, and Rochelle Easton Esposito. 1980. "ISOLATION OF SPO12–1 AND SPO13–1 FROM A NATURAL VARIANT OF YEAST THAT UNDERGOES A SINGLE MEIOTIC DIVISION." *Genetics* 96 (3): 567–88. https://doi.org/10.1093/genetics/96.3.567.

Kozar, Katarzyna, Maria A. Ciemerych, Vivienne I. Rebel, Hirokazu Shigematsu, Agnieszka Zagozdzon, Ewa Sicinska, Yan Geng, et al. 2004. "Mouse Development and Cell Proliferation in the Absence of D-Cyclins." *Cell* 118 (4): 477–91. https://doi.org/10.1016/j.cell.2004.07.025.

Kumagai, Akiko, and William G. Dunphy. 1996. "Purification and Molecular Cloning of Plx1, a Cdc25-Regulatory Kinase from Xenopus Egg Extracts." *Science* 273 (5280): 1377–80. https://doi.org/10.1126/science.273.5280.1377.

Larochelle, Marc, Danny Bergeron, Bruno Arcand, and François Bachand. 2019. "Proximity-Dependent Biotinylation Mediated by TurboID to Identify Protein-Protein Interaction Networks in Yeast." *Journal of Cell Science* 132 (11). https://doi.org/10.1242/jcs.232249.

Liu, Xing, Xu Liu, Haowei Wang, Zhen Dou, Ke Ruan, Donald L. Hill, Lin Li, Yunyu Shi, and Xuebiao Yao. 2020. "Phase Separation Drives Decision Making in Cell Division." *Journal of Biological Chemistry* 295 (39): 13419–31. https://doi.org/10.1074/jbc.REV120.011746.

Maundrell, K. 1990. "Nmt1 of Fission Yeast. A Highly Transcribed Gene Completely Repressed by Thiamine." *Journal of Biological Chemistry* 265 (19): 10857–64. https://doi.org/10.1016/s0021-9258(19)38525-4.

McDonald, J. Cooper, and George M. Whitesides. 2002. "Poly(Dimethylsiloxane) as a Material for Fabricating Microfluidic Devices." *Accounts of Chemical Research* 35 (7): 491–99. https://doi.org/10.1021/ar010110q.

Millar, J. B.A., P. Russell, J. E. Dixon, and K. L. Guan. 1992. "Negative Regulation of Mitosis by Two Functionally Overlapping PTPases in Fission Yeast." *EMBO Journal* 11 (13): 4943–52. https://doi.org/10.1002/j.1460-2075.1992.tb05601.x.

Mimura, Satoru, Takashi Seki, Seiji Tanaka, and John F.X. Diffley. 2004. "Phosphorylation-Dependent Binding of Mitotic Cyclins to Cdc6 Contributes to DNA Replication Control." *Nature* 431 (7012): 1118–23. https://doi.org/10.1038/nature03024.

Mochida, Satoru, Scott Rata, Hirotsugu Hino, Takeharu Nagai, and Béla Novák. 2016. "Two Bistable Switches Govern M Phase Entry." *Current Biology* 26 (24): 3361–67. https://doi.org/10.1016/j.cub.2016.10.022.

Moreno, Sergio, Amar Klar, and Paul Nurse. 1991. "Molecular Genetic Analysis of Fission Yeast

Schizosaccharomyces Pombe." *Methods in Enzymology* 194 (C): 795–823. https://doi.org/10.1016/0076-6879(91)94059-L.

Morgan, David O. 2007. *Primers in Biology The Cell Cycle Primers in Biology : Protein Structure and Function Forthcoming Titles :*

Mulvihill, Daniel P., Janni Petersen, Hiroyuki Ohkura, David M. Glover, and Iain M. Hagan. 1999. "Plo1 Kinase Recruitment to the Spindle Pole Body and Its Role in Cell Division in Schizosaccharomyces Pombe." *Molecular Biology of the Cell* 10 (8): 2771–85. https://doi.org/10.1091/mbc.10.8.2771.

Ni, Bin, Bhaswar Ghosh, Ferencz S. Paldy, Remy Colin, Thomas Heimerl, and Victor Sourjik. 2017. "Evolutionary Remodeling of Bacterial Motility Checkpoint Control." *Cell Reports* 18 (4): 866–77. https://doi.org/10.1016/j.celrep.2016.12.088.

Nobs, Jean Bernard, and Sebastian J. Maerkl. 2014. "Long-Term Single Cell Analysis of S. Pombe on a Microfluidic Microchemostat Array." *PLoS ONE* 9 (4). https://doi.org/10.1371/journal.pone.0093466.

Novak, Bela, John J. Tyson, Bela Gyorffy, and Attila Csikasz-Nagy. 2007. "Irreversible Cell-Cycle Transitions Are Due to Systems-Level Feedback." *Nature Cell Biology* 9 (7): 724–28. https://doi.org/10.1038/ncb0707-724.

Örd, Mihkel, Rainis Venta, K. Möll, E. Valk, and Mart Loog. 2019a. "Cyclin-Specific Docking Mechanisms Reveal the Complexity of M-CDK Function in the Cell Cycle." *Molecular Cell* 75 (1): 76-89.e3. https://doi.org/10.1016/j.molcel.2019.04.026.

———. 2019b. "Cyclin-Specific Docking Mechanisms Reveal the Complexity of M-CDK Function in the Cell Cycle." *Molecular Cell* 75 (1): 76-89.e3. https://doi.org/10.1016/j.molcel.2019.04.026.

Papadopoulou, Kyriaki, Szu Shien Ng, Hiroyuki Ohkura, Marco Geymonat, Steven G. Sedgwick, and Christopher J. McInerny. 2008. "Regulation of Gene Expression during M-G1-Phase in Fission Yeast through Plo1p and Forkhead Transcription Factors." *Journal of Cell Science* 121 (1): 38–47. https://doi.org/10.1242/jcs.019489.

Patterson, James O. 2017. "Quantitative Biology of Cell Cycle Decision Making - A Thesis Submitted for the Degree of Doctor of Philosophy University College London," no. August.

Peters, Jan Michael. 2006. "The Anaphase Promoting Complex/Cyclosome: A Machine Designed to Destroy." *Nature Reviews Molecular Cell Biology* 7 (9): 644–56. https://doi.org/10.1038/nrm1988.

Petronczki, Mark, Péter Lénárt, and Jan Michael Peters. 2008. "Polo on the Rise-from Mitotic Entry to Cytokinesis with Plk1." *Developmental Cell* 14 (5): 646–59.

https://doi.org/10.1016/j.devcel.2008.04.014.

Pickering, Mary, Mira Magner, Dan Keifenheim, and Nicholas Rhind. 2021. "The Fission Yeast S-Phase Cyclin Cig2 Can Drive Mitosis." *Genetics* 217 (1). https://doi.org/10.1093/GENETICS/IYAA002.

Pines, Jonathon. 2011. "Cubism and the Cell Cycle: The Many Faces of the APC/C." *Nature Reviews Molecular Cell Biology* 12 (7): 427–38. https://doi.org/10.1038/nrm3132.

Roy, Babhrubahan, Simon J.Y. Han, Adrienne N. Fontan, Soubhagyalaxmi Jema, and Ajit P. Joglekar. 2022. "Aurora B Phosphorylates Bub1 to Promote Spindle Assembly Checkpoint Signaling." *Current Biology* 32 (1): 237-247.e6. https://doi.org/10.1016/j.cub.2021.10.049.

Russell, Paul, and Paul Nurse. 1987. "Negative Regulation of Mitosis by Wee1+, a Gene Encoding a Protein Kinase Homolog." *Cell* 49 (4): 559–67. https://doi.org/10.1016/0092-8674(87)90458-2.

Samuel, J. M., N. Fournier, V. Simanis, and J. B.A. Millar. 2000. "SPO12 Is a Multicopy Suppressor of Mcs3 That Is Periodically Expressed in Fission Yeast Mitosis." *Molecular and General Genetics* 264 (3): 306–16. https://doi.org/10.1007/s004380000324.

Sancar, Aziz, Laura A. Lindsey-Boltz, Keziban Ünsal-Kaçmaz, and Stuart Linn. 2004. "Molecular Mechanisms of Mammalian DNA Repair and the DNA Damage Checkpoints." *Annual Review of Biochemistry* 73: 39–85. https://doi.org/10.1146/annurev.biochem.73.011303.073723.

Santaguida, Stefano, and Angelika Amon. 2015. "Short- and Long-Term Effects of Chromosome Mis-Segregation and Aneuploidy." *Nature Reviews Molecular Cell Biology* 16 (8): 473–85. https://doi.org/10.1038/nrm4025.

Santos, Silvia D.M., Roy Wollman, Tobias Meyer, and James E. Ferrell. 2012. "Spatial Positive Feedback at the Onset of Mitosis." *Cell* 149 (7): 1500–1513. https://doi.org/10.1016/j.cell.2012.05.028.

Schlessinger, Avner, Christian Schaefer, Esmeralda Vicedo, Markus Schmidberger, Marco Punta, and Burkhard Rost. 2011. "Protein Disorder-a Breakthrough Invention of Evolution?" *Current Opinion in Structural Biology* 21 (3): 412–18. https://doi.org/10.1016/j.sbi.2011.03.014.

Suárez, M. Belén, María Luisa Alonso-Nuñez, Francisco del Rey, Christopher J. McInerny, and Carlos R.Vázquez de Aldana. 2015. "Regulation of Ace2-Dependent Genes Requires Components of the PBF Complex in Schizosaccharomyces Pombe." *Cell Cycle* 14 (19): 3124–37. https://doi.org/10.1080/15384101.2015.1078035.

Sutani, Takashi, Tatsuro Yuasa, Takeshi Tomonaga, Naoshi Dohmae, Koji Takio, and Mitsuhiro Yanagida. 1999. "Fission Yeast Condensin Complex: Essential Roles of Non-SMC Subunits for Condensation and Cdc2 Phosphorylation of Cut3/SMC4." *Genes & Development* 13 (17):

2271–83. https://doi.org/10.1101/gad.13.17.2271.

Sveiczer, A., B. Novak, and J. M. Mitchison. 1996. "The Size Control of Fission Yeast Revisited."
Journal of Cell Science 109 (12): 2947–57. https://doi.org/10.1242/jcs.109.12.2947.

Swaffer, Matthew P., Andrew W. Jones, Helen R. Flynn, Ambrosius P. Snijders, and Paul Nurse.
2016. "CDK Substrate Phosphorylation and Ordering the Cell Cycle." *Cell* 167 (7): 1750-
1761.e16. https://doi.org/10.1016/j.cell.2016.11.034.

Tomson, Brett N., Rami Rahal, Vladimír Reiser, Fernando Monje-Casas, Karim Mekhail, Danesh
Moazed, and Angelika Amon. 2009a. "Regulation of Spo12 Phosphorylation and Its Essential
Role in the FEAR Network." *Current Biology* 19 (6): 449–60.
https://doi.org/10.1016/j.cub.2009.02.024.

Tomson, Brett N, Rami Rahal, Vladimír Reiser, Fernando Monje-Casas, Karim Mekhail, Danesh
Moazed, and Angelika Amon. 2009b. "Regulation of Spo12 Phosphorylation and Its Essential
Role in the FEAR Network." *Current Biology* 19 (6): 449–60.
https://doi.org/10.1016/j.cub.2009.02.024.

Torres-garcia, Sito, Lorenza Di Pompeo, Luke Eivers, Baptiste Gaborieau, Sharon A White, Alison
L Pidoux, Paulina Kanigowska, et al. 2021. "SpEDIT : A Fast and Efficient CRISPR / Cas9
Method for Fission Yeast [Version 1 ; Peer Review : 3 Approved]," 1–24. https://pubmed-
ncbi-nlm-nih-gov.insb.bib.cnrs.fr/33313420/.

Visintin, Rosella, Frank Stegmeier, and Angelika Amon. 2003. "The Role of the Polo Kinase Cdc5
in Controlling Cdc14 Localization." *Molecular Biology of the Cell* 14 (11): 4486–98.
https://doi.org/10.1091/mbc.e03-02-0095.

Willis, Nicholas A., Chunshui Zhou, Andrew E.H. Elia, Johanne M. Murray, Antony M. Carr,
Stephen J. Elledge, and Nicholas Rhind. 2016. "Identification of S-Phase DNA Damage-
Response Targets in Fission Yeast Reveals Conservation of Damage-Response Networks."
Proceedings of the National Academy of Sciences of the United States of America 113 (26):
E3676–85. https://doi.org/10.1073/pnas.1525620113.

Wood, Elizabeth, and Paul Nurse. 2013. "Pom1 and Cell Size Homeostasis in Fission Yeast." *Cell
Cycle* 12 (19): 3417–25. https://doi.org/10.4161/cc.26462.

FIGURE LEGENDS

Figure 1: Experimental evolution of the minimal cell cycle lacking the Wee1/Cdc25 feedback loop.
(A) Optical density measurements taken for each ministat during the experimental evolution assay. While the ministats used for budding yeast and fission yeast are designed to keep the OD constant, we find that at lower OD it is difficult to achieve, leading to important changes in OD during the experiment. In fact, the lab has since began using a eVOLVER instead, which is fully automatic with a feedback system to have much more reliable OD maintenance. **(B)** Schematic of the experimental evolution set up. Single colonies were inoculated in triplicate for each strain. **(C)** Generation time of each evolving population over the duration of the assay. **(D)** Size at division box plots for the ancestor, day 21 (D21) and day 65 (D65) for ministats M1, M2, M3, M4, and M7. Results similar to those for M4 and M7 were obtained for M5, M6, M8 and M9 (data not shown).

Figure 2: FACS profiles for populations from respective ministats for days 1, 35, and 70.
Wild type control (WT) indicates that expected FACS profile for asynchronous S. pombe populations. The appearance of a 1C peak implies larger percentage of cells cycling through G1 (extension of G1 phase) in an asynchronous population.

Figure 3: Characterisation of individual evolved clones from the evolved populations.
Three individual clones (1-3) were isolated for each evolving populations at the indicated days and characterised (generation time, **A**; size at division, **B**; co-variance of size at division, **C**) compared to the ancestor strains.

Figure 4: DNA content analysis of each set of sub-clones of the evolved MCN-AF populations at Day 1, Day 35, and Day 70.
DNA content was measure for asynchronous populations of the evolved clones for each for the evolved MCN-AF populations at the indicated days. As a reference, wild type (WT) is included.

Figure 5: Sequencing maps of genes with mutations in the different cell cycle networks during the experimental evolution assay
Each sequencing map corresponds to the respective vial (M1, M2, M3, M4, and M7). A subset of the genes that have accumulated mutations is indicated, and mapped according to when they are are predicted to have been mutated in the population during the experimental evolution assay. Stars represent the isolated evolved clones from the population that were sequenced.

Figure 6: Backcrossing results of M3.D70.3 evolved clones with MCN-AF ancestral strain.
Clone 3 of day 70 from vial M3 was backcrossed with the ancestral MCN-AF, and the generation time was determined for each of the individual spores. Populations from each spore were then fully sequenced, and the alleles for the genes identified in the initial whole population sequencing (M3.D70.3) were assigned (E: evolved, A: ancestral). A representative tetrad is shown. Bar chart (left panel) indicates the calculated generation time for each of the spores from the backcross. Table (right panel) indicates the allele for each candidate gene.

Figure 7: Schematic representation of fission yeast Spo12

Top panel: schematic of the fission yeast Spo12 protein. The location of the experimental evolution (EE) mutation variant, Q19X (black triangle) and the putative target sites for Cdc2 (red triangles) are indicated. Proteomic studies suggest that only S54 is phosphorylated by Cdk1 (Swaffer et al. 2016). The location of a conserved Fin1 target site (green triangle), which was identified by the Eukaryotic Linear Motif (ELM) resource (http://elm.eu.org/), is also indicated**.** Bottom panel: prediction of unstructured regions in Spo12 using the IUPpred2 tool (https://iupred2a.elte.hu/) for detecting short disordered domains.

Figure 8: Characterisation of Δ*spo12* and *spo12(S54A)* asynchronous populations

All experiments were performed in EMM6S at 32ºC. **(A)** Generation time (GT) and size at division (SAD) for the indicated strains. For GT, averages and standard errors of 3 experiments are shown. For SAD, averages of 3 experiments (*n*>100 for each experiment) and standard deviations of the full datasets are shown. **(B)** DNA contents analysis by flow cytometry. The 1C and 2C peaks are indicated. The shortening of G1 in the absence of Spo12 can be seen by a reduction of the 1C peak and an increased 2C peak compared to the MCN-AF. Δ*spo12* has no observable impact in both the WT and MCN backgrounds **(C)** Distribution of SAD data for the indicated strains. MCN-AF has a wider distribution compared to wild type (WT) and MCN due to the loss of size control. Loss of Spo12 reduces the average size but does not change the heterogeneous distribution. **(D)** Drop assays for the indicated strains on rich medium (YE4S), 3mM hydroxyurea (HU, depletes nucleotide pools), and 2.5μM camptothecin (CPT, inhibitor of Topoisomerase I). Serial dilutions of exponentially growing cells were spotted and the plates incubated at 32˚C. Note that low concentrations of the drugs were used, as cells carrying the MCN-AF module are hypersensitive to these stresses. At these concentrations, wild type cells are not affected. A-E: WT: wild type **(E)** Western blot analysis of total cell lysates in asynchronous populations of the indicated genotypes expressing *spo12* or *spo12(S54A)* that are HA-tagged (N-terminal tag). Tubulin was used as a loading control. **(F)** Blankophor staining of exponentially growing strains of the indicated genotypes. Scale bar = 10μm.

Figure 9: The characterisation of individual cells carrying Δ*spo12*

All experiments were performed with exponentially growing asynchronous cells grown in EMM6S at 32˚C. **(A)** DIC image of four of the traps used in our microfluidic devices. Scale bar = 10μm. **(B)** Comparison of the distribution of cell length between cells grown in a flask and imaged between a slide and a coverslip (slide), and cells injected into the microfluidic devices (chamber). Representative dataset from a single experiment (*n*>100). The median cell length with Median Absolute Deviation is shown. **(C)** Single-cell generation time for the indicated strains. The generation time for a single cell was determined as the time from birth (cytokinesis) until the next complete division into two daughter cells. Pooled data of three individual experiments (*n*>150 for each experiment). The median doubling times with Median Absolute Deviation are shown. **(D)** Percentage of non-dividing cells for the indicated strains. Cells were considered non-dividing when they failed to grow or divide over the course of the 10-hour time-lapse. Pooled data of three individual experiments with standard error bars (*n*>80 for each experiment). **(E)** Distribution in cell size at division for the indicated strains. Pooled data of three individual experiments (*n*>150 for each experiment). The median SAD with Median Absolute Deviation is indicated. **(F)** Generation

time plotted against cell length at birth for the indicated strains. Pooled data of three individual experiments (*n*>150 for each experiment). The slope values are shown, which were calculated from regression lines best fitted to the data.

Figure 10: Spo12 localisation
Maximum z-projections of cells expressing msGFPs-tagged Spo12. Nter = N-terminal tagging, Cter = C-terminal tagging. Images were acquired from exponentially growing asynchronous population in EMM6S at 32˚C. Scale bar = 10μm.

Figure 11: Levels of Spo12 and Spo12(S54A) in synchronised MCN cells
(A) Schematic of block and release of MCN cells. **(B)** Analysis of msGFP2::Spo12 and msGFP2::Spo12(S54A) localisation in synchronised MCN cells. MCN cells expressing either GFP fusion were synchronised and images were taken at the indicated times. Scale bar = 10 μm. **(C)** DNA content analysis of MCN strains with either msGFP2::Spo12 or msGFP2::Spo12(S54A). Cells were synchronised in G2 using a 2 h 45 min treatment with the 3-MBPP1 inhibitor of the MCN fusion protein (Coudreuse and Nurse 2010a), and released to synchronously re-enter the cell cycle. **(D)** Western blot analysis of N-terminally msGFP2-tagged Spo12 and Spo12(S54A) in MCN cells throughout the cell cycle. Tubulin was used as a loading control. **(E)** Percentage of binucleated cells after synchronization (*n*> 100 at each time point). Samples were analysed at 15-minute intervals. **(F)** Maximum projected z-stack image of synchronised MCN msGFP2::Spo12(S54A) cells from time point 10. Arrows indicate Spo12(S54A) localisation at the mitotic spindle. Scale bar = 10 μm.

Figure 12: Spo12 cleavage
Western blot analysis of total cell lysates from asynchronous populations of the indicated genotypes. Tubulin was used as a loading control. **(A)** Comparison of N-terminal and C-terminal tagging of Spo12 with msGFP2 for the indicated strains. **(B)** Analysis of Spo12 cleavage using either the N-terminal or C-terminal msGFP2 tag. **(C)** Analysis of the impact of the tag on Spo12 C-terminal cleavage.

Figure 13: Characterisation of mitosis in cells lacking Spo12
All experiments were done in EMM6S at 32˚C using microfluidic chips and a flow rate of fresh medium of 5 μL/min. **(A)** Examples of normal mitosis (top) and mitotic reversion (bottom). The times between successive images are indicated (min). Top panel: merge of frames from time-lapse experiments monitoring Plo1::GFP (green) and Nhp6::mCherry (red). Bottom panel: corresponding DIC images. Scale bar = 5 μm. **(B-D)** Distributions of the duration of mitosis (B), Plo1 recruitment at the SPB (C), and chromosome segregation (D) for the indicated strains. The duration of mitosis was defined as the time between the recruitment of Plo1 to the SPB and the complete separation of the chromosomes. The length of Plo1 residency at the SPB was defined from Plo1 enrichment to its disappearance. The duration of chromosome segregation was determined as the time between the loss of Plo1 enrichment at the SPB and the complete separation of the DNA into two masses. (B-D): Images were acquired every 2 minutes. Pooled data of three individual experiments (*n*>30 for each experiment). The median values with Median Absolute Deviation are shown. **(E)** The

percentage of cells undergoing full 'mitotic reversion' for the indicated genotypes. Pooled data of three individual experiments ($n>30$ for each experiment). Error bars: standard error of the mean.

Figure 14: Single-cell analysis of Cdk activity dynamics
All experiments were performed in EMM6S at 32˚C with a flow rate of 5 µL/min. Z-stack images were acquired and average nuclear intensity was determined from maximum projections using Fiji. Images were taken at 2 minute intervals. **(A)** Top panel: Representative images of synCut3::mCherry dynamics during cell division. Bottom panel: corresponding DIC images. The times between frames are indicated. Scale bar = 5 µm. **(B)** Histogram distributions of the peak synCut3::mCherry intensities in the indicated strains. Pooled data of a triplicate ($n>50$ for each experiment). **(C)** Quantification of nuclear synCut3::mCherry throughout the cell cycle in individual cells of the indicated genotypes. y-axis: average peak synCut3::mCherry intensities. For display purpose, the profiles were aligned to their peak synCut3::mCherry intensity. Representative experiment of a triplicate ($n>20$ for each experiment). Error bars show the standard deviation at each time point.

Figure 15: Loss of Spo12 in *wee1-50* and *cdc25-22* genetic backgrounds
(A-B) Distribution of size at division for the indicated genotypes. Data are from asynchronous populations grown in EMM6S at 25ºC. Data is from a pooled triplicate ($n>100$ cells per experiment). Number denotes average with standard deviation for indicate strains.

Figure 16: Overexpression of Cdk1 phosphorylated Spo12 potentiates Cdk Activity
All experiments were performed in EMM6S supplemented with thiamine at 32ºC with asynchronous populations. Each replicate was washed with either EMM6S with thiamine or without thiamine, and grown for a period of 36 hours in the respective conditions before characterisation. Strains grown with thiamine are denoted with a the "+" symbol (the expression of *spo12* or *spo12(S54A)* is repressed), and strains grown without thiamine are denoted with a "-" symbol (overexpression of *spo12* or *spo12(S54A)*). **(A)** Generation time (GT), size at division (SAD), and average synCut3::mCherry intensity for the indicated strains when grown with and without thiamine. n.d. :not determined. For GT, averages and standard errors of 3 experiments are shown. For SAD, averages of 3 experiments ($n>100$ for each experiment) and standard deviations of the full datasets are shown. For the synCut3::mCherry intensity, the average of 3 experiments *($n>50$* cells for each experiment) and standard deviations of the full datasets are shown. The average intensity was determined from cells with a visible synCut3::mCherry nuclear signal in an asynchronous population. **(B)** DNA content analysis for the indicated strains. The 1C and 2C peaks are indicated. **(C)** Distribution of SAD. This data corresponds to the measurements denoted in A. **(D)** Histograms of average synCut3::mCherry nuclear intensity. Average nuclear intensity was determined using Fiji. The data corresponds to the value shown in A. **(E)** Western blot analysis of 3xHA::Spo12 and 3xHA::Spo12(S54A) in the different expression conditions. All strains were built with the *Pnmt1::3xHA* construct, so we would be able to confirm that the overexpression works.

Figure 17: Overexpression of phosphorylated Spo12 in MCN-AF cells impairs growth
Representative Blankophor staining of exponentially growing MCN-AF *Pnmt1::3xHA::spo12* and MCN-AF *Pnmt1::3xHA::spo12(S54A)* under the different expression conditions. Scale bar = 10µm. Populations were grown in EMM6S supplemented with (+) or without (-) thiamine at 32ºC.

Figure 18: Analysis of Spo12 interaction with Cdc2 and impact on meiosis

(A) Western blot of GFP trap pull-down from whole cell lysate for msGFP2 N-terminally tagged Spo12 and Spo12(S54A). 500µg of lysate was used for each GFP trap assay. Immunostaining was done for GFP and Cdc2 (PSTAIR motif). Cdc2 is indicated at the 32kDa size. **(B)** Percentage of 4 spore, 3 spore, and 2 spore tetrads from the indicated crosses. Strains were crossed on EMM -N +glutamate at 25˚C. Data is from a single experiment (*n*>100 tetrads).

Supplementary Table 1

Strain	Genotype	Source
PN1	*h-*	Nurse Lab
PN4	*h+*	Nurse Lab
DC31	*h- cdc25-22*	Our Stock
DC76	*h- wee1-50*	Our Stock
DC561	*h+ leu1::Pcdc13::cdc13Scdc2as::cdc13UTR::ura4+ Dcdc2::KAN Dcdc13::NAT Dcig1::HYG Dcig2::KAN Dpuc1::leu2+ Dgsf2::KAN ura4-D18*	This Study
DC566	*h- leu1::Pcdc13::cdc13Scdc2T14AY15Fas::cdc13UTR::ura4+ Dcdc2::KAN Dcdc13::NAT Dcig1::HYG Dcig2::KAN Dpuc1::leu2+ Dgsf2::KAN ura4-D18*	This Study
DC595	*h- int::ura4+ int::leu2+ Dgsf2::KAN ura4-D18 leu1-32*	This Study
DC600	*h+ Drad3::KAN*	Our Stock
DC676	*h- Pcdc13::cdc13Scdc2as::cdc13UTR Dcdc2::KAN Dcig1::HYG Dcig2::KAN Dpuc1::HYG*	This Study
DC684	*h+ Pcdc13::cdc13Scdc2as::cdc13UTR Dcdc2::KAN Dcig1::HYG Dcig2::KAN Dpuc1::HYG Dgsf2::KAN*	This Study
DC752	*h+ Pcdc13::cdc13Scdc2T14AY15Fas::cdc3UTR Dcdc2::KAN Dcig1::HYG Dcig2::KAN Dpuc1::HYG*	This Study
DC778	*h- Dspo12::KAN*	This Study
DC916	*h- Nhp6::mCherry-ura4+ plo1::GFP-KAN*	This Study
DC958	*h+ Pcdc13::cdc13Scdc2T14AY15Fas::cdc13UTR Dcdc2::KAN Dcig1::HYG Dcig2::KAN Dpuc1::HYG Dspo12::KAN*	This Study
DC960	*h- Pcdc13::cdc13Scdc2T14AY15Fas::cdc13UTR Dcdc2::KAN Dcig1::HYG Dcig2::KAN Dpuc1::HYG Nhp6::mCherry::ura4+ plo1::GFP::KAN*	This Study
DC962	*h- Pcdc13::cdc13Scdc2T14AY15Fas::cdc13UTR Dspo12::KAN Dcdc2::KAN Dcig1::HYG Dcig2::KAN Dpuc1::HYG Nhp6::mCherry::ura4+ plo1::GFP::KAN*	This Study
DC995	*h- Dspo12::KAN ploI::GFP::KAN nhp6::mCherry::ura4+*	This Study
DC1055	*h+ Dspo12::KAN*	This Study
DC1058	*h+ Pcdc13::cdc13Scdc2T14AY15Fas::cdc13UTR Dcdc2::KAN Dpuc1::HYG Dcig1::HYG Dcig2::KAN spo12S54A*	This Study
DC1059	*h- spo12::L::msGFP2*	This Study
DC1060	*h- msGFP2::L::spo12*	This Study
DC1162	*h- 3xHA::spo12*	This Study
DC1068	*h+ Pcdc13::cdc13Scdc2T14AY15Fas::cdc13UTR Dcdc2::KAN Dpuc1::HYG Dcig1::HYG Dcig2::KAN msGFP2::L::spo12*	This Study

|		
DC1069	*h- Pcdc13::cdc13Scdc2as::cdc13UTR Dcdc2::KAN Dpuc1::HYG Dcig1::HYG Dcig2::KAN msGFP2::L::spo12*	This Study
DC1081	*h- Pcdc13::cdc13Scdc2as::cdc13UTR Dcdc2::KAN Dpuc1::HYG Dcig1::HYG Dcig2::KAN spo12::L::msGFP2*	This Study
DC1083	*h- Pcdc13::cdc13Scdc2T14AY15Fas::cdc13UTR Dcdc2::KAN Dpuc1::HYG Dcig1::HYG Dcig2::KAN spo12::L::msGFP2*	This Study
DC1134	*h- 3xHA::spo12::msGFP2*	This Study
DC1135	*h- Pnmt1::msGFP2*	This Study
DC1138	*h- Pcdc13::cdc13Scdc2T14AY15Fas::cdc13UTR Dcdc2::KAN Dpuc1::HYG Dcig1::HYG Dcig2::KAN msGFP2::L::spo12S54A*	This Study
DC1140	*h- Pcdc13::cdc13Scdc2as::cdc13UTR Dcdc2::KAN Dpuc1::HYG Dcig1::HYG Dcig2::KAN msGFP2::L::spo12S54A*	This Study
DC1155	*h- spo12::3xHA*	This Study
DC1160	*h- Pcdc13::cdc13Scdc2T14AY15Fas::cdc13UTR Dcdc2::KAN Dpuc1::HYG Dcig1::HYG Dcig2::KAN synCut3::mCherry::leu1+*	This Study
DC1161	*h- Pcdc13::cdc13Scdc2T14AY15Fas::cdc13UTR Dcdc2::KAN Dpuc1::HYG Dcig1::HYG Dcig2::KAN synCut3::mCherry::leu1+ Dspo12::KAN*	This Study
DC1162	*h- 3xHA::spo12*	This Study
DC1167	*h+ 3xHA::spo12S54A*	This Study
DC1170	*h- msGFP2::spo12S54A*	This Study
DC1174	*h+ Dspo12::KAN synCut3::mCherry::ura4+*	This Study
DC1178	*h+ synCut3::mCherry::ura4+*	This Study
DC1182	*h+ NAT::P3nmt1::3xHA::spo12 synCut3::mCherry::ura4+*	This Study
DC1183	*h+ NAT::P3nmt1::3xHA::spo12(S54A) synCut3::mCherry::ura4+*	This Study
DC1198	*h+ Pcdc13::cdc13Scdc2as::cdc13UTR Dcdc2::KAN Dpuc1::HYG Dcig1::HYG Dcig2::KAN 3xHA::spo12*	This Study
DC1199	*h+ Pcdc13::cdc13Scdc2T14YA15Fas::cdc13UTR Dcdc2::KAN Dpuc1::HYG Dcig1::HYG Dcig2::KAN 3xHA::spo12*	This Study
DC1200	*h+ Pcdc13::cdc13Scdc2as::cdc13UTR Dcdc2::KAN Dpuc1::HYG Dcig1::HYG Dcig2::KAN 3xHA::spo12(S54A)*	This Study
DC1201	*h+ Pcdc13::cdc13Scdc2T14AY15Fas::cdc13UTR Dcdc2::KAN Dpuc1::HYG Dcig1::HYG Dcig2::KAN 3xHA::spo12(S54A)*	This Study
DC1204	*h- Pcdc13::cdc13Scdc2as::cdc13UTR Dcdc2::KAN Dpuc1::HYG Dcig1::HYG Dcig2::KAN NAT::Pnmt1::3xHA::spo12 synCut3::mCherry::ura4+*	This Study
DC1205	*h- Pcdc13::cdc13Scdc2T14AY15Fas::cdc13UTR Dcdc2::KAN Dpuc1::HYG Dcig1::HYG Dcig2::KAN NAT::Pnmt1::3xHA::spo12 synCut3::mCherry::ura4+*	This Study
DC1206	*h+ Pcdc13::cdc13Scdc2as::cdc13UTR Dcdc2::KAN Dpuc1::HYG Dcig1::HYG Dcig2::KAN NAT::Pnmt1::3xHA::spo12(S54A) synCut3::mCherry::ura4+*	This Study
DC1207	*h- Pcdc13::cdc13Scdc2T14YA15Fas::cdc13UTR Dcdc2::KAN Dpuc1::HYG Dcig1::HYG Dcig2::KAN NAT::Pnmt1::3xHA::spo12(S54A) synCut3::mCherry::ura4+*	This Study
DC1226	*h? wee1-50 Dspo12::KAN*	This Study
DC1229	*h? cdc25-22 Dspo12::KAN*	This Study

FIGURE 1
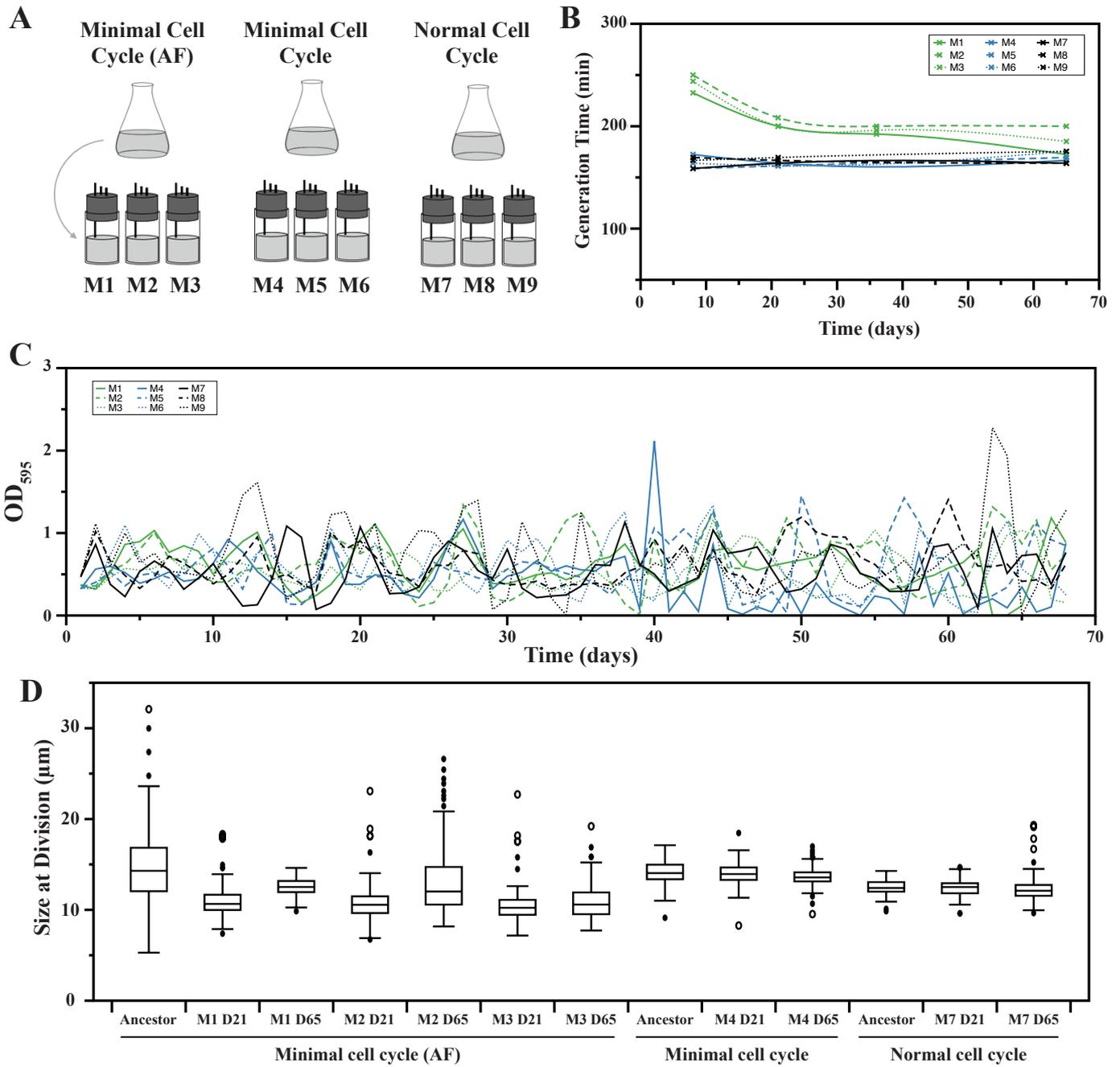
FIGURE 2
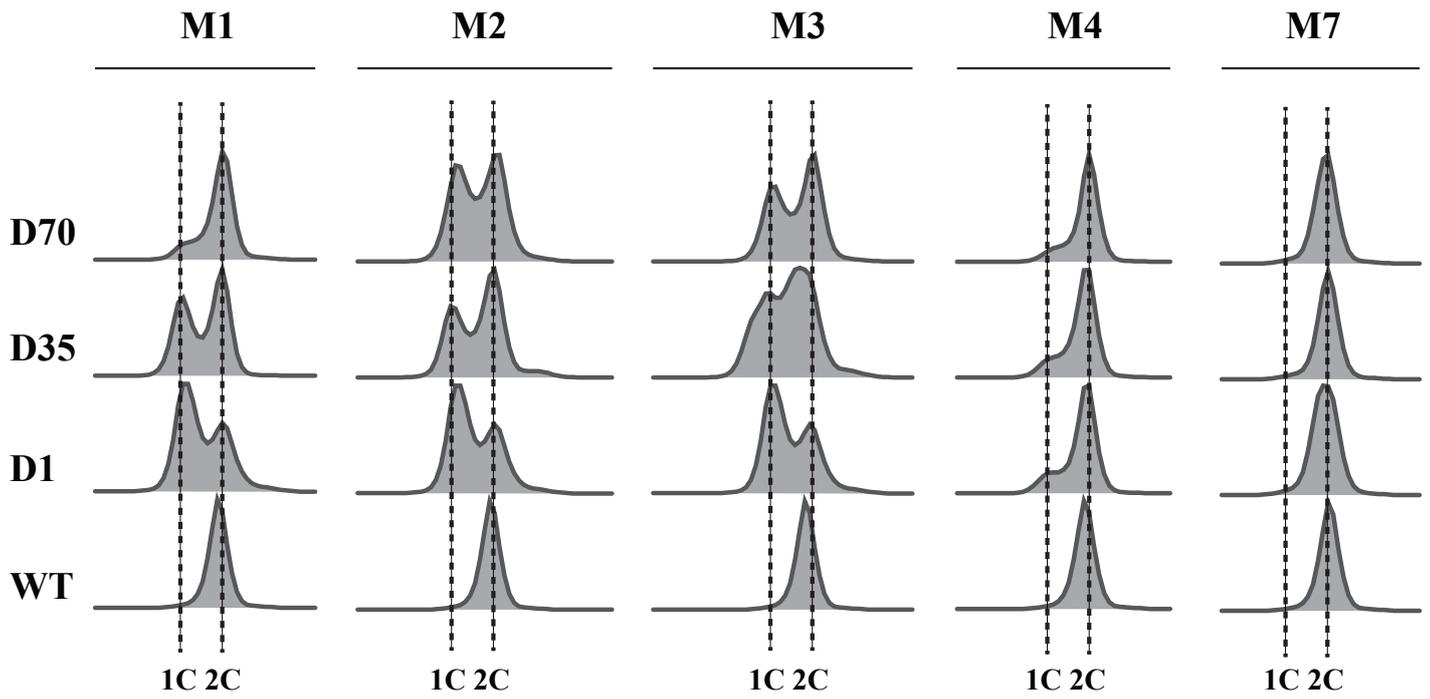
FIGURE 3
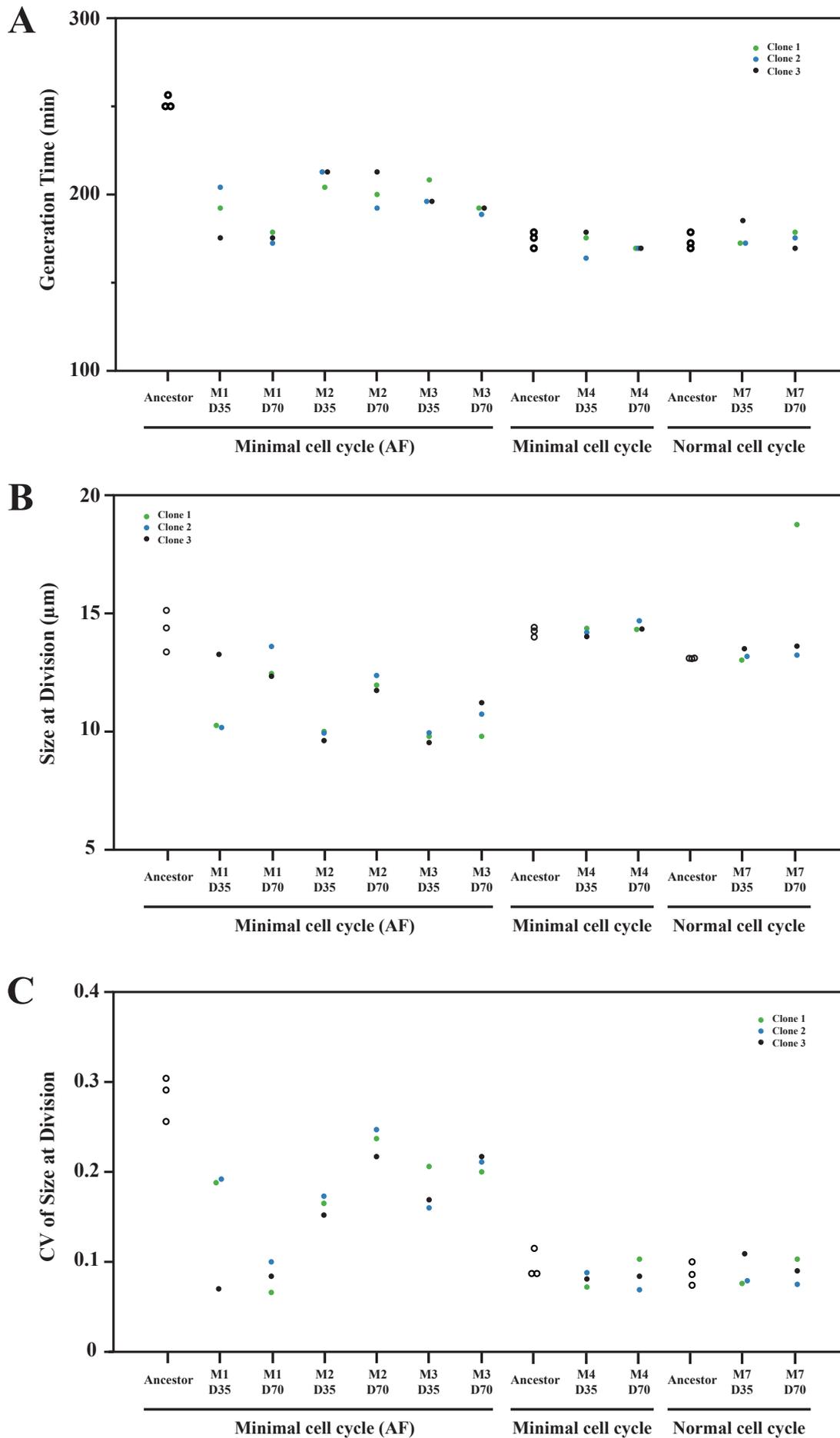
FIGURE 4

FIGURE 5

FIGURE 6

Generation Time (min)

300
200
100
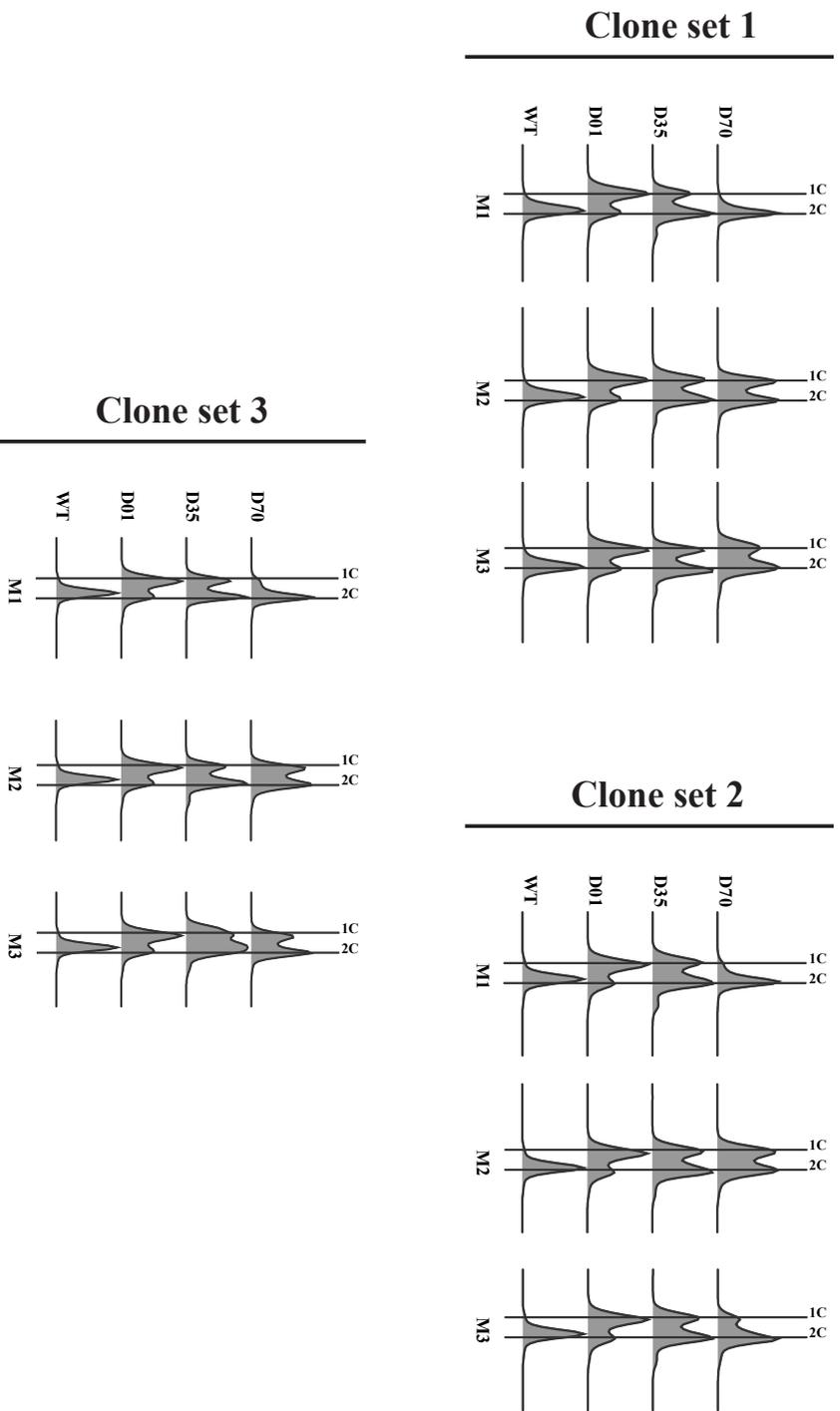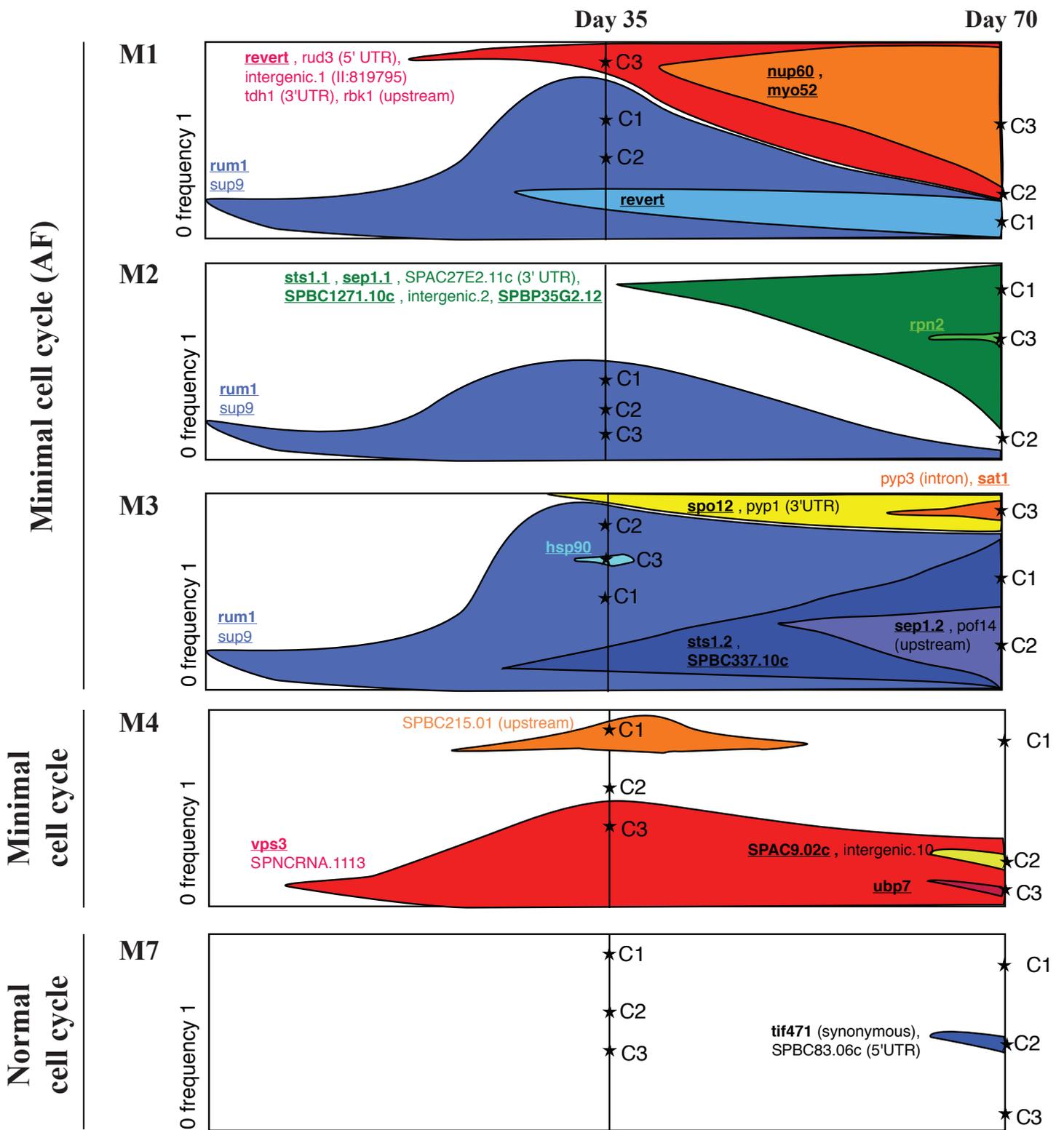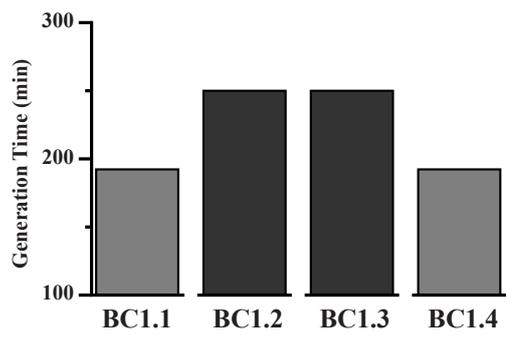
BC1.1 BC1.2 BC1.3 BC1.4

Variant	CHR	Position	Gene	BC1.1	BC1.2	BC1.3	BC1.4
26	I	1285542	SPAPB17E12.12c	E	E	A	A
28	I	2849147	spo12	E	A	A	E
32	I	5163245	pyp1	E	A	E	A
33	I	5299184	pyp3	A	E	E	A
43	II	3858142	sat1	E	A	A	E
44	III	1450442	SPCC61.05	E	A	A	E
Generation Time (min)				192.3	250.0	250.0	192.3

FIGURE 7

FIGURE 8

A

	Generation Time (min)	Size at Division (μm)
MCN-AF *spo12(S54A)*	142.53 ± 2.50	12.66 ± 1.82
MCN-AF Δ*spo12*	165.22 ± 3.84	12.18 ± 2.46
MCN-AF	185.78 ± 3.38	13.11 ± 2.66
MCN *spo12(S54A)*	143.42 ± 0.98	15.73 ± 1.41
MCN Δ*spo12*	145.43 ± 1.02	15.59 ± 1.49
MCN	143.47 ± 2.01	15.36 ± 1.34
spo12(S54A)	142.48 ± 1.93	14.12 ± 1.21
Δ*spo12*	136.82 ± 0.91	13.92 ± 0.99
WT	136.82 ± 0.91	13.84 ± 1.05

B

1C 2C

MCN-AF spo12(S54A)
MCN-AF Δspo12
MCN-AF
MCN spo12(S54A)
MCN Δspo12
MCN
spo12(S54A)
Δspo12
WT

C

% Cells

MCN-AF spo12(S54A)
MCN-AF Δspo12
MCN-AF
MCN spo12(S54A)
MCN Δspo12
MCN
spo12(S54A)
Δspo12
WT

Size at Division (μm)

D

YE4S   3mM HU   2.5uM CPT

WT
Δspo12
MCN
MCN Δspo12
MCN-AF
MCN-AF Δspo12
Δrad3

spo12(S54A)
MCN spo12(S54A)
MCN-AF spo12(S54A)

E

Wild type   MCN   MCN-AF
Control   WT   S54A   WT   S54A   WT   S54A

α-HA

α-Tubulin

F

WT   Δspo12   spo12(S54A)   MCN   MCN Δspo12

MCN spo12(S54A)   MCN-AF   MCN-AF Δspo12   MCN-AF spo12(S54A)

FIGURE 9

A

B

C

D

E

F

FIGURE 10
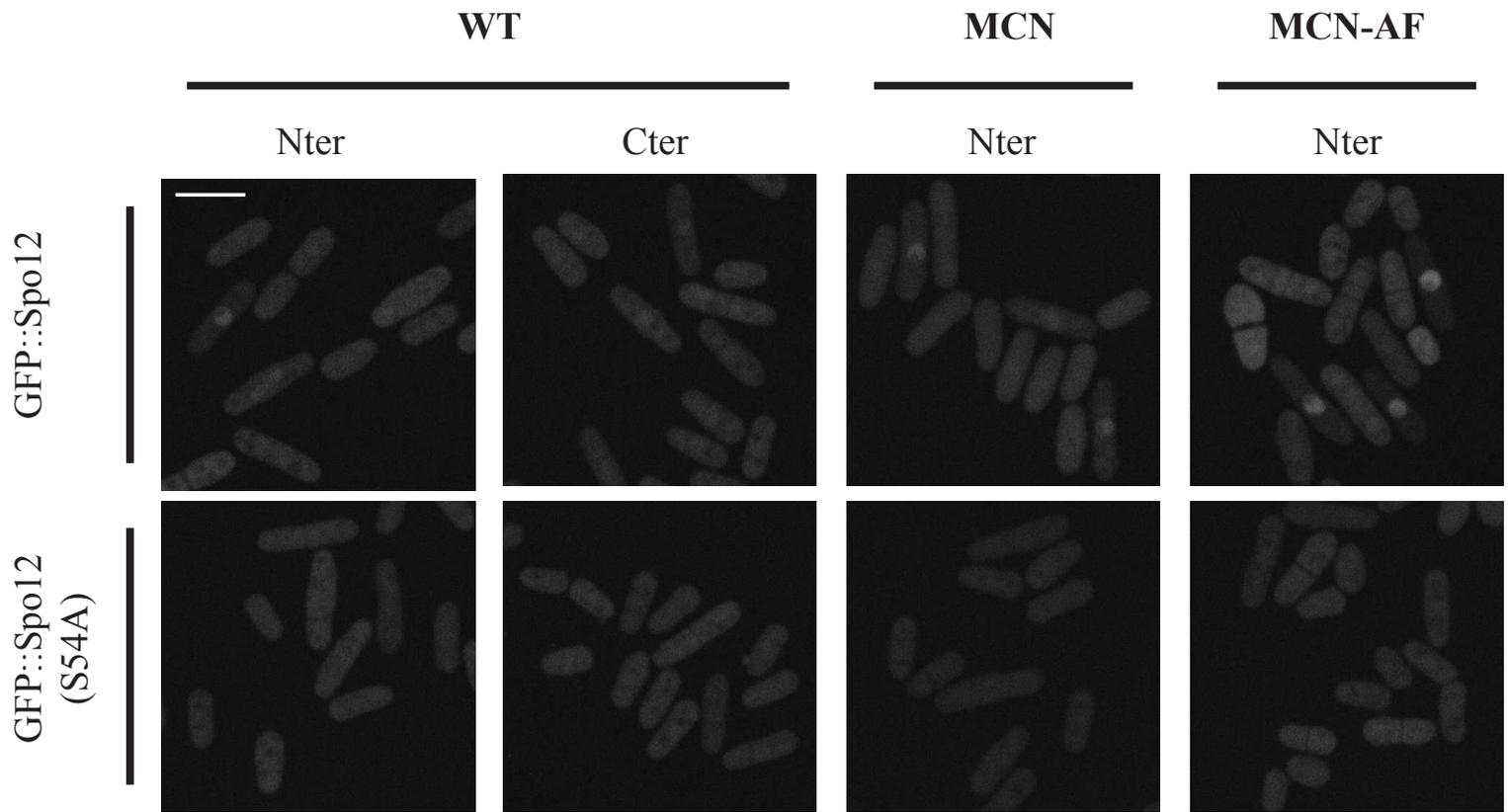
FIGURE 11

FIGURE 12

FIGURE 13

FIGURE 14

A

B

C

FIGURE 15

FIGURE 16

A

	w/ Thiamine			w/o Thiamine		
	Generation Time (min)	Size at Division (μm)	Average Cut3::mCherry Intensity (a.u.)	Generation Time (min)	Size at Division (μm)	Average synCut3::mCherry Intensity (a.u.)
MCN-AF *XS-spo12(S54A)*	140.7 ± 3.5	11.1 ± 1.8	n.d.	157.6 ± 2.1	12.5 ± 2.2	n.d.
MCN-AF *XS-spo12*	142.5 ± 0.9	10.8 ± 1.7	n.d.	260.3 ± 6.3	14.8 ± 3.0	n.d.
MCN *XS-spo12(S54A)*	123.1 ± 1.5	15.7 ± 1.0	3091.5 ± 521.6	146.5 ± 2.1	16.2 ± 1.3	3130.5 ± 597.2
MCN *XS-spo12*	120.9 ± 1.8	15.8 ± 1.1	2867.3 ± 555.4	153.0 ± 2.9	13.9 ± 1.1	3724.6 ± 897.9
WT *XS-spo12(S54A)*	118.9 ± 0.7	14.3 ± 0.9	2727.3 ± 787.8	142.5 ± 0.9	14.7 ± 1.0	2839.4 ± 1136.9
WT *XS-spo12*	120.3 ± 1.9	14.3 ± 1.1	2680.6 ± 593.3	147.5 ± 0.0	13.2 ± 0.9	4373.9 ± 1058.1
WT	118.8 ± 0.7	14.3 ± 1.1	n.d.	142.5 ± 0.9	14.4 ± 1.0	n.d.

B

D

WT — **MCN**

E

C

137

FIGURE 17

MCN-AF XS-Spo12

+   −

MCN-AF XS-Spo12(S54A)

+   −

FIGURE 18

A

GFP Trap Pull Down | Lysate
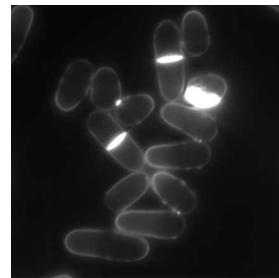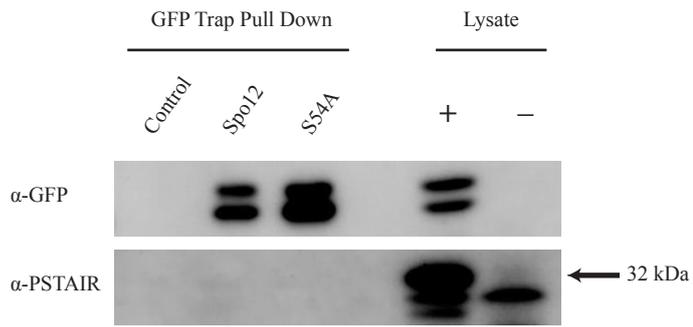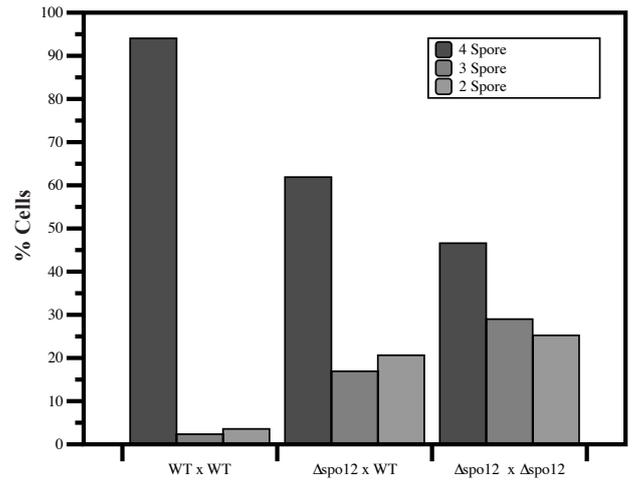
Control | Spo12 | S54A | + | −

α-GFP
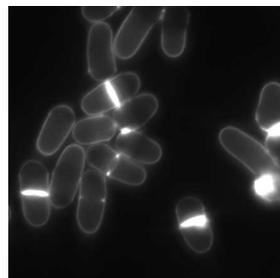
α-PSTAIR ⟵ 32 kDa

B

Chapter 3:

High-throughput mapping of cell cycle events in single fission yeast cells using live-cell imaging and automated image analysis

High-throughput mapping of cell cycle events in single fission yeast cells using live-cell imaging and automated image analysis

Joseph C. Ryan[1,2,*], Larisa Venkova[1,2,*], Théo Aspert[3], Gilles Charvin[3] and Damien Coudreuse[1,2]

[1] Institute of Biochemistry and Cellular Genetics, CNRS UMR 5095, Bordeaux, France

[2] Institute of Genetics and Development of Rennes, CNRS UMR 6290, Rennes, France

[3] University of Strasbourg, CNRS UMR 7156, Strasbourg, France

[*] These authors contributed equally to this work

Correspondence: damien.coudreuse@ibgc.cnrs.fr

This study is currently being finalized and is presented here as a manuscript in preparation.

ABSTRACT

Cell cycle progression is central to the biology of eukaryotic cells and organisms. While the temporal organization of cell cycle events and the mechanisms underlying the proper progression through the different cell cycle transitions have been the subject of thorough investigation, how the behaviors of individual cells impact population dynamics remains elusive. While single-cell studies have paved the way towards deciphering the maintenance and deregulation of cell cycle homeostasis, methods that combine the power of monitoring individual cells using high-throughput analyses are lacking. Here we take advantage of microfluidic devices coupled with a deep learning-based pipeline to generate a set of image classifiers that allow for automated mapping of cell cycle events in single fission yeast cells. This high-throughput, high-content and versatile method can be readily used without the need for further training of the analysis pipeline, making it an unprecedented resource for cell cycle studies in fission yeast.

INTRODUCTION

Cell cycle progression is a central aspect of the eukaryotic life cycle, delineating the proliferation of cells in colonies of unicellular organisms as well as in the tissues of multicellular species. Strikingly, despite drastically different sizes, morphological features and doubling times between species, cell cycle control relies on a highly conserved network of regulatory loops[1]. Thus, genetic models such as the budding and fission yeasts have played instrumental roles in our current knowledge of the processes that drive the orderly progression through the cell cycle. At the heart of the cell cycle control network are conserved enzymes of the cyclin-dependent protein kinase (CDK) family, which associate with various cyclins throughout the division cycle and trigger the main cell cycle events[1]. Cell proliferation and cell growth are intimately linked, and several mechanisms have been described that ensure the homeostasis of cell growth and division in populations of cells[1,2]. However, our understanding of the processes that prevent cell-to-cell heterogeneity and thereby promote the robustness of cell cycle progression between cells mostly relied on population studies. Such approaches neglect single-cell characteristics and do not provide us with an understanding of how the dynamic behaviors of individual cells impacts populations, how cell-to-cell variability may be buffered by dedicated mechanisms and how the deregulation of such pathways may lead to abnormal cell proliferation.

To circumvent the biases that are inherent to population studies and decipher how the behavior of cell populations is defined by the characteristics of individual cells, the analysis of single-cell properties has become an essential approach in cell cycle studies. In particular, live-cell imaging and the monitoring of cell cycle progression in individual cells have been widely used to unravel the temporal interplay between distinct cell cycle events in a given cell. Coupled with the ease of genetic engineering in amenable models such as yeast, which allows for expressing multiple non-overlapping fluorescent markers in live cells, and benefiting from the constant improvement of imaging techniques, this approach remains the method of choice for cell cycle studies. It allows for unraveling differences in the relative timing of discrete events with high temporal resolution and correlating these processes with the dynamic behavior of individually-tagged cell cycle factors.

However, a number of drawbacks inherent to these experiments have prevented researchers from taking full advantage of this strategy. First, in the majority of previously published studies, a tight control of the environment in which cells proliferate while under microscopic observation was not possible, introducing biases in the analyses and limiting the duration of the experiments. For

instance, imaging of proliferating yeast has been largely performed with cells growing on agar pads, despite the potential changes in nutritional and oxygen conditions over the course of a time-lapse as well as the mechanical stress imposed upon the cells by the assembly of the system. Second, the behavior of individual cells has mostly relied on the visual annotation of each cell by the researcher, making the process tedious and time-consuming, while also preventing the evaluation of large datasets. Indeed, determining the timing of cell cycle events, associating cell cycle transitions with the changes in specific fluorescent markers and evaluating key cellular features at different stages of the cell cycle is complex and cannot easily be performed for large numbers of cells. Interestingly, various methodologies have emerged that improve our capacity of monitoring large numbers of individual cells in more controlled conditions. In this context, microfluidic technologies have played a key role[3-8]. Not only are such systems compatible with high-resolution live-cell imaging, but their coupling with dedicated devices for control of medium-flow throughout the experiments makes it possible to perform long time-lapse studies in stable and pre-determined growth conditions. The emergence of standardized protocols for the design and custom fabrication of microchips compatible with live-cell imaging[9] has also represented a step forward compared to commercial solutions in which non-adherent cells such as yeast were subjected to mechanical stress. However, while these methods represented a breakthrough not only for studying cell proliferation at the single-cell level but also in a broad range of fields in cell biology, the analysis of data obtained using these approaches became a major bottleneck that naturally accompanied the possibility of monitoring a large number of cells. While the automated analysis of microscopic images has been broadly used, these methodologies are not straightforward and remain complex to develop and to implement. This is particularly the case when the goal is to extract a diversity of qualitative and quantitative parameters, or when monitoring the behavior of different fluorescent markers simultaneously expressed in the cells along with specific cell characteristics. This is even more challenging in populations that show a great degree of cell-to-cell heterogeneity.

Remarkably, approaches based on deep learning strategies have recently revolutionized image analysis in cell biology[10-12]. These methods are based on the use of neural networks that can analyze and accurately classify microscopy images. Following an initial phase of training of the networks to recognize the specific features used in a given experiment (*e.g.* changes in the localization of cell cycle markers), this allows for the automated analysis of large numbers of individual cells for virtually any pre-defined property. One such pipeline, referred to as DetecDiv, was recently developed to take advantage of the coupling of microfluidics with a deep learning-based approach to analyze replicative lifespan and cellular adaption to environmental stress in

budding yeast[12]. Importantly, this open-source and freely available software takes advantage of different types of neural networks, in particular a long short-term memory network (LSTM), which takes into account the temporal information provided in a time-lapse experiment. In other words, it integrates the time-dependency between successive images for a more accurate classification of dynamic events. Using this method, an impressive overlap was demonstrated between the ground truth dataset generated by the user and the automated analysis performed by the trained classification system[12]. Furthermore, the versatility of this pipeline and the ease of high-content data extraction from the automatic classification indicates that this platform may be developed to be a powerful tool for analyzing the dynamics of cell cycle progression and cellular homeostasis.

Here we provide a set of ready-to-use DetecDiv classifiers for the dissection of cell cycle progression in fission yeast. We have developed a specific microfluidic design dedicated to fission yeast, established a segmentation processor to focus on individual cells and used a set of fluorescent markers for determining the timing of cell cycle events. Using flow control systems to maintain constant growth conditions and automated quantification of a set of cellular parameters in cells with different genetic backgrounds, we show that our classifiers we make it possible to perform high-throughput analyses of a broad range of cellular features throughout the cell cycle at the single-cell level. This pipeline represents a powerful tool for cell cycle studies in fission yeast, an organism that has been at the forefront of key discoveries in this field. Importantly, the versatility of this platform and the possibility to build on the set of classifiers that we provide to further train the system for recognizing additional features or fluorescent markers will make this method a new standard in the studies of cell proliferation and behavior.

RESULTS AND DISCUSSION

A microfluidic design for tracking single fission yeast cells in a controlled environment

Tracking the division cycle of individual cells in a controlled environment is essential for extracting an unbiased temporal mapping of the processes underlying their cell cycle. In particular, maintaining the nutritional conditions throughout an experiment is essential, as changes in nutrient availability directly affect the cell cycle control network. For this, microfluidic systems are particularly advantageous, as they allow for the maintenance of a constant flow of medium throughout the chip. Given the very low overall volume of the channels in most microfluidic devices dedicated to live-cell imaging, low flows are sufficient to renew the entire environment of the cells in only a few seconds. However, this poses a problem when using non-adherent cells such as budding and fission yeast. Surface coating to promote the adhesion of these cells or mechanical blocking of the cells by deformation of cell chambers has been used to circumvent this issue, but both solutions remain problematic: the former is not very reliable and cells often detach when subjected to the flow of medium, while the latter induces mechanical stress on cells. We have previously used designs with separated chambers isolated from the flow but compatible with medium renewal through diffusion[13]. However, these systems are difficult to use as any imbalance in pressure in the flow channels on either side of the chamber during an experiment results in the flow through the chambers, thereby washing off the cells under observation. We therefore set out to adapt the single-cell trap design that was used with the DetecDiv platform[12] and make it compatible with fission yeast, as the original design was specifically developed for the smaller budding yeast cell. This design traps cells in small chambers that are open on both sides, with one side being wider than a cell, allowing for cell loading, and the other side being narrower than a cell, letting medium flow through without washing out the cell (Fig 1A-C). The microfluidic chip contains 8 individual channel networks, each comprising 2000 individual cell traps (Fig 1D). This makes it possible to perform several parallel experiments using a single microfluidic device. Cell injection was straightforward and efficient, allowing for the loading of >95% of the traps. Furthermore, applying a medium flow of 5 μL/min did not displace the loaded cells. To validate this device, we ascertained the cell cycle properties of wild-type cells growing in the traps under constant medium flow (Table 1). Compared to batch cultures, we observed no defects in cell size at division, a standard readout for cell cycle progression in fission yeast. In contrast, cycle times were significantly different, with cells in the chip growing slower than those in flasks. However, it is important to note that the cycle times in these two conditions are difficult to compare. Indeed, our

measurements of population doubling time are based on optical density measurements, while in the microdevice, the division time is determined for each individual cell. Furthermore, cell cycle duration in batch culture is established as population density increases over time, which means that cells are exposed to constantly changing nutritional environments. Finally, our data are consistent with the increase in doubling time that was previously reported when fission yeast cells were grown in microfluidic devices[14]. Altogether, these modifications of the original budding trap design made this system perfectly adapted to the tracking of single fission yeast cells.

A set of fluorescent markers for analysing cell cycle progression

In order to take advantage of our microfluidic system and deep learning software for automated image analysis, we set out to establish a basic combination of markers that can be used to extract an accurate, dynamic and high throughput mapping of the main cell cycle transition at the single-cell level. We therefore selected well-characterized fluorescently-tagged proteins, all expressed at their endogenous loci in fission yeast, to identify the G1/S transition, progression through mitosis, nuclear division and post-mitotic nuclear separation. Coupled with DIC imaging for determining the timing of cytokinesis and cellular parameters such as length and width, this would provide a powerful platform onto which one can build to determine how specific processes of interest may influence cell cycle progression.

To visualize nuclear dynamics, we used an Nhp6::mCherry fusion. Nhp6 is an HMG-box non-histone chromatin protein[15-17] that is present throughout the cell cycle and allows for monitoring nuclear behavior (Fig. 2A). In particular, this marker makes it possible to visualize the metaphase to anaphase transition, evaluate chromosome segregation defects as well as evaluate segregation dynamics, and identify potential segregation defects. It is also an easy-to-use marker for assessing the migration of the post-mitotic nuclei towards the old ends of the cells prior to cytokinesis. Next, the timing of mitotic entry and progression was determined using Plo1::GFP. The Polo-like kinase Plk1/Plo1 is a well-known and conserved factor that has key roles in cell cycle progression[1]. In the context of our method, Plo1 has been widely used as an early mitotic marker in fission yeast: it is recruited to the spindle pole body (SPB) at mitotic onset, which enables the monitoring of SPB duplication and separation, and mostly disappears as cells exit mitosis (Fig. 2A) [18-21]. We thus took advantage of a Tos4::GFP fusion protein to monitor this key cell cycle event (Fig. 2B). Finally, standard DIC images were integral to our method (Fig 2A, B), providing critical information such as the timing of cytokinesis (septation) as well as a number of parameters linked

to cell cycle progression and cell growth, including cell length and width. These were also essential for the segmentation of individual cells in traps where more than one cell was loaded (see below). Altogether, our approach was to then combine fluorescent and DIC imaging with cells expressing *nhp6::mCherry*, *plo1::GFP* and *tos4::GFP* to extract high-resolution maps of the main cell cycle events in fission yeast. Importantly, the classification system provided in this study represents a first fundamental step, and additional, more dedicated markers can easily be implemented in the deep learning platform to assess more specific processes in cell cycle progression.

Segmentation of the cells improves the quality of the classifiers

The dimensions of the cell traps in our microfluidic designs permitted the efficient loading of the cells. However, we often observed more than one cell per trap (Fig. 3A). To assess the quality of the neural network training in this context, we first used the Nhp6::mCherry marker, classifying cells in three categories: mono-nucleated, dividing and bi-nucleated. In this context, bi-nucleated cells were considered to switch to mono-nucleated cells when cytokinesis was observed, even if cell division was not fully complete. Note that we aimed at classifying only the cell located in the innermost part of the cell trap (Fig. 3A). We therefore applied two different strategies. First, we used non-processed images, considering that a large training set would be sufficient for accurate class assignment of the cell of interest. For this, we used a set of 222 single-cell time lapses (50 frames per trap – 11100 frames total) and a sequence classifier method. Once the network was trained, we performed an automatic classification of a second, entirely separate, dataset, which we also manually analyzed to compare the ground truth data with the results provided by the software (Fig. 3B). Interestingly, we found a relatively good correspondence for the mono-nucleated class, while the dividing and bi-nucleated categories appeared to be less promising. This is likely due to the fact that as growing fission yeast cells spend most of their life cycle as mononucleated G2 cells, mitosis, S phase and G1 combine to represent only ~30 % of the cell cycle. However, the limited quality of the automated classification may also result from the presence of multiple Nhp6::mCherry cells in the traps, providing additional signals that may be mis-interpreted with insufficient training (Fig. 3A). While increasing the training set may have circumvented this issue, we took an alternative approach, reasoning that our results could be improved if signals outside of the cell of interest were filtered out. We therefore used the corresponding DIC images to train the pipeline to automatically segment the target cell in each trap, separating the background (which includes the trap structure itself), the cell of interest and any other cells into three distinct categories (Fig. 3C). This was performed using the built-in segmentation feature of DetecDiv and manually

drawing the cells in a DIC dataset. Applying the same training / testing procedure as described above, we found the segmentation classifier to efficiently detect the contours of the cell of interest (Fig. 3D).

In order to take advantage of the segmentation classifier, we established a simple processor routine that consists of using the segmentation result as a mask to darken on the fluorescence images any pixel that is outside of the cell of interest. This way, subsequent training to generate other classifiers only takes into account the data from the cell of interest. We reasoned that this method to filter out signals from other cells may allow us to obtain more accurate classification results with training sets of the same size. To test this, we segmented the same datasets as above and used the masked images to train the system to recognize the mono-, bi-nucleated and dividing cells (Fig. 3E). Strikingly, while based on the same initial data, this classifier provided significantly more accurate results (Fig. 3F). Thus, all other subsequent trainings were performed using segmented datasets.

Training of the neural networks with different markers and cell cycle mapping

To obtain a full mapping of cell cycle events at the single-cell level, we next trained the networks to classify the two other markers, namely Plo1::GFP and Tos4::GFP. Importantly, while both Plo1 and Tos4 were tagged with the same fluorescent marker, their very distinct subcellular patterns and intensities (strong signal at the SPB vs diffuse and less intense nuclear staining, respectively) made it possible to generate two separate classifiers using each marker. Using the procedure as above, we trained and tested the networks to map these events, which are associated with mitosis and G1/S, respectively. These analyses are currently being finalized to generate the final versions of the classifiers.

Finally, we used time-lapse imaging of wild-type cells expressing all three markers to extract a complete and high-throughput mapping of cell cycle progression. These data will then be analyzed using our entire set of classifiers to demonstrate how this pipeline can be employed not only characterize the orderly and temporal progression through the cell cycle but also as a basis for the assessment of additional processes interacting with the cell cycle network. In addition, these analyses will also show the capacity of DetecDiv to perform complex analyses of biological processes based on several independent features, including the properties of diverse fluorescently-tagged markers and the morphological characteristics of the cells. The classifiers we have

established together with the designs of the chips can thus be utilised without further modification by any research team studying dynamic processes during the fission yeast division cycle.

Extracting quantitative data from the time-lapses and mapping cell cycle progression in cell cycle mutants

Interestingly, the segmentation procedure generates a mask that delineates the cell of interest, and we optimized the segmentation threshold to closely define cell edges. Thus, this mask can be used to extract a number of cellular characteristics, including cell length, diameter and calculated volume (using cell outlines to determine volume, thereby taking into account changes in diameter or morphology), and integrate these data with the differences in cell cycle progression in each individual cells (ongoing analysis using a dedicated Matlab module). While the masking process is not highly accurate, the possibility to obtain such data on a very large number of cells can be used to determine trends and compare the behaviors of different strains, providing the foundations for more in-depth and accurate studies.

Finally, as a proof-of-concept application of the method, we used this approach to analyze mutant genetic backgrounds. First, we took advantage of the *wee1-50* temperature sensitive allele [22-24]. Wee1 is a kinase that inhibits Cdc2 by direct phosphorylation and is part of the mitotic feedback loop that triggers the onset of mitosis[25]. In the absence of Wee1 function, cells advance in mitosis, divide at a smaller size and show an elongated G1. We therefore performed time-lapse experiments using *wee1-50* cells expressing all the markers for which we developed classifiers and the results will be analyzed with the DetecDiv pipeline. In addition, we will exploit the Minimal Cell cycle Network (MCN), a system that we previously described in which the fission yeast cell cycle is solely driven by the oscillation in activity of a single protein module consisting of a fusion between the cyclin B Cdc13 and Cdc2/Cdk1[26]. Importantly, the Cdc2 moiety of the fusion protein harbors a mutation (F89G) that makes it sensitive to dose-dependent and reversible inhibition by the small non-hydrolysable ATP analog 3-MBPP1[26,27]. Thus, treatment with 1 μM 3-MBPP1 blocks cells in G2, with cells elongating beyond their normal size at division. Release from the inhibitor allows cells to synchronously re-enter the cell cycle[26]. Using this method in our microfluidic devices, we anticipate that this artificially-controlled deregulation of cell cycle progression could be analyzed using the DetecDiv pipeline and classifiers presented above, further validating the method for cell cycle studies.

Conclusion

Cell cycle progression is a crucial biological process that is intimately linked with cell growth and the interaction of cells and organisms with their environment. While a large body of work has unraveled the conserved core network regulating the division cycle in eukaryotes, key aspects of the processes underlying the progression through the cell cycle remain poorly explored. In this context, single-cell studies have become essential for deciphering how the dynamic ordering and sequence of cell cycle events is brought about and maintained as well as how different signals impinge on the cell cycle network and alter its homeostasis. Due to their ease of manipulation and amenability to advanced genetic engineering, budding and fission yeast cells have proven to be models of choice for cell cycle studies. However, advances in live-cell imaging and environmental control using microfluidics are now allowing for generating high-volume and high-content datasets, making image analysis a critical bottleneck. Coupling the DetecDiv deep learning pipeline with dedicated microfluidic chips, we provide a set of ready-to-use classifiers that can easily be implemented for high-throughput mapping of the major cell cycle transitions in fission yeast and for extracting a set of cellular features associated with cell cycle progression. This represents a powerful foundation for future studies that can build on the proposed pipeline to study processes underlying cell cycle progression and the interplay between the division cycle and other cellular mechanisms.

MATERIALS AND METHODS

Fission yeast strains and growth conditions

Standard media and methods were used[28,29]. Strains used in this study are listed in Table 2. All experiments were performed in supplemented minimal medium (EMM6S) at 32 °C except otherwise noted. Inhibition of Cdc2 activity in analog-sensitive MCN cells was performed using the dose-dependent and reversible inhibitor 3-MBPP1 (A602960, Toronto Research Chemicals, Inc.) dissolved in DMSO at a stock solution of 10 mM.

Microfabrication

The design and fabrication of the microfluidic chips were performed as previously described, following standard microfabrication protocols[9]. In brief, the master mold was made from SU-8 2005 (trap layer – target thickness: 5 μm) and SU-8 2050 (channel layer – target thickness: 60 μm) photoresists (MicroChem Corp., USA) on standard silicon wafers using a spincoater (Laurell Technologies, USA) according to manufacturer's instructions. Photolithography was performed using high-resolution chrome masks (JD phototools, UK) and exposure to 365 nm UV light in a UV KUB 3 mask aligner (Kloe, France). The pre- and post-bake stages were 3 min long. This was followed by chemical development (PGMEA, Sigma-Aldrich). The mold was then treated with Silane (Acros Organics). Microfluidic chips were fabricated by casting a 10:1 mixture of PDMS (Sylgard 184, Dow Corning, USA) on the SU-8 Master mold and cured at 70 °C for 2 hours. Inlets were made with a 0.75 mm biopsy punch and the chip subsequently bonded to a microscopy-grade coverslip after plasma activation (Harrick Plasma, USA). The mask designs are available at (*Github URL to be provided*).

Microscopy

All time-lapse experiments were performed using an inverted Zeiss Axio Observer equipped with Plan-Apochromat 63X/1.4 NA immersion lens (Carl Zeiss Microscopy GmbH, Jena, Germany), a laser bench (Visitron Systems GmbH, Puchheim, Germany), a spinning disc confocal head (CSU-W1, Yokogawa Life Science, Japan) and a temperature control chamber (Okolab, Pozzuoli, Italy). Images were acquired using an Orca Flash 4.0V2 sCMOS camera (Hamamatsu Photonics, Hamamatsu, Japan) and the Visiview software (Visitron GmbH, Puchheim, Germany). Analyses were performed using DetecDiv in Matlab (Mathworks, Natick, USA).

Analysis of cell cycle properties

For determination of cell size at division, cells were stained with blankophor (1 mg/mL), and cell length was determined using the Pointpicker plugin in Fiji (National Institutes of Health, USA). For DNA content analysis, cells were fixed in 70% ethanol, washed in 50mM sodium citrate, treated with RNase A (0.1 mg/mL) and stained with propidium iodide (2 mg/mL). DNA content was assessed using a BD Accuri C6 flow cytometer. The fission yeast cell cycle has a short G1, and S phase occurs before cytokinesis. As a result, cells have a 2C DNA content for most of their division cycle. Appearance of a 1C peak reflects an elongation of G1.

Flow control during time-lapse experiments

Control of the flow of medium in microfluidic chips during time-lapse experiments was ensured using an OB1 pressure controller, a MUX valve matrix and high precision flow controllers (Elveflow, Paris, France). For all time-lapse experiments, a constant flow of 5 µL/min of pre-warmed medium was applied.

Classifiers and processors

All classifiers and processors that were established used the built-in properties of DetecDiv. The Nhp6::mCherry, Plo1::GFP and Tos4::GFP classifiers were image sequence classifiers using LSTM and CNN workflow. The segmentation classifier is based on a semantic segmentation (deeplab v3+). All of these project-independent classifiers as well as the masking processor are available at (*Github URL to be provided*)

References

1.   Morgan, D. O. *The Cell Cycle*. (New Science Press, 2007).
2.   Amodeo, A. A. & Skotheim, J. M. Cell-Size Control. *Cold Spring Harb Perspect Biol* **8,** a019083 (2016).
3.   El-Ali, J., Sorger, P. K. & Jensen, K. F. Cells on chips. *Nature* **442,** 403–411 (2006).
4.   Folch, A. & Toner, M. Microengineering of cellular interactions. *Annu Rev Biomed Eng* **2,** 227–256 (2000).
5.   Lee, P., Gaige, T. & Hung, P. Microfluidic systems for live cell imaging. *Methods Cell Biol.* **102,** 77–103 (2011).
6.   Paguirigan, A. L. & Beebe, D. J. Microfluidics meet cell biology: bridging the gap by validation and application of microscale techniques for cell biological assays. *Bioessays* **30,** 811–821 (2008).
7.   Whitesides, G. M. The origins and the future of microfluidics. *Nature* **442,** 368–373 (2006).
8.   Lee, S. S., Avalos Vizcarra, I., Huberts, D. H. E. W., Lee, L. P. & Heinemann, M. Whole lifespan microscopic observation of budding yeast aging through a microfluidic dissection platform. *Proc. Natl. Acad. Sci. U.S.A.* **109,** 4916–4920 (2012).
9.   McDonald, J. C. & Whitesides, G. M. Poly(dimethylsiloxane) as a material for fabricating microfluidic devices. *Acc. Chem. Res.* **35,** 491–499 (2002).
10.   Laine, R. F., Arganda-Carreras, I., Henriques, R. & Jacquemet, G. Avoiding a replication crisis in deep-learning-based bioimage analysis. *Nat. Methods* **18,** 1136–1144 (2021).
11.   Ghafari, M. *et al.* Complementary performances of convolutional and capsule neural networks on classifying microfluidic images of dividing yeast cells. *PloS one* **16,** e0246988 (2021).
12.   Aspert, T., Hentsch, D. & Charvin, G. DetecDiv, a generalist deep-learning platform for automated cell division tracking and survival analysis. *Elife* **11,** (2022).
13.   Chen, T. *et al.* A drug-compatible and temperature-controlled microfluidic device for live-cell imaging. *Open Biol* **6,** 160156 (2016).
14.   Nobs, J.-B. & Maerkl, S. J. Long-term single cell analysis of S. pombe on a microfluidic microchemostat array. *PloS one* **9,** e93466 (2014).
15.   Paull, T. T., Carey, M. & Johnson, R. C. Yeast HMG proteins NHP6A/B potentiate promoter-specific transcriptional activation in vivo and assembly of preinitiation complexes in vitro. *Genes & development* **10,** 2769–2781 (1996).
16.   Formosa, T. *et al.* Spt16-Pob3 and the HMG protein Nhp6 combine to form the nucleosome-binding factor SPN. *The EMBO journal* **20,** 3506–3517 (2001).

17. Gu, Y., Yam, C. & Oliferenko, S. Rewiring of cellular division site selection in evolution of fission yeasts. *Current biology : CB* **25,** 1187–1194 (2015).

18. Mulvihill, D. P., Petersen, J., Ohkura, H., Glover, D. M. & Hagan, I. M. Plo1 kinase recruitment to the spindle pole body and its role in cell division in Schizosaccharomyces pombe. *Molecular biology of the cell* **10,** 2771–2785 (1999).

19. Tanaka, K. *et al.* The role of Plo1 kinase in mitotic commitment and septation in Schizosaccharomyces pombe. *The EMBO journal* **20,** 1259–1270 (2001).

20. Kamenz, J., Mihaljev, T., Kubis, A., Legewie, S. & Hauf, S. Robust Ordering of Anaphase Events by Adaptive Thresholds and Competing Degradation Pathways. *Molecular cell* **60,** 446–459 (2015).

21. Kiang, L., Heichinger, C., Watt, S., Bähler, J. & Nurse, P. Cyclin-dependent kinase inhibits reinitiation of a normal S-phase program during G2 in fission yeast. *Molecular and cellular biology* **29,** 4025–4032 (2009).

22. Nurse, P. Genetic control of cell size at cell division in yeast. *Nature* **256,** 547–551 (1975).

23. Fantes, P. A. & Nurse, P. Control of the timing of cell division in fission yeast. Cell size mutants reveal a second control pathway. *Experimental cell research* **115,** 317–329 (1978).

24. Fantes, P. Epistatic gene interactions in the control of division in fission yeast. *Nature* **279,** 428–430 (1979).

25. Lundgren, K. *et al.* mik1 and wee1 cooperate in the inhibitory tyrosine phosphorylation of cdc2. *Cell* **64,** 1111–1122 (1991).

26. Coudreuse, D. & Nurse, P. Driving the cell cycle with a minimal CDK control network. *Nature* **468,** 1074–1079 (2010).

27. Bishop, A. C. *et al.* A chemical switch for inhibitor-sensitive alleles of any protein kinase. *Nature* **407,** 395–401 (2000).

28. Hayles, J. & Nurse, P. Genetics of the fission yeast Schizosaccharomyces pombe. *Annu. Rev. Genet.* **26,** 373–402 (1992).

29. Moreno, S., Klar, A. & Nurse, P. Molecular genetic analysis of fission yeast Schizosaccharomyces pombe. *Meth. Enzymol.* **194,** 795–823 (1991).

Table 1. Cell growth in the cell trap microfluidic device

Growth conditions	Generation time (min)	Size at division (µm)
Batch cultures	132.8 ± 0.9	13.7 ± 1.1
Microfluidic chip	170 ± 20	13.4 ± 0.9

Experiments were performed with wild-type cells in EMM6S at 32 °C. Generation time in batch cultures was determined using optical density measurements (OD_{595}, mean and standard error of 3 independent experiments). In the microfluidic chips, the cycle time was determined from cell birth (after cytokinesis) to the completion of the next cytokinesis (median and median absolute deviation for the pooled datasets of 3 independent experiments, $n>150$ for each assay). Size at division was measured when the division septum was formed, prior to the onset of cytokinesis. In batch cultures, blankophor staining was used (mean and standard deviation of the pooled data for 3 independent experiments, $n>100$ per experiment). In the microfluidic devices, this was based on septum visualization in DIC images (median and median absolute deviation of the pooled data for 3 independent experiments. $n>150$ for each experiment). The longer doubling time observed for cells grown in the microfluidic chip is consistent with what was observed in a previous study[14] (note that this earlier study used rich medium, in contrast to our experiments performed in EMM6S, in which cells grow slower).

Table 2. Fission yeast strains used in this study

Name	Genotype	Origin
PN1	*h- 972*	P. Nurse
DC1227	*h- nhp6::mCherry::ura4+ plo1::GFP::KAN tos4::GFP::KAN*	This study
DC1231	*h+ wee1-50 nhp6::mCherry::ura4+ plo1::GFP::KAN* *tos4::GFP::KAN*	This study
DC	*Pcdc13::cdc13Scdc2as::cdc13UTR Dcdc2::KAN Dcig1::HYG* *Dcig2::KAN Dpuc1::HYG nhp6::mCherry::ura4+* *plo1::GFP::KAN tos4::GFP::KAN*	This study

Figure 1

A. Schematic of a cell trap for fission yeast cells. **B.** Organization of the arrays of traps in a microfluidic chip. The different columns of traps have an offset of 7 μm to promote efficient cell loading. **C.** DIC image of the traps built in PDMS. **D.** Schematic of the full microfluidic chip design. Each chip allows for performing up to 8 parallel and independent experiments. Each channel integrates 2000 single cell traps. The green squares represent the trap areas (1.5 x 1.1 mm).

Figure 2

A. Mapping of cell cycle events using our microfluidic chip and the DetecDiv platform relied on specific fluorescent markers and DIC imaging. Nhp6::mCherry and Plo1::GFP were used to monitor the subcellular dynamics of the chromatin and the onset of mitosis, respectively. **B.** Tos4::GFP allowed for the identification of the G1/S transition. Representative images of time-lapse assays in our experimental conditions. The different categories used in our classification are indicated. Scale bars = 5 μm.

Figure 3

A. Representative image of a trap with more than one cell. Dashed line indicates the cell of interest, in the innermost area of the trap. Nhp6::mCherry signal from other cells may affect the training of the neural networks. **B.** Assessment of classifier quality when the software was trained using Nhp6::mCherry in non-segmented images. ROI: Region of Interest. Each ROI in an experiment consists of a single trap. The table compares the results from the manual annotation (Ground truth) with those from the automated pipeline on a testing dataset. This classifier was not efficient, mis-classifying between 12 and 34 % of cells each category. **C.** Segmentation procedure to train the neural networks on the cell of interest. The system was trained by drawing the cell of interest, additional cells and background in a set of ROIs. The testing set allowed the comparison of the manually drawn cells (middle panel) and automatically segmented cells (right panel). The threshold was adjusted to improve the accurate detection of the cell contours. The cell of interest in in green. **D.** Assessment of the quality of the segmentation qualifier as in *B*. These results show that the segmentation qualifier can be used to efficiently select and analyze only the cell of interest. **E.** Example of selection of the cell of interest using a processor that takes advantage of the segmentation mask to assign to each pixel outside the object an intensity of 0 (black). Data are as in *A*. **F.** Assessment of the quality of the Nhp6::mCherry classifier when training the neural network

on the same dataset as in *B*, but after segmentation and masking. These data show that the use of the masking strategy strongly improves the reliability of the classifier.
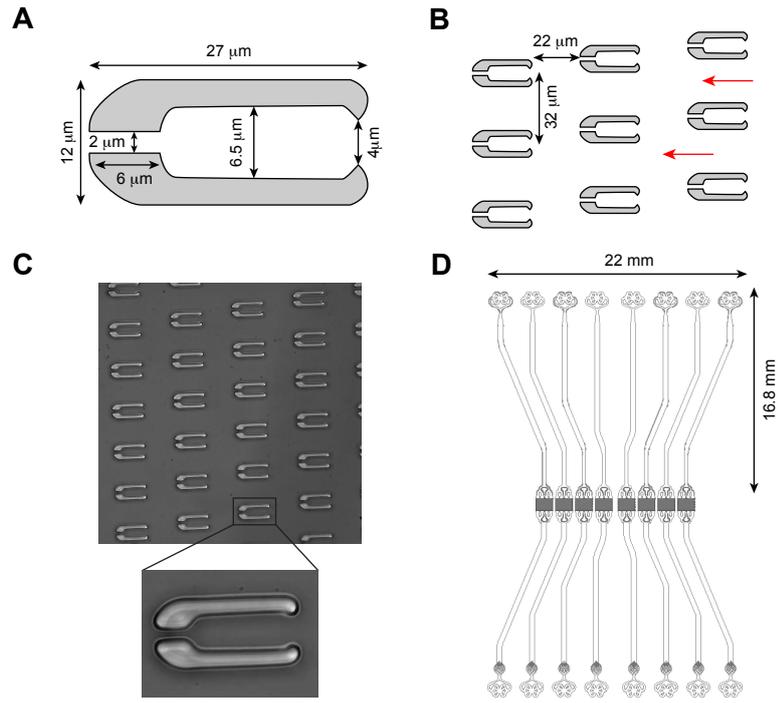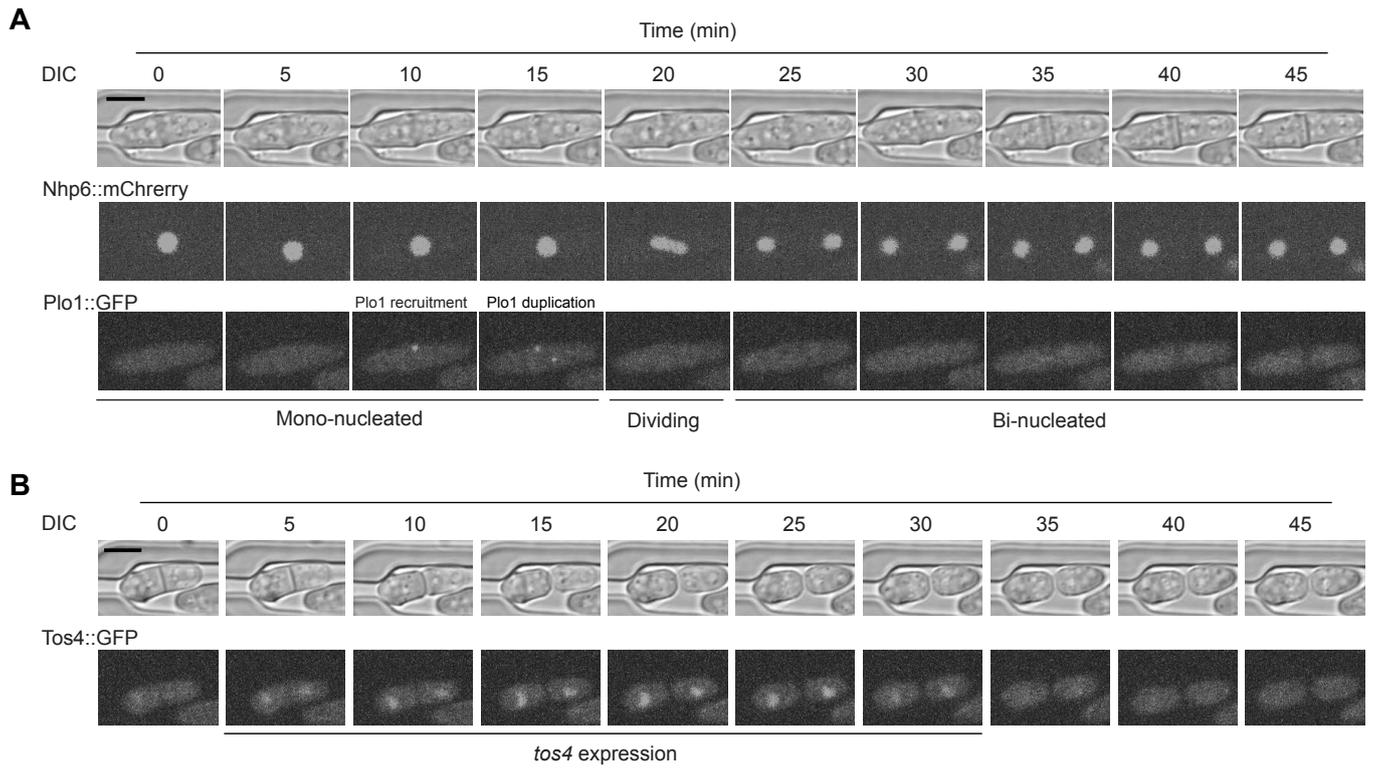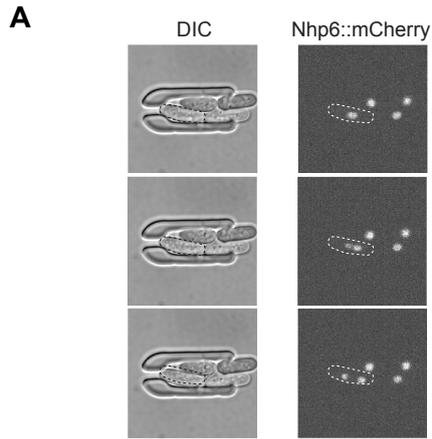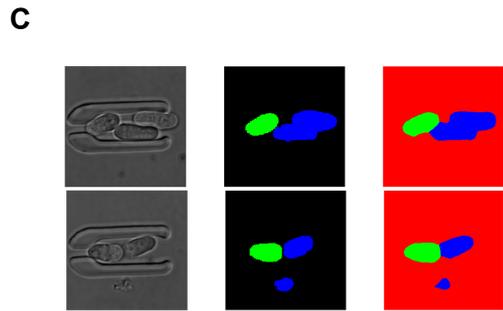
FIGURE 1

A

27 μm

12 μm

2 μm

6 μm

6.5 μm

4 μm

B

22 μm

32 μm

C

D

22 mm

16.8 mm

FIGURE 2

A

Time (min)

DIC

| 0 | 5 | 10 | 15 | 20 | 25 | 30 | 35 | 40 | 45 |

Nhp6::mChrerry

Plo1::GFP

Plo1 recruitment   Plo1 duplication

Mono-nucleated   Dividing   Bi-nucleated

B

Time (min)

DIC

| 0 | 5 | 10 | 15 | 20 | 25 | 30 | 35 | 40 | 45 |

Tos4::GFP

tos4 expression

FIGURE 3

FIGURE 3

Chapter 4:

Fluorescence exclusion – a rapid, accurate and powerful method for measuring yeast cell volume

Summary

Cells exist in a broad range of shapes and sizes across and within different species, and it is apparent that regulation of their size is a shared feature. The manner by which cells regulate their size remains elusive, with a bulk of our knowledge deriving from models that have morphologically regular shapes, such as yeast. However, many of the techniques available do not include the analysis of cell volume. Cell volume a complex and important trait that is modulated by both genetic and environmental factors. Indeed, proteins such as enzymes are highly influenced by changes in concentrations, while exchanges the cells have with the environment are dependent on surface area. Additionally, changes in cell volume has been linked to the cell cycle, where although fission yeast cells stop growing and maintain their shape during mitosis, mammalian cells undergoing mitosis demonstrate a more transient phase rounding and changes in volume. These examples emphasise an importance of volume in dissecting size control in cells, as it would be a more informative parameter.

To this end, our lab has adapted a newly developed technique for measuring cell volume in mammalian cells for the use in fission yeast. The fluorescent exclusion method (FXm) involves a specifically designed microfluidic chip where cells are measured in the presence of a fluorescently labelled dextran, which does not permeate the cell membrane, where the displaced local reduction in fluorescence can be used to determine the volume of the a cell. In addition to adapting this methodology to yeast, we have also improved the image analysis pipeline, providing more high-throughput analysis. This study provides a quick and reliable way to measure cell volume in fission yeast. Lastly, we have also demonstrated that we can track single-cell volume changes over time by combing FXm with time-lapse microscopy. A unique strategy that will allow us to dissect growth dynamics and size modulations, aiding our understanding of cell volume is regulated in fission yeast.

The Company of
Biologists

TOOLS AND RESOURCES

Fluorescence exclusion – a rapid, accurate and powerful method for measuring yeast cell volume

Daniel García-Ruano[1], Larisa Venkova[2,3], Akanksha Jain[1], Joseph C. Ryan[1], Vasanthakrishnan Radhakrishnan Balasubramaniam[1], Matthieu Piel[2] and Damien Coudreuse[1,3,*]

ABSTRACT

Cells exist in an astonishing range of volumes across and within species. However, our understanding of cell size control remains limited, owing in large part to the challenges associated with accurate determination of cell volume. Much of our comprehension of size regulation derives from yeast models, but even for these morphologically stereotypical cells, assessment of cell volume has mostly relied on proxies and extrapolations from two-dimensional measurements. Recently, the fluorescence exclusion method (FXm) was developed to evaluate the size of mammalian cells, but whether it could be applied to smaller cells remained unknown. Using specifically designed microfluidic chips and an improved data analysis pipeline, we show here that FXm reliably detects subtle differences in the volume of fission yeast cells, even for those with altered shapes. Moreover, it allows for the monitoring of dynamic volume changes at the single-cell level with high time resolution. Collectively, our work highlights how the coupling of FXm with yeast genetics will bring new insights into the complex biology of cell growth.

KEY WORDS: Cell volume, Yeast, Fluorescence exclusion

INTRODUCTION

Cell volume is a complex trait that is modulated by both genetic and environmental components (Amodeo and Skotheim, 2016; Cook and Tyers, 2007; Lloyd, 2013; Marshall et al., 2012; Mueller, 2015). It has an impact on a host of processes (Pedersen et al., 2001; Zhurinsky et al., 2010), playing important roles in tissue architecture and contributing to the overall size and shape of an organism. At the single-cell level, volume and surface area not only define how cells interact with their environment but also determine their intracellular chemistry and organization. Strikingly, deregulation of cell size has dramatic consequences and is a hallmark of aging and cancer (Li et al., 2015; Pietras, 2011; Yang et al., 2011).

In proliferating cells, volume is linked to cell cycle progression. Specific stages of the cell cycle are associated with differential changes in cell size and morphology, and the dynamics of cell growth are complex across species. For instance, although fission yeast cells stop growing and maintain their shape during mitosis, mammalian cells undergoing division show a transient phase of rounding and volume alteration (Lancaster et al., 2013; Zlotek-Zlotkiewicz et al., 2015). In addition, cell size checkpoints were proposed to be central to the fission yeast cell cycle, allowing for the coordination of growth and division (Fantes, 1977; Fantes and Nurse, 1978, 1977). These mechanisms reduce cell-to-cell heterogeneity, thereby maintaining size homeostasis. Modulation of cell size is also triggered by environmental changes, and cell cycle exit is often associated with a decrease in cell volume. For example, yeast cells exposed to nitrogen or glucose starvation enter quiescence with a significantly reduced size (Sun and Gresham, 2021). Interestingly, increases in cell volume were observed during long-term experimental evolution in bacteria and proposed to contribute to improved proliferation (Grant et al., 2021; Lenski and Travisano, 1994; Mongold and Lenski, 1996). The volume of dividing cells may therefore result from the necessary balance between growth advantages and evolutionary trade-offs.

The mechanisms underlying size control have been the focus of in-depth investigation. Although several pathways have been described (Amodeo and Skotheim, 2016; Cook and Tyers, 2007; Lloyd, 2013; Marshall et al., 2012; Mueller, 2015), whether they represent the key processes that ensure size homeostasis remains unclear. Surprisingly, how cells measure and control their geometric characteristics is still poorly understood, and multiple models that are not mutually exclusive have been proposed: cells may divide (1) when reaching a specific size (sizer), (2) after a defined time following a landmark event (timer) and (3) after having produced a fixed amount of mass, at a rate that depends on birth size (adder). Although these possibilities are supported by experimental and theoretical studies (Fantes and Nurse, 1977; Mueller, 2015; Soifer et al., 2016; Sveiczer et al., 1996; Taheri-Araghi et al., 2015), general conclusions are difficult to draw. This may be due in part to the diversity of measurements used to describe cell size, including volume, surface area, length or dry mass. The question remains whether one or a combination of these characteristics is more relevant for size regulation and whether different cell types rely on the same or distinct parameters. Thus, although the sizes and shapes of individual cell types are considered as hallmarks of cell identity, no unifying principles for size control have emerged.

Experimentally, size regulation has been difficult to investigate, in particular in complex eukaryotes. In mammalian cells, this has been hampered by the challenges of genetic manipulation and the lack of simple methods for accurate measurement of cell volume. Therefore, unicellular eukaryotes such as the budding and fission yeasts remain the models of choice for deciphering the bases of this critical cellular feature, and different concepts have emerged that may provide robust ways of regulating size, including titration mechanisms and dependence on geometric parameters (Amodeo

[1]Institute of Genetics and Development of Rennes, UMR 6290, CNRS – University of Rennes 1, 35043, Rennes, France. [2]Institut Curie and Institut Pierre Gilles de Gennes, PSL Research University, CNRS UMR 144, 75005, Paris, France. [3]Institute of Biochemistry and Cellular Genetics, UMR 5095 CNRS - Bordeaux University, 33077, Bordeaux, France.

*Author for correspondence (damien.coudreuse@ibgc.cnrs.fr)

L.V., 0000-0001-5721-7962; A.J., 0000-0002-9299-1248; J.C.R., 0000-0002-1098-7158; V.R.B., 0000-0001-8052-4119; M.P., 0000-0002-2848-177X; D.C., 0000-0003-2534-1621

Journal of Cell Science

1

and Skotheim, 2016; Facchetti et al., 2019; Martin and Berthelot-Grosjean, 2009; Moseley et al., 2009). However, how cells monitor their dimensions and how size variation triggers a corrective response is not fully understood.

Owing to the cylindrical morphology of fission yeast cells, length at division has been widely used as a proxy for cell size. Despite the ease of measuring cell length, this approach is limited and does not allow for deciphering the complexity of size control. First, cell volume is more critical to cell biology and biochemistry than length. Second, differences in diameter along individual cells (Fig. 1A,B; Fig. S1A), which are usually ignored, have a stronger impact on cell volume than length: the size of a rod-shaped cell is linearly dependent on its length but varies with the square and cube of its radius. Finally, length at division restricts the analysis to a small fraction of the population, and morphology mutants or cells grown in conditions that induce alteration of their dimensions cannot be studied using this method. To investigate the control of yeast cell volume, different techniques have been applied. These include volume calculation from geometrical assumptions, three-dimensional (3D) reconstruction from two-dimensional imaging data, extrapolation of volume from cell outline detection, and complex approaches using micromechanical devices (Baybay et al., 2020; Bryan et al., 2010, 2014; Facchetti et al., 2019; Model, 2018; Pan et al., 2014; Zegman et al., 2015). However, these strategies are either low throughput, difficult to establish, or rely on various assumptions and complex image processing. In particular, given the impact of cell diameter on cell volume (Fig. 1A,B; Fig. S1A), accurate evaluation of cell size based on the detection of cell outlines requires these measurements to be highly precise (Baybay et al., 2020; Zegman et al., 2015). Therefore, although these methods represent important steps for addressing size control, a more direct, simple and unbiased technique is necessary.

Recently, a fluorescence exclusion method (FXm) was developed for evaluating the volume of morphologically diverse mammalian cells (Cadart et al., 2018, 2017). FXm relies on microfluidic devices in which cells are imaged in the presence of a fluorescently labelled dextran that does not cross the plasma membrane. Thus, using chambers of known height, the local reduction in fluorescence due to the presence of a cell allows for the determination of its volume with high accuracy (Fig. 1C; Cadart et al., 2017). FXm presents a number of advantages over other known and often complex approaches (Bottier et al., 2011; Cadart et al., 2017; Model, 2018; Zlotek-Zlotkiewicz et al., 2015; see also Discussion). It was validated through measurement of artificial substrates of different heights, and data obtained using mammalian cells were highly comparable to those from atomic force microscopy analyses (Bottier et al., 2011). Furthermore, results from FXm and profilometer measurements for thin polydimethylsiloxane (PDMS) strips were
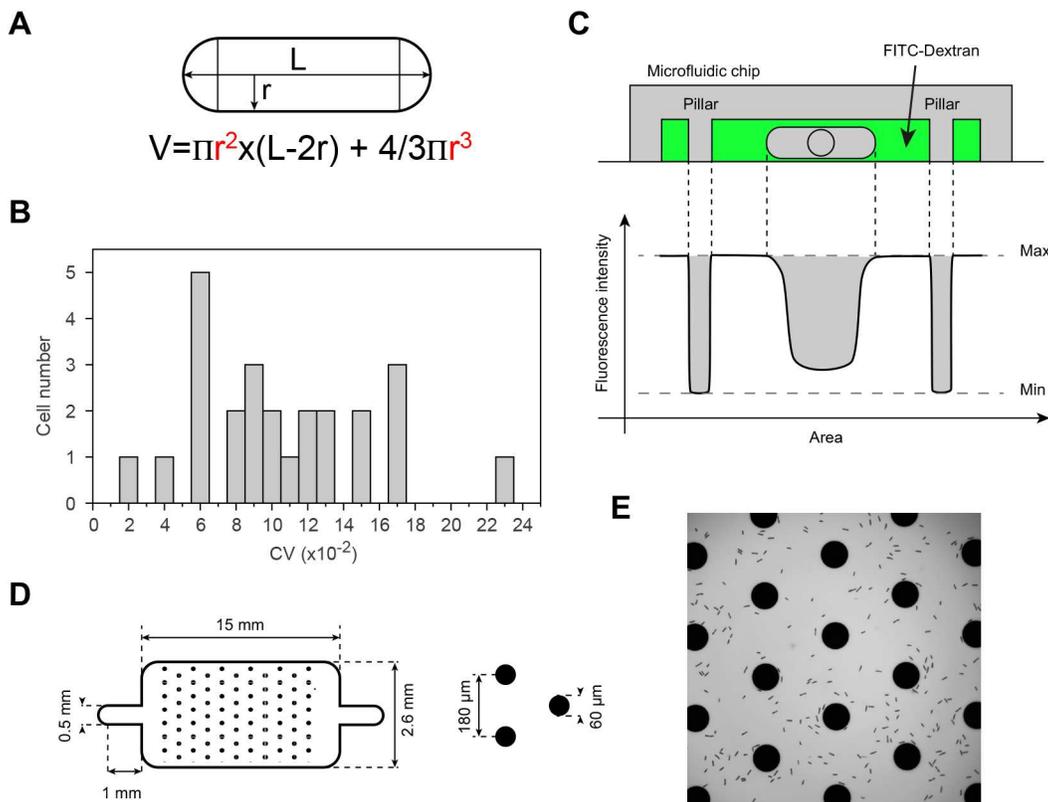

Fig. 1. Cell volume and microfluidic chips for FXm. (A) The geometric model of a fission yeast cell is based on a cylinder with half spheres at both ends. Differences in radius (r) thus have a stronger impact on volume (V) than those in cell length (L). (B) Distribution of the coefficients of variation (CV) of cell volume at division for 25 cells, determined using the geometric model. For each cell, length at division and width at five different positions were measured (Fig. S1A). Cell volume was then calculated using each width measurement, and the CV was determined for each cell. (C) Schematic of the principles of FXm. Top: cells are injected in a FXm chip (see D) in the presence of FITC–Dextran. Pillars are integrated for ceiling support and image normalization. Single-plane images (see E) are acquired for analysis. Bottom: after normalization, cell volume is determined from the loss of fluorescence (gray area; the internal height of the chip must be measured). Although this schematic represents the fluorescence along a scan line for ease of visualization, FXm relies on the assessment of fluorescence intensity over the entire area in which the cell of interest is located. (D) Schematic of the chambers used for fission yeast. Left: design and dimensions (not to scale). Right: pillars are 60 μm in diameter and separated by 180 μm. (E) Image of fission yeast cells in an FXm experiment (before image normalization).

similar (Braïni et al., 2018), highlighting the potential of this method. Importantly, FXm is unaffected by morphological alterations and is compatible with the monitoring of high numbers of cells. However, whether this approach could be used for much smaller cells such as yeast remained unclear, as this would require microdevices with significantly lower internal chambers. For example, HeLa cells are $\sim$20 µm in height with a volume of $\sim$1500 µm³ at birth and $\sim$3000 µm³ at division (Cadart et al., 2018, 2019). In contrast, fission yeast cells divide at a length of $\sim$14 µm and a diameter of $\sim$4 µm, with a calculated volume ranging from 120 µm³ to 200 µm³, depending on growth conditions and width measurements (Navarro and Nurse, 2012; Nurse, 1975).

Here, we use the fission yeast as a model and demonstrate that FXm is a groundbreaking tool for measuring the volume of small cells. We engineer specific microdevices for yeast cells, provide an improved pipeline to perform large-scale analyses, and assess the reproducibility and sensitivity of the system. Furthermore, we demonstrate the compatibility of FXm with multi-color imaging for evaluating single-cell volume in specific subpopulations. We finally show that combining FXm with time-lapse experiments will represent a unique strategy for deciphering growth dynamics and size modulation, in particular when taking advantage of yeast genetics. Interestingly, our results suggest that the use of FXm to re-evaluate previous models will be essential for understanding how cell volume is regulated in fission yeast, with implications for the general principles of cell size control in eukaryotes.

RESULTS
Microfluidic devices for yeast cell volume measurement
FXm is simple and potentially compatible with cells of any type and shape, making it ideal for investigating size control in genetically amenable models such as yeast. However, to ensure an optimal dynamic range for accurate volume measurements, the height of the microfluidic chamber must be of the same order of magnitude as that of the cells. Indeed, the exclusion of fluorescent molecules in a microsystem several times higher than the cell would only marginally impact the total fluorescence intensity in the region of interest, affecting the reliability of the results. Microdevices employed for mammalian cells are therefore not adapted to fission yeast, which require chambers of $\sim$4–7 µm in height. Interestingly, such reduced dimensions were suggested to be advantageous for the accuracy of FXm (Model, 2020).

This design constraint led us to build specific devices for yeast cells. For this, we determined the optimal pillar density, which has to be high enough to prevent the collapse of the chambers without reducing the throughput of the method. Indeed, cells close to these pillars are excluded from analysis due to the bias introduced in the measurements by the presence of neighboring structures (Cadart et al., 2017). We therefore tested chambers with various inter-pillar distances and found 180 µm (Fig. 1D), coupled with an optimized cell concentration and preparation procedure, to be the most reliable combination for assessing high numbers of cells in a single frame (Fig. 1E, Materials and Methods).

Measuring single yeast cell volume with FXm
FXm image analysis consists of three steps: image normalization, cell selection and volume calculation. The concepts underlying these different aspects of FXm and the extraction of volume from fluorescence measurements have been thoroughly described (Bottier et al., 2011; Cadart et al., 2017; Zlotek-Zlotkiewicz et al., 2015). However, the use of a low-magnification objective (see Materials and Methods), the size of yeast cells and the high number of cells in

a frame make it labor intensive to manually select individual cells using the existing code that was established for mammalian cells. Interestingly, the normalization procedure generates a mask that separates pillars and cells from the background (Cadart et al., 2017). Because the majority of objects extracted at this step correspond to valid individual cells, we took advantage of this mask and developed a Python script to assist the user in cell selection. Thus, instead of manually delineating each region of interest for analysis (Fig. 2A, top), this tool offers two distinct strategies:

First, a user-guided selection mode can be chosen, in which cells pre-selected by the normalization mask are magnified and individually displayed (Fig. 2A, bottom), allowing the user to rapidly exclude incorrect objects (e.g. dust particles, cell aggregates). This makes the analysis of a large number of cells easier and faster. We validated this method by first assessing the volumes of haploid versus diploid cells and found that diploids were almost twice as large as haploids (1.84-fold, Fig. 2B; Fig. S1B). In addition, we analyzed cells with more subtle differences in volume, comparing wild type with the well-described *wee1-50^ts* (small) and *cdc25-22^ts* (large) temperature-sensitive cell cycle mutants grown at permissive temperature (Fantes, 1979; Fantes and Nurse, 1978; Nurse, 1975). Our results demonstrated significant differences in volume between these strains (Fig. 2C; Fig. S1C). Interestingly, our data for *wee1-50^ts* were similar to those obtained using a Coulter Multisizer (Table S1, $\sim$5% difference), but the latter reported lower volumes for both wild-type (-19%) and *cdc25-22^ts* (-23%) cells compared to FXm. This is consistent with a known drawback of the Coulter Multisizer, which underestimates the size of rod-shaped particles (Bryan et al., 2012; Cavicchi et al., 2015): small *wee1-50^ts* cells are closer to spherical objects and thus less sensitive to this bias.

Second, an automated selection can be applied. To exclude cell aggregates or small dead cells, a threshold is used based on the interquartile range (IQR) of the population data. This is more appropriate than absolute cut-offs, which need to be adjusted from strain to strain. After testing different approaches, we found that excluding values that are one IQR above or below the third and first quartiles, respectively, was optimal for obtaining results similar to those from the user-guided method (Fig. 2D). Importantly, our code also allows for tuning the outlier threshold and displays the total number of objects as well as the number and percentage of discarded measurements on each side of the spectrum. The user can thus evaluate the quality of the data and apply a manual analysis when necessary.

Finally, our script also integrates the option of separating the selected cells in different groups, making it possible to determine the volumes of distinct subpopulations, for instance based on additional fluorescence markers (see below).

Collectively, our results suggest that FXm can be used for measuring yeast cell volume, and the improvements brought by our analysis code facilitate FXm while providing additional options to the user for more complex studies. Interestingly, although manual selection is the most accurate approach, we show that automated analysis with outlier exclusion allows a rapid assessment of high numbers of cells while remaining sufficiently reliable for screening the volumes of many strains.

Robustness of FXm for measuring yeast cell volume
The necessity of using microchips of reduced height may represent a challenge for precisely measuring the volume of individual yeast cells. Indeed, in these conditions, the difference between the minimum (pillar) and maximum (no cell) fluorescence intensities (Fig. 1C), as well as the extent of fluorescent molecule displacement
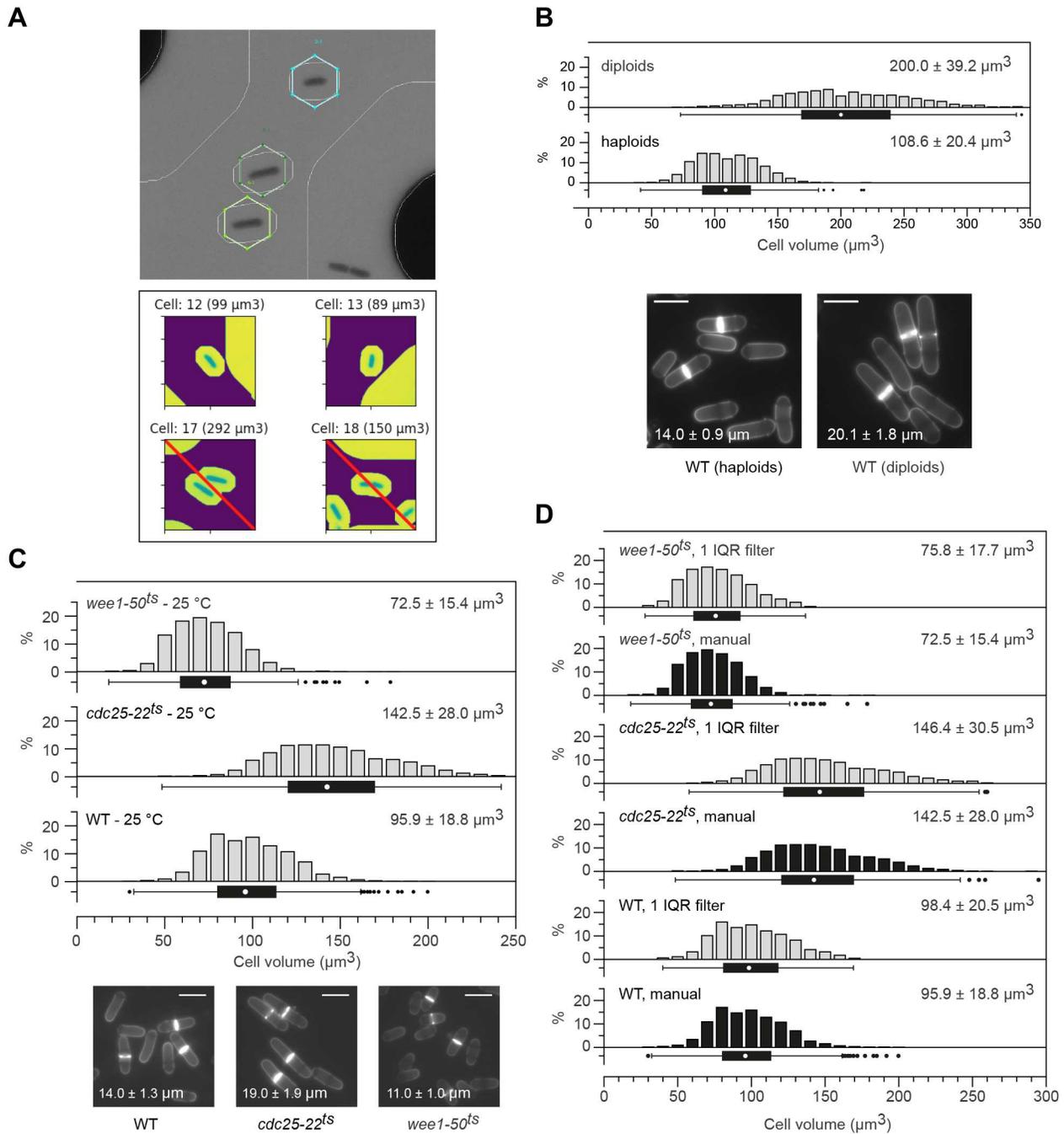
Fig. 2. Measuring yeast cell volume by FXm. (A) Top: representative image showing the selection of individual cells using the original FXm code. Each valid cell must be identified from the FITC image (Fig. 1E; the area shown is magnified for display purposes) and the regions of interest (hexagons) manually drawn for quantification. Bottom: representative image showing the new FXm pipeline, which takes advantage of the normalization mask for cell selection. All objects are automatically identified and displayed individually at higher magnification. Cell aggregates (left), recently divided cells (right) or artifacts can be excluded by the user (red barred). (B) Top: comparison of volume distributions in populations of wild-type (WT) haploid and diploid fission yeast cells by FXm. Cells were grown in EMM6S at 32°C. Pooled datasets ($n \geq 1073$) for three independent experiments ($n \geq 207$ for each replicate, Fig. S1B). Values outside of the plot range (n^*) were excluded: $n^* \leq 1$ for each replicate. Bottom: Blankophor images, cell length at division (LAD) is indicated (averages with s.d. for pooled datasets of three independent experiments, $n \geq 100$ for each replicate). Scale bars: 10 µm. In EMM6S, WT cells have a volume similar to that in EMM (compare with Figs 3–7) but a reduced LAD (compare with Fig. 4A, Fig. 5A, Fig. 6 and Fig. 7), suggesting a difference in cell width between these conditions. (C) Top: WT, and wee1-50^ts and cdc25-22^ts temperature-sensitive strains were grown at the permissive temperature of 25°C and their volumes measured by FXm. Pooled datasets ($n \geq 1144$) of three independent experiments ($n \geq 337$ for each replicate, Fig. S1C). $n^* \leq 6$ for each replicate. Bottom: Blankophor images with LAD (averages with s.d. for pooled datasets of three independent experiments, $n \geq 100$ for each replicate). Scale bars: 10 µm. WT cells at 25°C have a reduced volume and LAD compared to those at 32°C (compare with Figs 3–7). (D) Comparison of FXm results using manual (black) versus automated [gray, 1 interquartile range (IQR) filter] cell selection. Data for manual selection are from Fig. 2C. For automated selection, (1) the same images as for the manual method were used, pooling data from all replicates, and (2) a filter was applied that excludes entries that are 1 IQR above and below quartile (Q)3 and Q1 (n^{**}), respectively (unfiltered selected objects: $n \geq 1390$, excluded objects $n^{**} \leq 200$). The overlap between the two approaches for both correctly assigned cells and outliers is between 87% and 92%. In B–D, graphs are histograms with box and whiskers plots, indicating the minimum, Q1, median (white dot), Q3 and maximum, with outliers determined by 1.5 IQR. Median volumes with median absolute deviations (m.a.d.) are shown.

in the presence of a cell, are inherently low. This may render the technique more susceptible to noise.

To evaluate whether FXm provides high quality results for yeast, we measured the size of wild-type fission yeast cells, comparing both the median volumes and volume distributions from independent experiments. To this end, we analyzed five replicates from separate devices built from the same 5.53 μm mold. Remarkably, we obtained reproducible data with a median volume

for the pooled dataset of 104.8 μm^3 (s.e.m., 1.7 μm^3; Fig. 3A). This is consistent with previous results established by complex image processing (Baybay et al., 2020), validating FXm for size monitoring in yeast. Comparing our individual datasets, we found that alterations up to ~10% in median volume at the population level can occur between replicates of the same strain. This likely results from biological variations and differences in local or global chamber heights (see Materials and Methods). Thus, changes
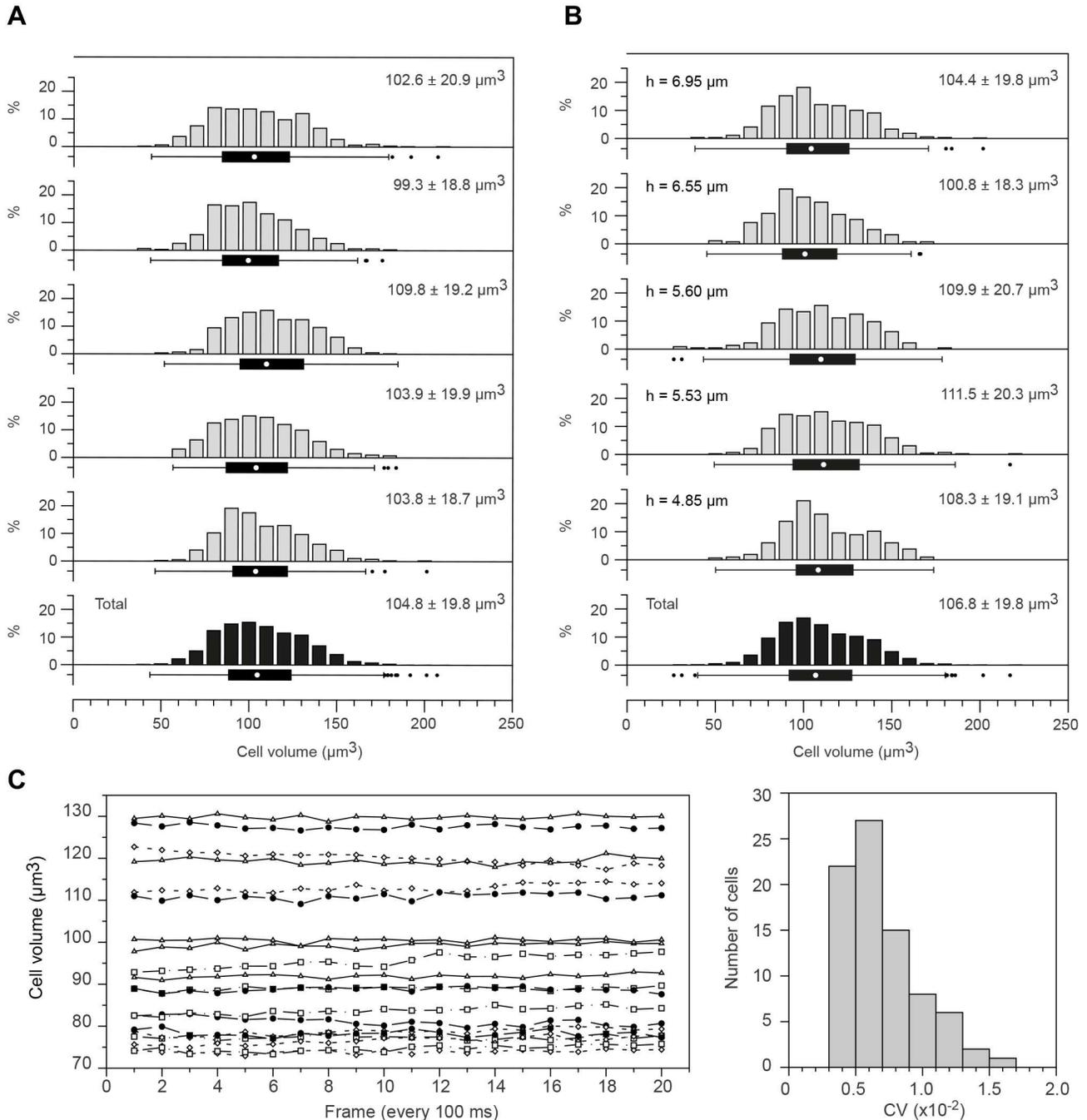

Fig. 3. Robustness of FXm for measuring yeast cell volume. (A) Measurements of WT fission yeast in five independent experiments (gray) and the total pooled dataset (black). Chamber height: 5.53 μm; $n \geq 316$ for each replicate, $n=2266$ for the total dataset; $n^* \leq 1$ for each replicate. (B) Measurements of WT cells from a single culture using five distinct devices of the indicated heights (gray) and the total pooled dataset (black). $n \geq 225$ for each replicate, $n=1777$ for the total dataset; $n^*=0$ for each replicate. In A and B, graphs are as in Fig. 2. (C) 20 consecutive FXm images were acquired (100 ms exposure per image over a total time of 2 s), and the volumes of 81 individual cells were followed throughout the experiment (left). For display purposes, 20 representative cells are shown. The generation time of WT cells in these conditions is ~140 min. The coefficients of variation (CV) in volume were determined for each cell (right). The average CV for all 81 cells is 0.0071±0.0028, corresponding to a precision in cell volume measurement of 0.71%.

below this conservative threshold should be interpreted with caution, as they are in the range of the observed experimental variability between replicates. To test whether this threshold could be improved by increasing sample size, we used six independent measurements and compared all combinations of non-overlapping triplicates (*n*>900 for each pooled dataset). In this context, we found that the maximum difference between two datasets was less than 6.5% (Table S2), suggesting that the threshold for distinguishing strains with different median volumes depends on the sample size and number of repeats. Note that when using the geometric model for fission yeast (Fig. 1A) and a constant diameter of 4 µm, an increase in volume at division of 6.5% results from an increase in length at division from 14 µm to ∼14.8 µm. The same alteration in volume with a constant length at division of 14 µm is brought about by an increase in diameter of ∼0.1 µm. These changes in length and width are at or below the minimal difference that can be reliably determined by light microscopy in *Schizosaccharomyces pombe*, thus further highlighting the sensitivity of FXm for yeast cell volume measurement. Finally, we evaluated the reproducibility of the volume distributions observed in our experiments (Table S3) and demonstrated the robustness of FXm for describing the volume profiles of asynchronous populations.

Next, we evaluated potential sources of technical variability associated with FXm. First, inconsistencies in chamber height contribute to differences in volume between replicates (see Materials and Methods). Indeed, we showed that when measuring the respective volumes of two distinguishable wild-type strains within a single chip, the variability threshold can be lowered even when scoring similar numbers of cells (6.6% versus 10%; compare Fig. S2 and Fig. 3A). Importantly, in contrast to the impact of errors in cell width measurements when using conventional approaches (Fig. 1A), FXm data are only linearly affected by differences in chamber dimensions, making this technique less sensitive to experimental variation. Nevertheless, as standard microfabrication procedures make it difficult to generate highly reproducible chamber heights, we set out to assess how changes in the dimensions of different molds may impact volume determination. To this end, we produced microchips of various heights and measured the size of wild-type fission yeast cells by FXm. Surprisingly, the median volumes and volume distributions were comparable (Fig. 3B; Table S3, median volume of the pooled datasets, ∼106.8 µm^3; s.e.m. for the five replicates, 1.9 µm^3), showing that data obtained with different devices can be reliably compared. Furthermore, to ascertain measurement noise at the single-cell level beyond chamber height, we determined the volumes of individual cells over a series of 20 successive images acquired every 100 ms (Fig. 3C). Considering that cell size does not significantly change within this 2 s time window, our results show that the variability inherent to FXm is very limited (<2%), even with such low chambers.

Altogether, these experiments demonstrate that FXm with specifically adapted microfluidic chips is robust and compatible with the analysis of yeast cell volume, producing highly reproducible results.

Small variations in cell dimensions and population heterogeneity

Our initial evaluation of FXm experimental variability suggests that changes in median volume ≥6.5% between strains or growth conditions can be reliably detected (Fig. 3). To confirm this, we first determined the volume of cells showing a marginal difference in length at division compared to wild type. To this end, we took advantage of a strain for which proliferation relies on a minimal cell

cycle control network (MCN). In this background, cell proliferation is solely dependent on the activity of a single cyclin–cyclin-dependent kinase (CDK) complex (Coudreuse and Nurse, 2010). Interestingly, while behaving similarly to wild type, MCN cells show a minor increase in length at division of ∼7% (Fig. 4A, top). At constant diameter (4 µm), the length values we measured are predicted to contribute to a similar increase in volume according to the geometric model of *S. pombe*. Surprisingly, FXm measurements showed a median volume difference of 17% between these strains (Fig. 4A, bottom; Fig. S3A, compare WT and MCN). This suggests that the change in size between wild-type and MCN cells is not solely the result of an increase in cell length (Fig. 4A). Next, building on the results in Fig. 2C and Fig. 3A, we compared wild-type cells grown at 32°C with those grown at 25°C using large sample sizes and five independent replicates (Fig. 4B; Fig. S3B). Our analyses established a difference of ∼9% in median volume between these conditions. Finally, we investigated whether even smaller alterations in volume at the population level could be detected as cells progressively change size over time. To this end, we used MCN cells, which harbor an alteration in CDK that makes it sensitive to dose-dependent inhibition by non-hydrolysable ATP analogs (Bishop et al., 2000; Coudreuse and Nurse, 2010). This allowed us to synchronize cells at G2/M (Fig. S3C,D) and monitor volume changes throughout the following G2 with high time resolution (Fig. 4C). Even considering the variability at certain time points (−1.3% at T=100 and +0.1% at T=135, compared to T=95 and T=130, respectively), small increases in volume (<5%, Fig. S7A) could be measured. These experiments demonstrate the high sensitivity of FXm in this context.

Another critical parameter in our understanding of cell size homeostasis is the size distribution in the population. This reflects the cell-to-cell heterogeneity in cell cycle progression and the strength of the size control. Most studies in fission yeast have focused on variability in length at division. However, not only does this exclude the majority of cells, but our results above suggest that evaluating volume distribution may lead to different conclusions. To determine whether FXm allows for monitoring alterations in size profiles, we took advantage of MCN cells in which the target residues of the conserved Wee1–Cdc25 feedback loop on CDK are substituted (T14A Y15F, MCN-AF). Loss of this mitotic switch results in an increase in cell-to-cell variability in length at division (Coudreuse and Nurse, 2010). In our experimental conditions, we found that these cells are shorter than wild type (Fig. 4A). As anticipated, we also observed a broader distribution of cell volume in MCN-AF compared to MCN and wild-type cells (Fig. 4D). Remarkably, the relative changes in median volume versus length at division between MCN-AF, MCN and wild type provide insights into the dimensions that are altered in these strains (Fig. 4A; Table S4): while MCN-AF and MCN appear to differ only in length (same ratios for volume versus length at division), our data suggest that both strains show an increase in diameter compared to wild type (differing ratios). This was consistent with the measured differences in cell width at division, although they fall below the margin of error (Fig. 4A).

Altogether, these results demonstrate that FXm is easy, sensitive and more robust to experimental errors than previously used methods requiring cell width determination. It enables the monitoring of small alterations in cell volume and changes in size homeostasis in populations of yeast cells. Coupling this approach with traditional cell length measurements is also a promising approach for investigating fission yeast volume regulation, providing novel and more in-depth information on cell size and geometry.
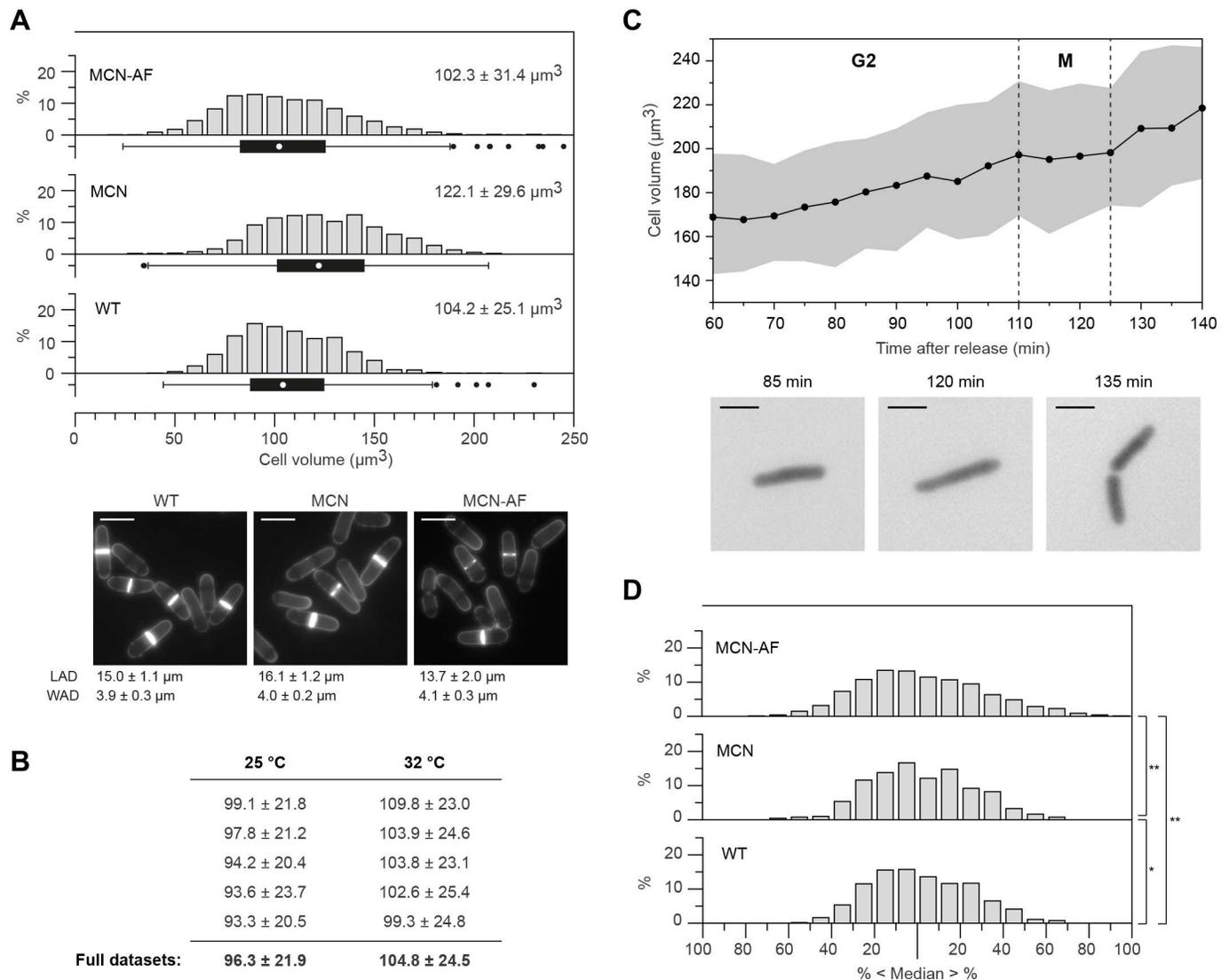
Fig. 4. FXm detects subtle changes in cell volume and size distribution. (A) Top: Blankophor images with LAD and width at division (WAD) (averages with s.d. for pooled datasets of three independent experiments, $n \geq 100$ and $n \geq 60$ per replicate for LAD and WAD, respectively). Although the changes in WAD are consistent with our conclusions based on FXm and LAD (see below), they should be interpreted with caution as they are below the limit of reliable measurement. Scale bars: 10 µm. Bottom: volume measurement of WT, minimal cell cycle control network (MCN) and MCN cells in which the target residues of the conserved Wee1–Cdc25 feedback loop on CDK are substituted (MCN-AF). Pooled datasets ($n \geq 913$) of three independent experiments ($n \geq 172$ for each replicate, Fig. S3A). $n^* \leq 1$ for each replicate. Graphs are as in Fig. 2. (B) Comparison of the median volumes (µm³) for five independent replicates of WT at 25°C and 32°C. Full datasets are in Fig. S3B. Difference in median cell volume: 8.8%. (C) MCN cells grown in EMM6S at 32°C were G2 arrested using 1 µM 3-MBPP1 for 160 min and allowed to synchronously re-enter the cell cycle by washing off the inhibitor (Coudreuse and Nurse, 2010) (Fig. S3C). 50 min after release, cells were injected in a FXm chip and images were acquired every 5 min throughout the next G2, after the first round of cell division (60 min, Fig. S3D). Top: median volumes at the indicated time points (black line, automated cell selection) with IQR (gray area). The higher volume for MCN cells compared to other figures results from the initial G2 block, during which cells grow without dividing. Cell cycle phases are indicated. G2 growth rate: 0.59 µm³/min (linear regression from 60 min to 110 min, before the mitotic plateau). As anticipated, no growth was observed during mitosis. From 125 min to 140 min, the automated selection does not separate newly divided cells (17.4%, 25.9% and 25.5% of the selected objects at 130, 135 and 140 min, respectively, are pairs of cells). This results in an apparent increased growth rate after mitosis, although additional time points would be required for a robust conclusion. The delay in cell cycle progression compared to Fig. S3D is likely due to the growth conditions in the chips without medium flow (see Fig. 8A). For each time point, $214 \leq n \leq 278$ (unfiltered automatically selected objects). Outliers were removed using the 1 IQR filter (see Fig. 2D, $28 \leq n^{**} \leq 49$, representing a maximum of 18% of the selected objects). Bottom: representative images of cells in FXm chips at 85 min (G2), 120 min (M) and 135 min. Scale bars: 10 µm. (D) Volume distribution for the indicated strains as a percentage of the median volume. Data are as in A. $n^* \leq 10$. The two-sample Kolmogorov–Smirnov test was used for comparing population distributions. *$P < 0.05$; n.s., non-significant ($P > 0.05$).

Measuring the size of cells with altered geometries and morphologies

The use of length as a proxy for fission yeast size is particularly problematic when studying mutants or conditions in which cellular aspect ratio and shape are altered. Strategies using cell outline detection to extrapolate volume may not be sufficiently reliable in

this situation, given the influence of minor changes in diameter on cell volume.

In this context, we determined the volumes of various strains showing defects in morphology and shape by FXm. First, we assessed strains lacking Rga2, Rga4 or Rga6, which are members of the RhoGAP family. These factors are involved in polarized growth,
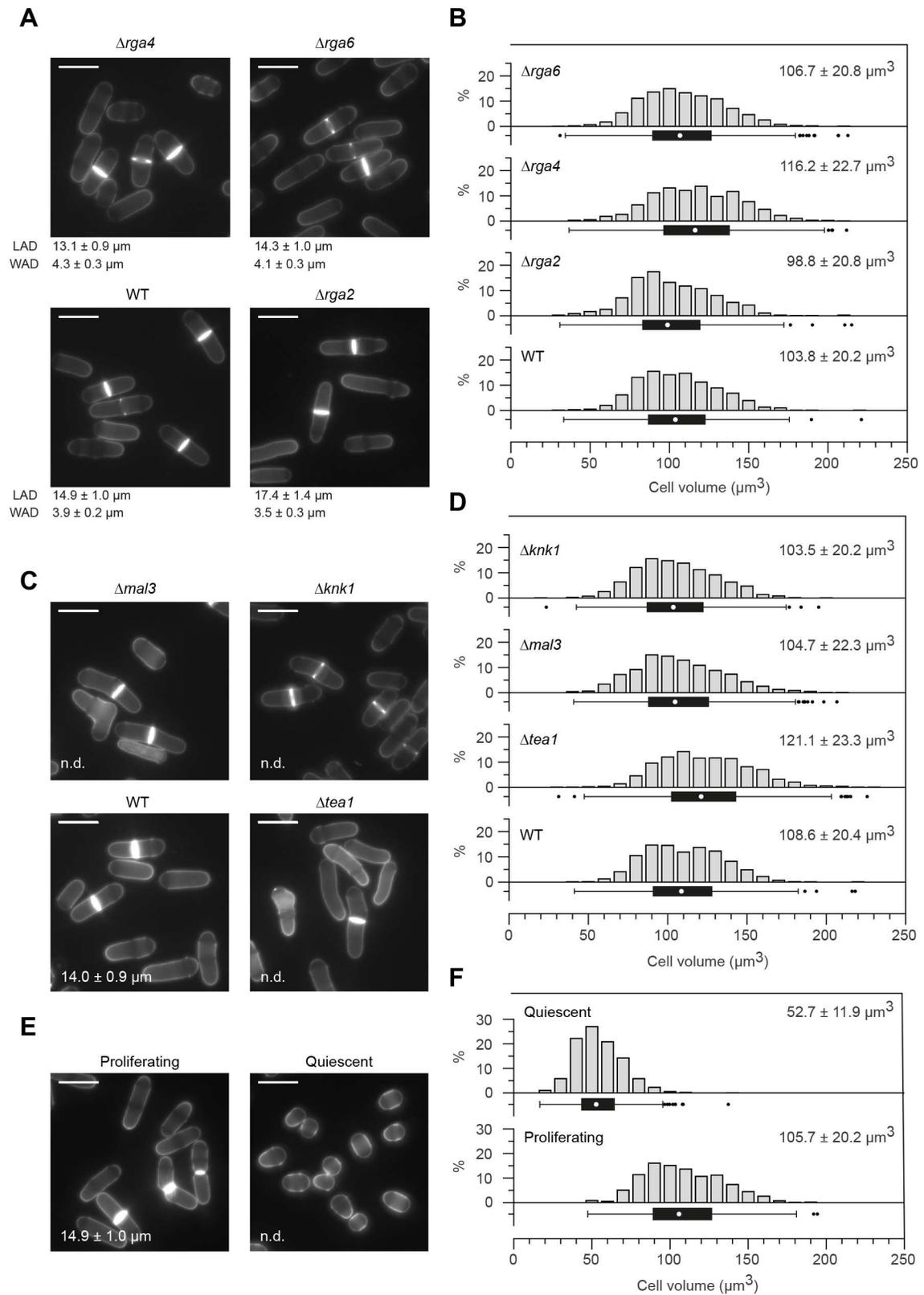
Fig. 5. See next page for legend.

and their loss impacts cell geometry (Das et al., 2007; Revilla-Guarinos et al., 2016; Soto et al., 2010; Villar-Tajadura et al., 2008). When ranking these strains according to their lengths at division, we found that Δ*rga2* cells are the longest, followed by Δ*rga6* and Δ*rga4* (Fig. 5A). Strikingly, FXm, which is independent of cell geometry, ranked the strains differently, with Δ*rga4* and Δ*rga2* cells having the largest and smallest volumes, respectively (Fig. 5B; Fig. S4A).

Fig. 5. Measuring the volume of yeast cells with altered morphologies. (A,C) Blankophor images. Scale bars: 10 µm. (A) LAD and WAD are indicated (averages with s.d. for pooled datasets of three independent experiments, $n \geq 100$ and $n \geq 60$ for each replicate for LAD and WAD, respectively). As for Fig. 4A, such small differences in WAD should be interpreted with caution. (C) LAD is indicated (averages with s.d. for pooled datasets of three independent experiments, $n \geq 100$ for each replicate). n.d., not determined. (B) Volume measurement of the strains in A. Pooled datasets ($n \geq 832$) of three independent experiments ($n \geq 268$ for each replicate, Fig. S4A). $n^* \leq 1$ for each replicate. (D) Volume measurement of the strains in C. Pooled datasets ($n \geq 940$) of three independent experiments ($n \geq 230$ for each replicate, Fig. S4B) are shown. $n^* = 0$ for each replicate. Data for WT are from Fig. 2B (haploids). (E) Blankophor images of proliferating and quiescent WT cells. For quiescent cells, samples were taken 24 h after the culture reached OD$_{595}$=0.4. For proliferating cells, LAD is shown (average with s.d. for pooled dataset of three independent experiments, $n \geq 100$ for each replicate). Scale bars: 10 µm. (F) Volume measurement of the cells in E. Pooled datasets ($n \geq 965$) of three independent experiments ($n \geq 238$ for each replicate, Fig. S5). $n^* = 0$ for each replicate. In C and D, experiments were carried out in EMM6S due to the presence of auxotrophies in some of the strains (Table S5). In B, D and F, graphs are as in Fig. 2.

Next, we assessed the size of cells for which length can be difficult to measure or inherently inaccurate due to morphological alterations. To this end, we used bent cells ($\Delta knk1$, $\Delta tea1$) as well as cells with significant shape defects and irregular diameters ($\Delta mal3$) (Beinhauer et al., 1997; Mata and Nurse, 1997; Scheffler et al., 2014) (Fig. 5C). As anticipated, although cell length at division could not be determined without excluding a significant fraction of the cells, FXm allowed us to establish the profiles of cell volume in these populations and compare them with wild-type cells (Fig. 5D; Fig. S4B). This again highlights the power of this method for studying size control mechanisms independently of cell morphology. Interestingly, in cells with abnormal shapes, both the median volume and size distribution may change (Fig. 5A–D; Fig. S4), potentially reflecting alteration of their cell cycle organization and associated growth patterns. This opens the door to investigating how cell shape may delineate the complex interplay between growth and division at the single-cell level.

Finally, we evaluated FXm data for significantly smaller cells that have stopped dividing. Upon glucose exhaustion, fission yeast cells exit the cell cycle and enter quiescence, which is associated with a dramatic reduction in size. Given the shape of these arrested cells (Fig. 5E), determining their length and width to extrapolate their volume is unreliable. In contrast, FXm established high-quality profiles of cell volume for these populations (Fig. 5F; Fig. S5). This will allow for investigating the impact of cell size on cell physiology and aging in this critical cellular state.

Collectively, this set of experiments demonstrates the versatility of FXm, which provides an unprecedented ability to measure the size of any strain, irrespective of cell morphology and physiological status. Our results also suggest that previous conclusions on size control in fission yeast may need to be re-evaluated using FXm.

Measuring the volume of subpopulations
The experiments presented so far have focused on the determination of cell volume in entire populations. However, extracting the size of cells in specific subpopulations is critical for understanding how different processes may interact with the mechanisms that underlie cell size control and how cell growth and proliferation are coupled. Thus, combining FXm with intracellular fluorescent markers would represent a powerful method to take advantage of yeast genetics and explore the complexity of size regulation in different conditions and throughout the cell cycle. Similarly, this could allow for

discriminating between distinct strains expressing specific markers in a complex population, opening the door to exploring non-cell autonomous processes that may affect volume regulation.

As a proof-of-concept, we determined cell volume at mitosis, using the non-histone chromatin-associated protein Nhp6 coupled to mCherry. First, we validated that nuclear Nhp6::mCherry did not induce any significant signal in the fluorescein isothiocyanate (FITC) channel under FXm conditions (Fig. S6A). This also showed that the slightly reduced volume of these cells compared to wild type (Fig. 6A; Fig. S6B) results from an alteration in Nhp6 function due to the tag rather than a bias from mCherry fluorescence. Using our improved FXm code, we segmented the population of binucleated cells (~11% of the total number of cells) and determined their median volume (~126.5 µm^3, compared to ~93.5 µm^3 for mononucleated cells, Fig. 6B). The partial overlap between mononucleated and binucleated cells is consistent with the interruption of growth during mitosis: cell size does not change during nuclear division, and growth only resumes in G1. Note that the volume of binucleated cells measured in our assay is consistent with previous calculations of cell volume at division (Nurse, 1975) but differs from those presented in a more recent study (Navarro and Nurse, 2012). Altogether, our experiments validate the possibility of combining FXm with additional markers in yeast for more complex investigations of cell size control and dynamics.

Dynamic changes in fission yeast cell volume at the population and single-cell levels
Next, we tested FXm for assessing dynamic changes in yeast cell size. First, we ascertained whether coupling time course experiments with FXm allows for following induced alterations in cell volume over time using asynchronous populations. A wide range of growth conditions [e.g. heat stress (Vjestica et al., 2013), osmotic stress (Millar et al., 1995), change in nutrient availability (Fantes and Nurse, 1977; Petersen, 2009)], as well as experimental modulation of specific cellular pathways, can trigger cell size changes. Understanding the dynamics of such changes may be key to determining the implication of these processes in cell size homeostasis. To evaluate FXm in this context, we took advantage of the analog sensitivity of MCN cells. Indeed, reducing CDK activity in fission yeast using this method leads to an increase in cell size (Chen et al., 2016; Coudreuse and Nurse, 2010). We therefore measured cell volume in asynchronous MCN cells at 40 min intervals (~1/4 of the cell cycle) after treatment with 0.05 µM 3-MBPP1 (Fig. 7). Our data show that MCN cells progressively increase their volume, up to 1.7-fold after one doubling time. Strikingly, comparison of the volume versus length at division ratios throughout the experiment (Table S4) suggests complex dynamics in the respective modulations of length and diameter upon CDK inhibition. This demonstrates that FXm (1) can be used to follow short-term alterations in median cell size and size distribution in asynchronous yeast populations, and (2) provides new perspectives for our understanding of how the geometrical dimensions of cells contribute to their volume.

We then asked whether FXm could be applied to analyze individual yeast cells in time-lapse experiments. To this end, the injection inlets in our chips were enlarged (from 2.5 mm to 4 mm), acting as nutritional reservoirs to maintain stable growth conditions. As fission yeast cells are non-adherent, this assay also required pre-coating of the chip coverslips with lectin. In this setup, we observed a linear increase in volume during each cell cycle and a plateau in size around the time of cell division, corresponding to the well-described growth arrest at mitosis (Mitchison, 1957; Mitchison and
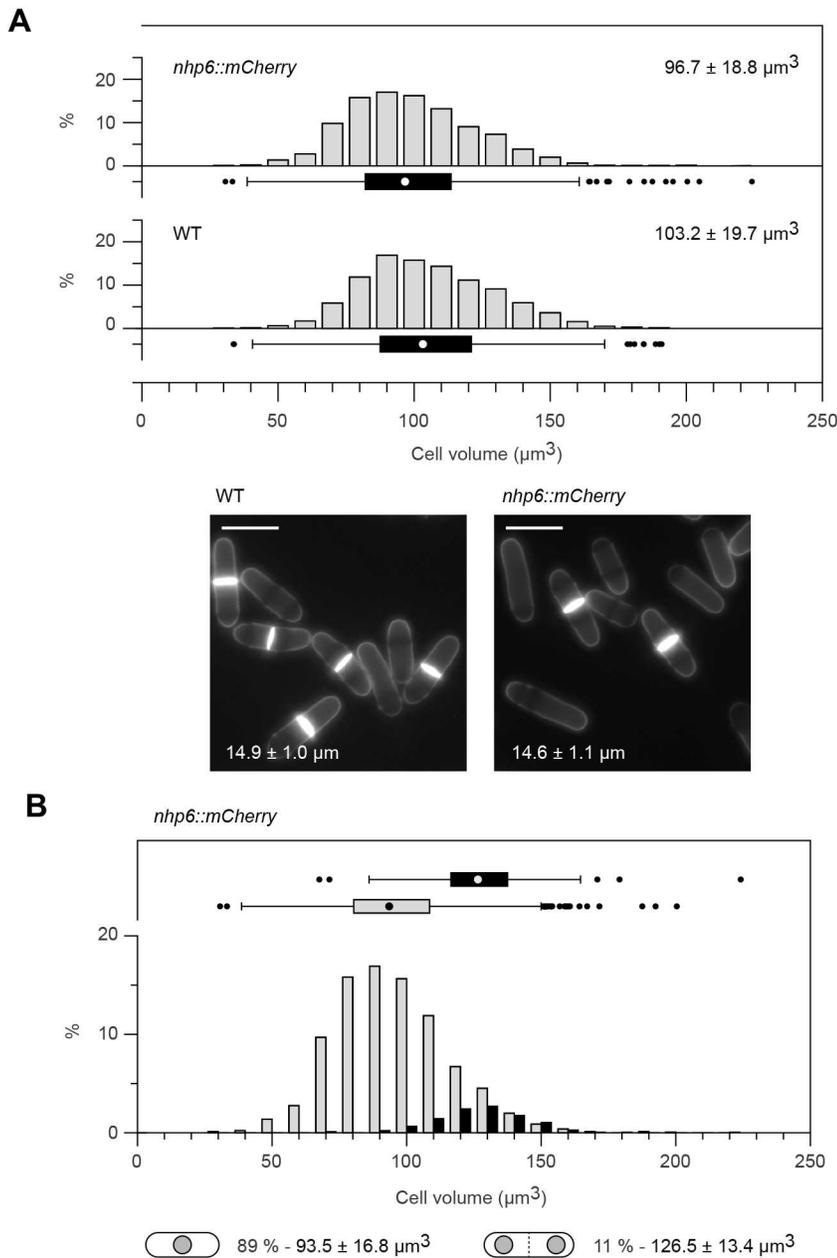
A

Fig. 6. FXm is compatible with the use of fluorescent markers. (A) Top: volume measurement of WT and cells expressing *nhp6::mCherry*. Pooled datasets (*n*≥1568) of three independent experiments (*n*≥499 for each replicate, Fig. S6B). *n**=0 for each replicate. Median volume values with m.a.d. are shown. The difference in median volume is above the 6.5% threshold (Mood's test: *P*<10⁻⁸). The two-sample Kolmogorov–Smirnov test was used for comparing population distributions on normalized data: *P*=0.96, indicating that the distributions are not different. Bottom: Blankophor images with LAD (averages with s.d. for pooled datasets of three independent experiments, *n*≥110 for each replicate). Scale bars: 10 µm. (B) Volume comparison between mononucleated (gray, *n*=1619) and binucleated (black, *n*=196) cells in the population of *nhp6::mCherry* cells. Percentages and median volumes with m.a.d. are indicated. Binucleated cells include both septated (dashed line) and non-septated cells. In A and B, graphs are as in Fig. 2.

B

Nurse, 1985) (Fig. 8A). However, cells divided at smaller sizes in succeeding cell cycles, suggesting that the built-in reservoirs are insufficient to ensure a favorable growth environment throughout our assay. We therefore applied a constant flow of fresh medium containing FITC–Dextran (∼3–5 µl/min) for the entire duration of the experiments. Using this method, we did not detect any consistent reduction in cell volume at division after each cycle (Fig. 8B). Furthermore, the growth rate (see Materials and Methods) was significantly higher than without medium renewal (Fig. 8).

These data demonstrate that FXm is a unique tool for monitoring the volume dynamics of small cells with a high time resolution and for detecting changes in growth rate at the single-cell level. This will allow for investigating the immediate responses of cells to environmental perturbations and the behaviors of separate yeast cell lineages. In addition, this will make it possible to relate volume at birth, growth rate and volume at division for a given cell. Coupled with additional markers, this technique thus offers an unprecedented

entry into the investigation of cell size control and its interplay with other complex cellular processes.

DISCUSSION

Regulation of cell volume is critical for eukaryotic organisms, but the mechanisms underlying this process are still unclear. Yeast models have played a pioneering role in deciphering this complex trait and remain at the forefront of this very active research field. However, the difficulty of accurately measuring cell volume in these small unicellular organisms has been an obstacle for our understanding of size control and homeostasis. Here we show that the FXm is ideal for evaluating the volume of yeast cells in diverse contexts. It provides high quality data on the volume profiles of yeast populations irrespective of cell morphology and physiological state, allows for single-cell analysis of volume changes with high time resolution and is compatible with the use of additional fluorescent markers. Our experiments also demonstrate that FXm
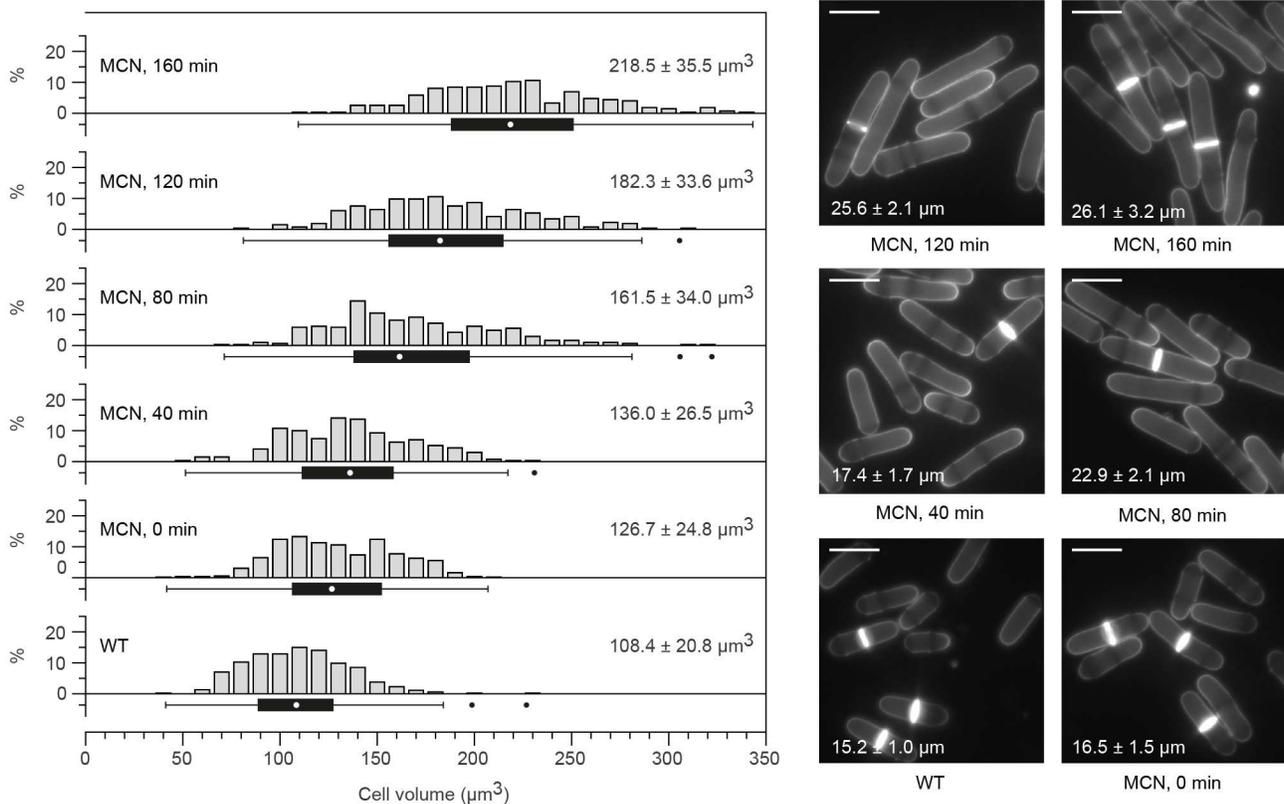
Fig. 7. Dynamic changes in cell volume at the population level. Left: FXm measurement of MCN cells after treatment with 0.05 µM 3-MBPP1. Samples were collected every 40 min after inhibitor addition ($n \geq 265$ at each time point). $n^* \leq 2$ for each dataset. Untreated WT cells were used as a control ($n = 528$). Graphs are as in Fig. 2. Right: Blankophor images with average LAD and s.d. $n \geq 100$ for WT and MCN (0, 120 and 160 min). For the 40 min and 80 min time points, the initial delay in mitosis due to inhibitor treatment leads to a reduction in the number of dividing cells, making it difficult to obtain similar numbers for the calculation of LAD ($n = 45$ and $n = 22$, respectively). Septation indices: WT, 11.5%; MCN 0 min, 20.4%; MCN 40 min, 1%; MCN 80 min, 2%; MCN 120 min, 15.5%; MCN 160 min, 26.9%; $n \geq 400$ for each time point. Scale bars: 10 µm.

gives researchers unique access to in-depth analyses of yeast cell volume dynamics and their coupling with cell cycle progression, integrating the size of cells at all stages of their division cycle. Furthermore, combining FXm with time-lapse imaging represents an unprecedented tool for exploring the changes in growth rate and cellular geometry that occur not only during proliferation or upon major transitions such as quiescence entry and exit, but also when cells respond to acute challenges.

In addition to the versatility and power of this method, FXm is cost effective and easy to implement. All steps of the microfabrication process, from generating the molds to producing the chips, can be performed using standard microfabrication techniques that are now widespread and available within many research teams or in the constantly increasing number of microfabrication facilities. FXm does not require complex microscopy setups, allows for the rapid measurement of a high number of cells and is less biased by measurement errors compared to strategies that rely on cell width. Furthermore, it is based on single-plane imaging, limiting bleaching and phototoxicity, and is not affected by the position of each cell along the *z*-axis, a particular advantage when using non-adherent cells. Finally, the treatment of FXm images is simple and does not require advanced segmentation processes or high computing power. At this stage, the main drawback of FXm is in the measurement of the volumes of individual cells within colonies and dense populations: this requires manual segmentation of each cell, and the direct proximity to a high number of other cells impacts the results. Thus, given the limited disadvantages of FXm compared to its ease

of implementation, robustness and accuracy, we believe that this technique will become a new standard for investigating cell size control in yeast, with implications for our knowledge of size regulation in complex eukaryotes.

Interestingly, our work led to a number of observations that may question existing models of cell size regulation. First, research on *S. pombe* size control and its interplay with cell cycle progression has mostly been based on the assumption that the diameter of proliferating haploid fission yeast cells is (1) constant from one cell to another and (2) homogenous along their growing axis. Our results clearly indicate that these assumptions can lead to incorrect conclusions when comparing strains, as shown using various mutants (Figs 4, 5). In this context, FXm has the advantage of being a direct method for volume measurement that does not rely on any pre-conceived idea of cell geometry. Coupling FXm with cell length measurements also offers an additional level of understanding of cell size dynamics. For example, our data suggest that when cells are arrested in their division cycle through CDK inhibition, the geometric changes that occur over time are surprisingly complex, with length and volume alterations showing different kinetics (Table S4, MCN+3-MBPP1). Similarly, we find that simplifying the architecture of cell cycle control or growing cells in distinct environments has unanticipated impacts on cell geometry, affecting both cell length and diameter (Table S4).

Focusing on subpopulations, as is the case when using cell length at division as a proxy for cell size, may also hamper our comprehension of important processes linking cell growth,
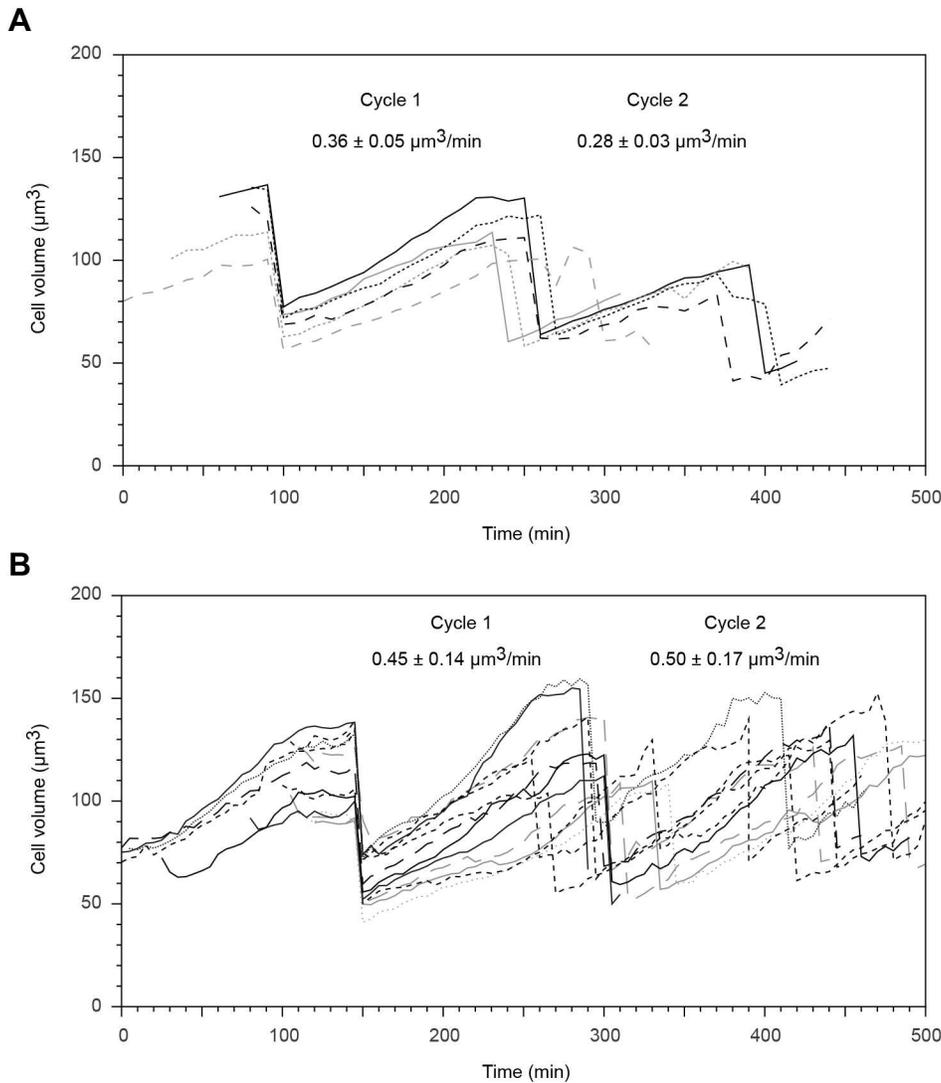
A

B

Fig. 8. Real-time monitoring of single-cell volume by FXm. (A,B) Time-lapse experiments using WT without (A) and with (B) medium flow containing FITC–Dextran (3–5 µl/min). Individual traces represent the volumes of single-cell lineages (at each division, only one of the two daughter cells is further monitored). The traces are aligned to the first division (Materials and Methods). This approach allows for measuring differences in single-cell volume that are close to the experimental noise (compare Fig. 3C and Fig. S7B). Volumes were measured every 10 min and 5 min for A and B, respectively. Average growth rates with s.d. are shown. The growth rate in B is consistent with that obtained from the bulk analysis of a synchronized population (Fig. 4C).

morphology and proliferation. For instance, the apparent changes in size distribution that we observed in morphology mutants suggest that the interplay between growth rate and cell cycle phases may be altered in these cells. This may shed light on potentially novel inputs and mechanisms that modulate cell size dynamics. In this context, the different cell geometries of *rga* mutants, as indicated by our comparisons of volume versus cell length at division ratios (Table S4), may represent a promising strategy for uncovering the key parameters used by cells to 'monitor' their size.

Our work demonstrates that previous models that describe the way cell size is regulated in fission yeast need to be revisited using FXm. Together with the wealth of knowledge on size control in this organism, this approach will provide new insights into the processes that underlie the biology of cell growth. Interestingly, the investigation of cellular processes has been enriched by the use of natural yeast isolates. In fission yeast, these strains are known to be less homogenous in morphology and overall size (Jeffares et al., 2015). FXm may therefore make it possible to fully exploit this unique resource and take advantage of advanced population genetics strategies to decipher the regulation of cell size. Although we use fission yeast as a proof-of-concept model, our results also

show that FXm can be applied to any type of cell over a broad range of sizes. Our studies therefore establish the versatility and power of FXm for investigating cell volume homeostasis and its regulation in small cells and model organisms, contributing to our general understanding of the modulation of cellular dimensions and scaling in eukaryotes.

MATERIALS AND METHODS
Fission yeast strains and methods
Standard methods and media were used (Hayles and Nurse, 1992; Moreno et al., 1991). All the strains used in this study are detailed in Table S5. The deletions of *rga2*, *rga4*, *rga6*, *mal3*, *knk1* and *tea1* have already been described (Soto et al., 2010; Villar-Tajadura et al., 2008; Beinhauer et al., 1997; Mata and Nurse, 1997; Revilla-Guarinos et al., 2016; Scheffler et al., 2014). All experiments were carried out in non-supplemented minimal medium (EMM) at 32°C, except otherwise noted. Auxotrophic and diploid strains were grown in EMM supplemented with adenine, histidine, leucine, uridine, lysine and arginine (EMM6S). To inhibit CDK activity in analog-sensitive MCN strains, the 3-MBPP1 inhibitor {4-amino-1-tert-butyl-3-(3-methylbenzyl)pyrazolo[3,4-d]pyrimidine; A602960, Toronto Research Chemicals, North York, Canada} was dissolved in dimethyl sulfoxide (DMSO) at stock concentrations of 10 mM or 0.4 mM and added to liquid

cultures at a final concentration of 1 µM or 0.05 µM. The percentage of binucleated cells (Fig. S3D) was determined from heat fixed samples on microscope slides (70°C for 5 min) stained with a 11:1 solution of Blankophor (1 mg/ml): 4′,6-diamidino-2-phenylindole (DAPI; 1 µg/ml).

Measurement of cell volume using a Coulter Multisizer

Cells were grown in EMM at 25°C and resuspended in dedicated cuvettes containing Isoton (Beckman Coulter, Brea, CA). Cell volume was measured using a Coulter Multisizer 4 (Beckman Coulter) with a 30 µm aperture tube.

Microfabrication of FXm chips

PDMS microfluidic chips for FXm were prepared following standard microfabrication protocols (McDonald and Whitesides, 2002). In brief, master molds were made by spin coating SU-8 2005 resin (MicroChem Corp., Newton, MA) on silicon wafers using a spin coater (Laurell Technologies, North Wales, PA) according to the manufacturer's instructions. Microstructures were then generated using high-resolution chrome masks (JD Phototools, Oldham, UK) and 365 nm UV exposure (UV KUB 3, Kloe, Montpellier, France) followed by PGMEA (propylene glycol monomethyl ether acetate; Sigma-Aldrich, St Louis, MO) development. For each mold, the height of the structures was determined as the average of three measurements perpendicular to the long axis of the design (Fig. 1D) using a Veeco Wyko NT9100 optical profilometer (Veeco Instruments, Plainview, NY). Molds showing significant variability between the three height measurements were discarded. Nevertheless, local variations in chip dimensions may occur during the microfabrication process. When using a single averaged chamber height, biases may therefore be introduced in the evaluation of cell size depending on the position of the cell in the chip. Thus, when even higher accuracy is needed, further reduction of the experimental error can be achieved by using regional chamber heights. For this, the chip can be divided into sub-areas, identifying each area by introducing markers in the mask used for microfabrication and measuring the height of each area using a profilometer. Volume determination can then be made with more specific parameters depending on the position of the cell within the chamber.

To produce chips for FXm, a 10:1 mixture of PDMS (Sylgard 184, Dow Corning, Midland, MI) was cast on the SU-8 master mold and allowed to cure at 70°C for 2 h. Inlets were then made using 2.5 mm or 4 mm biopsy punches, and chips were bonded to microscopy-grade coverslips by plasma activation (Harrick Plasma, Ithaca, NY). As the pillars are used not only to support the chip ceiling but also for the normalization and volume calculation (Cadart et al., 2017), particular attention must be paid to the integrity of these structures and their proper bonding to the coverslip. In addition, for accurate measurements, we recommend using freshly fabricated chips.

Preparation of fission yeast cells for FXm

To perform FXm experiments, exponentially growing fission yeast cells were sampled at an optical density between 0.25 and 0.45 at 595 nm (OD_{595}). To limit the formation of cell aggregates, a mild sonication cycle of 5 s at 10% amplitude (Branson 450 Digital Sonifier, Emerson Electric Co., St Louis, MO) was applied. This treatment had no effect on the results we obtained by FXm (data not shown). In order to maximize the number of cells that can be measured on a single FXm image in our chip design, cells were concentrated to ~5.5×10^7 cells/ml in their own conditioned minimal medium (note that to prevent bias in our volume measurements, we did not use rich medium, which is autofluorescent). FITC–Dextran was then added to the sample (FD10S, Sigma-Aldrich) at a final concentration of 1 mg/ml, and cells were loaded into the chip shortly before image acquisition. For evaluating the volume of quiescent cells, cells were grown in EMM at 32°C and sampled 24 h after they reached OD_{595}=0.4.

Microscopy

All microscopy experiments were carried out using an inverted Zeiss Axio Observer (Carl Zeiss Microscopy GmbH, Jena, Germany) equipped with a Lumencor Spectra X illumination system and an Orca Flash 4.0V2 sCMOS camera (Hamamatsu Photonics, Hamamatsu, Japan). Acquisition was

performed using the VisiView software (Visitron Systems GmbH, Puchheim, Germany). A Plan-Apochromat 63×/1.4 NA immersion lens and a Plan-Apochromat 20×/0.8 NA Ph2 lens (Carl Zeiss Microscopy GmbH) were used for cell length measurements and FXm, respectively. FXm requires the capture of all the fluorescence from the area of the chamber under observation (Cadart et al., 2017). This is most easily achieved using low-magnification lenses with low numerical apertures. Higher-magnification objectives with low NA may be compatible with FXm and the chamber height used in our experiments. However, as a reference, we tested FXm with a 63×/1.4 NA lens (Carl Zeiss Microscopy GmbH) and found that it led to a slight overestimation of cell volume (data not shown), as is expected when not all fluorescence light from the chamber is acquired. Thus, comparing the data from a 20× low NA with those obtained using a given high-magnification lens is a pre-requisite for performing robust FXm analysis with such an objective. For routine volume measurements, the acquisition parameters were 100 ms exposure at 20% illumination power, and 30–40 images were taken across the entire chamber to limit potential bias due to local changes in chamber height. For the time-lapse experiments in Fig. 8, 100 ms exposure at 10% illumination power was used.

Image analysis

Cell length and width at division were determined from Blankophor images (1 mg/ml Blankophor solution, A108741, Ambeed Inc., Arlington Heights, IL) using FIJI (National Institutes of Health, Bethesda, MD) and the Pointpicker plug-in. For the Blankophor images in Figs 2, 4–7, brightness and contrast were adjusted for display purposes. For routine volume measurements, images were first normalized using a custom MATLAB software (Cadart et al., 2017). This code can be obtained from M.P. upon request. Cell selection and volume calculation were subsequently performed using the normalization mask with a new, specifically developed Python interface (see Results, script available at https://github.com/SyntheCell/select-pombe-fxm/). For all figures except Fig. 2D, Fig. 4C and Fig. 8, cell selection was done using the manual mode. For Fig. 2D and Fig. 4C, automated cell identification was used. Our Python code is not adapted to tracking the volume of individual cells in long time-lapse experiments (Fig. 8), as slight cell movements make it difficult to reliably follow single cells over time when using the normalization mask pre-selection. For these assays, we therefore used the original MATLAB software (Cadart et al., 2017). Note that except for the time-lapses in Fig. 8, we systematically excluded cells that were undergoing cytokinesis but that had not fully separated into two individual daughter cells; this population is similarly excluded in studies using cell length at division.

FXm time-lapse and analysis using fission yeast

As fission yeast cells are non-adherent, FXm time-lapses required coverslips to be coated in order to prevent cells from moving inside the chambers, which would hamper data acquisition and analysis. To this end, 10 µl of 1 mg/ml filtered lectin was spread in a rectangle of ~10×5 mm at the center of the coverslips and allowed to dry at 37°C. The coverslips were then washed once with filtered ultra-pure water and dried at 37°C. For experiments without medium flow (Fig. 8A), inlets of 4 mm in diameter were made in the PDMS chips using the appropriate biopsy punch. Five microliters of cells prepared as described above were loaded in one inlet, and both inlets were then filled with 45 µl EMM containing the FITC–Dextran dye. Cells were then allowed to flow into the chambers prior to imaging. For time-lapse experiments using medium flow (Fig. 8B), two successive layers of lectin were applied as above and inlets of 0.75 mm in diameter were fabricated. Cells were then loaded by depositing a drop of cells prepared as above over one of the inlets, and a mild vacuum was applied at the other inlet using the tip of a 10 ml pipet connected to a vacuum pump. The loaded chip was then connected to a flow control system (pressure generator and flow controller, Elvesys, Paris, France), and a flow of medium (~3-5 µl/min) containing the FITC–Dextran dye was used throughout the experiment. For the time-lapse experiments, the two daughter cells after a division were manually delineated during the analysis and only one of them was followed for further investigation (Fig. 8). To validate this manual segmentation, we measured the same ten pairs of sister cells at birth five consecutive times. This led to an average coefficient of variation for all 20

cells of 0.019±0.011 (s.d.), corresponding to a precision of 1.1%. Similarly, the total volume of each pair of sister cells was measured five consecutive times, and we compared the average value of these five measurements with the sum of the average volumes of each sister cells determined as above. The average of the relative difference between total volume and sum of sister cell volumes for all ten pairs was 1.3±1.0% (s.d.). The growth rate of each cell was determined by calculating the slopes of the traces during each cycle. This was obtained by linear regression considering the volume at birth (when an invagination is detected) as the first time point and excluding the mitotic plateau: entry into mitosis was assigned to the last point prior to a strong reduction of growth (when two consecutive points on the graph decrease the slope).

Statistical analyses

All statistical analyses were performed in Python using the SciPy module (Fig. 4D, Fig. 6A; Table S3).

Peer review history

The peer review history is available online at https://journals.biologists.com/jcs/article-lookup/doi/10.1242/jcs.259392.

References

Amodeo, A. A. and Skotheim, J. M. (2016). Cell-size control. *Cold Spring Harb. Perspect. Biol.* **8**, a019083. doi:10.1101/cshperspect.a019083

Baybay, E. K., Esposito, E. and Hauf, S. (2020). Pomegranate: 2D segmentation and 3D reconstruction for fission yeast and other radially symmetric cells. *Sci. Rep.* **10**, 16580. doi:10.1038/s41598-020-73597-w

Beinhauer, J. D., Hagan, I. M., Hegemann, J. H. and Fleig, U. (1997). Mal3, the fission yeast homologue of the human APC-interacting protein EB-1 is required for microtubule integrity and the maintenance of cell form. *J. Cell Biol.* **139**, 717-728. doi:10.1083/jcb.139.3.717

Bishop, A. C., Ubersax, J. A., Petsch, D. T., Matheos, D. P., Gray, N. S., Blethrow, J., Shimizu, E., Tsien, J. Z., Schultz, P. G., Rose, M. D. et al. (2000). A chemical switch for inhibitor-sensitive alleles of any protein kinase. *Nature* **407**, 395-401. doi:10.1038/35030148

Bottier, C., Gabella, C., Vianay, B., Buscemi, L., Sbalzarini, I. F., Meister, J.-J. and Verkhovsky, A. B. (2011). Dynamic measurement of the height and volume of migrating cells by a novel fluorescence microscopy technique. *Lab. Chip* **11**, 3855-3863. doi:10.1039/c1lc20807a

Braïni, C., Mottolese, A., Ferrante, I., Monnier, S. and Villard, C. (2018). High-resolution volume imaging of neurons by the use of fluorescence eXclusion method and dedicated microfluidic devices. *J. Vis. Exp.* **133**, e56923. doi:10.3791/56923

Bryan, A. K., Goranov, A., Amon, A. and Manalis, S. R. (2010). Measurement of mass, density, and volume during the cell cycle of yeast. *Proc. Natl. Acad. Sci. USA* **107**, 999-1004. doi:10.1073/pnas.0901851107

Bryan, A. K., Engler, A., Gulati, A. and Manalis, S. R. (2012). Continuous and long-term volume measurements with a commercial Coulter counter. *PLoS One* **7**, e29866. doi:10.1371/journal.pone.0029866

Bryan, A. K., Hecht, V. C., Shen, W., Payer, K., Grover, W. H. and Manalis, S. R. (2014). Measuring single cell mass, volume, and density with dual suspended microchannel resonators. *Lab. Chip* **14**, 569-576. doi:10.1039/C3LC51022K

Cadart, C., Zlotek-Zlotkiewicz, E., Venkova, L., Thouvenin, O., Racine, V., Le Berre, M., Monnier, S. and Piel, M. (2017). Fluorescence eXclusion measurement of volume in live cells. *Methods Cell Biol.* **139**, 103-120. doi:10.1016/bs.mcb.2016.11.009

Cadart, C., Monnier, S., Grilli, J., Sáez, P. J., Srivastava, N., Attia, R., Terriac, E., Baum, B., Cosentino-Lagomarsino, M. and Piel, M. (2018). Size control in mammalian cells involves modulation of both growth rate and cell cycle duration. *Nat. Commun.* **9**, 3275. doi:10.1038/s41467-018-05393-0

Cadart, C., Venkova, L., Recho, P., Lagomarsino, M. C. and Piel, M. (2019). The physics of cell-size regulation across timescales. *Nat. Phys.* **15**, 993-1004. doi:10.1038/s41567-019-0629-y

Cavicchi, R. E., Carrier, M. J., Cohen, J. B., Boger, S., Montgomery, C. B., Hu, Z. and Ripple, D. C. (2015). Particle shape effects on subvisible particle sizing measurements. *J. Pharm. Sci.* **104**, 971-987. doi:10.1002/jps.24263

Chen, T., Gómez-Escoda, B., Munoz-Garcia, J., Babic, J., Griscom, L., Wu, P.-Y. J. and Coudreuse, D. (2016). A drug-compatible and temperature-controlled microfluidic device for live-cell imaging. *Open Biol.* **6**, 160156. doi:10.1098/rsob.160156

Cook, M. and Tyers, M. (2007). Size control goes global. *Curr. Opin. Biotechnol.* **18**, 341-350. doi:10.1016/j.copbio.2007.07.006

Coudreuse, D. and Nurse, P. (2010). Driving the cell cycle with a minimal CDK control network. *Nature* **468**, 1074-1079. doi:10.1038/nature09543

Das, M., Wiley, D. J., Medina, S., Vincent, H. A., Larrea, M., Oriolo, A. and Verde, F. (2007). Regulation of cell diameter, For3p localization, and cell symmetry by fission yeast Rho-GAP Rga4p. *Mol. Biol. Cell* **18**, 2090-2101. doi:10.1091/mbc.e06-09-0883

Facchetti, G., Knapp, B., Flor-Parra, I., Chang, F. and Howard, M. (2019). Reprogramming Cdr2-dependent geometry-based cell size control in fission yeast. *Curr. Biol.* **29**, 350-358.e4. doi:10.1016/j.cub.2018.12.017

Fantes, P. A. (1977). Control of cell size and cycle time in Schizosaccharomyces pombe. *J. Cell Sci.* **24**, 51-67. doi:10.1242/jcs.24.1.51

Fantes, P. (1979). Epistatic gene interactions in the control of division in fission yeast. *Nature* **279**, 428-430. doi:10.1038/279428a0

Fantes, P. and Nurse, P. (1977). Control of cell size at division in fission yeast by a growth-modulated size control over nuclear division. *Exp. Cell Res.* **107**, 377-386. doi:10.1016/0014-4827(77)90359-7

Fantes, P. A. and Nurse, P. (1978). Control of the timing of cell division in fission yeast. Cell size mutants reveal a second control pathway. *Exp. Cell Res.* **115**, 317-329. doi:10.1016/0014-4827(78)90286-0

Grant, N. A., Abdel Magid, A., Franklin, J., Dufour, Y. and Lenski, R. E. (2021). Changes in cell size and shape during 50,000 generations of experimental evolution with Escherichia coli. *J. Bacteriol.* **203**, e00469-e00420. doi:10.1128/JB.00469-20

Hayles, J. and Nurse, P. (1992). Genetics of the fission yeast Schizosaccharomyces pombe. *Annu. Rev. Genet.* **26**, 373-402. doi:10.1146/annurev.ge.26.120192.002105

Jeffares, D. C., Rallis, C., Rieux, A., Speed, D., Převorovský, M., Mourier, T., Marsellach, F. X., Iqbal, Z., Lau, W., Cheng, T. M. K. et al. (2015). The genomic and phenotypic diversity of Schizosaccharomyces pombe. *Nat. Genet.* **47**, 235-241. doi:10.1038/ng.3215

Lancaster, O. M., Le Berre, M., Dimitracopoulos, A., Bonazzi, D., Zlotek-Zlotkiewicz, E., Picone, R., Duke, T., Piel, M. and Baum, B. (2013). Mitotic rounding alters cell geometry to ensure efficient bipolar spindle formation. *Dev. Cell* **25**, 270-283. doi:10.1016/j.devcel.2013.03.014

Lenski, R. E. and Travisano, M. (1994). Dynamics of adaptation and diversification: a 10,000-generation experiment with bacterial populations. *Proc. Natl. Acad. Sci. USA* **91**, 6808-6814. doi:10.1073/pnas.91.15.6808

Li, Q., Rycaj, K., Chen, X. and Tang, D. G. (2015). Cancer stem cells and cell size: a causal link? *Semin. Cancer Biol.* **35**, 191-199. doi:10.1016/j.semcancer.2015.07.002

Lloyd, A. C. (2013). The regulation of cell size. *Cell* **154**, 1194-1205. doi:10.1016/j.cell.2013.08.053

Marshall, W. F., Young, K. D., Swaffer, M., Wood, E., Nurse, P., Kimura, A., Frankel, J., Wallingford, J., Walbot, V., Qu, X. et al. (2012). What determines cell size? *BMC Biol.* **10**, 101. doi:10.1186/1741-7007-10-101

Martin, S. G. and Berthelot-Grosjean, M. (2009). Polar gradients of the DYRK-family kinase Pom1 couple cell length with the cell cycle. *Nature* **459**, 852-856. doi:10.1038/nature08054

Mata, J. and Nurse, P. (1997). tea1 and the microtubular cytoskeleton are important for generating global spatial order within the fission yeast cell. *Cell* **89**, 939-949. doi:10.1016/S0092-8674(00)80279-2

McDonald, J. C. and Whitesides, G. M. (2002). Poly(dimethylsiloxane) as a material for fabricating microfluidic devices. *Acc. Chem. Res.* **35**, 491-499. doi:10.1021/ar010110q

Millar, J. B., Buck, V. and Wilkinson, M. G. (1995). Pyp1 and Pyp2 PTPases dephosphorylate an osmosensing MAP kinase controlling cell size at division in fission yeast. *Genes Dev.* **9**, 2117-2130. doi:10.1101/gad.9.17.2117

Mitchison, J. M. (1957). The growth of single cells. I. Schizosaccharomyces pombe. *Exp. Cell Res.* **13**, 244-262. doi:10.1016/0014-4827(57)90005-8

Mitchison, J. M. and Nurse, P. (1985). Growth in cell length in the fission yeast Schizosaccharomyces pombe. *J. Cell Sci.* **75**, 357-376. doi:10.1242/jcs.75.1.357

Model, M. A. (2018). Methods for cell volume measurement. *Cytom. A* **93**, 281-296. doi:10.1002/cyto.a.23152

Model, M. (2020). Comparison of cell volume measurements by fluorescence and absorption exclusion microscopy. *J. Microsc.* **280**, 12-18. doi:10.1111/jmi.12929

Mongold, J. A. and Lenski, R. E. (1996). Experimental rejection of a nonadaptive explanation for increased cell size in Escherichia coli. *J. Bacteriol.* **178**, 5333-5334. doi:10.1128/jb.178.17.5333-5334.1996

Moreno, S., Klar, A. and Nurse, P. (1991). Molecular genetic analysis of fission yeast Schizosaccharomyces pombe. *Meth. Enzymol.* **194**, 795-823. doi:10.1016/0076-6879(91)94059-L

Moseley, J. B., Mayeux, A., Paoletti, A. and Nurse, P. (2009). A spatial gradient coordinates cell size and mitotic entry in fission yeast. *Nature* **459**, 857-860. doi:10.1038/nature08074

Mueller, R. L. (2015). Genome biology and the evolution of cell-size diversity. *Cold Spring Harb. Perspect. Biol.* **7**, a019125. doi:10.1101/cshperspect.a019125

Navarro, F. J. and Nurse, P. (2012). A systematic screen reveals new elements acting at the G2/M cell cycle control. *Genome Biol.* **13**, R36. doi:10.1186/gb-2012-13-5-r36

Nurse, P. (1975). Genetic control of cell size at cell division in yeast. *Nature* **256**, 547-551. doi:10.1038/256547a0

Pan, K. Z., Saunders, T. E., Flor-Parra, I., Howard, M. and Chang, F. (2014). Cortical regulation of cell size by a sizer cdr2p. *Elife* **3**, e02040. doi:10.7554/eLife.02040.029

Petersen, J. (2009). TOR signalling regulates mitotic commitment through stress-activated MAPK and Polo kinase in response to nutrient stress. *Biochem. Soc. Trans.* **37**, 273-277. doi:10.1042/BST0370273

Pedersen, S. F., Hoffmann, E. K. and Mills, J. W. (2001). The cytoskeleton and cell volume regulation. *Comp. Biochem. Physiol. A Mol. Integr. Physiol.* **130**, 385-399. doi:10.1016/S1095-6433(01)00429-9

Pietras, A. (2011). Cancer stem cells in tumor heterogeneity. *Adv. Cancer Res.* **112**, 255-281. doi:10.1016/B978-0-12-387688-1.00009-0

Revilla-Guarinos, M. T., Martín-García, R., Villar-Tajadura, M. A., Estravís, M., Coll, P. M. and Pérez, P. (2016). Rga6 is a fission yeast Rho GAP involved in Cdc42 regulation of polarized growth. *Mol. Biol. Cell* **27**, 1409-1551. doi:10.1091/mbc.E15-12-0818

Scheffler, K., Recouvreux, P., Paoletti, A. and Tran, P. T. (2014). Oscillatory AAA[+] ATPase Knk1 constitutes a novel morphogenetic pathway in fission yeast. *Proc. Natl. Acad. Sci. USA* **111**, 17899-17904. doi:10.1073/pnas.1407226111

Soifer, I., Robert, L. and Amir, A. (2016). Single-cell analysis of growth in budding yeast and bacteria reveals a common size regulation strategy. *Curr. Biol.* **26**, 356-361. doi:10.1016/j.cub.2015.11.067

Soto, T., Villar-Tajadura, M. A., Madrid, M., Vicente, J., Gacto, M., Pérez, P. and Cansado, J. (2010). Rga4 modulates the activity of the fission yeast cell integrity MAPK pathway by acting as a Rho2 GTPase-activating protein. *J. Biol. Chem.* **285**, 11516-11525. doi:10.1074/jbc.M109.071027

Sun, S. and Gresham, D. (2021). Cellular quiescence in budding yeast. *Yeast* **38**, 12-29. doi:10.1002/yea.3545

Sveiczer, A., Novak, B. and Mitchison, J. M. (1996). The size control of fission yeast revisited. *J. Cell Sci.* **109**, 2947-2957. doi:10.1242/jcs.109.12.2947

Taheri-Araghi, S., Bradde, S., Sauls, J. T., Hill, N. S., Levin, P. A., Paulsson, J., Vergassola, M. and Jun, S. (2015). Cell-size control and homeostasis in bacteria. *Curr. Biol.* **25**, 385-391. doi:10.1016/j.cub.2014.12.009

Villar-Tajadura, M. A., Coll, P. M., Madrid, M., Cansado, J., Santos, B. and Pérez, P. (2008). Rga2 is a Rho2 GAP that regulates morphogenesis and cell integrity in S. pombe. *Mol. Microbiol.* **70**, 867-881. doi:10.1111/j.1365-2958.2008.06447.x

Vjestica, A., Zhang, D., Liu, J. and Oliferenko, S. (2013). Hsp70-Hsp40 chaperone complex functions in controlling polarized growth by repressing Hsf1-driven heat stress-associated transcription. *PLoS Genet.* **9**, e1003886. doi:10.1371/journal.pgen.1003886

Yang, J., Dungrawala, H., Hua, H., Manukyan, A., Abraham, L., Lane, W., Mead, H., Wright, J. and Schneider, B. L. (2011). Cell size and growth rate are major determinants of replicative lifespan. *Cell Cycle* **10**, 144-155. doi:10.4161/cc.10.1.14455

Zegman, Y., Bonazzi, D. and Minc, N. (2015). Measurement and manipulation of cell size parameters in fission yeast. *Methods Cell Biol.* **125**, 423-436. doi:10.1016/bs.mcb.2014.10.011

Zhurinsky, J., Leonhard, K., Watt, S., Marguerat, S., Bähler, J. and Nurse, P. (2010). A coordinated global control over cellular transcription. *Curr. Biol.* **20**, 2010-2015. doi:10.1016/j.cub.2010.10.002

Zlotek-Zlotkiewicz, E., Monnier, S., Cappello, G., Le Berre, M. and Piel, M. (2015). Optical volume and mass measurements show that mammalian cells swell during mitosis. *J. Cell Biol.* **211**, 765-774. doi:10.1083/jcb.201505056
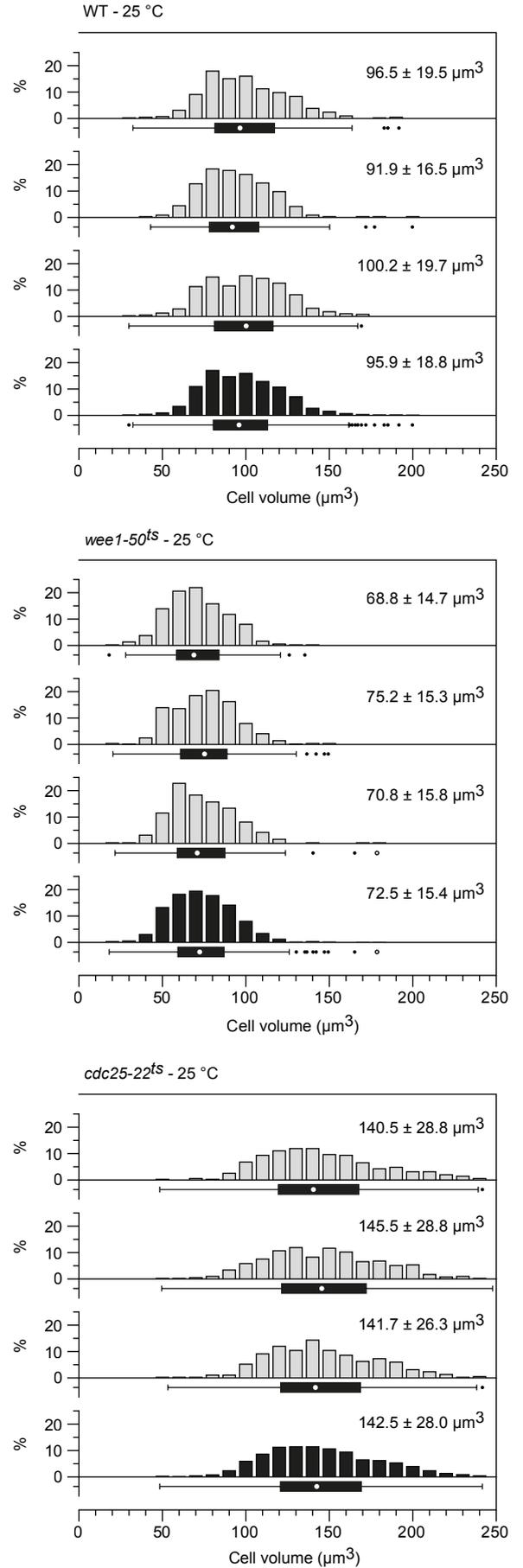
Figure S1

A
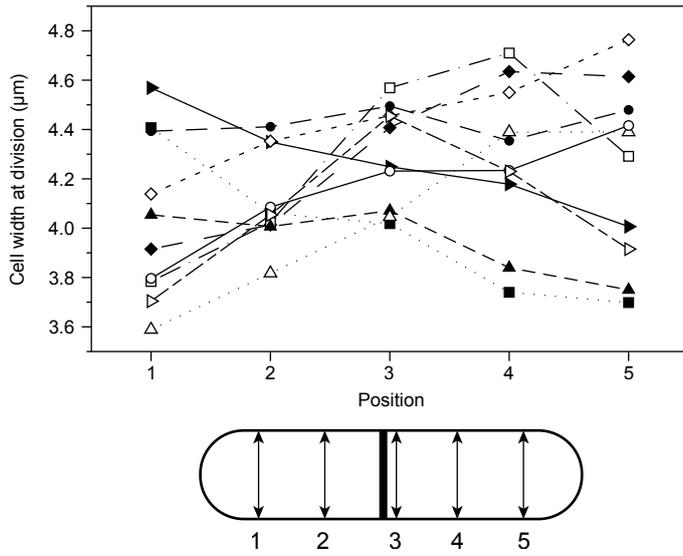
B
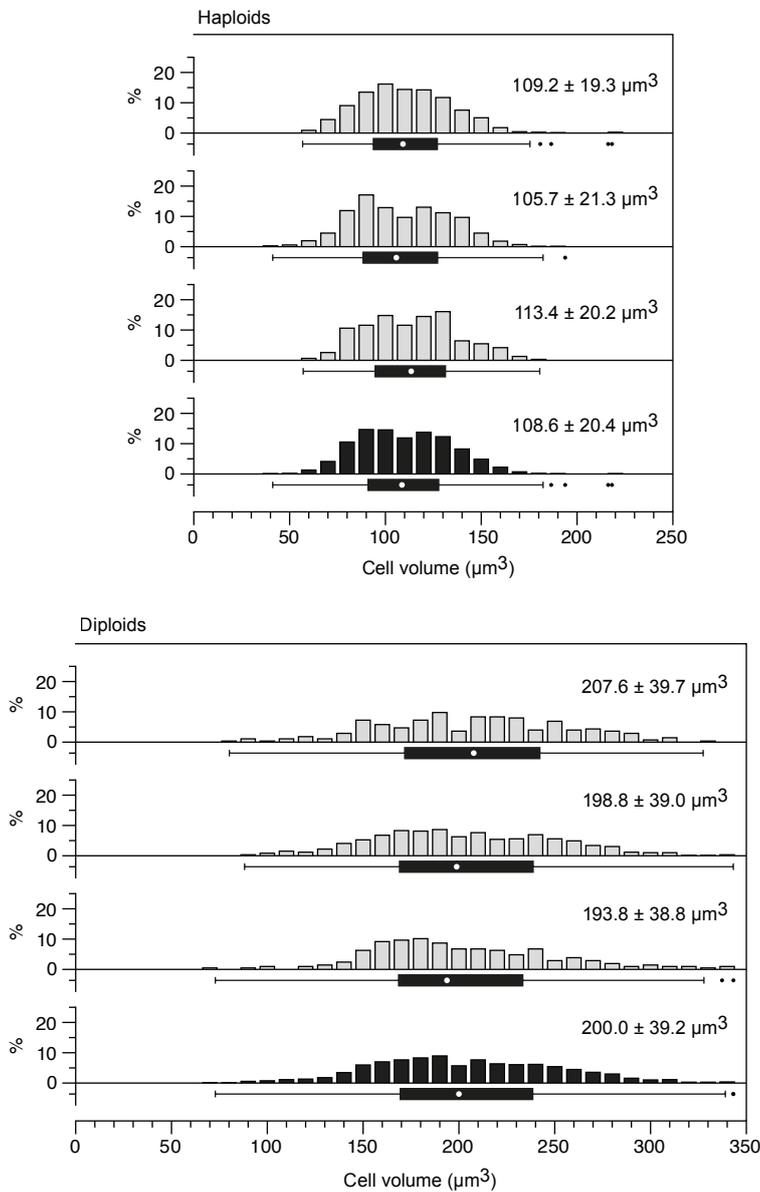
C

Fig. S1. Supporting data for Fig. 1B and Fig. 2. A. Cell width was measured at 5 different positions along 25 individual cells (bottom schematic). For display purposes, a subset of 10 individual cells is shown. When using the geometric model for size determination (Fig. 1A), this results in a broad range of cell volume for a given cell, depending on the diameter used (see coefficients of variation in Fig. 1B). **B.** Volume measurement by FXm of the indicated strains. All the replicates (grey) used for the data presented in Fig. 2B are shown. For each strain, the bottom histogram (black) and box plot are the same as in Fig. 2B. **C.** Volume measurement by FXm of the indicated strains. All the replicates (grey) used for the data presented in Fig. 2C are shown. For each strain, the bottom histogram (black) and box plot are the same as in Fig. 2C. Graphs are as in Fig. 2. For each replicate in *B*: 1) Haploids: $n{\geq}311$, diploids: $n{\geq}207$ and 2) values outside of the plot range were excluded (haploids: $n{*}{=}0$; diploids: $n{*}{\leq}1$). For each replicate in *C*: 1) wild type (WT): $n{\geq}337$, *cdc25-22*^{ts}: $n{\geq}353$, *wee1-50*^{ts}: $n{\geq}374$ and 2) values outside of the plot range were excluded (WT: $n{*}{=}0$; *cdc25-22*^{ts}: $n{*}{\leq}4$, *wee1-50*^{ts}: $n{*}{=}0$).
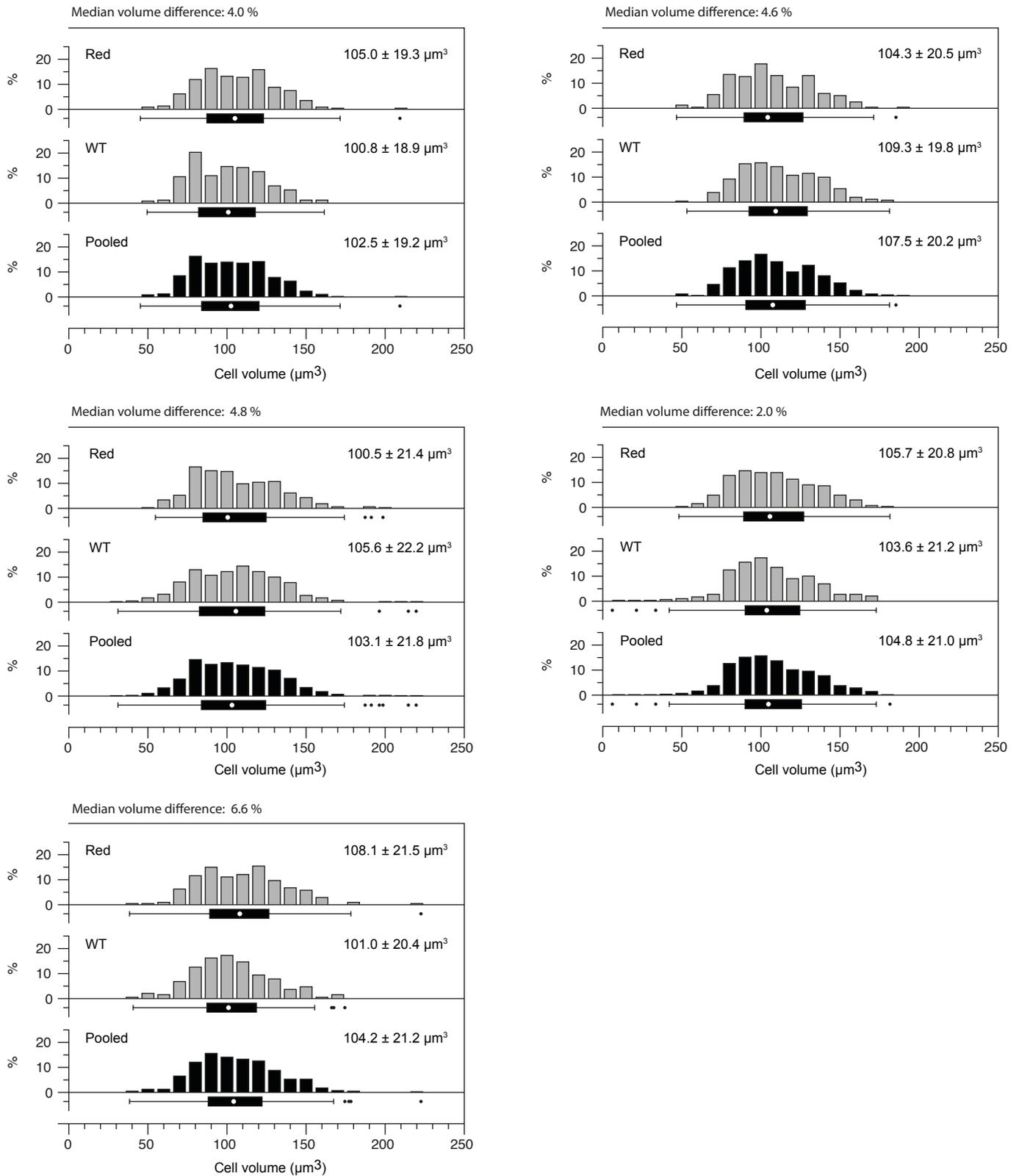
Figure S2

Fig. S2. Measurement of distinct wild-type strains within a single chamber.
Volume measurement by FXm of two separate cultures within individual chips. Wild type
cells (WT) and cells expressing a red fluorescent protein in an otherwise wild type
background (Red, DC432 in Table S5) were mixed in equal proportions and injected in FXm
chambers for volume measurement. Both strains are phenotypically wild type.
Discrimination between the strains was made possible using the red fluorescence. 5
independent experiments are shown, with the volume measurements for each strain as well as
the pooled datasets (black). Graphs are as in Fig. 2. For each assay, $191<n<409$ per strain and
values outside of the plot range were excluded ($n_*\leq1$). The differences in median volume
between the two strains in each chip are indicated. These data show that eliminating
variations in chamber height within and between chips allows for reducing the threshold for
determining volume differences between strains without increasing sample size.
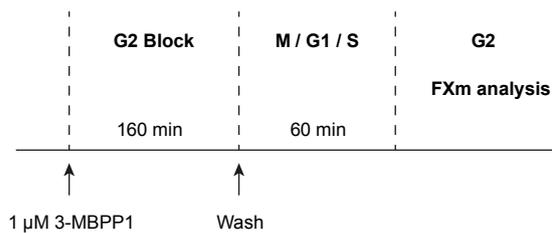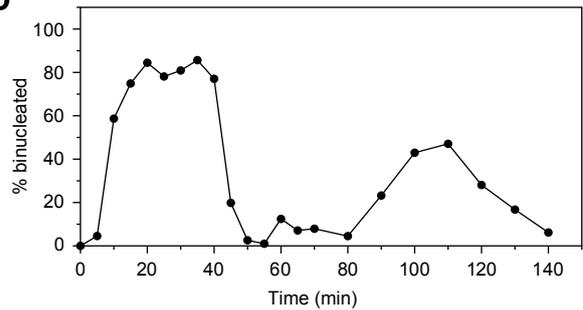
Figure S3
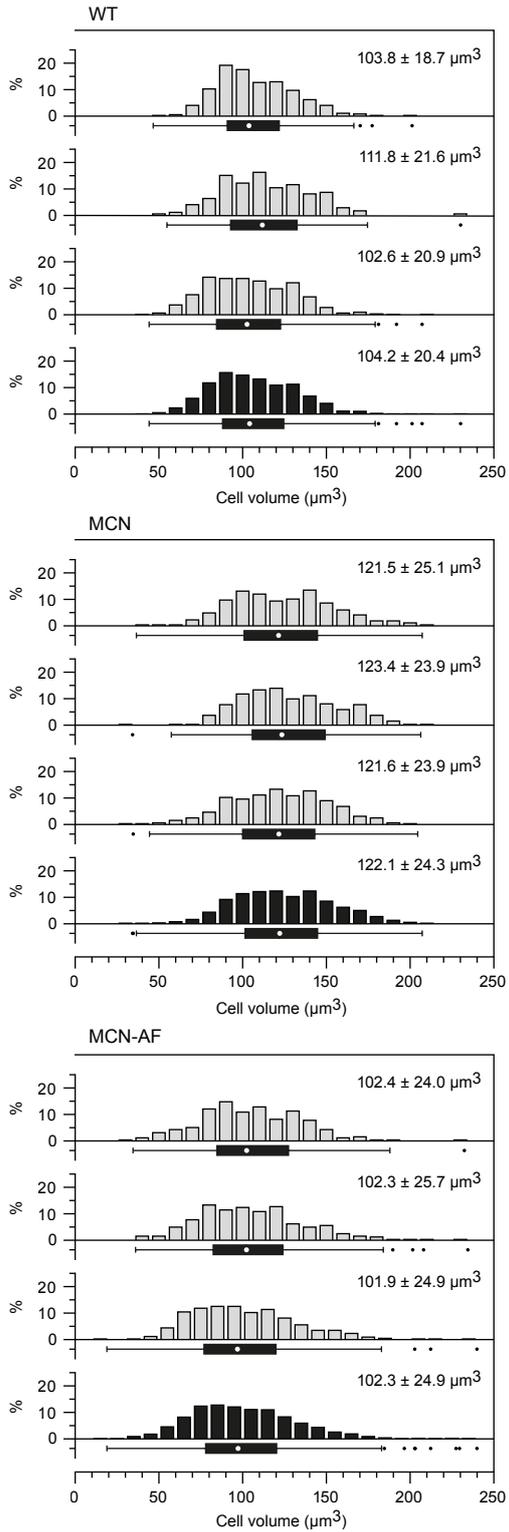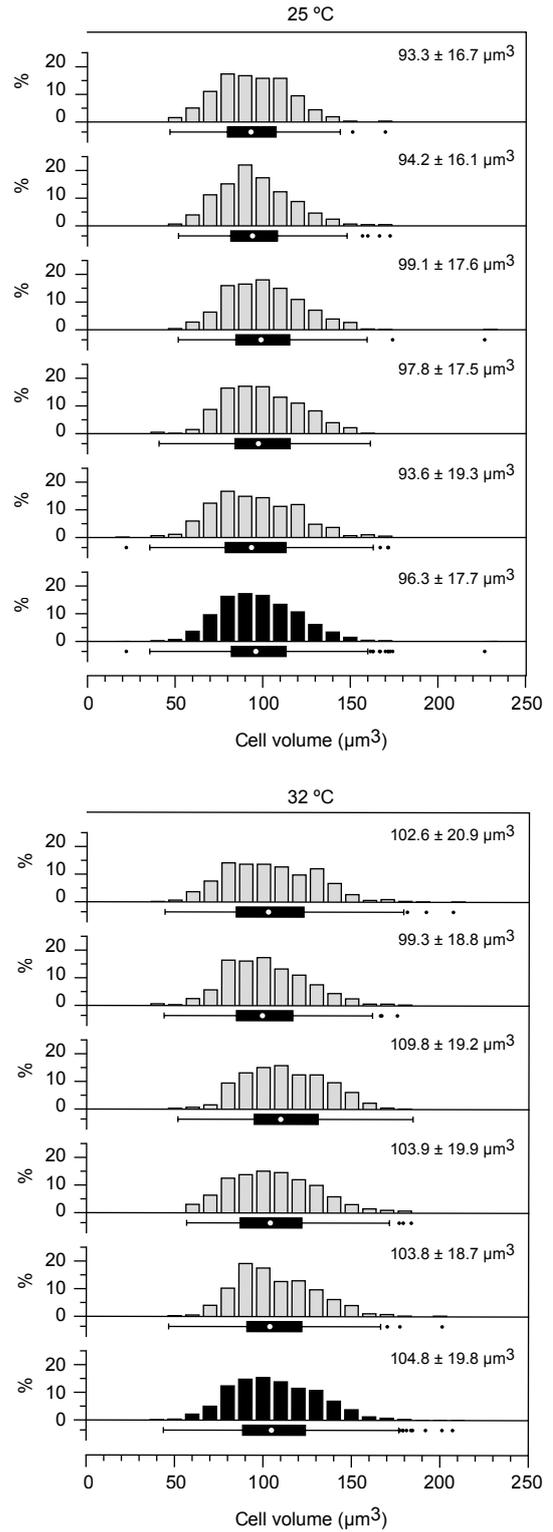
Fig. S3. Supporting data for Fig. 4. A. Volume measurement by FXm of the indicated strains. All replicates (grey) used for the data presented in Fig. 4A are shown. For each strain, the bottom histogram (black) and box plot are the same as in Fig. 4A. For wild type (WT), the 1st and 3rd datasets are as in Fig. 3A (last and 1st datasets respectively). Graphs are as in Fig. 2. For each replicate: 1) WT: $n \geq 172$, MCN: $n \geq 267$, MCN-AF: $n \geq 257$ and 2) values outside of the plot range were excluded (WT: $n* = 0$; MCN: $n* = 0$, MCN-AF: $n* \leq 1$). **B.** Measurements for five independent experiments (grey) and for the total pooled datasets (black) using wild-type cells grown at 25 °C (top panel) or 32 °C (bottom panel). Data at 32 °C are as in Fig. 3A. For the data at 25 °C, $n \geq 316$ for each replicate, $n = 2706$ for the total dataset; no values were outside of the plot range ($n* = 0$ for each replicate). Graphs are as in Fig. 2. The median volume values with median absolute deviations are also shown in Fig. 4B. **C.** Schematic of the experimental protocol for the data in Fig. 4C. **D.** Percentage of binucleated cells after synchronization ($n \geq 178$ at each time point). Samples were analyzed at 5 min intervals for the first 70 min and then at 10 min intervals. This experiment is independent from that in Fig. 4C and was entirely performed in culture flasks. It was used to determine the time window (T=60 to 140 min) after the release from the G2 block during which images would be acquired for Fig. 4C.
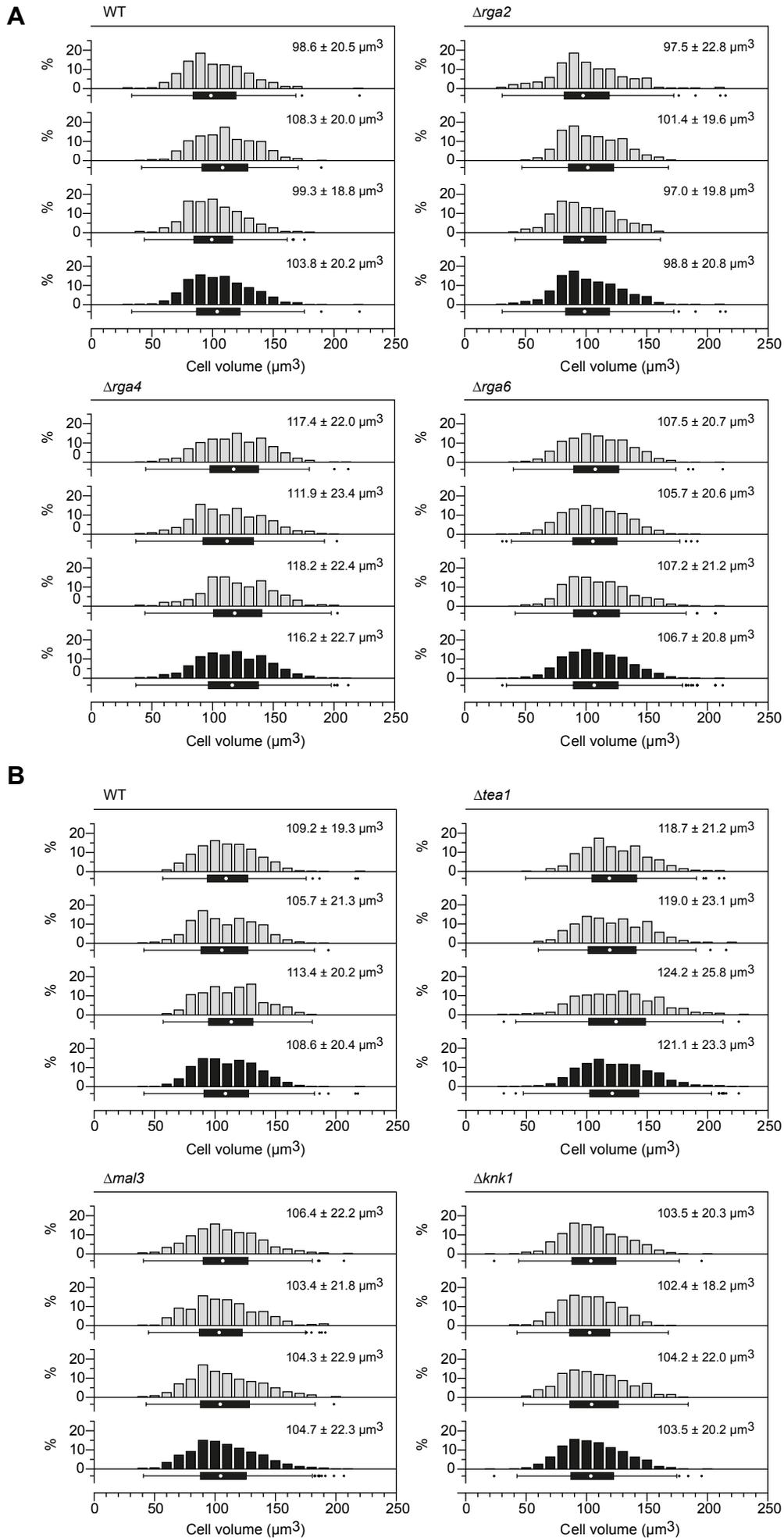
Figure S4

Fig. S4. Supporting data for Fig. 5B, D. A. Volume measurement by FXm of the indicated strains. All replicates (grey) used for the data presented in Fig. 5B are shown. For each strain, the bottom histogram (black) and box plot are the same as in Fig. 5B. For wild type (WT), the 1st dataset is as in Fig. 3A (4th dataset). Graphs are as in Fig. 2. For each replicate: 1) WT: $n \geq 316$, $\Delta rga2$: $n \geq 268$, $\Delta rga4$: $n \geq 348$, $\Delta rga6$: $n \geq 766$ and 2) values outside of the plot range were excluded (WT: $n* \leq 1$; $\Delta rga2$: $n*=0$, $\Delta rga4$: $n*=0$, $\Delta rga6$: $n*=0$). **B.** Volume measurement by FXm of the indicated strains. All the replicates (grey) used for the data presented in Fig. 5D are shown. For each strain, the bottom histogram (black) and box plot are the same as in Fig. 5D. Graphs are as in Fig. 2. For each replicate: 1) wild type (WT): $n \geq 311$, $\Delta tea1$: $n \geq 230$, $\Delta mal3$: $n \geq 242$, $\Delta knk1$: $n \geq 398$ and 2) no values were outside of the plot range ($n*=0$ for each strain).

Figure S5
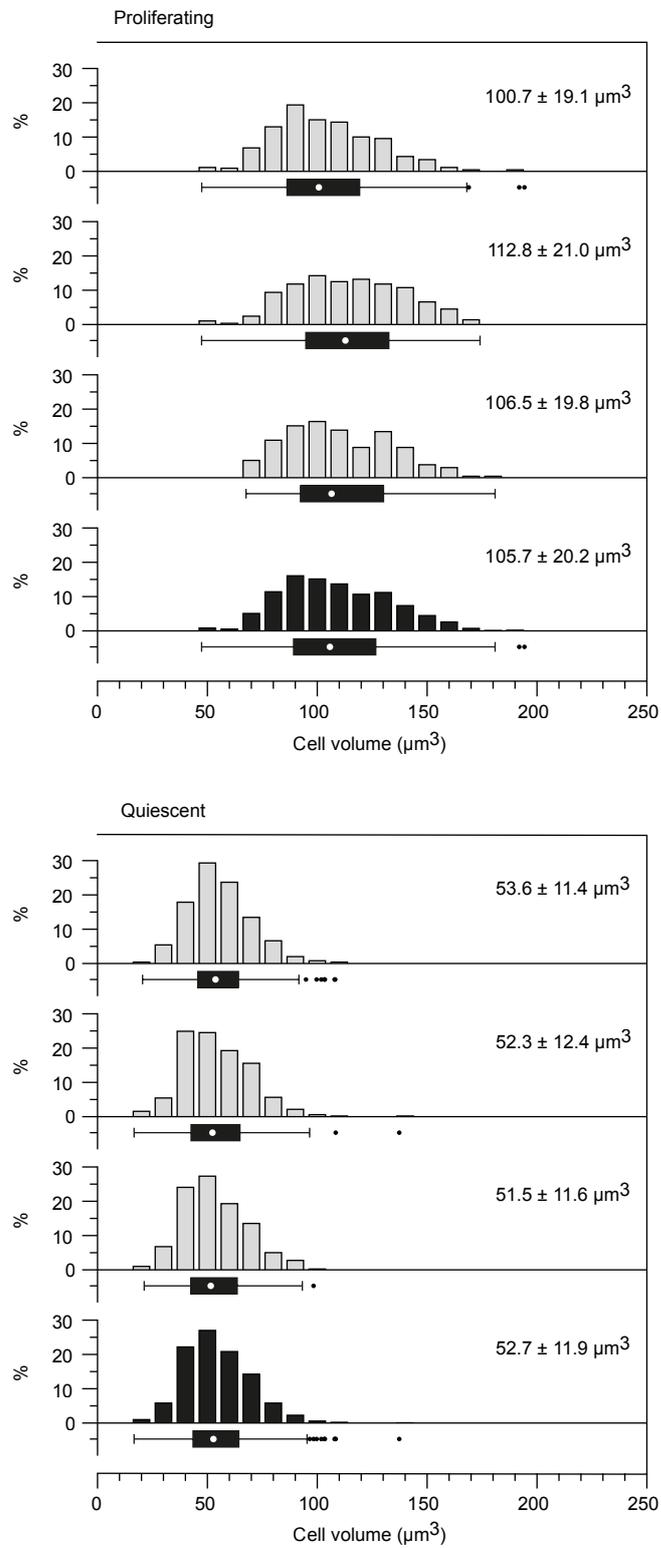
Fig. S5. Supporting data for Fig. 5F. Volume measurement by FXm of proliferating *vs*. quiescent wild type fission yeast cells. All the replicates (grey) used for the data presented in Fig. 5F are shown. For each strain, the bottom histogram (black) and box plot are the same as in Fig. 5F. Graphs are as in Fig. 2. For each replicate: 1) proliferating: $n{\geq}238$, quiescent: $n{\geq}399$ and 2) no values were outside of the plot range ($n_*=0$).

Figure S6

A
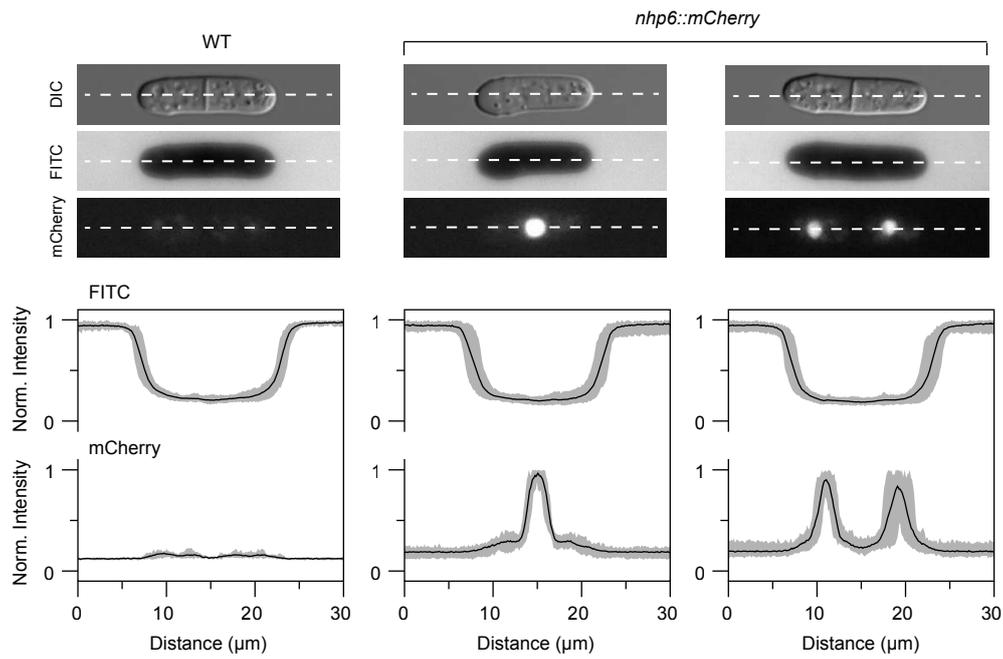
B

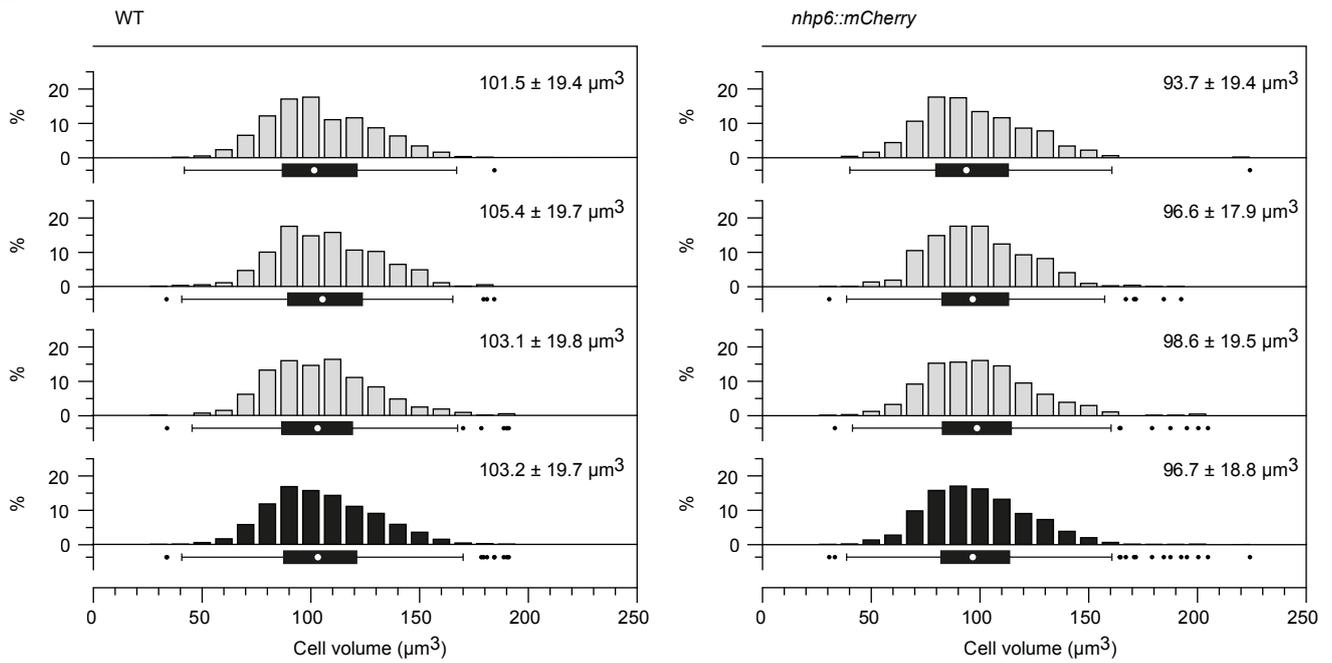**Fig. S6. Supporting data for Fig. 6. A.** Top panel: representative images of wild type (WT) and *nhp6::mCherry* cells in the DIC (top), FITC (middle) and mCherry (bottom) channels. Equivalent numbers of cells of both strains were mixed and imaged in the presence of the FITC-Dextran dye. Dashed lines indicate the path of the fluorescence intensity scans presented in the bottom panel. Bottom panel: quantification of the fluorescence intensity in both channels. 30 μm scan lines were drawn using Fiji (National Institutes of Health), manually centered on the cells, and fluorescence intensities along the scan lines were determined. In the FITC channel as well as in the mCherry channel for *nhp6::mCherry* cells, values were normalized to the maximum intensities measured for each cell. For wild type in the mCherry channel, values were normalized to the maximum intensity measured in the complete dataset of Nhp6::mCherry positive cells. Black lines: averages of all the intensity profiles (n=12 for each cell type). The grey areas are delineated by the maximum and minimum intensities at each position in the complete datasets. **B.** Volume measurement by FXm of the indicated strains. All the replicates (grey) used for the data presented in Fig. 6A are shown. For each strain, the bottom histogram (black) and box plot are the same as in Fig. 6A. Graphs are as in Fig. 2. For each replicate: 1) WT: $n \geq 506$, *nhp6::mCherry*: $n \geq 499$ and 2) values outside of the plot range were excluded (WT: $n_* \leq 1$; *nhp6::mCherry*: $n_* = 0$).

Figure S7

A
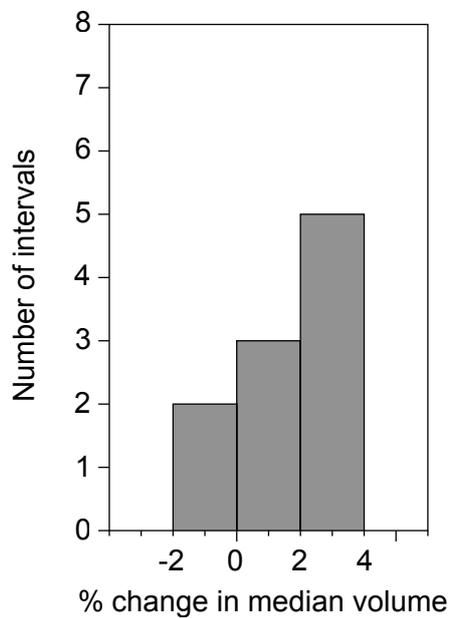
B
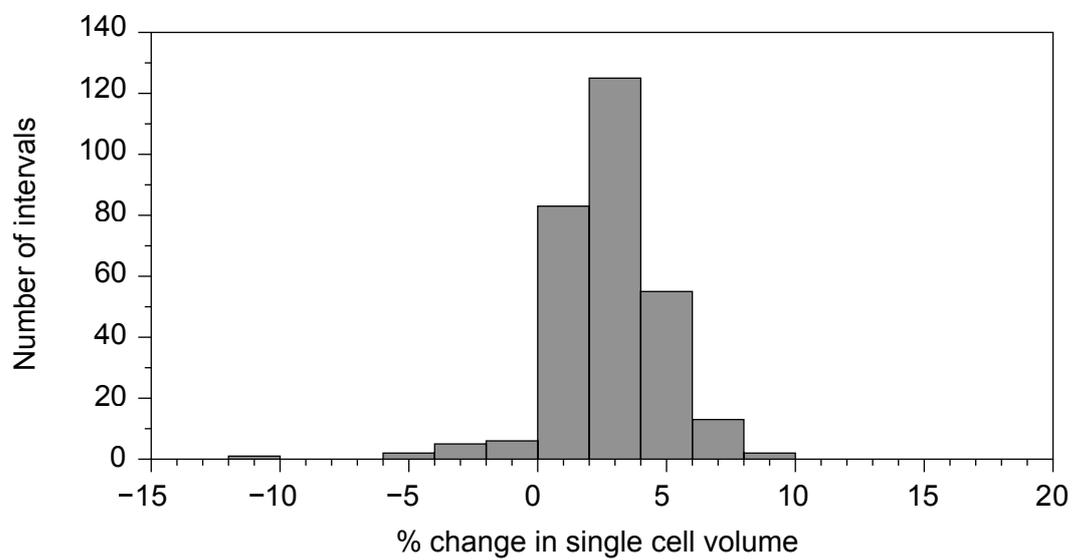
Fig. S7. Supporting data for Fig. 4C and Fig. 8B. A. Histogram of the percentage changes in median volume between successive volume measurements in Fig. 4C. For each point from T=60 to T=110 min (entry into mitosis), the percentage change in median volume was calculated with respect to the previous time point (*n*=10). **B.** Histogram of the percentage changes in single-cell volume between successive volume measurements in Fig. 8B. For each cell, the percentage change in volume was calculated with respect to the previous time point. This was performed during the 1st cycle, from cell birth to the next mitosis (*n*=13, corresponding to 292 intervals).

Table S1. Measurement of cell volume by Coulter Multisizer

	Cell number (x10^3)	Volume (μm^3)
WT at 25 ºC	39	88
	45.7	77.4
	44	79.7
	47	78
	Average	**80.8**
wee1-50^{ts} at 25 ºC	43	69.2
	45.2	67.3
	41.5	69.9
	43.9	70.8
	Average	**69.3**
cdc25-22^{ts} at 25 ºC	32.6	115.5
	30	117.2
	31.2	116.2
	34	114.7
	Average	**115.9**

Table S2. Comparison of median cell volume between pooled triplicates of wild type cells

Samples in triplicate 1	Samples in triplicate 2	% difference
1 2 3	4 5 6	2.57
1 2 4	3 5 6	4.99
1 2 5	3 4 6	3.76
1 2 6	3 4 5	0.92
1 3 4	2 5 6	0.4
1 3 5	2 4 6	1.17
1 3 6	2 4 5	5.76
1 4 5	2 3 6	6.14
1 4 6	2 3 5	1.25
1 5 6	2 3 4	0.49

Data from 6 independent experiments (results from Fig. 3A and an additional dataset with *n*=553)
For comparison, in each pair of triplicates, the largest sample is taken as the 100% reference.

Table S3. Comparison of volume distribution between replicates

Figure	Sample 1	Sample 2	p-value
3A	1	2	0.0948449
	1	3	0.7619098
	1	4	0.5097842
	1	5	0.0047651
	2	3	0.4611871
	2	4	0.5760033
	2	5	0.7318095
	3	4	0.9356956
	3	5	0.0528163
	4	5	0.1073448
3B	1	2	0.1199342
	1	3	0.1610272
	1	4	0.8936139
	1	5	0.7136720
	2	3	0.8454095
	2	4	0.3487484
	2	5	0.5213805
	3	4	0.4580455
	3	5	0.4616116
	5	4	0.8019842
Pooled datasets[*]	3A	3B	0.1262570

p-values are from two-sample Kolmogorov-Smirnov tests.

As variability in chamber height linearly affects cell volume when using FXm, all datasets are normalized to their respective medians.

All p-values except 3A- sample 1 vs 5 are greater than 0.05, indicating no differences between the volume distributions of the replicate samples.

[*] Comparison of the pooled datasets from Fig. 3A and 3B.

Table S4. Comparison of strains based on volume *vs.* length at division

		Comparison	V* ratio	LAD** ratio	Data
WT diploids in EMM6S		WT haploids in EMM6S	1.84	1.44	Fig. 2B
cdc25-22^{ts} at 25 ºC		WT at 25 ºC	1.49	1.36	Fig. 2C
wee1-50^{ts} at 25 ºC		WT at 25 ºC	0.76	0.79	Fig. 2C
MCN		WT	1.17	1.07	Fig. 4A
MCN-AF		WT	0.98	0.91	Fig. 4A
MCN-AF		MCN	0.84	0.85	Fig. 4A
Δ*rga2*		WT	0.95	1.17	Fig. 5A, B
Δ*rga4*		WT	1.12	0.88	Fig. 5A, B
Δ*rga6*		WT	1.03	0.96	Fig. 5A, B
nhp6::mCherry		WT	0.94	0.98	Fig. 6A
MCN + 3-MBPP1	40 min	MCN + 3-MBPP1 / 0 min	1.07	1.05	Fig. 7
	80 min	MCN + 3-MBPP1 / 0 min	1.27	1.39	Fig. 7
	120 min	MCN + 3-MBPP1 / 0 min	1.44	1.55	Fig. 7
	160 min	MCN + 3-MBPP1 / 0 min	1.72	1.58	Fig. 7
WT in EMM6S at 32 ºC		WT in EMM at 32 ºC	1.04	0.93	Fig. 2B, 4A
WT at 25 ºC		WT at 32 ºC	0.92	0.93	Fig. 2C, 4A

* V: volume; ** LAD: cell length at division

Table S5. Fission yeast strains used in this study

Name	Genotype	Origin
PN1	*h- 972*	P. Nurse
DC1114	*h-/h- 972 diploid*	This study
PN143	*h- cdc25-22*	P. Nurse
PN369	*h- wee1-50*	P. Nurse
DC432	*h+ NAT::Padh1::RFP::Tadh1*	This study
DC676	*h- Pcdc13::cdc13Scdc2as::cdc13UTR Δcdc2::KAN Δcig1::HYG Δcig2::KAN Δpuc1::HYG*	This study
DC753	*h- Pcdc13::cdc13Scdc2T14AY15Fas::cdc13UTR Δcdc2::KAN Δcig1::HYG Δcig2::KAN Δpuc1::HYG*	This study
DC1099	*h+ Δrga2::KAN*	This study
DC1102	*h- Δrga4::KAN*	This study
DC1100	*h+ Δrga6::KAN*	This study
DC1131	*h- nhp6::mCherry::ura4+*	This study
PN1687	*h- Δtea1::ura4+ ura4-D18*	P. Nurse
PN3718	*h- Δmal3::his3 ade6-M210 leu1-32 ura4-D18 his3-D1*	P. Nurse
TP474	*h- Δknk1::KAN ade6-M210 leu1-32 ura4-D18*	P. Tran

Chapter 5:
General Discussion

The work presented in this thesis combines the framework of synthetic biology with the tool of experimental evolution to uncover previously unknown pathways involved in cell cycle regulation. By utilising the unique properties of a synthetic Minimal Cell cycle Network in fission yeast (MCN, Coudreuse and Nurse 2010), we were able to explore the evolutionary strategies that cells can employ to overcome the loss of normally essential regulatory mechanisms for proliferation. Remarkably, our results demonstrate that modulation of poorly understood processes can compensate, at least partially, for the loss of the highly conserved Wee1/Cdc25 feedback loop. Such mechanisms would have been difficult to identify in wild-type cells due to the overarching dominance of this regulatory feedback loop. This thesis has focused primarily on dissecting one of the evolved mechanisms responsible for recovering the proliferation potential of cells lacking the mitotic entry switch. We demonstrated that loss of the small and highly disordered protein, Spo12, promotes the growth of MCN cells in which the Wee1/Cdc25 target sites are mutated. We further showed that Spo12 is involved in a positive feedback loop on Cdk activity at mitosis onset.

The first step of this study consisted of a 70-day experimental evolution assay that was performed using three distinct fission yeast strains: one with a normal cell cycle control network (wild-type cells, WT), and two minimal cell cycle control networks (MCN and MCN-AF; in the MCN-AF background, the T14 and Y15 residues of Cdc2/Cdk1, which are the Wee1 target sites, are mutated into A and F, respectively). During the course of the evolution assay, the populations were maintained at constant vegetative growth, allowing for the selection of faster growing cells. This experimental set up allowed us to explore two key questions: 1) Does the simplified cell cycle control network remain robust despite the lack of complexity compared to the wild-type network (WT vs. MCN), and 2) what pathways can be targeted by evolution in cells lacking strict control over entry into mitosis to overcome the inherent loss in proliferative potential of the MCN-AF cells. First, based on the characterisation of evolved WT and MCN populations presented in this work, we can see that cells with a simplified cell cycle control network do not appear to have inherent pressures to re-complexify, nor are they any less robust when maintained in prolonged vegetative growth compared to WT. This is a striking result, as it further contributes to a growing body of evidence that the fundamental principle of the cell cycle is to maintain the correct oscillation of Cdk activity (Fisher and Nurse 1996; Coudreuse and Nurse 2010b; Santamaría et al. 2007). However, the increased layers of complexity in the normal cell cycle control network

compared to the MCN may still be significant in maintaining the integrity of the cell cycle in specific growth conditions and further studies will be necessary to explore this question. In fact, work from our team has showed that MCN and WT cells have very properties when in quiescence and different chronological aging profile (unpublished data).

Next, in order to study the evolutionary strategies that cells can employ to overcome the loss of the Wee1/Cdc25 feedback loop, we specifically explored one of the genetic alterations that was identified in our experimental evolution assay. Indeed, a single point mutation in the *spo12* gene that results in a disruption of the Spo12 protein was found to be causal for the observed improvement in growth of evolved MCN-AF cells. This improved proliferative potential was accompanied with a shortening of the G1 phase and reduction of size at division (SAD). Interestingly, these improvements appeared to be common characteristics for each of the independently evolved MCN-AF populations, implying that improved growth in the context of this assay involves returning to a cell cycle state that is more similar to that in WT cells. The loss of Spo12 function was confirmed to be responsible for the recovered proliferative capacity of MCN-AF cells, as full deletion of the open reading frame demonstrated clear benefits for growth compared to the parental, at both the population and single cell levels.

The role of Spo12 in fission yeast remained unknown, and does not share function with its homolog in budding yeast, which is involved in the early Cdc14 release as part of the FEAR network (Chen et al. 2006; Samuel et al. 2000). Interestingly, fission yeast Spo12 (90aa) is much smaller compared to budding yeast SPO12 (173aa), with only a small conserved Spo12 domain surrounded by largely disorganised structures. Within the Spo12 domain, there are two putative Cdk target sites, one of which having been shown to be phosphorylated by Cdc2/Cdk1 (Swaffer et al. 2016). This demonstrates a clear functional interaction between Spo12 and Cdc2/Cdk1. Indeed, our results further show that Spo12 functions as a potentiator of Cdk activity, and is part of a novel positive feedback loop on cyclin B/Cdk1. Spo12 is translocated to the nucleus in a Cdk dependent manner at the onset of mitosis where it remains transiently until anaphase. Interestingly, the cellular levels of Spo12 do not change throughout the cell cycle. It is in fact its Cdk-induced translocation to the nucleus at mitosis that appears to mediate an increase in Cdk activity. Thus, our work demonstrates for the first time that Spo12 is a novel regulator of Cdk activity that functions in a spatial positive feedback loop on Cdc2. While we have uncovered the way Cdc2 regulates

Spo12, the mechanism responsible for Spo12 potentiation of Cdk activity remains unclear. However, we expect to uncover this through the identification of interactors of Spo12 using the TurboID tag combined with mass spectrometry (Larochelle et al. 2019).

Our study showed that the loss of Spo12 function was sufficient to improve the growth of cells lacking the mitotic entry switch by reducing Cdk activity levels. Indeed, we found that MCN-AF populations have a higher percentage of non-dividing cells compared to WT, which is reduced by abrogating Spo12 function. We hypothesise that the higher percentage of cells that fail to divide in MCN-AF cultures is due to the increased instance of cells entering mitosis prematurely, which would lead to the inability to complete chromosome segregation correctly. This is a result of a more gradual increase in Cdk activity during G2 caused by the absence of the Wee1/Cdc25 feedback loop, which then leads to cells reaching the M phase threshold sooner. Remarkably, our data suggest that, in contrast to one of the commonly accepted models, MCN-AF cells do not show higher overall Cdk activity than WT. This also implies that the Cdk mitotic threshold may be lower than anticipated and that there is an important overshoot in Cdk activity as WT cells enter mitosis. By decreasing Cdk activity during this phase of the cell cycle via loss of Spo12 function, more time is provided during G2, as the time at which the Cdk mitotic threshold is reached is delayed. This facilitates the full completion of genome duplication and more optimal preparation of chromosome segregation, thereby reducing the occurrence of deleterious entry into mitosis. Therefore, we propose that cells lacking the mitotic entry switch can overcome its loss to improve proliferation by reducing Cdk activity at the onset of mitosis without affecting its dynamic progressive profile. Altogether, our results hint at the possibility of Spo12 acting as an archaic regulator of Cdk activity at mitosis, which has had its function minimised through the evolution of the more dominant Wee1/Cdc25 feedback loop. Alternatively, Spo12 function may be crucial in more specific environments that are not reproduced in laboratory conditions. The results from this work also demonstrate the significant added value of the experimental evolution approach this project has taken, as it would not have been easy to uncover such a pathway in more standard strategies or in alternative models, given the importance of the mitotic entry switch.

A significant part of the data presented in this work has been generated through single cell analysis of dynamic events in the cell cycle, which was only possible due to the novel experimental techniques utilised. Specifically, analysis of single cells was done using time-

lapse experiments that combined microfluidics and high-resolution microscopy. From this we were able to monitor cell cycle progression, which allowed us to track the real-time dynamic changes of relevant markers that were tagged with fluorescent proteins. We generated large amounts of time-lapse images from these experiments, which were then used to produce quantitative and qualitative data to characterise the role of Spo12 in cell cycle progression. However, in order to acquire meaningful data from these assays, it was necessary to score a significant number of cells for each experiment. This was a time-consuming aspect of our work, as it required manual scoring of all independent markers. This in itself is a common bottleneck in the analysis of time-lapse microscopy images. Indeed, while the capacity to acquire high-content data has significantly increased, in particular via the development of novel technologies such as microfluidics, automated image analysis remains a complex task that requires very specific expertise. Thus, while we did not use it in the context of the Spo12 study, we set out to improve this aspect of our work by implementing a recently developed pipeline for automatic image analysis, DetecDiv. This platform is a very versatile software that utilises deep-learning techniques to train neural networks for the high-throughput analysis of single-cell imaging data (Aspert, Hentsch, and Charvin 2022). Combined with a novel microfluidic chip design, DetecDiv was initially developed to investigate the replicative lifespan of individual budding yeast cells in different growth conditions. The goal of this part of our work was to adapt this pipeline to the analysis of the fission yeast cell cycle. Importantly, our approach probed for the first time the capacity of Detecdiv to determine the temporal organisation of a complex process based on 1) single-cell segmentation and 2) the use of several fluorescent markers within the same strain, a strategy that was not tested in the original study. This work was performed in collaboration with Dr. Gilles Charvin, who developed Detecdiv.

First, we adapted the microdevice design for fission yeast by modifying the structures that allow for trapping and monitoring individual cells. Second, we developed novel classifiers for the analysis of specific cellular characteristics (e.g. cell length and volume) and cell cycle events using fluorescent markers (e.g. onset of S and M). This involved training the neural network with data acquired through time-lapse experiments with strains harbouring the specific cell cycle markers Nhp6::mCherry (DNA), Plo1::GFP (mitosis), and Tos4::GFP (G1/S). We validated our results by using the trained network to automatically analyse datasets that were previously scored manually, allowing us to compare the results with the ground truth characterisations. In parallel, we constructed new strains that express our

different reporters while having altered cell cycle properties, which will serve as a proof-of-concept for the newly trained pipeline's ability to extract meaningful data from time-lapse images of cell cycle events. While this study is still being finalised, we have now successfully used Detecdiv to map cell cycle events and cell cycle dynamics at the single-cell level. Altogether, this will represent a powerful tool for the fission yeast community, as it will allow the high-throughput analysis of cell cycle time-lapse data producing robust quantitative and qualitative data. Indeed, as we have used general markers for monitoring cell cycle events in fission yeast, other labs will be able to directly utilise our trained network to process their own datasets when using these same markers. This tool will also allow us to re-inforce the results obtained by manual scoring in our Spo12 study. Furthermore, due to the versatility of the DetecDiv pipeline, it will be possible for others to contribute to this open-source software and share classifiers trained using alternative markers, generating a database of ready-to-use tools for image analysis. Our study represenst the first step in this dynamic. Finally, as we now demonstrate how combining Detecdiv with a complex set of markers is a powerful tool for analysing any process in a high-throughput manner, we believe that this work will also be of interest in other fields and for labs using other models than fission yeast.

Finally, as part of this thesis, we looked to examine the changes in cell size regulation that occur in the absence of Spo12. This was done using cell length at division measurements as a proxy for cell size, a classical approach to determine the effectiveness of size control in fission yeast. However, an alternative metric that is now broadly utilised in our team for monitoring cell size is cell volume. Cell volume is a more relevant measure of cell size, as it is more critical to cell physiology than cell length. Indeed, significant changes in cell volume result in alteration of intracellular biochemistry, and surface area, which is also linked to volume, defines the interaction of cells with their environment. Importantly, in the context of the rod-shaped fission yeast cell, the measurement of cell length ignores potential small changes in cell diameter, despite their strong impact on cell volume. Thus, by measuring the dynamic changes in the volume of fission yeast cells during the cell cycle, we may gain novel insights into the mechanisms responsible for the improved proliferation of the evolved MCN-AF clones. However, a method for directly measuring the volume of yeast cells was lacking, and all existing techniques available for this have strong biases. We therefore implemented a novel methodology for measuring cell volume in fission yeast using a strategy initially developed for mammalian cells as a starting point (García-Ruano et al. 2022). In this paper, we demonstrate that changes in cell volume can be accurately monitored at the single-cell

level using microfluidics and a dedicated analysis pipeline. This exciting tool will improve our understanding of how cells regulate their size and potentially be used to uncover novel insights into the alternative pathways of proliferation. In particular, the lab will assess cell volume in the context of our Spo12 study. To conclude, the work presented in this manuscript was centered on the investigation of Spo12, where we have implicated its role in a novel positive feedback loop on Cdk activity. Additionally, we were prompted to improve the type of analysis that we performed, so this manuscript also details the implementation of a novel and powerful tool for microfluidic time-lapse analysis.

References

Aspert, Théo, Didier Hentsch, and Gilles Charvin. 2022. "DetecDiv, a Generalist Deep-Learning Platform for Automated Cell Division Tracking and Survival Analysis." *ELife* 11 (August): 2021.10.05.463175. https://doi.org/10.7554/eLife.79519.

Chen, C.-T., M.-P. Peli-Gulli, V. Simanis, and D. McCollum. 2006. "S. Pombe FEAR Protein Orthologs Are Not Required for Release of Clp1/Flp1 Phosphatase from the Nucleolus during Mitosis." *Journal of Cell Science* 119 (21): 4462–66. https://doi.org/10.1242/jcs.03220.

Coudreuse, Damien, and Paul Nurse. 2010a. "Driving the Cell Cycle with a Minimal CDK Control Network." *Nature* 468 (7327): 1074–80. https://doi.org/10.1038/nature09543.

Fisher, D. L., and P. Nurse. 1996. "A Single Fission Yeast Mitotic Cyclin B P34cdc2 Kinase Promotes Both S-Phase and Mitosis in the Absence of G1 Cyclins." *EMBO Journal* 15 (4): 850–60. https://doi.org/10.1002/j.1460-2075.1996.tb00420.x.

García-Ruano, Daniel, Larisa Venkova, Akanksha Jain, Joseph C. Ryan, Vasanthakrishnan Radhakrishnan Balasubramaniam, Matthieu Piel, and Damien Coudreuse. 2022. "Fluorescence Exclusion - a Rapid, Accurate and Powerful Method for Measuring Yeast Cell Volume." *Journal of Cell Science* 135 (13). https://doi.org/10.1242/jcs.259392.

Larochelle, Marc, Danny Bergeron, Bruno Arcand, and François Bachand. 2019. "Proximity-Dependent Biotinylation Mediated by TurboID to Identify Protein-Protein Interaction Networks in Yeast." *Journal of Cell Science* 132 (11). https://doi.org/10.1242/jcs.232249.

Samuel, J. M., N. Fournier, V. Simanis, and J. B.A. Millar. 2000. "SPO12 Is a Multicopy Suppressor of Mcs3 That Is Periodically Expressed in Fission Yeast Mitosis." *Molecular and General Genetics* 264 (3): 306–16. https://doi.org/10.1007/s004380000324.

Santamaría, David, Cédric Barrière, Antonio Cerqueira, Sarah Hunt, Claudine Tardy, Kathryn Newton, Javier F. Cáceres, Pierre Dubus, Marcos Malumbres, and Mariano Barbacid. 2007. "Cdk1 Is Sufficient to Drive the Mammalian Cell Cycle." *Nature* 448 (7155): 811–15. https://doi.org/10.1038/nature06046.

Swaffer, Matthew P., Andrew W. Jones, Helen R. Flynn, Ambrosius P. Snijders, and Paul Nurse. 2016. "CDK Substrate Phosphorylation and Ordering the Cell Cycle." *Cell* 167 (7): 1750-1761.e16. https://doi.org/10.1016/j.cell.2016.11.034.

Titre: Adaptation cellulaire à la dérégulation du cycle de division

Mots clés: Cycle cellulaire, Cdk, levure de fission, évolution expérimentale, biologie synthétique

Résumé: La progression du cycle cellulaire est un processus essentiel dont la régulation est hautement conservée chez les eucaryotes. Les protéines kinases dépendantes des cyclines (Cdks) sont des composants clés du réseau de contrôle du cycle cellulaire et interagissent avec diverses cyclines pour conduire une prolifération cellulaire robuste. Un mécanisme de régulation de l'activité des Cdk, connu sous le nom de boucle de rétroaction Wee1/Cdc25, est hautement conservé dans les cellules eucaryotes et est essentiel dans les cellules de type sauvage. Nous avons précédemment démontré que les cellules MCN dépourvues des boucles de rétroaction Wee1/Cdc25 conservées (appelées MCN-AF) sont étonnamment viables. Cependant, les cellules MCN-AF présentent un taux de croissance significativement réduit. Après avoir réalisé une évolution expérimentale avec les cellules MCN-AF, nous avons identifié un certain nombre de mutations liées à une amélioration de la croissance en l'absence de la boucle de rétroaction Wee1/Cdc25.

Spo12 est une petite protéine nucléaire de fonction inconnue, dont nous avons montré que, lorsqu'elle est perturbée, elle améliore la croissance des cellules MCN-AF et raccourcit la durée de la phase G1. En effet, je démontre que Spo12 joue un rôle dans une nouvelle boucle de rétroaction sur l'activité de la Cdk, qui, lorsqu'elle est perturbée, réduit l'activité globale de la Cdk au cours du cycle cellulaire. En outre, j'ai également adapté avec succès un pipeline d'analyse d'images automatisé pour permettre l'acquisition de données à haut débit à partir de laps de temps complexes de marqueurs du cycle cellulaire, ce qui constituera un outil utile pour la communauté des levures de fission. Enfin, j'ai également contribué au développement d'une méthodologie de mesure du volume en time-lapse, dans le cadre d'un projet plus large visant à mesurer avec précision le volume chez la levure de fission.

Title: Alternative paths to proliferation

Keywords : Cell cycle, Cdk, fission yeast, experimental evolution, synthetic biology

Abstract: Cell cycle progression is an essential process whose regulation is highly conserved among eukaryotes. Cyclin-dependent protein kinases (Cdks) are key components of the cell cycle control network and interact with various cyclins to drive robust cell proliferation. A regulatory mechanism of Cdk activity, known as the Wee1/Cdc25 feedback loop, is highly conserved in eukaryotic cells and is essential in wild type cells. We previously demonstrated that MCN cells lacking the conserved Wee1/Cdc25 feedback loops (referred to as MCN-AF) are surprisingly viable. However, MCN-AF cells show a significantly reduced growth rate. After performing experimental evolution with MCN-AF cells, we identified a number of mutations linked to an improvement of growth in the absence of the Wee1/Cdc25 feedback loop.

Spo12 is a small nuclear protein of unknown function, which we have shown, when disrupted, will improve the growth of MCN-AF cells and shorten G1 phase length. Indeed, I demonstrate that Spo12 has a role in a novel feedback loop on Cdk activity, which when disrupted will reduce overall Cdk activity during the cell cycle. Furthermore, I have also successfully adapted an automated image analysis pipeline to provide high-throughput data acquisition from complex time-lapses of cell cycle markers, which will be a useful tool for the fission yeast community. Lastly, I have also contributed to the development of a time-lapse volume measurement methodology, as part of a larger project to accurately measure volume in fission yeast.